Air Injection Technique to Mitigate Liquefaction beneath Shallow Foundations

Abdulhakim Zeybek

Department of Engineering

University of Cambridge

This dissertation is submitted for the degree of

Doctor of Philosophy

Clare Hall

November 2017

Declaration

I hereby declare that this dissertation is the result of my own work and includes nothing which is the outcome of work done in collaboration except where specified in the text. It is not substantially the same as any that I have submitted, or, is being concurrently submitted for a degree or diploma or other qualification at the University of Cambridge or any other University or similar institution. I further state that no substantial part of my dissertation has already been submitted, or, is being concurrently submitted for any such degree, diploma or other qualification at the University of Cambridge or any other University or similar institution. This dissertation contains fewer than 65,000 words including appendices, bibliography, footnotes, tables and equations and has no more than 150 figures.

Abdulhakim Zeybek

November 2017

Signed: _____

Date: _____

Acknowledgements

I would like to thank many people who contributed in some way to this PhD research. First and foremost, I thank my supervisor, Professor Gopal Madabhushi, for giving me an opportunity to undertake my work in his research group. His tremendous support and guidance through all the stages of my research were invaluable. My thanks also go to Dr Stuart Haigh and Dr Giovanna Biscontin for their helpful suggestions along the way.

I am very grateful to the Ministry of National Education (M.E.B.) of Turkey for their financial support during the course of this study.

Every result described in this research was accomplished with the excellent assistance and support of the technical staff at the Schofield Centre. I would like to express my sincere gratefulness to Kristian Pether, John Chandler and Mark Smith for making parts for the tests and running the centrifuge, to Chris McGinnie for wiring or fixing countless instruments and to Richard Adams for his constant help during the preparation of the tests. I am also grateful to Anama Lowday and Magdalena Charytoniuk for their help with administrative issues.

I would like to thank my colleagues for their kind friendship, invaluable help and stimulating discussions throughout the years. I particularly owe my gratitude to Stephan Van Eeden, Srikanth Madabhushi, Dr Raz Jabary, Thejesh Kumar Garala, Stefan Ritter and Jad Boksmati. They made my life at the centre more enjoyable. I am indebted to Dr Peter Kirkwood and Dr Orestis Adamidis for answering all of my questions about centrifuge testing. I want to thank Dr Njemile Faustin, Dr Aliasger Haiderali and Dr Jennifer Upton for proofreading the first draft of this thesis. I also thank many colleagues Jeffrey, Gue, Talia, Andrei and Fiona for their great friendship and kindness.

Last but not the least, this thesis is dedicated to my dear parents Ramazan and Sahinaz, my beloved wife Betul and my daughter Zeyneb. I would not have reached this stage without the unconditional love and support of my wife and the encouragement of my parents, to whom I owe everything.

Abstract

Historical and recent earthquakes often remind the need for taking precautions against earthquake-induced liquefaction damage that structures on shallow foundations can suffer. Air injection technique has the potential to improve the soil supporting new and existing structures. There is, however, little research on its application and performance beneath existing shallow foundations. The aim of this research was to provide a comprehensive view of the air injection technique by conducting well-controlled dynamic centrifuge and 1-g shaking table tests, along with static soil column experiments in the laboratory.

Detailed analysis of the test results highlighted that air injection was an effective way of minimising the soil-softening and loss of shear stiffness associated with earthquake-induced liquefaction. A decreasing trend in the magnitude of excess pore pressures and foundation settlements was observed with decreasing degree of saturation. Air injection technique was also found to perform better under increased confining stresses.

Injecting air in a controlled manner (e.g. applying low air injection rate and pressure) was shown to be crucial for the safety of foundations. A wider and more uniformly desaturated zone was achieved with increasing air injection pressure, but which concurrently increased the settlements that shallow foundations experienced. It was also found that most of the air could remain entrapped in partially saturated soil under different simulated field conditions for a long period of time, which indicated the long-term reliability of the mitigation accomplished.

Particle image velocimetry was utilised to identify deformation mechanisms that develop underneath and in the ground surrounding shallow foundations. It was shown that foundations resting on saturated soil settled excessively. Foundation settlements were predominantly driven by deviatoric strains, and a bearing capacity failure mechanism did form. When air was injected into saturated soil, air reduced the build-up of excess pore pressures as it contracted during dynamic loading but increased soil compressibility. Deviatoric strain-induced deformations significantly reduced, which resulted in much smaller settlements. The observed settlements were principally caused by volumetric strains that arose from increased soil compressibility. Given the depth of liquefaction reduced significantly for air-injected partially saturated soil, a complete bearing capacity failure mechanism could not occur. The lower the degree of saturation, the shallower and more localised the deformations were observed.

Table of Contents

List of Figures V
List of Tables IX
Nomenclature XI
Chapter 1 Introduction 1
1.1 Problem Statement 1
1.2 Research Aims and Objectives 4
1.3 Thesis Outline 6
Chapter 2 Literature Review 8
2.1 Introduction 8
2.2 Soil Liquefaction 8
2.2.1 Definition and Mechanism of Soil Liquefaction 9
2.2.2 Frameworks for Soil Liquefaction 12
2.2.3 Undrained Behaviour of Sand under Cyclic Loading 14
2.3 Design Practice for Liquefaction Hazard Evaluation 16
2.3.1 Liquefaction Susceptibility 16
2.3.2 Triggering (Initiation) of Liquefaction 16
2.3.3 Consequences of Liquefaction 18
2.3.4 Prediction of Settlement 19
2.3.5 Traditional Liquefaction Mitigation Techniques 21
2.3.6 Limitations of Current Design Practice 22
2.4 Desaturation of Soil as a Liquefaction Treatment Method 24
2.4.1 Historical Review of Soil Desaturation Methods 24
2.4.2 Air Injection as a Liquefaction Countermeasure 25
2.5 Saturation in Soils 26
2.6 Shear Strength and Liquefaction Resistance of Soils 28
2.6.1 Effect of Matric Suction on Effective Stress 28
2.6.2 Theoretical Effect of Air Injection on Pore Fluid Compressibility 30
2.6.3 Theoretical Effect of Air Injection on Excess Pore Water Pressure 33
2.6.4 Effects of Soil Compressibility on Liquefaction Resistance 34
2.7 Summary 35
Chapter 3 Modelling Techniques 36
3.1 Introduction 36

3.2 Dynamic Centrifuge Modelling 37
3.2.1 The Theory of Centrifuge Modelling 37
3.2.2 The Turner Beam Centrifuge 39
3.2.3 The Stored Angular Momentum (SAM) Earthquake Actuator 40
3.2.4 Model Containers 41
3.2.5 Instrumentation 42
3.2.6 Data Acquisition 47
3.3 Centrifuge Tests 48
3.3.1 Model Foundations 48
3.3.2 Model Preparation-Sand Pouring 53
3.3.3 Model Preparation-Saturation 55
3.3.4 Model Preparation-Desaturation via Air Injection 56
3.3.5 PIV Setup 59
3.3.6 Centrifuge Testing Procedure 60
3.4 1-g Shaking Table Tests 64
3.4.1 Shaking Table at the Schofield Centre 64
3.4.2 Model Foundation 64
3.4.3 Model Preparation-Sand Pouring and Saturation 64
3.4.4 Model Preparation-Desaturation via Air Injection & Chemical 66
3.4.5 Shaking Table Testing Procedure 66
3.5 Analysis Techniques 69
3.5.1 Data Processing and Data Presentation 69
3.5.2 Geo-PIV Analysis 69
3.5.3 Potential Errors 70
Chapter 4 Physical Modelling of Air Injection 74
4.1 Introduction 74
4.2 The Execution of Air Injection 74
4.2.1 Air Injection Pressure versus Settlement 75
4.2.2 Air Injection Pressure versus Soil Deformations 77
4.2.3 Control of Air (Injection)-Induced Foundation Settlement 79
4.3 Assessment of Degree of Saturation, Sr 79
4.3.1 Degree of Saturation Based on Mass-Volume Relationships 81
4.3.2 Degree of Saturation Based on Soil Moisture Sensors 83
4.4 Distribution of Entrapped Air Bubbles 84
4.4.1 Effective Air-Entrapped Zones 84
4.4.2 Impact of Distribution of Air Bubbles on the Seismic Response 87

4.5 Summary 89
Chapter 5 Durability of Partial Saturation 90
5.1 Introduction 90
5.2 Possible Field Conditions and Simplifications 91
5.3 1-D Vertical Soil Column Tests 92
5.3.1 Design of 1-D Vertical Soil Column Apparatus 92
5.3.2 Model Preparation 95
5.3.3 De/Saturation of 1-D Vertical Soil Column Specimens 95
5.4 Durability of Entrapped Air 97
5.4.1 Durability under Hydrostatic Conditions 97
5.4.2 Durability under Hydraulic Flow 99
5.4.3 Durability under Varying Pressure 99
5.4.4 Durability under Earthquake Loading 102
5.4.5 Seismic Response under the Combined Field Conditions 103
5.5 Summary 105
Chapter 6 Dynamic Behaviour of Partially Saturated Soils 106
6.1 Introduction 106
6.2 Important Parameters for the Dynamic Response of Partially Saturated Soils 107
6.2.1 Degree of Saturation 107
6.2.2 Confining Stress Level (Vertical Stress) 122
6.2.3 Bearing Pressure 128
6.2.4 Earthquake Motion Characteristics 134
6.3 Dynamic Response of Level Bed of Partially Saturated Soils 142
6.3.1 Co-Seismic and Post-Seismic Behaviour 142
6.4 Summary 146
Chapter 7 Deformation Mechanisms: Shallow Foundations 148
7.1 Introduction 148
7.2 Response beneath and around Foundation 149
7.2.1 Deformation Mechanisms during the Seismic Events 149
7.2.2 Deformation Mechanisms during the Air Injection Process 155
7.3 Experimentally Observed Deformation Mechanisms 157
7.4 Effects of Key Parameters on Soil Deformations 158
7.4.1 Degree of Saturation 158
7.4.2 Confining Stress (Vertical Stress) 161
7.4.3 Foundation Bearing Pressure 165
7.4.4 Earthquake Amplitude 168

7.5 Summary 170
Chapter 8 Simplified Methodology to Estimate the Settlement of Partially Saturated Soils 172
8.1 Introduction 172
8.2 Settlement Evaluation Methods in State of Practice 173
8.2.1 Free-Field Settlement 173
8.2.2 Foundation Settlement 174
8.3 A Simple Methodology for Settlement Prediction 176
8.3.1 The Basis for the Methodology 176
8.3.2 Framework for the Methodology 177
8.3.3 Evaluation of the Model Parameters 180
8.3.4 Validity of the Methodology 183
8.4 Post-Liquefaction Reconsolidation of Soil 185
8.4.1 Reconsolidation Settlement 185
8.4.2 Permeability and One-Dimensional Stiffness 186
8.4.3 Centrifuge Test Results 187
8.5 Summary 188
Chapter 9 Conclusions and Future Research 190
9.1 Research Conclusions 191
9.1.1 Physical Modelling of Air Injection and Durability of Air 191
9.1.2 Performance of Air Injection as a Liquefaction Mitigation Measure 192
9.1.3 Deformation Mechanisms 194
9.1.4 Methodology for Prediction of Settlement 197
9.2 Implications to Design Practice 197
9.2.1 Design of Air Injection 197
9.2.2 Reliability of Air Injection 198
9.2.3 Extent of Desaturated Zones 198
9.3 Research Limitations and Future Research 198
9.3.1 Experimental Modelling 199
9.3.2 Numerical Modelling 200
References 201
Appendix-A Centrifuge Test Programme and Model Layouts 211

List of Figures

Chapter 1

Figure 1.1– Typical liquefaction-induced building damage..... 2

Chapter 2

Figure 2.1– Flow chart for the assessment of liquefaction.. 11
Figure 2.2– Critical State framework for soil liquefaction..... 13
Figure 2.3– Characteristic state for saturated sands.. 14
Figure 2.4– Stress paths and stress-strain curves.. 15
Figure 2.5– Key elements of soil liquefaction study.. 16
Figure 2.6– Liquefaction-induced damage in Adapazari.. 19
Figure 2.7– Proposed charts for the prediction of post-earthquake volumetric strains.. 20
Figure 2.8– Influence of degree of saturation on the liquefaction resistance of soils. 24
Figure 2.9– Schematic illustration of the in situ air injection technique. 25
Figure 2.10– Schematic of fully, partially and unsaturated soil zones.. 27
Figure 2.11– SWRC and suction stress for a loose Hostun sand deposit. 29
Figure 2.12– Schematic representation of a partially saturated soil element. 32
Figure 2.13– Variation of potential bulk modulus of pore fluid with degree of saturation and effective stress. 33
Figure 2.14– Potential volumetric strain vs liquefaction resistance ratio.. 34

Chapter 3

Figure 3.1– A view of the Turner beam centrifuge at the University of Cambridge. 39
Figure 3.2– A view and schematic illustration of the SAM earthquake actuator..... 40
Figure 3.3– A view of the model containers. 42
Figure 3.4– A view of the instruments used during the experiments. 43
Figure 3.5– A view of the model foundation used in the centrifuge experiments. 49
Figure 3.6– The spring support system attached to the foundation. 50
Figure 3.7– A view of the model foundations instrumented with MEMS accelerometers. 52
Figure 3.8– Particle size distribution for the HN31 Hostun sand. 53
Figure 3.9– A view of the automatic sand pourer and instruments installed. 54

Figure 3.10– Saturation of the centrifuge models through CAM-Sat system. 56
Figure 3.11– A view and sketch of the air injection control system. 57
Figure 3.12– A view of the air injectors tested in a water-filled tank. 59
Figure 3.13– A view of the fully assembled centrifuge model loaded. 60
Figure 3.14– Typical input acceleration-time histories recorded in the centrifuge tests.. 63
Figure 3.15– A view of the shaking table and model setup. 65
Figure 3.16– A view of the overhead hopper and instruments installed during sand pouring.66
Figure 3.17– Model layout for 1-g shaking table models. 68
Figure 3.18– Co-seismic and post-seismic settlements based on PIV and LVDT..... 72

Chapter 4

Figure 4.1– Time histories of pressure, change in fluid height and foundation settlement recorded during the air injection process.. 77
Figure 4.2– Typical air injection-induced soil deformations. 78
Figure 4.3– Time histories of pressure and degree of saturation in the air injection phase.... 82
Figure 4.4– Time histories of degree of saturation. 83
Figure 4.5– Distribution of air bubbles. 86
Figure 4.6– Digital image of soil specimen.. 87
Figure 4.7– Variation of excess pore pressure ratios with distance from the air injector. 88

Chapter 5

Figure 5.1– Schematic illustration of the 1-D vertical soil column test apparatus. 94
Figure 5.2– Typical test setup for the vertical soil column tests. 95
Figure 5.3– Typical test data corresponding to de/saturation of the soil column specimens.. 96
Figure 5.4– Variation of degree of saturation under hydrostatic condition at 1-g. 98
Figure 5.5– Variation of degree of saturation under hydrostatic condition at 70-g. 98
Figure 5.6– Variation of degree of saturation under upward and downward water flow. 99
Figure 5.7– Variation of degree of saturation under increasing g-level..... 100
Figure 5.8– Photos of model cross-sections recorded during centrifuge swing-down. 101
Figure 5.9– Soil deformations during centrifuge swing-down.. 101
Figure 5.10– Variation of degree of saturation under horizontal shaking. 102
Figure 5.11– Seismic settlement of a level deposit at different stages of centrifuge test. 104

Chapter 6

Figure 6.1– Typical foundation settlement-time, acceleration-time and settlement-degree of saturation histories. 109

Figure 6.2– Differential settlements between the foundation and the soil surface..... 110

Figure 6.3– Typical excess pore pressure-time and depth-excess pore pressure histories beneath foundations. 113

Figure 6.4– Typical excess pore pressure-time histories in the free-field. 115

Figure 6.5– Time histories of hydraulic gradients recorded during and after earthquakes. .. 117

Figure 6.6– Variation of excess pore pressure head with depth and time. 118

Figure 6.7– Typical amplification/attenuation ratios for foundation and foundation soil. ... 120

Figure 6.8– Typical shear stress-strain loops recorded in the free-field (Section 1). 121

Figure 6.9– Time histories of settlement and excess pore pressure ratios (1-g testing). 124

Figure 6.10– Time histories of settlement and excess pore pressure ratios (high-g testing). 125

Figure 6.11– Time histories of excess pore pressure ratios in the free-field (high-g testing) 126

Figure 6.12– Typical shear stress-strain loops recorded in the free-field (Section 3). 127

Figure 6.13– Time histories of heavy and light footing settlement and input acceleration. . 130

Figure 6.14– Foundation settlement versus degree of saturation. 131

Figure 6.15– Time histories of excess pore pressures beneath heavy and light foundations. 132

Figure 6.16– Amplification/attenuation ratios for the heavy and light foundations. 133

Figure 6.17– Time histories of settlement and acceleration during successive earthquakes. 136

Figure 6.18– Time histories of excess pore pressure ratios beneath the light foundation. 138

Figure 6.19– Excess pore pressure ratios beneath foundations vs peak input accelerations. 139

Figure 6.20– FFTs of the horizontal input and foundation accelerations (first 17 cycles). .. 141

Figure 6.21– FFTs of the horizontal foundation accelerations recorded at varying cycles... 141

Figure 6.22– Free-field settlement, excess pore pressure and input motion time histories... 143

Figure 6.23– Free-field settlements and excess pore pressures. 145

Figure 6.24– Free-field post-seismic (reconsolidation) settlements. 145

Chapter 7

Figure 7.1– Typical photos of cross-sections of the models.. 150

Figure 7.2– Displacement vector fields beneath heavy foundations at the end of 17 acceleration cycles. 151

Figure 7.3– Accumulation of soil deformations beneath shallow foundations and foundation settlements during half-cycles near the beginning of the earthquake. 153

Figure 7.4– Soil displacement vectors during the air injection process. 156
Figure 7.5– Effect of degree of saturation on deformation mechanisms.. 159
Figure 7.6– Accumulated horizontal soil displacements. 160
Figure 7.7– Ultimate soil displacements at 1-g shaking table tests... 162
Figure 7.8– Ultimate soil displacements at 1-g shaking table test (chemical treatment)..... 163
Figure 7.9– Soil displacements accumulated during 17 acceleration cycles in CT7EQ1..... 164
Figure 7.10– Accumulated displacement contours for saturated soils. 166
Figure 7.11– Accumulated displacement contours for partially saturated soils. 167
Figure 7.12– Accumulated soil displacements for saturated soils during successive earthquake events. 169
Figure 7.13– Accumulated soil displacements for partially saturated soils during successive earthquake events. 170

Chapter 8

Figure 8.1– Predicted vs measured foundation settlement for saturated soils. 175
Figure 8.2– Predicted vs measured foundation settlement for partially saturated soils. 176
Figure 8.3– Schematic representation of saturated and partially saturated soil behaviour. .. 177
Figure 8.4– Schematic representation of a uniform soil layer divided into n sub-layers..... 178
Figure 8.5– Schematic flow chart of the proposed methodology. 179
Figure 8.6– Change of liquefaction resistance and excess pore pressure ratio with degree of saturation. 181
Figure 8.7– Predicted vs measured excess pore pressure ratios. 182
Figure 8.8– Relationship between pore pressure ratio and volumetric strain.. 183
Figure 8.9– Estimated total ground surface settlement vs measured centrifuge data. 184
Figure 8.10– Variation of permeability with effective stress.. 187
Figure 8.11– Predicted reconsolidation settlement vs measured centrifuge data. 188

Appendix-A

Figure A.1– Model layout for centrifuge tests CT1, CT2 and CT3.... 221
Figure A.2– Model layout for centrifuge tests CT4, CT5, CT6 and CT7.. 222
Figure A.3– Model layout for centrifuge test CT8..... 223
Figure A.4– Model layout for centrifuge tests CT9 and CT10.. 224

List of Tables

Chapter 2

Table 2.1 – A list of traditional methods of liquefaction mitigation. 21

Chapter 3

Table 3.1 – Main scaling laws in centrifuge modelling. 38
Table 3.2 – Typical details of the instrumentation. 44
Table 3.3 – Characteristics of the model foundations. 52
Table 3.4 – Geotechnical properties of HN31 Hostun sand. 53
Table 3.5 – Centrifuge testing programme. 62
Table 3.6 – 1-g shaking table testing programme. 67
Table 3.7 – Sensitivity of basic soil parameters to measurement errors. 73

Chapter 4

Table 4.1 – Typical settlement data corresponding to the air injection phase..... 79
Table 4.2 – Typical degree of saturation data corresponding to the air injection phase. 82

Chapter 5

Table 5.1 – Testing programme for the durability of air and typical test results. 93

Chapter 6

Table 6.1 – Approximate relative densities during successive events. 137
Table 6.2 – Percentage reduction in foundation settlement during successive events. 137

Chapter 7

Table 7.1 – Mechanisms of deformations in the partially saturated soils. 157

Chapter 8

Table 8.1 – Experimental settlements vs predictions of the free-field methodologies..... 174

Appendix-A

Table A.1 – Testing programme for CT1. 211
Table A.2 – Testing programme for CT2. 212

Table A.3 – Testing programme for CT3. 213
Table A.4 – Testing programme for CT4. 214
Table A.5 – Testing programme for CT5. 215
Table A.6 – Testing programme for CT6. 216
Table A.7 – Testing programme for CT7. 217
Table A.8 – Testing programme for CT8. 218
Table A.9 – Testing programme for CT9. 219
Table A.10 – Testing programme for CT10. 220

Nomenclature

Roman Symbols

a	Acceleration
B	Foundation width
B	Skempton's pore pressure coefficient
C	Concentration (%)
c_v	Coefficient of consolidation
D	Grain diameter
D_L	Depth of liquefiable layer
D_r	Relative density
e	Voids ratio
E_0	One-dimensional stiffness
g	Acceleration of gravity
G_s	Specific gravity
H	Height of model foundation
H_s	Height of soil
i	Hydraulic gradient
K	Bulk modulus
k	Hydraulic conductivity
$K\alpha$	Correction factor for the influence of initial static shear stress in CRR
$K\sigma$	Correction factor for the influence of overburden pressure in CRR
M	Magnitude of earthquake
n	Porosity
N	Scaling factor
N_{vG}	van Genuchten fitting parameter
N_1	SPT blow counts
$N_{1\text{-}60}$	Energy corrected SPT blow counts
N_{liq}	Number of cycles to reach liquefaction
P	Injection Pressure
p	Mean stress

P_0 Absolute hydrostatic pressure

q Bearing pressure

q Deviatoric stress

r_d Stress reduction coefficient

r_u Excess pore pressure ratio

S Settlement

S_r Degree of saturation

T Period

t Time

u Pore pressure

U_c Uniformity coefficient

V_p Compressional wave velocity

z Depth

Δe Change in void ratio

Δh Change in fluid level

Δp Change in pore pressure

Δu Excess pore pressure

Greek Symbols

α_{vG} van Genuchten fitting parameter

χ Effective stress parameter

ε Strain

γ Shear strain

γ_s Unit weight of soil

γ_f Unit weight of fluid

ν Kinematic viscosity

ψ Matric suction

ρ Density

σ Normal stress

σ_c Confining Stress

σ_s Suction stress

σ_1 Major principal stress

σ_3 Minor principal stress

τ Shear stress

φ Friction angle

Superscripts

′ Effective (for stress)

Subscripts

a pore air

ave average

com compressibility

epp excess pore (fluid) pressure

f foundation

f pore fluid

hyd hydrostatic

inj injection

max maximum

min minimum

net net

o initial

part partially saturated

sat saturated

v vertical

vol volumetric

w pore water

Acronyms / Abbreviations

AEV Air Entry Value

ChSL Characteristic State Line

CPT Cone Penetration Test

CRR Cyclic Resistance Ratio

CS Critical State

CSL Critical State Line

CSR Cyclic Stress Ratio

CVR Critical Voids Ratio

DA Double Amplitude

EU European Union

FFT Fast Fourier Transforms

FL Failure Line

HDPE High-Density Polyethylene

HPMC Hydroxypropyl Methylcellulose

LVDT Linear Variable Displacement Transducer

MEMS Micro-Electro-Mechanical Systems

Mh Horizontal MEMS accelerometer

MS Model Scale

Mv Vertical MEMS accelerometer

NEMISREF NEw Methods of MItigation of Seismic Risk on Existing Foundations

PIA Peak Input Acceleration

PIV Particle Image Velocimetry

PPT Pore Pressure Transducer

PS Prototype Scale

PSD Particle Size Distribution

PT Phase Transformation

PTFE Polytetrafluoroethylene

SAM Stored Angular Momentum

SPT Standard Penetration Test

Chapter 1

Introduction

1.1 Problem Statement

Earthquake-induced liquefaction is one of the most devastating phenomena contributing to damage to geotechnical structures. Over the last 50 years, liquefaction-induced damage has been a recurrent feature of many moderate to strong earthquakes. In particular, structures built on shallow foundations have suffered severe damage, as borne out by recent earthquakes in Turkey (Bray et al. 2004), Chile (Bertalot et al. 2013), Japan (Bhattacharya et al. 2011) and New Zealand (Cubrinovski et al. 2011). Figure 1.1 presents prime examples of liquefaction-related failures, whereby the ground beneath the foundation liquefied and no longer offered sufficient capacity to support the overlying structure. Although many residential buildings maintained their structural integrity, they suffered large settlements and/or rotations. Therefore, they could no longer be used and needed to be demolished. This type of failure indicates that the buildings were built on the liquefiable ground without consideration of protective measures for potential liquefaction damage. There are still a large number of structures built on saturated deposits of liquefiable soils in seismic zones worldwide. As they continue to be highly vulnerable to liquefaction-induced damage during future earthquake events, there is an urgent need to develop cost-effective liquefaction mitigation measures that can assist in preventing economic loss and even casualties/fatalities.

For many years, engineers have conducted research programmes to develop different types of liquefaction remediation techniques. The majority of proposed measures are often prohibitively expensive owing to their installation costs. In addition, their application to the foundation soils of existing structures is usually limited.

In less developed countries, there is often a lack of finance and regulation to incorporate any countermeasure against liquefaction. In developing countries, investment priorities are usually the important projects in urban areas, and there is often limited budget for the rest of the structures. Therefore, existing structures still remain at risk. Moreover, even in developed countries, the advanced seismic design codes allow for the construction of safe new structures, but the existing structures are often not well protected against liquefaction.

A rigorous seismic design approach for liquefaction mitigation of existing buildings is still lacking. For instance, Eurocode 8 (British Standards Institution 2004) suggests that

"*Ground improvement against liquefaction should either compact the soil to increase its penetration resistance beyond the dangerous range, or use drainage to reduce the excess pore-water pressure generated by ground shaking*".

The success of soil densification and drains as a way of mitigating liquefaction effects is well established, but they might not be best suited for use with existing structures, as will be discussed in section 2.3.6.

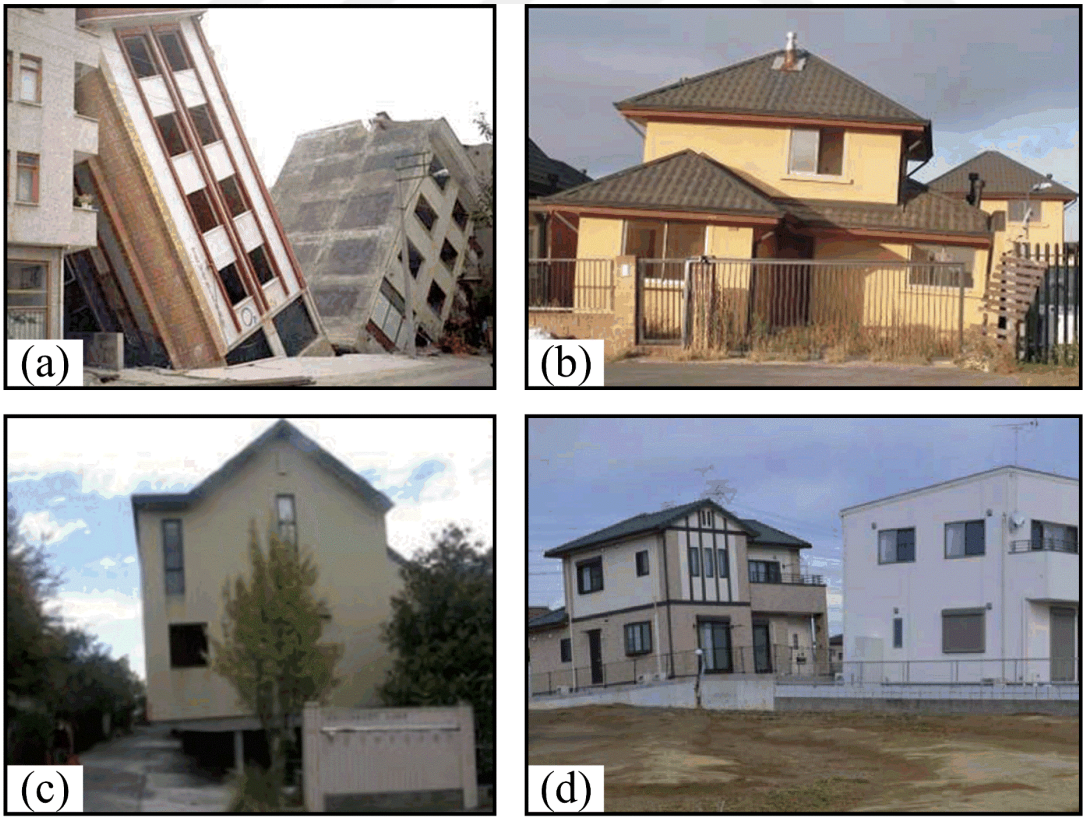

Figure 1.1– Typical liquefaction-induced building damage.
a) 1999 Kocaeli, Turkey b) 2010 Maule, Chile c) 2011 Tohoku, Japan and d) 2011 Christchurch, New Zealand (photographs courtesy of NISEE, University of California, Berkeley).

In recent years, a number of researchers have directed their attention towards the development of innovative and cost-effective liquefaction mitigation techniques that can be implemented beneath the foundation of existing structures as well as at new construction sites. A large collaborative research project called NEMISREF- New Methods of Mitigation of Seismic Risk on Existing Foundations is a good example of this research effort. This EU funded project was carried out as a co-operation between several academic institutions and engineering companies across Europe. The ultimate goal of the project was to develop new geotechnical foundation types and economic mitigation schemes for the seismic upgrade of existing structures, considering site effects and soil structure interaction. As part of the NEMISREF project, the performance of several methods for liquefaction remediation of existing buildings was investigated through integrated centrifuge experiments and numerical modelling efforts (e.g. Mitrani and Madabhushi 2008).

The increasing liquefaction resistance of soil with decreasing degree of saturation has been known for a long time. Nevertheless, it was not until 2003 that researchers started realising the need to develop liquefaction mitigation measures based on this concept. Since then, a few research attempts have been made to examine the technical feasibility of the desaturation techniques that comprise the artificial formation of air/gas bubbles within the liquefiable soil deposits. Air injection, amongst these techniques, has become more attractive to researchers and practitioners. Despite the promising nature of air injection, very little experimental research is available on this technique. This has left an important gap in the basic understanding of the mechanisms by which air injection can mitigate liquefaction effects and in the identification of the critical parameters that play a significant role in its efficacy. In particular, the way that air injection affects the seismic behaviour of liquefiable soils and the deformation mechanisms that generate shallow foundation settlements are not properly understood, and they still require scientific elucidation.

Particular emphasis of the research presented in this thesis is placed on the settlement response of soil deposits during and after earthquakes. Over the past 40 years, design approaches have been developed to estimate earthquake-induced settlement of soil layers. These methodologies have mostly focused on '*dry*' or '*saturated*' soil conditions since they are categorised as the worst case scenarios for the compression of void space and liquefaction. On the other hand, partially saturated soils can also exist naturally or can be formed artificially in many seismically active zones. To date, the co-seismic and post-seismic response of partially saturated soils have

not been extensively studied. Consequently, significant knowledge gaps have remained in the fundamental understanding of the stress-strain-strength behaviour of partially saturated soils, in particular during the excess pore pressure generation. Furthermore, although it is crucial for design engineers to be able to adequately assess the impact of the presence of air in pore fluid on the deformation mechanisms that contribute to settlement, this still remains elusive.

This thesis describes a research programme conducted to examine important parameters and basic mechanisms that are involved in the mitigation of liquefaction effects using the air injection technique. It attempts to:

- improve the basic understanding of this particular technique,
- offer insights that can pave the way for developing effective guidelines for its use,
- describe the deformation response of saturated and partially saturated soils beneath shallow foundations and in the free field,
- highlight the uncertainties involved with academic understanding of liquefaction and the shortcomings of semi-empirical methodologies commonly used in current design practice to predict the settlement of a level ground and shallow foundation.

1.2 Research Aims and Objectives

Air injection can potentially offer an economical solution for existing buildings with shallow foundations resting on liquefiable soil deposits. It is currently used, but on a small-scale. This is probably due to the lack of a complete and deep understanding on the seismic response of partially saturated soils and partly due to the lack of effective guidelines to engineers for its use. This research intends to provide answers to the questions surrounding the impact of artificial air/gas generation within the liquefiable soil layers. The ultimate aim is to enhance the use of this particular technique in engineering design practice.

This research uses a scientific approach to the problems under consideration based on a combination of physical modelling at 1-g (shaking table and one-dimensional (1-D) vertical soil column tests) and in a geotechnical centrifuge. The main objectives of the research are to:

- examine the importance of the parameters which affect the performance of air injection technique and which are essential considerations in design practice, such as the

appropriate execution of air injection beneath existing shallow foundations and distribution of entrapped air within the soil layers,

- experimentally study the long-term durability of entrapped air in soil deposits under different simulated field conditions (main engineering concern),
- identify the most important parameters that affect the co-seismic and post-seismic behaviour of saturated and partially saturated soils,
- assess the influence of degree of saturation, confining stress, foundation bearing pressure and duration & amplitude of the earthquake motion on the seismic response of saturated and partially saturated soils and shallow foundations,
- capture the deformation mechanisms that develop beneath shallow foundations resting on the saturated and partially saturated soils,
- highlight the shortcomings of the simplified methodologies currently used for the estimation of settlement.

In this thesis, the terms '*saturated soil*' and '*partially saturated soil*' will be used for the '*unimproved sand models*' and '*sand models improved with air injection*', respectively. The research objectives presented above will be accomplished by conducting several tests on the saturated and partially saturated soils.

- The saturated soil tests (benchmark) will be used to gain an increased understanding of the behaviour of shallow foundations resting on deposits of liquefiable soils.
- The results of partially saturated soil tests will be compared to those of saturated soil tests to assess the relative success of air injection in preventing liquefaction-induced damage, with an emphasis on the excess pore pressure generation and dissipation, foundation and ground surface settlement and acceleration.
- The way that air injection functions will be investigated by means of particle image velocimetry (PIV) technique. The deformation mechanisms that contribute to ground surface and foundation settlement will be directly observed and identified.
- A simple, effective stress based methodology will be introduced to predict the settlement of partially saturated soils in the free-field. The supporting basis of this methodology and its framework will be presented.

1.3 Thesis Outline

- **Chapter 1** is an introductory chapter that highlights some of the shortcomings in research and current design practice, along with the research objectives of this thesis.

- **Chapter 2** critically reviews the previous research relevant to the study presented in this thesis. The fundamental understanding and concepts of soil liquefaction, related problems and mitigation of liquefaction-induced damage are described. This is followed by a review of soil desaturation as a way of mitigating liquefaction damage and theoretical concepts associated with this approach.

- **Chapter 3** describes the experimental apparatus and testing procedures used in this study. Details of each test are briefly outlined in chapter 3, and further details are given in appendix-A.

- **Chapter 4** examines the critical parameters for the effective application of air injection beneath existing foundations (e.g. air injection pressure). The importance of the distribution of air and the geometry of the desaturated zone for the performance of air injection is also assessed.

- **Chapter 5** explores the durability of entrapped air in soil deposits under different simulated field conditions, in an attempt to offer insights into the long-term reliability of desaturation techniques.

- **Chapter 6** examines the parameters that influence the performance of air injection as a way of counteracting liquefaction and affect the overall dynamic response of saturated and partially saturated soils beneath shallow foundations. In addition, it explores the dynamic response of level ground of saturated and partially saturated soils. The observed behaviour in saturated soils provides an understanding of the problem and highlights important parameters for the effectiveness of air injection technique in reducing the foundation settlements during liquefaction.

- **Chapter 7** identifies the critical deformation mechanisms that develop beneath shallow foundations resting on the saturated and partially saturated soils. The displacement vector fields and their contours obtained from PIV analysis are used. The observed mechanisms are compared to evaluate how air injection works and minimises the respective contributions of each deformation mechanism to the overall foundation settlements. Furthermore, it examines what mechanisms become dominant when such parameters as degree of saturation and bearing pressure change.

- **Chapter 8** discusses the shortcomings of the current state of practice methodologies used for the prediction of level ground and foundation settlement. It shows the use of a simple methodology for estimating the settlement of partially saturated soils in the free-field.

- **Chapter 9** gives a summary of the main thesis findings and conclusions. Moreover, needs for areas of future work are discussed.

Chapter 2

Literature Review

2.1 Introduction

In this chapter, the literature relevant to this thesis is presented in several sections. Early sections begin with an overview of the present scientific understanding of the seismic liquefaction phenomenon, the triggering conditions, progress and its effects on geotechnical structures. A number of remediation schemes currently available in design practice for liquefaction-induced problems are reviewed. The most important limitations of the current liquefaction mitigation methods, particularly for the existing structures are discussed briefly. Later sections of this chapter review the published literature on desaturation techniques as a liquefaction countermeasure, with an emphasis on the air injection technique. Fundamental aspects of desaturation methods and the principles assisting the liquefaction resistance of soils are discussed. It must be noted that key papers that propose interesting and valuable ideas are presented here. Further literature pertaining to the explored ideas will be given at the beginning of each chapter.

2.2 Soil Liquefaction

Saturated, cohesionless soils may undergo liquefaction during an earthquake loading, depending on such parameters as relative density (D_r), degree of saturation (S_r), effective confining stress (p') and boundary conditions that determine the pore fluid drainage.

It has been long known that dry, cohesionless soils, such as loose sands, have a tendency to contract when sheared. During an earthquake loading, air-filled voids collapse due to cyclic shear strains, and soil grains try to move into a denser state. When dry soils are saturated with

an almost incompressible pore fluid, usually water in the field, the pore fluid must move for volumetric contraction to happen during the earthquake. However, if drainage from the soils cannot occur quickly due to the rate of the loading, suggestive of globally undrained loading, excess pore pressures develop. The generation of excess pore pressures can lead to a significant reduction in effective stresses. Once the excess pore pressures build up high enough, and effective stresses drop to near zero values, liquefaction is said to have occurred. Physically, liquefaction of soils results in a loss of particle contacts between the soil grains and a significant drop of shear stiffness. Excess pore pressures dissipate once the earthquake ceases. If the soil layer is singly draining (e.g. the bedrock is impermeable), the pore fluid flows upwards during the dissipation, and the surface of the soil layers remains liquefied for a longer period of time. Geotechnical structures founded on these soil deposits are subjected to great risk of failure, such as one resultant incidence being the excessive settlement of residential buildings built on shallow foundations.

Since the 1964 Niigata earthquake, a great body of research has produced an array of definitions, criteria and frameworks for the liquefaction phenomena, and they will be outlined in the subsequent sections.

2.2.1 Definition and Mechanism of Soil Liquefaction

Earthquake-induced liquefaction became a major topic in the aftermath of the 1964 Good Friday earthquake in Alaska and Niigata earthquake in Japan. Over the years, liquefaction studies have produced an array of definitions that often contradict each other. Many of the definitions of liquefaction-related phenomena are based on the undrained response of sand to shearing. Coelho (2007) remarks that it is unfeasible to find a definition that covers all the phenomena associated with liquefaction. This section discusses only some of the available definitions and criteria.

Casagrande (1936) postulated that liquefaction is a change from an interlocked grain structure to a flow structure due to particle re-alignment that progresses through the soil. Based on load controlled drained shear box tests, he proposed the existence of a '*critical voids ratio, CVR*' that separated contractive and dilative soils. The critical voids ratio concept suggested that sands looser than *CVR* were susceptible to liquefaction and could liquefy during shear, whereas sands denser than *CVR* would be safe against this type of failure and would never liquefy. This approach, however, did not appropriately establish the influence of effective confining stress,

and assumed a constant critical voids ratio independent of confining stress. It is now generally accepted that Casagrande's original notion of critical voids ratio is incorrect. Even Arthur Casagrande himself recognised this and moved from his original view of *CVR* to the steady state concept proposed by Poulos (1981).

Seed and Lee (1966) investigated the cyclic behaviour of saturated, cohesionless soils using undrained triaxial tests. The soil samples were subjected to cyclic axial stress under a given confining stress. Based on the test results, the term '*initial liquefaction*' was introduced to describe the condition in which the excess pore pressures that gradually developed under shear, Δu, reached the initial effective stress, σ'_{vo}, for the first time. For such cases, the excess pore pressure ratio, r_u, is equal to one ($r_u = \frac{\Delta u}{\sigma'_{vo}} = 1$). Seed and Lee (1966) suggested that immediately after initial liquefaction, loose sand may develop '*full liquefaction*' where a complete loss of shear strength occurs over a large strain amplitude, and the sand flows like a dense fluid. On the other hand, after initial liquefaction, dense sand can undergo gradual soil-softening since it is able to dilate at larger strains, which reduces excess pore pressures and causes retrieving some of its strength. Arthur Casagrande (Green and Ferguson 1971) used the term '*cyclic mobility*' to describe the gradual softening of a dense, saturated sand under cyclic loading. This term was later used by Seed (1979) to describe the condition '*peak cyclic pore pressure ratio of 100% with limited strain potential*'. Ishihara (1993) specified the onset of liquefaction for different sand densities and soil types (clean sands to sands containing fines) using the definition of initial liquefaction and added the requirement for a double amplitude of axial strain at 5% within 20 cycles.

It is noted that the definition of initial liquefaction (r_u=1) is conventionally used for soils in one-directional element testing (e.g. an ordinary simple shear test), which can simulate the influence of cyclic loading in one direction only. On the other hand, actual earthquake events produce multi-directional loading, during which excessive strains can develop even for lower r_u values. The resistance of soils during multi-directional tests is consequently lower than that during one-directional tests. Based on multi-directional cyclic simple shear testing, Kammerer (2002) observed that $r_u \approx 0.65$ marks the point above which softening was intensified, and the onset of softening allowed increased strains.

In addition, unlike in the traditional laboratory experiments that involve uniform cycles of loading, actual earthquakes in the field produce irregular and non-uniform loading, in terms of both amplitude and frequency. For most earthquake events, the maximum excess pore pressure

is often reached at the largest peak ground acceleration, which usually occurs during the first few cycles of the earthquake loading. This indicates that the definition of Ishihara (1993) can be valid for the element testing, but ceases to be true for sites subjected to real earthquakes.

Kramer (1996) provided two broad categories of liquefaction phenomena: flow liquefaction and cyclic mobility. Flow liquefaction occurs under monotonic or cyclic loading when the static (driving) shear stress required for equilibrium is greater than the undrained steady state shear strength of the soil. The soil in its liquefied state is driven by the static shear stress towards a sudden flow failure. The saturated, loose cohesionless soils are very sensitive to flow liquefaction. Cyclic mobility, however, occurs when the driving shear stress is smaller than the steady state shear strength of the soil. The deformations develop incrementally, and they are driven by both dynamic and static shear stresses. Both dense and loose sands can undergo cyclic mobility. A level deposit of saturated sand, where static shear stress does not exist, can be a special case of cyclic mobility. The deformation is driven by dynamic shear stress only. Robertson et al. (1994) categorised liquefaction phenomena as flow and cyclic liquefaction (figure 2.1). They distinguished between cyclic liquefaction and cyclic mobility, depending on the driving shear stress being higher or lower compared to dynamic shear stress.

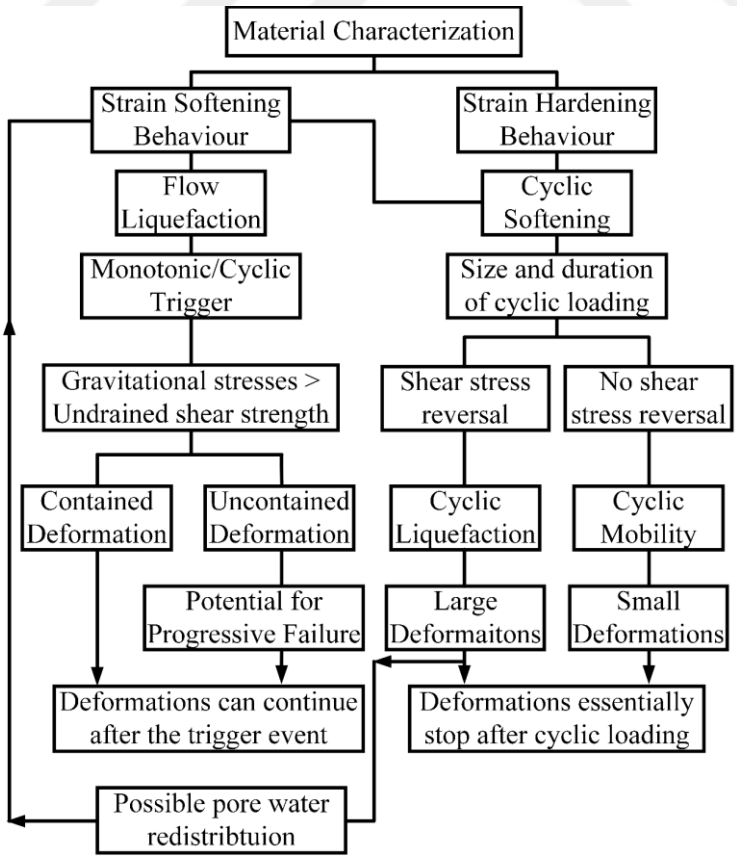

Figure 2.1– Flow chart for the assessment of liquefaction, after Robertson et al. (1994).

Schofield (1981) and later Muhunthan and Schofield (2000) had a comprehensive explanation of liquefaction. They stated that excess pore pressure rise and corresponding near zero effective stress is a necessary condition for liquefaction to happen in soil, but that the formation of cracks/fractures and presence of high hydraulic gradients are also necessary. It was reported that micro-fissures could open in saturated soil as the effective stresses, and therefore contact stresses between the particles, reduce under cyclic shear stresses. In the presence of high hydraulic gradients, this can cause liquefaction.

In this thesis, for the sake of simplicity, the initial liquefaction criterion (r_u= 1), which considers the excess pore pressures being equal to the initial vertical effective stress, is used to define liquefaction. It must be emphasised, though, that this approach has some deficiencies in defining the state of soils, as discussed below.

Firstly, the presence of shallow foundations on the ground directly affects the total stress in the underlying soil. In this case, the soil may need much higher excess pore pressures to liquefy, as discussed in section 6.2.3.3. Coelho et al. (2007), based on dynamic centrifuge experiments, showed that the free-field soil completely liquefied, whereas the soil column underneath the foundations remained unliquefied. Secondly, the build-up of excess pore pressures during the earthquake loading reduces the effective stress. The distribution of foundation-induced stresses in the soil also changes with the onset of liquefaction. The change in the stress distribution under the foundations causes the variations of total and effective stress (Ghosh and Madabhushi 2007). Hence, the effective stress recorded at any given location and any particular time of the earthquake loading must be considered for the appropriate definition of liquefaction.

2.2.2 Frameworks for Soil Liquefaction

Several theoretical frameworks have been proposed to capture the complex cyclic behaviour of saturated soils and to gain an increased understanding of the liquefaction phenomena. The '*Critical State*' framework postulates that soil elements at critical state deform continuously at constant volume and shear stress (Schofield and Wroth 1968). This state is depicted as a single line '*Critical State Line, CSL*' in q- p'- v space. The critical state is unique and independent of the initial state of a given soil. When shearing takes place slowly at the same confining stress (p'), the soil looser than CSL contracts. The soil denser than CSL dilates to reach the CSL.
The Critical State framework was applied for much of the liquefaction research in the Schofield Centre of Cambridge University (e.g. Lee (1985) and Venter (1987)). Such research led to a

simplified illustration of the critical state framework for liquefaction described by Muhunthan and Schofield (2000), as presented in figure 2.2. When a loose soil element on the '*wet side*' of the critical state is subjected to cyclic shear stresses under undrained conditions, excess pore pressures increase due to its contractive nature, causing a decrease in effective confining stress, p'. Once the stress path crosses the fracture surface, soil particles lose contact stresses, which brings about a significant loss of strength during liquefaction.

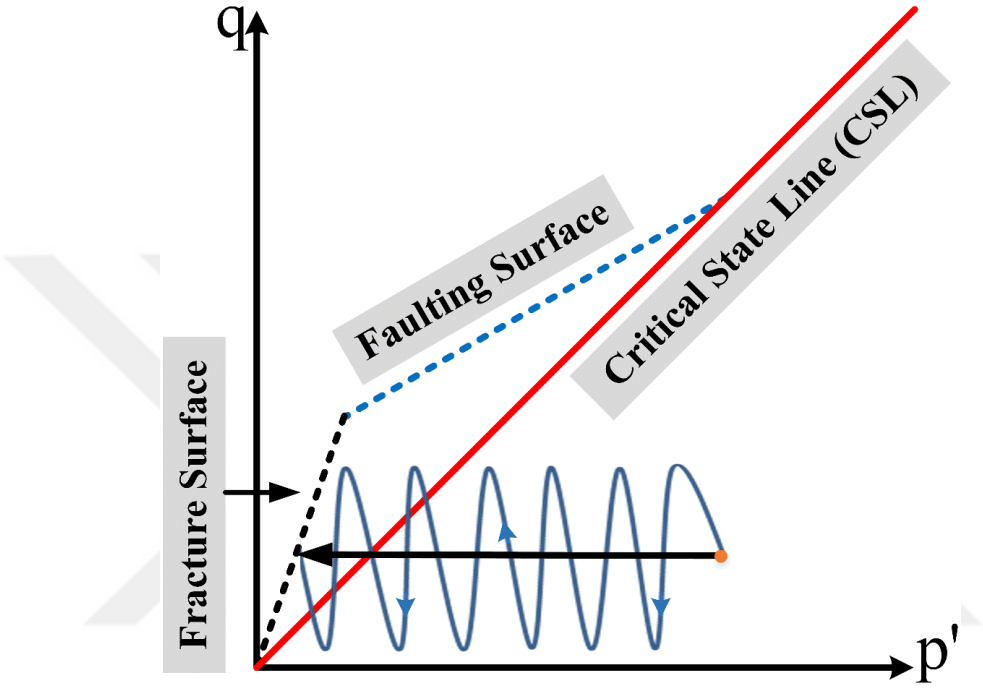

Figure 2.2– Critical State framework for soil liquefaction, after Muhunthan and Schofield (2000).

Ishihara et al. (1975) examined the behaviour of loose soils under cyclic loading and introduced a concept of the '*Phase Transformation Line*, *PTL*'. This line marks the boundary between the contractive and dilative response of soil under shear. A similar observation was made quite independently by Luong and Sidaner (1981) during their study on the undrained response of sand under cyclic loading. They named this boundary the '*Characteristic State Line, ChSL*'; above which sand exhibits dilative behaviour (*surcharacteristic region*) and below which contractive behaviour of sand is observed (*subcharacteristic region*), as seen in figure 2.3. It was shown that in q- p' space the characteristic state line could be expressed as a single line in both compression and extension side. The slope of the line on the extension side was shallower.

With these features, both phase transformation and characteristic state concepts seem to be analogous to the critical state framework. The main difference is that the stress path of the soil element must stay on the critical state line once it reaches the CSL. However, for the characteristic state concept, the soil changes behaviour (from contractile to dilatant) when its

stress path crosses the characteristic state (or phase transformation) line before reaching the failure line. This implies that it has a gentler slope than the critical state line.

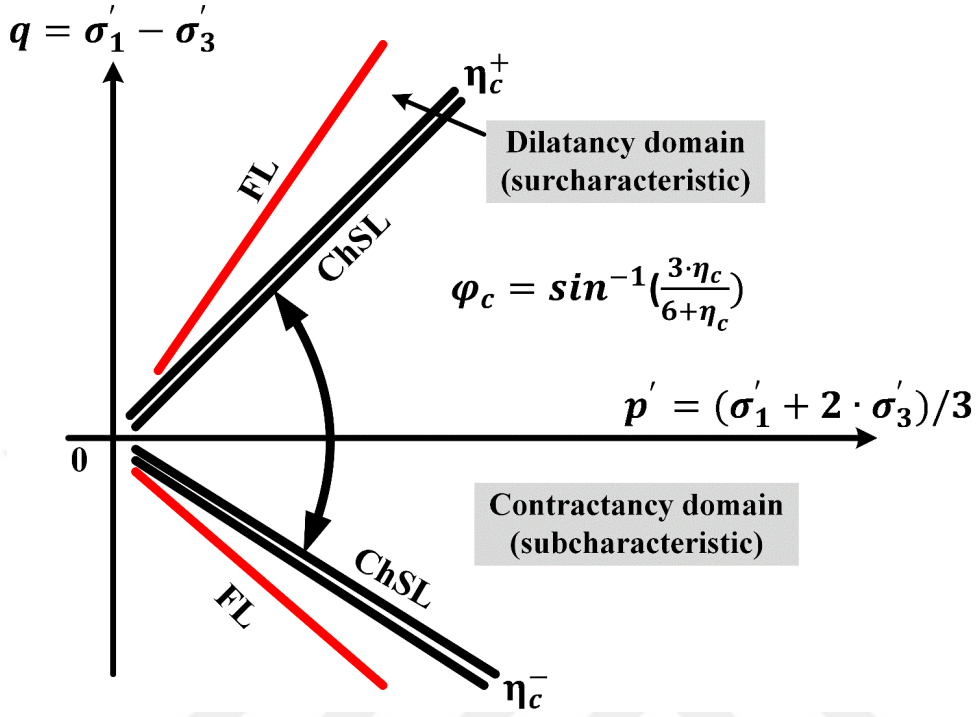

Figure 2.3– Characteristic state for saturated sands, after Luong and Sidaner (1981).

2.2.3 Undrained Behaviour of Sand under Cyclic Loading

The traditional perception of liquefaction is based on undrained element tests. In literature, the generation of excess pore pressure and soil softening process are examined extensively under cyclic loading. An extensive review of such studies is considered beyond the scope of this thesis. The study of Ishihara (1985) who examined the behaviour of loose and dense samples through undrained cyclic torsional tests is presented below as an example (figure 2.4).

Figure 2.4 shows that the qualitative behaviour of loose and dense sand was similar. For both types of sand, as excess pore pressures accumulated with each cycle and effective confining stresses dropped, the stress path of the sands moved towards a state of zero-effective stress. Once the phase transformation line was crossed, the applied shear stresses caused the dense sand to strongly dilate and regain some strength. On the other hand, the loose sand showed only little dilative behaviour on crossing the phase transformation line, and needed more strains to exhibit this behaviour. Unlike the progressive cyclic shear strain increase in the dense sand (indicating cyclic mobility), the shear strains, relatively smaller for the initial cycles, rapidly increased as significant excess pore pressures were generated, and this led to large strains in

the loose sand (indicative of full liquefaction). It is noted that dilation and associated excess pore pressure cycles at double the frequency of the applied loading were observed when the phase transformation line was crossed twice in one cycle (producing a typical butterfly pattern).

The validity of the traditional view of globally undrained liquefaction event has been challenged by recent centrifuge studies (e.g. Coelho (2007) and Adamidis (2017)). Examining liquefiable sand, it is found that the actual earthquake loading of the soil is not truly undrained. Some settlement of the soil surface occurs during an earthquake loading, indicating a partially drained event. A more in-depth discussion on this phenomenon will be given in section 6.3 while the aspects of the dynamic response of liquefiable soils are examined.

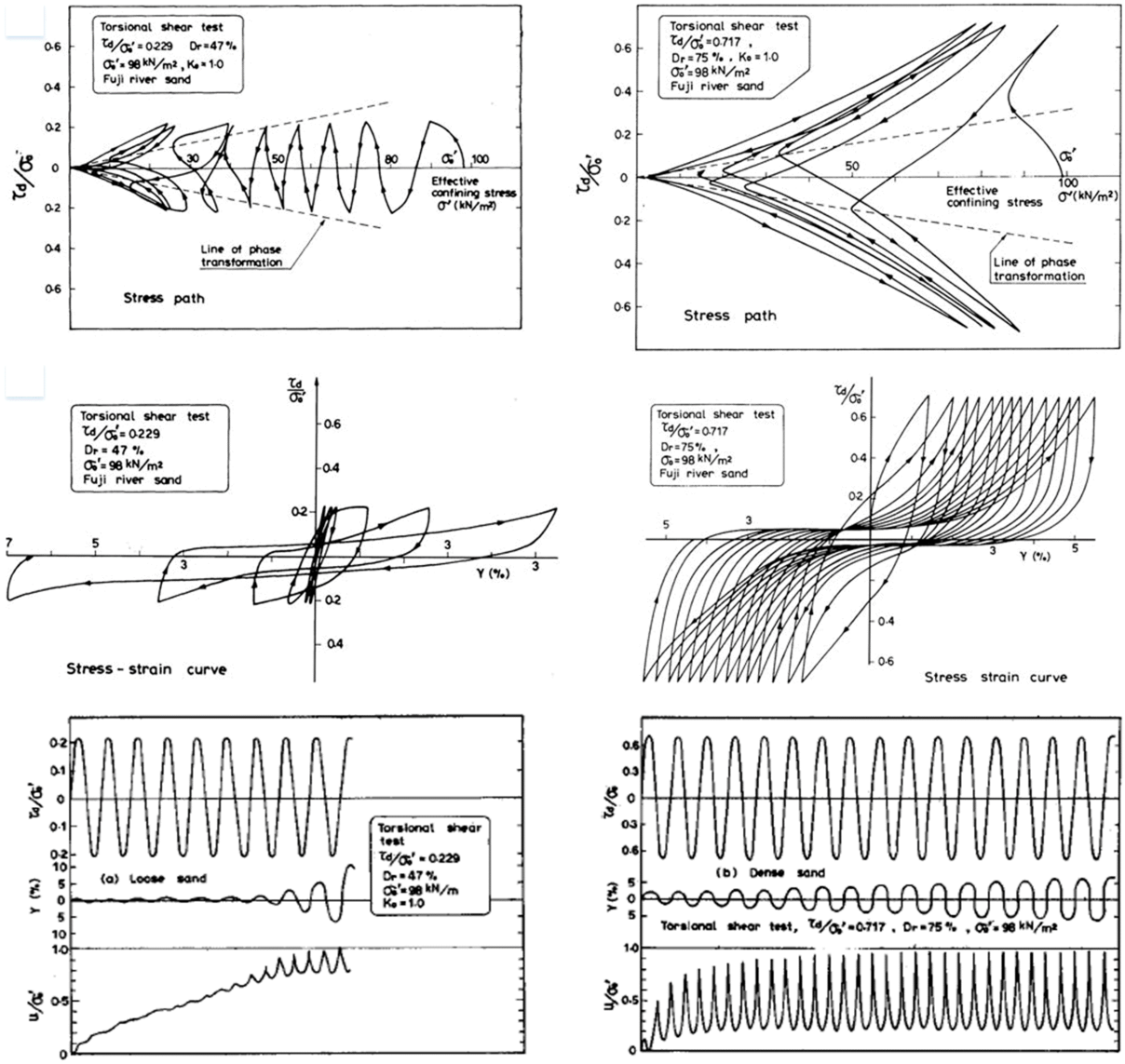

(a) Loose sand (b) Dense sand

Figure 2.4– Stress paths and stress-strain curves, after Ishihara (1985).

2.3 Design Practice for Liquefaction Hazard Evaluation

In current design practice, engineers typically follow five major steps to evaluate the potential hazards associated with earthquake- induced soil liquefaction at a site (see figure 2.5).

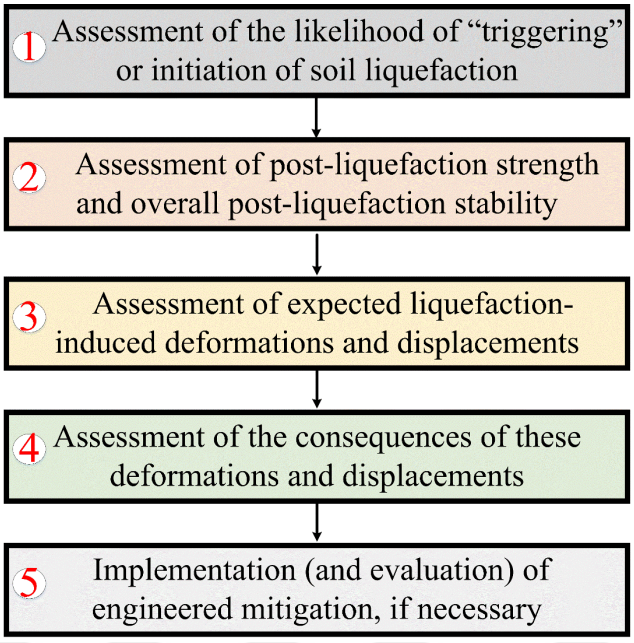

Figure 2.5– Key elements of soil liquefaction study, after Seed et al. (2003).

2.3.1 Liquefaction Susceptibility

The hazard evaluation procedure becomes meaningful only when a soil deposit at a given site is found to be potentially liquefiable. The liquefaction susceptibility of soil deposits is usually assessed based on the qualitative evaluation of certain criteria. Kramer (1996) identified three broad categories of liquefaction susceptibility: historical criteria, geological and compositional criteria (e.g. soil type) and state criteria (void ratio and effective stress).

2.3.2 Triggering (Initiation) of Liquefaction

If the soil deposit is vulnerable to earthquake-induced liquefaction, the initiation of liquefaction is quantitatively investigated. This is typically carried out through the empirical relationships based on the correlation of observed field behaviour with in situ '*index*' tests, such as Standard Penetration Test (SPT) or Cone Penetration Test (CPT). Many approaches are available to engineers for the quantitative evaluation, such as the semi-empirical '*simplified procedure*' (Seed and Idriss 1971) and cyclic strain approach (Dobry et al. 1982). Nevertheless, in current

design practice, the most common, widely used, methods are based on the simplified procedure. During the following decades, in the light of new findings from the case studies and element testing efforts, some updates and modifications have been made to the original simplified procedure to incorporate the recent findings (e.g. Idriss and Boulanger 2006). Fundamental aspects of the simplified procedure are outlined below.

2.3.2.1 Simplified Procedure

The simplified procedure relates the earthquake-induced loading, defined as the cyclic stress ratio (*CSR*), to the cyclic stress ratio required to cause liquefaction of a soil deposit (*CRR*). The comparison of the computed *CSR* and *CRR* allows for the estimation of the safety factor against liquefaction.

The cyclic stress ratio, *CSR*, at a depth *z* is calculated considering an equivalent uniform cyclic shear stress ratio, $\frac{\tau_{ave}}{\sigma'_{vo}}$, for an earthquake of magnitude of 7.5 ($M = 7.5$):

$$CSR = \frac{\tau_{ave}}{\sigma'_{vo}} = 0.65 \cdot \left(\frac{a_{max}}{g}\right) \cdot \left(\frac{\sigma_{vo}}{\sigma'_{vo}}\right) \cdot r_d \tag{2.1}$$

where a_{max}, g, σ_{vo} and σ'_{vo} are the peak ground surface acceleration, gravitational acceleration and initial total and effective stress, respectively. The stress reduction coefficient, r_d, considers the flexibility of the soil column and is used for the calculation of acceleration at the desired depth. An array of methods were established for the assessment of r_d values (e.g. Idriss and Boulanger (2006) and Cetin et al. (2004)).

The equivalent uniform cyclic shear stress cycles are described by three parameters: amplitude, frequency and number of cycles.

The loading applied to an element of in situ soil during an actual earthquake is erratic and non-uniform. Due to the sophistication of simulating realistic earthquake loading in the laboratory, the concept of equivalent number of uniform stress cycles proposed by Seed and Idriss (1971) is widely used in current design practice. In this approach, the cyclic shear stress ratio is often assumed to be some percentage (usually 65%) of the peak stress (acceleration) of the design earthquake. The peak cyclic stress ratio is converted to an equivalent cyclic stress ratio, which is assumed to be a representative of the remaining cycles of the applied loading. It must be noted, though, that while uniform equivalent loading can be applicable to liquefaction based studies in the laboratory (e.g. cyclic triaxial), it may be impractical for real earthquake events that apply non-uniform loadings, as discussed in section 2.2.1.

In current design practice, the number of loading cycles is deemed important and computed based on the magnitude of the anticipated earthquake, whereas the impact of the frequency of the earthquake loading is frequently disregarded. The frequency content of stress cycles is often assumed to have an insignificant effect on liquefaction potential within the range of frequencies in engineering practice (Liu et al. 2001). With regard to this assumption, due to the complexities of using realistic loading frequencies in element tests for liquefaction analysis, the frequency content effects on cyclic resistance are commonly neglected for the sake of accuracy in cyclic test control and measurements. However, this simplification may be inaccurate for liquefiable deposits under earthquake loading in the field, particularly when the natural frequency of the liquefiable ground is higher than the predominant frequency of the earthquake motion.

The cyclic resistance ratio, *CRR*, for sands is commonly computed for an earthquake magnitude of 7.5. The simplified procedure was developed for low static shear stress and low overburden pressures only. Therefore, correction factors are applied to extrapolate the simplified method to varying high overburden stresses (K_σ) and initial static shear stresses (K_α).

2.3.3 Consequences of Liquefaction

If the initiation of liquefaction at a site is a potentially serious risk, engineers need to assess whether the consequences of the liquefaction are tolerable. Earthquake-induced liquefaction of soil deposits has severe and diverse effects on the site and built environment. The detrimental impact can be observed in the form of settlement in the free-field (Liu and Dobry 1997), sand boils (Brennan and Madabhushi 2005), lateral spreading (Youd et al. 2002) and uplift of the buried structures (Chian and Madabhushi 2012).

2.3.3.1 Liquefaction Effects on Shallow Foundations

Residential buildings with shallow foundations are the most common structures around the world. Over the years, in the aftermath of the strong or moderate earthquakes, many buildings resting on liquefiable ground have suffered significant damage. The liquefaction of soil has caused complete foundation bearing failure, leaving buildings excessively tilted or sunk (see figure 2.6). Cyclic softening of the foundation soil has also led to partial bearing failure or limited punching of foundations into the ground. Prime examples of extensive liquefaction-induced damage to buildings on shallow foundations are presented by the 1999 Kocaeli, Turkey earthquake (Sancio et al. 2002) and the 2010 Maule, Chile earthquake (Bertalot et al. 2013).

In the event of Kocaeli earthquake, many buildings in the city of Adapazari sunk into the ground with almost no tilting and heaving of the surrounding ground (figure 2.6a), laterally displaced over softened ground (figure 2.6b), settled with significant tilting due to the non-uniform vertical deformation (figure 2.6c) and suffered bearing capacity failure (figure 2.6d).

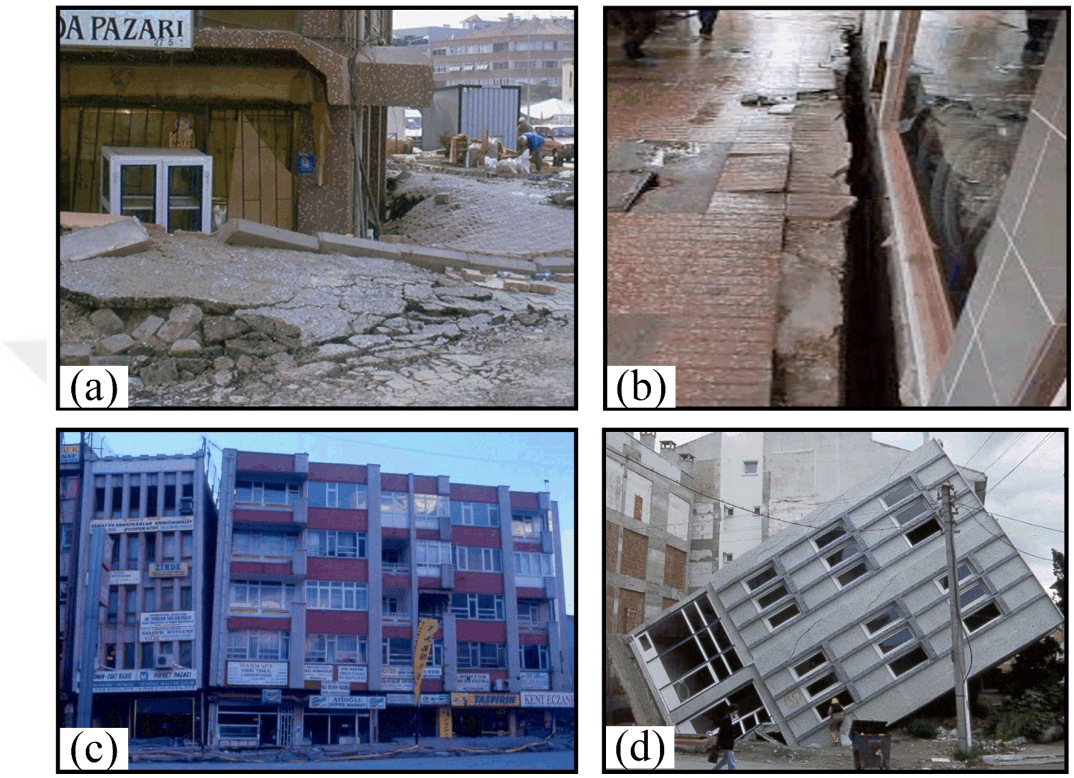

Figure 2.6– Liquefaction-induced damage in Adapazari, courtesy of NISEE, University of California, Berkeley.

2.3.4 Prediction of Settlement

If the overall stability of a site or structure is unacceptable, the expected liquefaction-induced deformations and their detrimental effects are evaluated. Structures on shallow foundations often respond with excessive settlement during an earthquake-induced liquefaction event, as discussed above. Settlement receives the most attention due to its harmful effects on structures.

The current state of practice for the evaluation of liquefaction-induced settlements of saturated soil deposits relies on the procedures developed based on the assumption of globally undrained liquefaction event. These methodologies often predict the one-dimensional, post-earthquake, free-field settlement of saturated soil deposits. Figure 2.7 shows an array of semi-empirical models, typically presented in a chart form. Using these methods, the expected volumetric strains are often related to the demand (*CSR*) and the capacity (*SPT* blow counts, N_1). It is a common practice to correct the *CSR* and N_1 values for the accuracy of the predictions.

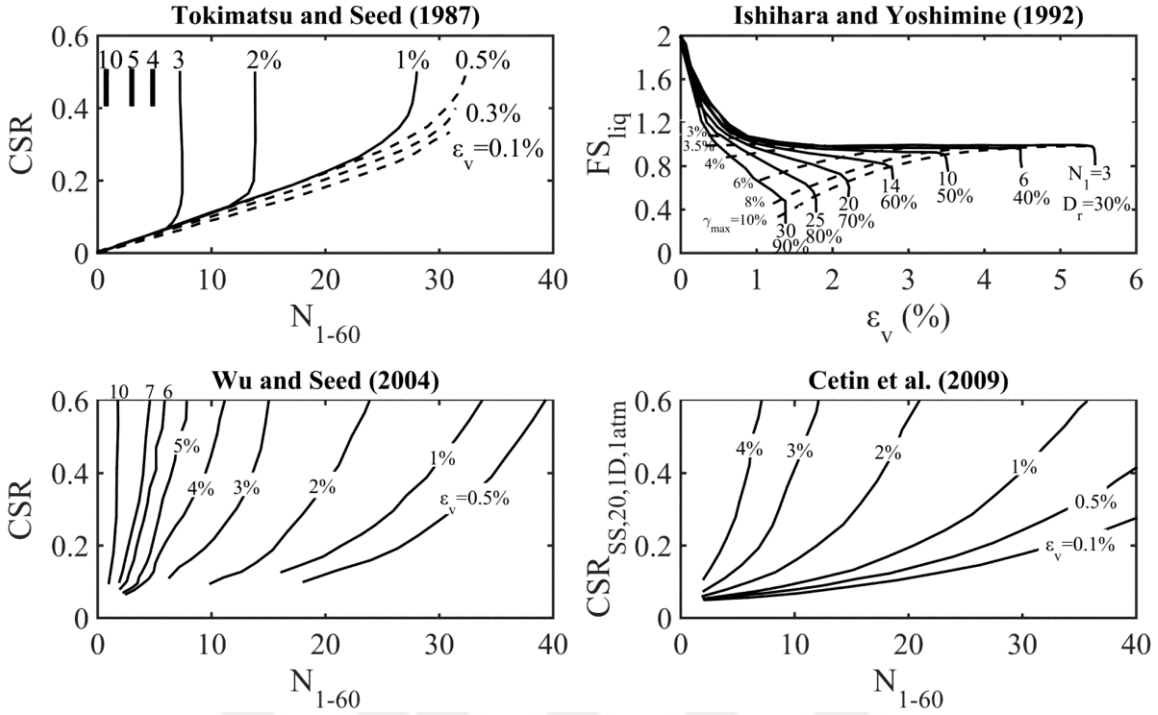

Figure 2.7– Proposed charts for the prediction of post-earthquake volumetric strains (reproduced).

In current design practice, liquefaction-induced settlement of structures on shallow foundations is also frequently estimated using the semi-empirical, free-field methodologies. It is commonly assumed that the structures will settle along with the ground on which they rest. However, this approach is inaccurate. Applying free-field procedures to soils underneath the foundation is not correct since they do not incorporate important conditions and parameters that can potentially affect the liquefaction and foundation behaviour (Rollins and Seed 1990). More recent studies show that in order to design and implement an effective site-specific liquefaction remediation technique, potential consequences of liquefaction and building performance objectives should be thoroughly understood, *a priori*. Dashti et al. (2010) indicated that potential consequences of liquefaction (e.g. settlement) strongly depend on the characteristics of the earthquake (e.g. intensity and duration), the properties of a liquefiable soil layer (e.g. relative density, hydraulic conductivity and depth of liquefiable layer) and features of the structure in question (e.g. foundation width, bearing pressure, static shear stress ratio and slenderness of the structure). In current design practice, the foundation width and depth of the liquefiable layer have received the most attention. Researchers often normalise the foundation settlement with the depth of the liquefiable layer (e.g. Liu and Dobry 1997). Based on an extensive centrifuge study, Dashti et al. (2010), Bertalot et al. (2013) and some other researchers have challenged the validity of this approach for thinner liquefiable soil layers. Additional background information relevant to this aspect will be given in chapter 8.

2.3.5 Traditional Liquefaction Mitigation Techniques

Engineered mitigation of an unacceptable liquefaction hazard is needed when satisfactory performance of a site and structure cannot be reliably assured (e.g. the expected liquefaction-induced deformations and displacements exceed the safety and serviceability limits of the structure). Mitigation schemes are mainly proposed to either (1) strengthen the structure to withstand the consequences of liquefaction or (2) eliminate or minimise the risks and effects of liquefaction through ground improvement measures. Over the years, research on this area has produced an increasing suite of engineering options, and a brief list of the major mitigation techniques is given in table 2.1. No attempt is made here to provide a comprehensive discussion of all the available improvement methods as it is not directly relevant to the scope of this study.

Liquefaction mitigation techniques can be broadly categorised as those to:

- expedite the drainage and dissipation of excess pore water pressures,
- increase the liquefaction resistance of soil physically or chemically,
- limit the cyclic shear strains, such as introducing stiff elements into the soil.

Table 2.1 – A list of traditional methods of liquefaction mitigation, adapted from Seed et al. (2003).

General Category	Mitigation Methods	Notes
I. Excavation and/ or compaction	(a) Excavation and disposal of liquefiable soils (b) Excavation and recompaction (c) Compaction (for new fill)	
II. In situ ground densification	(a) Compaction with vibratory probes (e.g.: Vibroflotation, Terraprobe, etc.) (b) Dynamic consolidation (Heavy tamping) (c) Compaction piles (d) Deep densification by blasting (e) Compaction grouting	Can be coupled with installation of gravel columns Can also provide reinforcement
III. Selected other types of ground treatment	(a) Permeation grouting (b) Jet grouting (c) Deep mixing (d) Drains (deep grains; sand grains; pre-fabricated strip drains) (e) Surcharge pre-loading (f) Structural fills	Many drain installation process also provide in situ densification
IV. Berms, dikes, sea walls, and other edge containment structures/systems	(a) Structures and/or earth structures built to provide edge containment and thus to prevent large lateral spreading	
V. Deep foundations	(a) Piles (installed by driving or vibration) (b) Piers (installed by drilling or excavation)	Can also provide ground densification
VI. Reinforced shallow foundations	(a) Grade beams (b) Reinforced mat (c) Well-reinforced and/or post-tensioned mat (d) 'Rigid' raft	

Seed et al. (2003) stated that the selection and implementation of liquefaction mitigation techniques requires a thorough evaluation of critical parameters that include (a) applicability, (b) effectiveness, (c) verifiability of the reliability of the mitigation achieved, (d) cost and (e) other sources of concern (e.g. environmental issues). The applicability and effectiveness of liquefaction remediation methods can be assessed based on field and experimental studies. Mitchell et al. (1995) provided a comprehensive discussion of the performance of various remediation methods employed at different sites: gravel drains, deep soil mixing, compaction methods (e.g. vibrocompaction and compaction piles) and grouting methods (e.g. compaction and chemical grouting). Improved and unimproved sites were examined following moderate to strong-sized earthquakes. They reported that improved sites were observed to perform better compared with adjacent unimproved sites. Structures on the remediated sites suffered much smaller liquefaction-induced settlement, lateral displacement and damage. Similarly, Soga (1998) documented that the sites improved with vibro-compaction or sand compaction piles experienced considerably less deformation than the adjacent unimproved sites. Buildings with shallow foundations on remediated sites were affected to a lesser degree by liquefaction. Besides the case studies, several experimental research programmes have been undertaken to garner scientific-based knowledge on the different liquefaction mitigation measures, such as the use of vertical drains (Brennan and Madabhushi 2002), stone columns (Adalier et al. 2003), inclined micro-piles, geomembrane and rigid containment walls (Mitrani 2006) and densification (Coelho et al. 2007). The field and experimental evidence indicate that liquefaction mitigation methods can be effective at reducing the risk and potential effects of liquefaction when performed correctly.

2.3.6 Limitations of Current Design Practice

The design of liquefaction mitigation measures is currently carried out based on an evaluation of the cost-benefit ratio and seismic performance. The detrimental effects that they might have on surrounding structures, ground motion propagation and environment are usually not assessed properly. Another major limitation of current design practice is the lack of a proper understanding of the mechanisms by which mitigation measures affect the performance of ground and foundation. The design decisions are often made based on case studies, rather than scientific concepts.

Despite a large range of available ground improvement techniques, the majority of traditional liquefaction mitigation methods are not easy to use beneath or adjacent to existing structures

(Gallagher et al. 2007). Moreover, techniques applicable to existing structures are often financially demanding and not easily accessible. They are, therefore, employed solely for the important and large projects. Cooke and Mitchell (1999) suggested that compaction techniques or inserting stone columns can cause settlement and vibration of buildings, which can be permanently damaging to the superstructure during retrofitting. Dynamic loadings in the neighbourhood, which are crucial in a dense urban environment, can be another issue for the densification of the ground. The use of grouting can be harmful to the environment although it can allow for installation with minimal vibration and level of noise. Due to environmental concerns, many chemical grouts are under the scrutiny of public opinion (Karol 2003). Lowering the groundwater table (e.g. by means of drainage tunnels or deep wells) may cause land subsidence, which can render its application for the built-environment less practical.

In recent years, considering the limitations of the traditional methods described above and with the availability of new materials, relatively new alternative concepts have become the focus of a concentrated research effort. This has promoted the development of a new research area called non-disruptive soil improvement methods. The non-disruptive methods of liquefaction mitigation can be examined in three major groups: passive site remediation, bio-geotechnical (or bio-mediated) systems and soil desaturation (or induced partial saturation). The principle of passive site remediation concept is based on the slow injection of a stabilising material (colloidal silica or bentonite grout) beneath or around the foundations of existing structures on liquefiable soils (Gallagher and Mitchell 2002). The interdisciplinary research between microbiology, geochemistry and civil engineering has highlighted the potential use of biological processes to improve the soil properties and offered sustainable, cost-effective solutions for the mitigation of liquefaction (DeJong et al. 2010). The ability of microbial-induced calcite precipitation (MICP) methods to mitigate the liquefaction effects is verified through experimental studies. Multiple microbial processes that enhance the liquefaction resistance of soil are identified for MICP, such as urea hydrolysis that induces cementation (Montoya et al. 2013) and denitrification that desaturates soil (He et al. 2013). Although these alternative methods show promise as a way of mitigating liquefaction risk, they are still quite new. There is a pressing need for further investigation and development to clarify the doubtful aspects of these methods and gain a full understanding of their seismic performance. Only in that case, can they be reliably implemented in practice. In this thesis, the desaturation of soil through air injection technique has been chosen for study. An overview of this method is given in the following sections.

2.4 Desaturation of Soil as a Liquefaction Treatment Method

2.4.1 Historical Review of Soil Desaturation Methods

Published studies based on cyclic element testing often report that the liquefaction resistance of soils strongly depends on degree of saturation, S_r. Some of the data available in the literature was collected and presented in figure 2.8. In these papers, liquefaction resistance was defined by the cyclic stress ratio (CSR) required to cause liquefaction at a certain number of cycles, N_{liq}. They considered the liquefaction criteria based on the soil samples reaching 5% double amplitude (DA) of axial strain under constant cyclic stress condition.

It is clear in figure 2.8 that the cyclic liquefaction resistance of soils increases significantly as S_r reduces. For the same cyclic stress ratio, the number of cycles to reach liquefaction increases with decreasing degree of saturation.

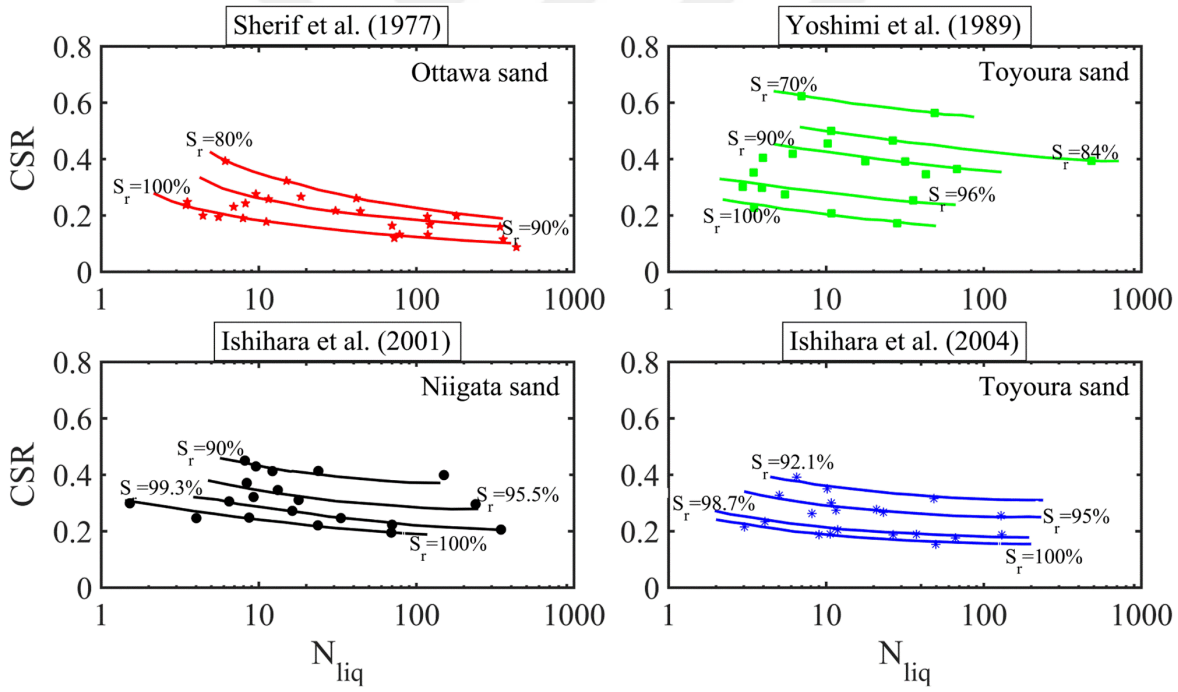

Figure 2.8– Influence of degree of saturation on the liquefaction resistance of soils.

Although the beneficial effects that reducing S_r has on the liquefaction resistance of soils have been documented since the early days of liquefaction studies, adequate attention has not been paid to the use of this concept in the treatment of earthquake-induced liquefaction. In recent years, a few researchers have sought to benefit from this feature of soils and attempted to explore the technical feasibility of ground remediation techniques that can assist in reducing S_r of soils through the generation of air/gas bubbles. The most popular air/gas generation

techniques are electrolysis (Yegian et al. 2007), drainage-recharge of pore fluid (Yegian et al. 2007), air injection (Okamura et al. 2011), use of chemical compound such as sodium perborate (Eseller-Bayat et al. 2013) and utilising denitrifying bacteria-biogas (He et al. 2013). These techniques can be implemented at new sites as well as beneath existing structures. Of the methods proposed, air injection may be deemed the most appropriate to use for existing buildings with shallow foundations. This can be mainly ascribed to its cost-effectiveness, eco-friendliness and practicality. As the material used for this method is an inexpensive material (air), the main concern is just the cost of the installation itself, bringing down the total cost of the geotechnical construction (Okamura and Tomida 2015). Moreover, it is a trouble-free alternative to the soil improvement methods that use synthetic man-made materials and chemicals (e.g. epoxy and cement), reducing the environmental impact.

2.4.2 Air Injection as a Liquefaction Countermeasure

Air injection technique relies on the artificial injection of air into the saturated, liquefiable soil deposit without causing significant hydro-fracture. The pressurised air is pumped into the ground, and small-sized air bubbles are trapped between the voids. This potentially reduces the degree of saturation of soil deposit. A schematic illustration of the air injection technique employed beneath a shallow foundation of an existing building on site is shown in figure 2.9.

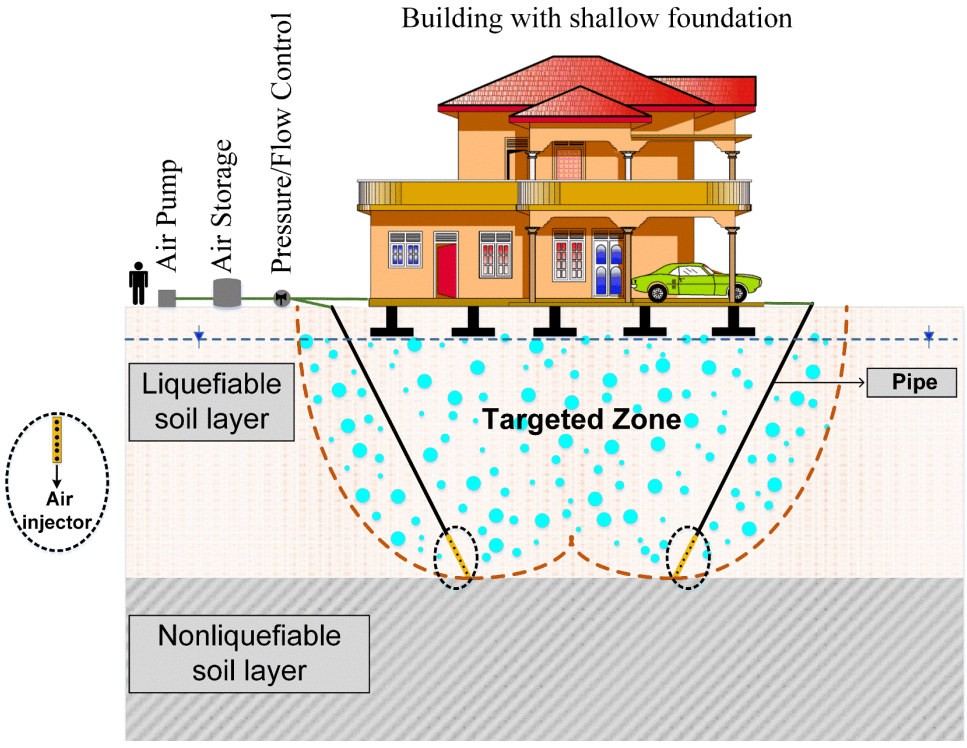

Figure 2.9– Schematic illustration of the in situ air injection technique.

In one case study, Okamura et al. (2003) observed an indirect form of in situ desaturation that happened during a sand compaction pile (SCP) application. They postulated that this was caused by the significant quantities of air that expelled as the air was ejected from the tip of casing pipe. After several years, Okamura et al. (2006) obtained high quality undisturbed frozen samples from six different sites where the ground had been previously improved with SCP. Inspection of these samples indicated that degrees of saturation of soils were just slightly higher than those measured shortly after the SCP installation. They concluded that air bubbles injected in the improved soil can remain entrapped for a long time, at least 26 years.
In this thesis, the durability of air bubbles in the partially saturated soil was investigated experimentally and will be discussed in chapter 5.

In addition to the long-term durability of air in soil, the applicability and effectiveness of air injection to desaturate ground in the free field was investigated by Okamura et al. (2011) conducting an in situ air injection test. The test results suggested that air injection can be used effectively in the field to desaturate the ground and enhance the liquefaction resistance of soil.

In fact, there is a paucity of research directed towards the air injection technique. Existing studies reviewed here have assisted in establishing some of the important parameters for this method. Nevertheless, more research is needed to gain a better understanding and provide some design recommendations, specifically for its application beneath the foundation of existing buildings. It is noted that the emphasis in this thesis is on the air injection technique. However, the conclusions drawn can be valid for circumstances where the soil improvement is accomplished from the desaturation of the ground, irrespective of the technique employed.

2.5 Saturation in Soils

The terminologies, often used to describe the conditions of natural soil deposits, are '*fully or nearly saturated*', '*unsaturated*', '*partially saturated*' and '*gassy*' (Tsukamoto et al. 2014). The distinction between such conditions can be made as shown in figure 2.10. The term '*gassy*' is used for the marine deposits below a groundwater table, and they can form as a consequence of biological activities (Mitchell and Santamarina 2005). In geotechnical engineering, soils encountered under shallow foundations are often unsaturated (vadose zone) or saturated. '*Unsaturated*' soils can be found above the current or historic-high groundwater table, and the pores are filled with air and meniscus water. Pore water pressures are usually negative in these

soils due to capillary suction. When the soil layers are below the groundwater table, they are frequently deemed '*fully saturated*' with water. In this case, almost all pore spaces are filled with water, and pore water pressures are positive relative to the atmospheric pressure. In addition, '*partially saturated*' soil layers below the groundwater table can also exist naturally or can be formed artificially. Partially saturated soils obviously have lower S_r than saturated soils owing to the existence of air bubbles trapped within the pore fluid.

It is worth noting, though, that there is a difference between unsaturated soils with a vadose zone above the groundwater table due to the capillarity and partially saturated soils below the groundwater table with entrapped air bubbles. Studies on the unsaturated soil behaviour often use the term '*partially saturated*' to describe the soil condition above the groundwater table. The difference between them is believed to be intangible and due to semantics. However, this research considers the definition of Tsukamoto et al. (2014), and the term '*partial saturation'* is interpreted to refer to the condition where air exists below the groundwater table as bubbles surrounded by the pore fluid (e.g. occluded air).

It can be seen in figure 2.10 that air in soils can be found in a continuous or occluded form. Air usually takes the continuous form well above the groundwater table. The critical S_r level below which the air phase generally becomes continuous is around 80% (Fredlund and Rahardjo 1993). The continuous air phase in the soil structure decreases with increasing soil depth and closer to the groundwater table. Occluded air bubbles become predominant when the air entry value, *AEV*, of a given soil is reached.

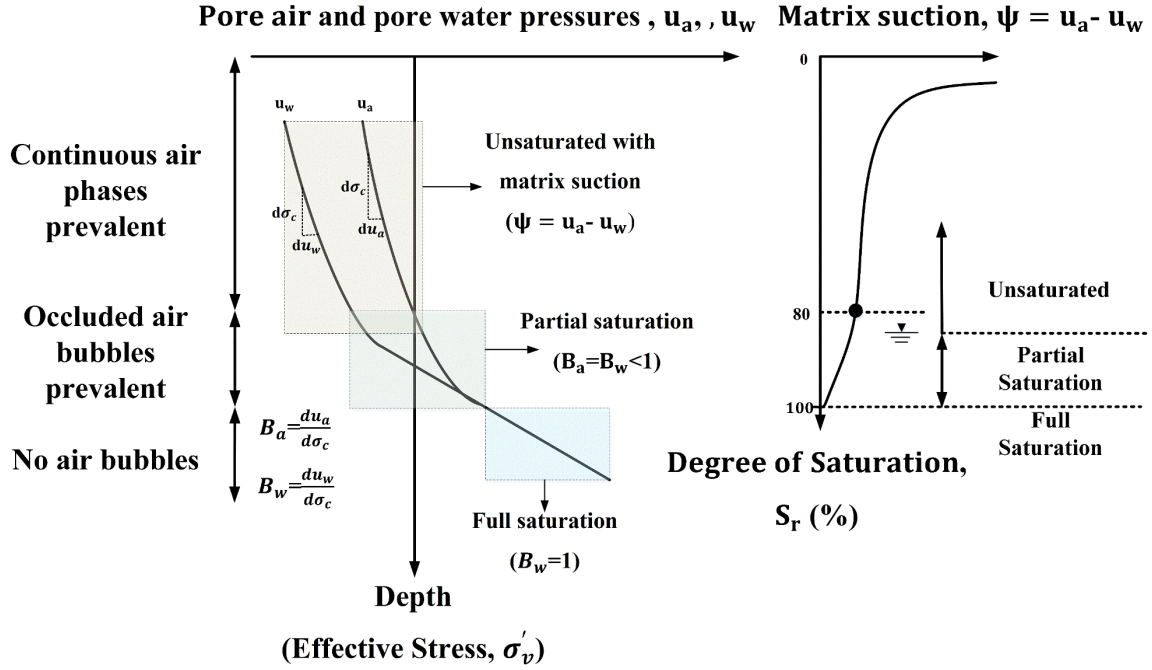

Figure 2.10– Schematic of fully, partially and unsaturated soil zones, adapted from Tsukamoto et al. (2014).

2.6 Shear Strength and Liquefaction Resistance of Soils

In conventional partially saturated soil mechanics, effective stresses and hence strength of soils increase due to the matric suction, ψ, effect (Bishop 1959). Matric suction forms in soil layers owing to the surface tension at the pore-air and pore-water interface within soil structures. The interaction of surface tension with soil structures enhances the shear resistance and strength of soils (to be discussed further in section 2.6.1).

For liquefiable soil deposits with a high fines content (e.g. sands with non-plastic silts), the matric suction can have a significant impact on the effective stresses. For many liquefiable soil deposits with low fines content (e.g. clean sands), the matric suction can, however, only be important in the shallow soil layers. The contribution of matric suction reduces with increasing soil depth and becomes negligible compared to the large effective stresses at a depth of practical concern (see figure 2.10). In this case, the liquefaction resistance of soils is primarily controlled by the compressibility of the pore fluid (Okamura and Soga 2006). Air bubbles in the soil pores decrease the bulk modulus and increase the compressibility of pore fluid that is the air-water mixture. During an earthquake loading, air bubbles contract (shrink), which subsequently assists in reducing or preventing the build-up of excess pore pressures and in increasing the liquefaction resistance of soil deposits (to be explained in more detail in the ensuing sections).

2.6.1 Effect of Matric Suction on Effective Stress

Inter-particle stresses are of importance for the mechanical and hydraulic behaviour of soils. The effective stress, σ', of Terzaghi (1943) is commonly used to identify the strength and deformation response of dry and saturated soils that have the two phases. The definition of the effective stress is unique for these soils. However, partially saturated soils have three phases, and there is no unique effective stress state defined for them. Effective stresses of these soils can be calculated using different relationships and concepts that consider the matric suction, ψ, and degree of saturation, S_r. Bishop (1959) proposed a relationship (equation 2.2) to define the effective stresses for the partially saturated soils.

$$\sigma' = \sigma - u_a + \chi \cdot (u_a - u_w) \tag{2.2}$$

where σ is the total stress, u_a is the pore air pressure, u_w is the pore fluid pressure, $(\sigma - u_a)$ is the net normal stress, χ is the effective stress parameter, and $(u_a - u_w)$ is the matric suction.

Building upon the concept of the single state variable (Bishop 1959), a concept of Suction Stress Characteristic Curve (SSCC) was proposed to define the effective stresses of partially saturated soils. Lu et al. (2010) suggested the use of soil-water retention curve (SWRC) to compute the effective stresses for these soil deposits (see equation 2.3). It was shown that the suction stress, σ_s, is a function of matric suction. For soils with high N_{vG} values (typically greater than 1.5), as S_r reduces from full saturation, the suction stress reaches its highest value at an intermediate S_r and decreases back to zero for lower S_r values.

$$\sigma' = (\sigma - u_a) + \sigma_s = (\sigma - u_a) + \frac{u_a - u_w}{\{1+[\alpha_{vG}\cdot(u_a-u_w)]^{N_{vG}}\}^{(N_{vG}-1)/N_{vG}}} \tag{2.3}$$

where α_{vG} and N_{vG} are the fitting parameters for the van Genuchten (1980) SWRC.

Lins et al. (2009) studied the SWRC of clean Hostun sand by conducting a series of steady state and transient state tests. Using the published test data, variation of the matric suction with degree of saturation is replotted for a loose deposit of Hostun sand in figure 2.11.

For this type of sand, the suction value at the residual degree of saturation is 2.8 kPa, and the value of N_{vG} is 7.825. Using the van Genuchten SWRC fitting parameters, variation of the suction stress with degree of saturation is also depicted in figure 2.11.

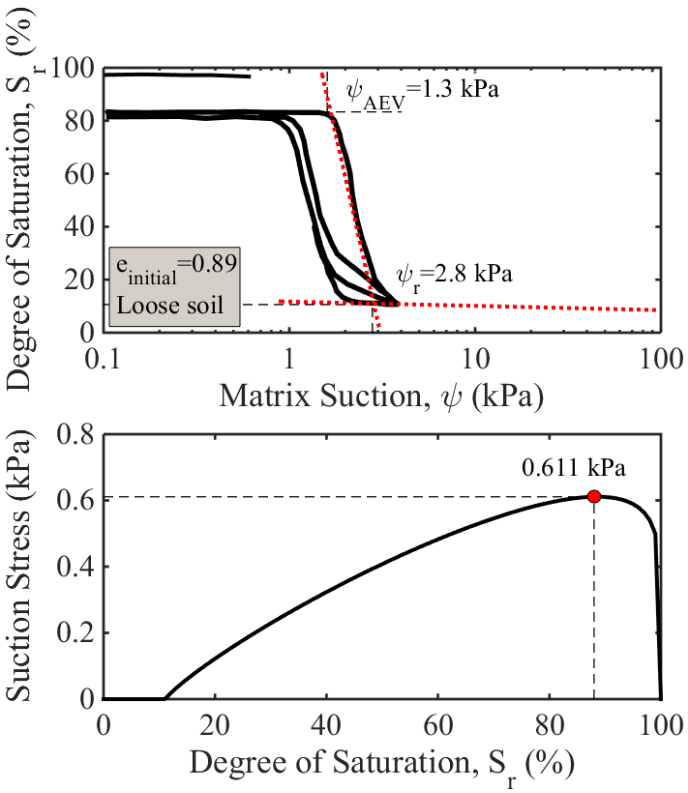

Figure 2.11– SWRC and suction stress for a loose Hostun sand deposit.

It is evident that the suction stress increases with decreasing S_r and reaches its maximum value at S_r of 88%. The peak suction stress at this saturation level is however 0.611 kPa only. This indicates that the influence of matric suction on effective stresses is minor for this type of sand. Hence, for a liquefiable deposit of Hostun sand, matric suction effect on effective stresses can be negligible in comparison with the large effective stresses at a depth of practical concern.

2.6.1.1 Effect of Surface Tension on Matric Suction

Fredlund and Rahardjo (1993) argued that for partially saturated soils with high S_r values, air often exists in the form of occluded bubbles. The diameters of the bubbles become generally smaller or the same size as the soil particles. In this condition, pore-air and pore-water ought to have virtually equal pressures if the surface tension between air and water is neglected. Similarly, Houlsby (1997) claimed that in the occluded air bubble state, the surface tension can be ignored as the relative velocity of the air-water interface and the soil solid is small.

A simple analysis regarding the effect of surface tension on matric suction is given here. The relationship between matric suction ($\psi = u_a - u_w$) and surface tension (T_s) is given as:

$$u_a - u_w = \frac{2T_s}{R_s} \tag{2.4}$$

where R_s is the radius of the curvature.

If the radius of the curvature is assumed to be roughly equal to the half of the average particle size of the soil (D_{50}), the following equation is produced:

$$u_a - u_w = \frac{4T_s}{D_{50}} \tag{2.5}$$

The D_{50} value for Hostun sand is 0.480 mm (see table 3.4). If the surface tension of water at a temperature of 20 ℃ is taken to be 0.07286 N/m, the matric suction value calculated based on equation 2.5 will be 0.607 kPa.

2.6.2 Theoretical Effect of Air Injection on Pore Fluid Compressibility

The influence of entrapped air bubbles on the pore fluid compressibility is shown theoretically. A schematic representation of a partially saturated soil element is shown in figure 2.12. A soil mass with a pore fluid (typically water) and occluded air bubbles is under an initial effective stress of σ'_{v0}. The occluded bubbles are in equilibrium with the surrounding pore fluid at the

similar pressure. When an external pressure (Δp) is applied, air and pore fluid pressure will experience the same excess pressure (Δp). Under undrained conditions, the volume change due to the applied pressure can be empirically related to the change in air and pore fluid pressure separately (Fredlund and Rahardjo 1993). This can be quantified by the compressibility or its inverse bulk modulus (K). For the pore pressure change (Δp), the volumetric strains of water (ε_w) and air (ε_a) can be defined as:

$$\varepsilon_w = \frac{\Delta p}{K_w} \tag{2.6}$$

$$\varepsilon_a = \frac{\Delta p}{K_a} \tag{2.7}$$

Introducing the Boyle's law, equation 2.7 can be rewritten as follows:

$$\varepsilon_a = \frac{\Delta p}{K_a} = \frac{\Delta p}{P_0 + \Delta p} \tag{2.8}$$

The volumetric strains of the pore fluid (air-water mixture), ε_f, can be given as follows:

$$\varepsilon_f = \frac{\Delta p}{K_f} = [(1 - S_r)\,\varepsilon_a + S_r\,\varepsilon_w] = \Delta p\,[\frac{1 - S_r}{K_a} + \frac{S_r}{K_w}] \tag{2.9}$$

where P_0 is the absolute hydrostatic pressure, S_r is the degree of saturation of soil mass and K_a, K_w and K_f are the bulk modulus of the pore-air, pore-water and pore-fluid, respectively. Okamura and Soga (2006) suggested that the second term in equation 2.9, $\frac{S_r}{K_w}$, can be neglected since the bulk modulus of water is substantially larger than that of air. Air dissolution into water is also not taken into account. Assuming that the soil grains are incompressible, the volumetric strain of the soil mass (ε_v) induced by pore pressure change (Δp) is expressed as below:

$$\varepsilon_v = \frac{\Delta p}{K_a}(1 - S_r)\,\frac{e}{e+1} = \frac{\Delta p}{P_0 + \Delta p}(1 - S_r)\,\frac{e}{e+1} \leq \frac{\sigma'_{v0}}{P_0 + \sigma'_{v0}}(1 - S_r)\,\frac{e}{e+1} = \varepsilon_v^* \tag{2.10}$$

where e is the void ratio of the soil mass. The bulk modulus of the pore fluid is expressed as:

$$K_f = \frac{1}{\frac{1 - S_r}{K_a} + \frac{S_r}{K_w}} = \frac{(P_0 + \Delta p)\,K_w}{(1 - S_r)\,K_w + (P_0 + \Delta p)\,S_r} \leq \frac{(P_0 + \sigma'_{v0})\,K_w}{(1 - S_r)\,K_w + (P_0 + \sigma'_{v0})\,S_r} = K_f^* \tag{2.11}$$

The volumetric strain of the soil and bulk modulus of the pore fluid attain their highest values when Δp reaches its maximum possible value (σ'_{v0}) during an earthquake loading. The highest volumetric strain of the soil and bulk modulus of the pore fluid are termed potential volumetric strain (ε_v^*) and potential bulk modulus (K_f^*), respectively.

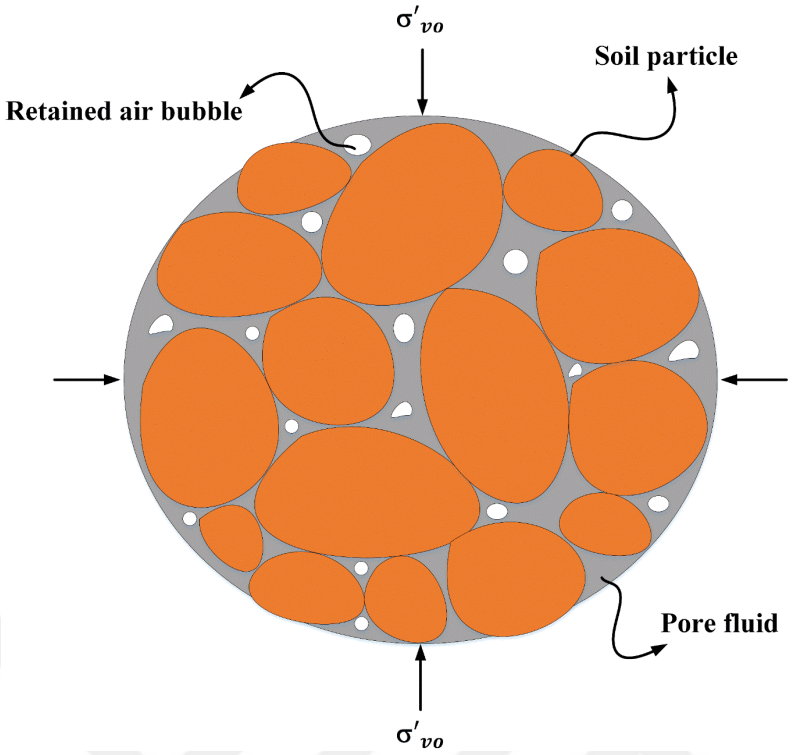

Figure 2.12– Schematic representation of a partially saturated soil element.

2.6.2.1 Compressibility of the Pore Fluid

The potential bulk modulus of the pore fluid is calculated using equation 2.11, and its variation with degree of saturation and effective stress is shown in figure 2.13. Ideally, the bulk modulus of water, K_w, can be taken as 2×10^6 kPa, and water is deemed virtually incompressible. The bulk modulus of the pore fluid (air-fluid mixture), K_f, in the partially saturated soils, however, decreases substantially with a small reduction from the complete saturation (S_r=100%). K_f remains unchanged with effective stress if the soil is fully saturated ($K_f = K_w$), whereas it significantly varies when S_r reduces even by 1% from full saturation.

The theoretical consideration above indicates that the compressibility of the pore fluid and soil mass ought to increase substantially following the desaturation of soil with air injection. Under an earthquake loading, the reduction in the volume of air due to excess pore pressure generation should generate settlement. It is worth to mention that this analysis might be more practical for the partially saturated soils that have relatively high S_r values ($\geq$ 80%), for which the pore fluid is continuous, and tiny air bubbles exist in the non-continuous, occluded form.

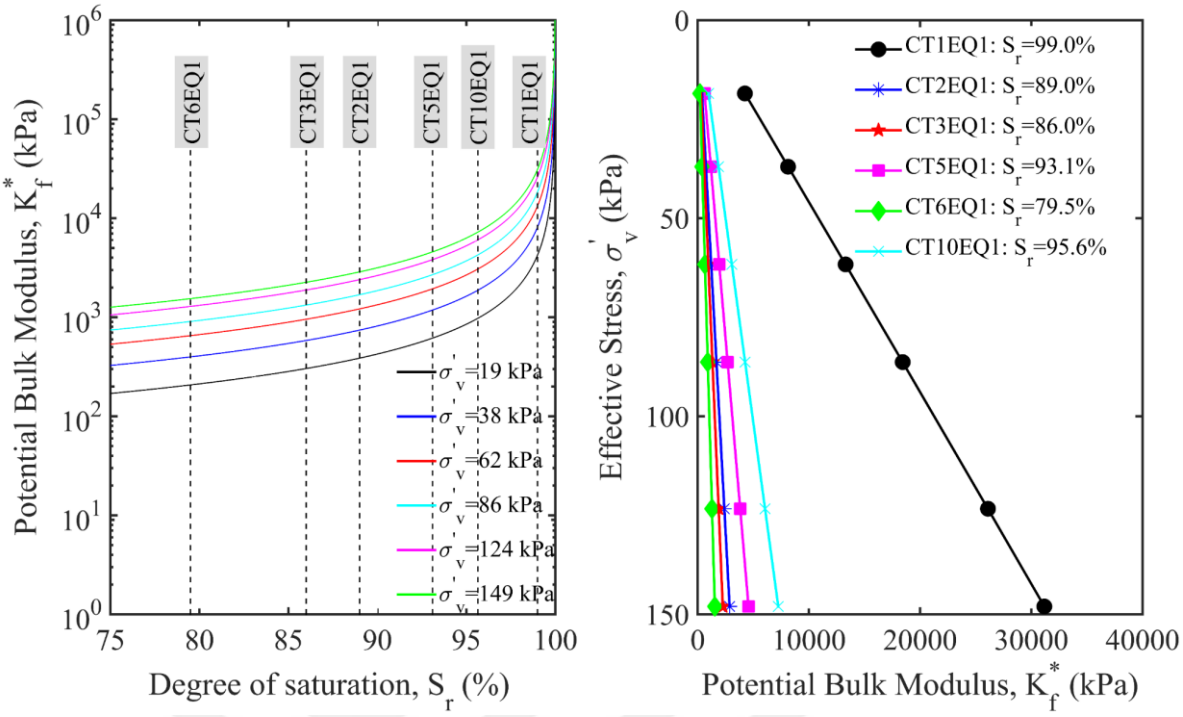

Figure 2.13– Variation of potential bulk modulus of pore fluid with degree of saturation and effective stress.

2.6.3 Theoretical Effect of Air Injection on Excess Pore Water Pressure

Finn et al. (1976) derived an expression for the build-up of excess pore water pressure (Δu) in the saturated sand during one loading cycle of simple shear tests, as shown in equation 2.12.

$$\Delta u = \frac{\Delta\varepsilon_{vd}}{\frac{1}{\overline{E_r}} + \frac{n}{K_w}} \tag{2.12}$$

Δu : Excess pore pressure per load cycle

$\Delta\varepsilon_{vd}$: Net volumetric strain increment that corresponds to the decrease in volume happening during a loading cycle in drained case

$\overline{E_r}$: One-dimensional rebound modulus of soil skeleton at an effective stress, σ_v'

n : Porosity of the soil

K_w : Bulk modulus of water

When air is injected into the deposits of saturated soils, the parameter that will change is the bulk modulus of water. In this case, the term K_w will be replaced with the bulk modulus of air-water mixture (K_f). The expression in equation 2.13 can be used for the partially saturated soils.

$$\Delta u = \frac{\Delta\varepsilon_{vd}}{\frac{1}{\overline{E_r}} + n\left[\frac{(S_r)}{K_w} + \frac{(1-S_r)}{K_a}\right]} \tag{2.13}$$

It can be deduced from equation 2.13 that the magnitude of excess pore pressures that develop during a cyclic loading depends on degree of saturation of the soil mass and bulk modulus of air bubbles. Excess pore pressures that can be generated in partially saturated soils are expected to be less than those in saturated soils due to increased compressibility of the pore fluid.

2.6.4 Effects of Soil Compressibility on Liquefaction Resistance

Various researchers, who had an interest in the influence of increased soil compressibility on the liquefaction resistance of partially saturated soils, conducted several static and dynamic element tests in order to improve the understanding on this aspect.

Okamura and Soga (2006) constructed a database from various cyclic triaxial tests available in the literature. The liquefaction resistance was defined by the cyclic stress ratio to cause DA=5% in 20 cycles. The liquefaction resistance of partially saturated soils was normalised with that of saturated soils, which was subsequently termed as liquefaction resistance ratio. In addition, potential volumetric strains, ε_v^*, given by equation 2.10 were calculated based on the consideration of maximum excess pore pressures that can be generated in the triaxial samples, which were equal to effective confining stresses, σ'_c. Based on this data set, they produced a best-fit relationship between liquefaction resistance ratio and potential volumetric strain (see figure 2.14). It can be seen in this figure that the data from different types of soils at varying densities and effective confining stresses lie along the same curve. The liquefaction resistance of partially saturated soils increases dramatically as the compressibility of the soils increases.

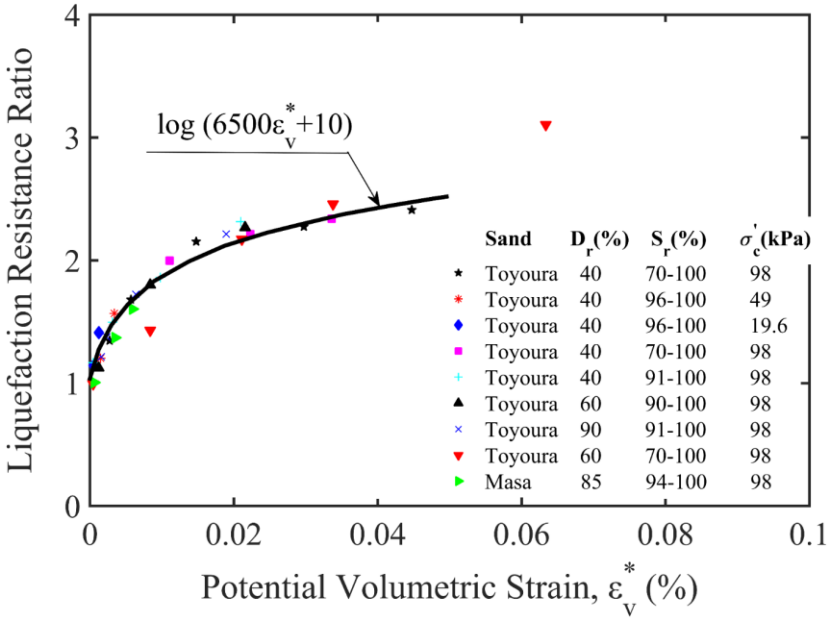

Figure 2.14– Potential volumetric strain vs liquefaction resistance ratio (adapted from Okamura and Soga 2006).

2.7 Summary

This chapter presented a review of salient research on liquefaction and air injection technique as a way of mitigating liquefaction effects.

First of all, some of the uncertainties over the definition of liquefaction were highlighted. A brief overview of the important concepts used for the liquefaction analysis (e.g. critical state, phase transformation and characteristic state) was given in this chapter. Since the undrained element tests are at the core of the liquefaction-related studies, typical results from undrained element tests under cyclic loading were briefly discussed. Furthermore, the current design practice for hazard evaluation, comprising liquefaction triggering, its effects particularly beneath shallow foundations and the methods used as a liquefaction resistance measure, was briefly outlined.

In the second part, the use of desaturation techniques as a liquefaction countermeasure was discussed, particularly focusing on the air injection technique. The theoretical relationships relevant to the effect of air on the soil and pore fluid response were presented.

Chapter 3

Modelling Techniques

3.1 Introduction

The use of field data from real earthquakes, by constructing fully-instrumented sites, would be ideal to investigate air injection as a way of mitigating liquefaction effects beneath shallow foundations. However, quantitative field data for the problem under consideration is quite rare as acquiring such data is extremely challenging. The valid data allowing full depiction of soil behaviour and true assessment of the performance of air injection should therefore be obtained by other means. Numerical modelling can be an effective tool since it can allow for the incorporation of complex geometry, non-linearity and interaction effects. However, it requires a thorough understanding of the problem and an accurate, well-calibrated constitutive model. To date, very little experimental research is available on the performance of air injection technique, and its understanding is incomplete. A comprehensive knowledge of the partially saturated soil behaviour also remains elusive, and its constitutive behaviour is not fully known. All of these factors would render numerical modelling counterproductive. In this research, the air injection technique was examined using physical modelling in a geotechnical centrifuge and on a 1-g shaking table. In particular, centrifuge tests are expected to provide reliable information that virtually matches the in situ response of soil recorded during earthquake events. They ought to offer sensible data at relatively low cost and under repeatable conditions.

In this chapter, the apparatus and testing procedures for the dynamic centrifuge and 1-g shaking table tests are described. Each modelling technique is explained separately, with a particular focus on the dynamic centrifuge testing. The theory behind each modelling technique is briefly discussed. Information regarding the model foundations and the soil used, preparation and de/saturation of the models and the test programmes for the experiments are presented. Finally,

techniques used to analyse the test data, some of the limitations of the apparatus and potential sources of error are discussed.

3.2 Dynamic Centrifuge Modelling

3.2.1 The Theory of Centrifuge Modelling

Full or large-scale testing at the Earth's gravity (1-g) is a viable alternative for civil engineering problems. The response of fully instrumented sites and shallow foundations can be monitored during real earthquakes. However, constructing full-scale prototypes is very costly and time-consuming. This issue can be resolved to some extent by means of small-scale 1-g physical modelling techniques. For a linear system, the response of a small-scale model is expected to be the same as the response of its prototype. For geotechnical problems, the stress-strain characteristics of real soils are highly non-linear, and their mechanical behaviour strongly depends on the stress level. This introduces a challenge for geotechnical engineers. In order to achieve a realistic response for full-scale scenarios, the same level of stresses needs to be recreated in the small-scale models.

Since the 1970s, centrifuge modelling has become an effective way to study complex geotechnical problems using small-scale models. The principle of centrifuge modelling is to subject scaled-down models to an increased gravitational field and accomplish the stress and strain similarities at homologous points in the soil between model and prototype, which is the simplified version of the full-scale system. It must be highlighted that for an accurate representation of the stress-strain response in a small-scale centrifuge model, boundary conditions need to be correctly accounted for. Furthermore, the fundamental physical characteristics of the geotechnical problem should be successfully captured by the prototype.

In geotechnical centrifuge testing, a scaled model is N times smaller than the prototype, and it is subjected to a centrifugal acceleration that is N times of Earth's gravity (Nxg). As part of centrifuge testing, a range of appropriate scaling factors must be applied to convert between model scale and prototype scale quantities. Based on the dimensional analysis, Schofield (1980) and Schofield (1981) derived a set of scaling laws for a range of different parameters, both in static and dynamic events. The scaling laws derived for the parameters which are of interest to this study are summarised in table 3.1.

Centrifuge modelling has some drawbacks, as in the other form of research tools. Madabhushi (2014) discussed some of the limitations and the source of errors that are inherent to centrifuge modelling. They mainly comprise (a) the variation of gravity field within the centrifuge model: the acceleration field increases with radius, and g-level does not remain constant over the entire depth of the centrifuge model, (b) the radial acceleration field: g-level varies across any horizontal plane within the centrifuge model, (c) particle size effects: the size of the particles in the centrifuge model is not decreased, which may influence the formation of shear bands and (d) coriolis error. In order to minimise the impact of these effects on the experimental data, the overall radius of the centrifuge is usually kept larger compared to the height of the model.

Table 3.1 – Main scaling laws in centrifuge modelling.

Parameter	Scale: Model/Prototype[(a)]	Dimensions
Length	1/N	L
Mass	$1/N^3$	M
Stress	1	$ML^{-1}T^{-2}$
Strain	1	1
Force	$1/N^2$	MLT^{-2}
Seepage Velocity	N [(b)]	LT^{-1}
Time (seepage event)	$1/N^2$ [(b)]	T
Time (dynamic event)	1/N	T
Frequency	N	T^{-1}
Acceleration	N	LT^{-2}
Velocity	1	LT^{-1}

[(a)] For a centrifuge acceleration of N×g; [(b)] Use of the same fluid in the model and prototype

The scaling laws were derived for '*diffusion'* or '*static*' events such as consolidation and '*dynamic*' events such as an earthquake. The time in diffusion events scales as $1/N^2$ between the model and prototype, whereas it scales as $1/N$ in dynamic events, as seen in table 3.1. The incompatibility in the time-scaling can be confronted by using a pore fluid that is N times more viscous than the water (Lambe and Whitman 1982). Using a highly viscous pore fluid in dynamic centrifuge models is a well-established procedure. A range of different pore fluids, such as silicone oil (Lee 1985) and methylcellulose (Stewart et al. 1998), have been used for viscosity-scaling. Despite the common use of this approach, a few researchers have raised some doubts about the effects of high-viscosity fluids on the experimental data. Bolton and Wilson (1990) indicated that increasing the pore fluid viscosity affects the damping characteristics of the soil. In comparison with water, the use of silicone oil having a viscosity of 100 cSt at 75 Hz was shown to produce an increase in the damping ratio by a factor of 2. However, Madabhushi (1994) demonstrated, based on the centrifuge tests with water and high-viscosity

silicone oil, that the sensitivity of damping to the pore fluid viscosity is very small indeed. Moreover, Ellis et al. (2000), based on extensive resonant column tests, noted that viscous damping might be significant for the problems where loading frequency is high, and strain amplitudes are small, such as a small magnitude of earthquakes. However, no evidence was found to claim that the energy required to generate a given value of excess pore pressure ratio, r_u, would be influenced by the viscous damping in the liquefaction problems. In this research, it was assumed that the viscous damping is relatively small compared to the material damping in the soil, and the viscous damping effects are negligible.

Another way of removing the discrepancy in time scaling is to change the soil permeability used in the model by scaling the size of particles down. Hazen's empirical relationship for sands indicates that the D_{10} size particles need to be scaled down by a factor of $\sqrt{N}$, and this necessitates the use of $\sqrt{N}$ times smaller soil particles in the model. However, changing the particle sizes can cause a significant change in the stress-strain behaviour of the soil.

3.2.2 The Turner Beam Centrifuge

The dynamic centrifuge tests presented in this thesis were conducted using the Turner beam centrifuge at the Schofield Centre of Cambridge University (see figure 3.1). The centrifuge has a capacity of carrying a package of up to 1 ton at the acceleration of 150-g. It has a 10 m arm and two swinging platforms at each end. In its current form, the model is placed on one (blue) end, and the counterweight mass is loaded on the other (red) end. When swung up, the top surface of the swinging platforms is at a radius of 4.125 m. Electrical and hydraulic slip rings are available on the centrifuge central spindle. Electric power, fibre optics, water and air lines can therefore be easily conveyed to the model package through these slip rings. Moreover, they enable data connections between the control room, computers on the beam and model package. More details about the Turner beam centrifuge are available elsewhere (Madabhushi 2014).

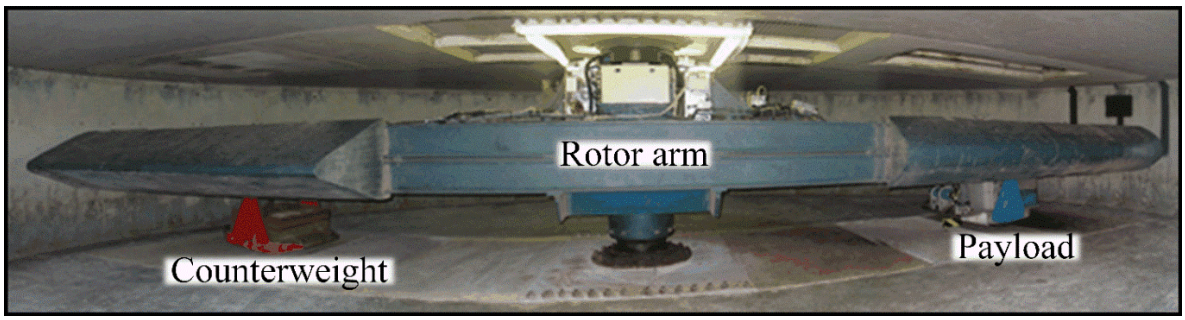

Figure 3.1– A view of the Turner beam centrifuge at the University of Cambridge.

3.2.3 The Stored Angular Momentum (SAM) Earthquake Actuator

In this research, earthquake motions for the dynamic centrifuge tests were generated using a Stored Angular Momentum (SAM) earthquake actuator. A view and schematic diagram of the SAM actuator are shown in figure 3.2. It is a mechanical actuator and works, very basically, by storing the energy required for the earthquake in a pair of flywheels. These flywheels are rotated by a simple three-phase motor. The speed of the flywheels is selected according to the frequency of the desired earthquake motion. A rod attached to the flywheels reciprocates through a fast-acting hydraulic clutch. An electronic timer engages the clutch for the required duration of the earthquake through the control of pneumatic valves. Once the clutch is pressurised and grabs the reciprocating rod, the earthquake commences. The shaking is transmitted to the model package via a connecting rod that passes through a pivot. Eventually, lateral shaking motion of a rack beneath the model package is produced. It is worth noting that the adjustment of the location of the pivot allows for controlling the displacement magnitude of the shaking.

The SAM actuator generates simple sinusoidal pseudo-harmonic input motions with a desired frequency, duration and controlled magnitude. This system is reliable and simple; however, it can produce only two types of earthquakes: (1) a single frequency and a single amplitude of earthquake motion of a known duration and (2) an earthquake motion of decreasing magnitude and decreasing frequency (sine-sweep). The SAM actuator can function at centrifugal accelerations of up to 100-g. It also allows for firing successive earthquakes, depending on the capacity of the accumulator. Further information regarding the development of the SAM actuator can be found in Madabhushi et al. (1998).

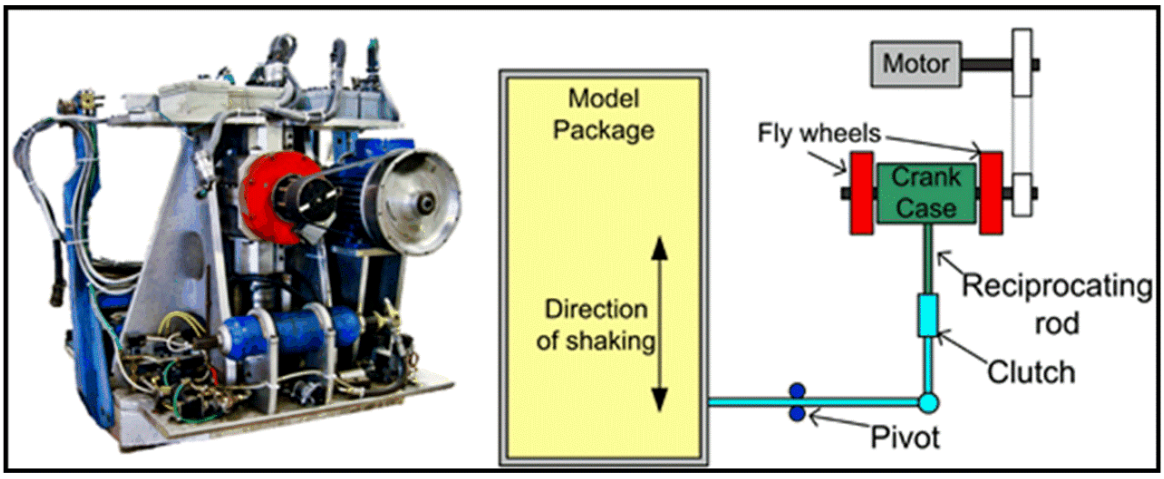

Figure 3.2– A view and schematic illustration of the SAM earthquake actuator.

3.2.4 Model Containers

The soils in the field are considered to be semi-infinite. Centrifuge models are, by their very nature, finite and have a limited lateral extent. To realistically simulate the field conditions, containers, containing centrifuge models, must be able to minimise the boundary effects on the response of soil. Earthquake-induced liquefaction problems involve significant excess pore pressure generation and dramatic changes of shear stiffness in each cycle. This, however, may not be replicated by the model container walls whose stiffness remains unaltered. The stiffness of the model boundaries may not match the dynamic stiffness of the soil, and some wave reflections by the boundaries back into the soil can occur. This can cause boundary effects on the response of soil. To prevent this, laminar model containers are widely used in modelling the liquefaction problems. The concept of such a container is that it has zero lateral stiffness, and hence its deformation is driven by the soil deformation (Madabhushi 2014).

In this research, two types of model containers were employed for the dynamic centrifuge tests. The choice of the model container for the majority of the tests was often dictated by the need to have a transparent side to conduct high-speed photogrammetry. For this purpose, a rigid container with a thick and transparent Perspex side (window box) was used. Moreover, a laminar box was utilised quite separately for two of the centrifuge experiments. A view of the centrifuge model containers is shown in figure 3.3.

The laminar model container, described by Brennan et al. (2006), consists of a stack of 25 rectangular aluminium frames that can roll on top of each other through a series of roller bearings. It uses an inner rubber bag that is made of latex to contain the pore fluid within the model container and create a flexible barrier around the soil.

Due to the technical difficulties in designing and manufacturing a flexible container with a transparent side wall, the window box available at the Schofield Centre was used. This box has three metal sides and one transparent Perspex side, which makes a cross-section of the model visible. Plane strain conditions can be approximated in this visible cross-section. The Perspex window is very smooth to keep the friction at the interface to a minimum. Further details about the window box can be found in Cilingir and Madabhushi (2011). As mentioned previously, this type of model container may cause boundary effects due to its rigid end walls and affect the model response, particularly when liquefaction is reached. A soft putty-like material called Duxseal® was, therefore, used at the container end walls to minimise boundary effects in the

direction of earthquake loading. The Duxseal absorbs the incident stress waves and reduces the amount of wave energy that is reflected back into the soil. Steedman and Madabhushi (1991) showed that it could successfully reduce the stress wave reflections by about two-thirds.

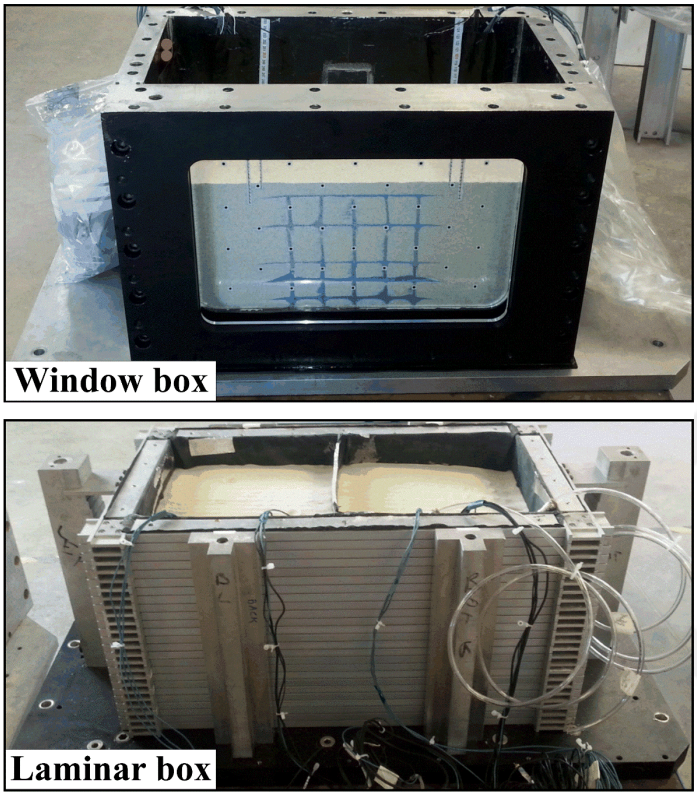

Figure 3.3– A view of the model containers.

3.2.5 Instrumentation

In centrifuge modelling, the rationale behind the selection of the instruments used is often based on the requisite for accurately capturing the model behaviour at high gravity with minimum interference. The robustness of the instruments also needs to be sufficient so that they can operate under high g-levels. In this research, different types of instruments were used to acquire the data from the tests. A view of these instruments is presented in figure 3.4. The specification for each instrument is also summarised in table 3.2. These instruments were usually miniature, yet robust. They also had flexible connection cables, allowing for minimising the disturbance on the centrifuge models during the installation process. Detailed descriptions of some of these instruments can be found in Knappett (2006) and Stringer et al. (2010).

A brief outline regarding the general virtues and limitations of each instrument is given below, along with a brief discussion of the specific problems faced during the use of these instruments.

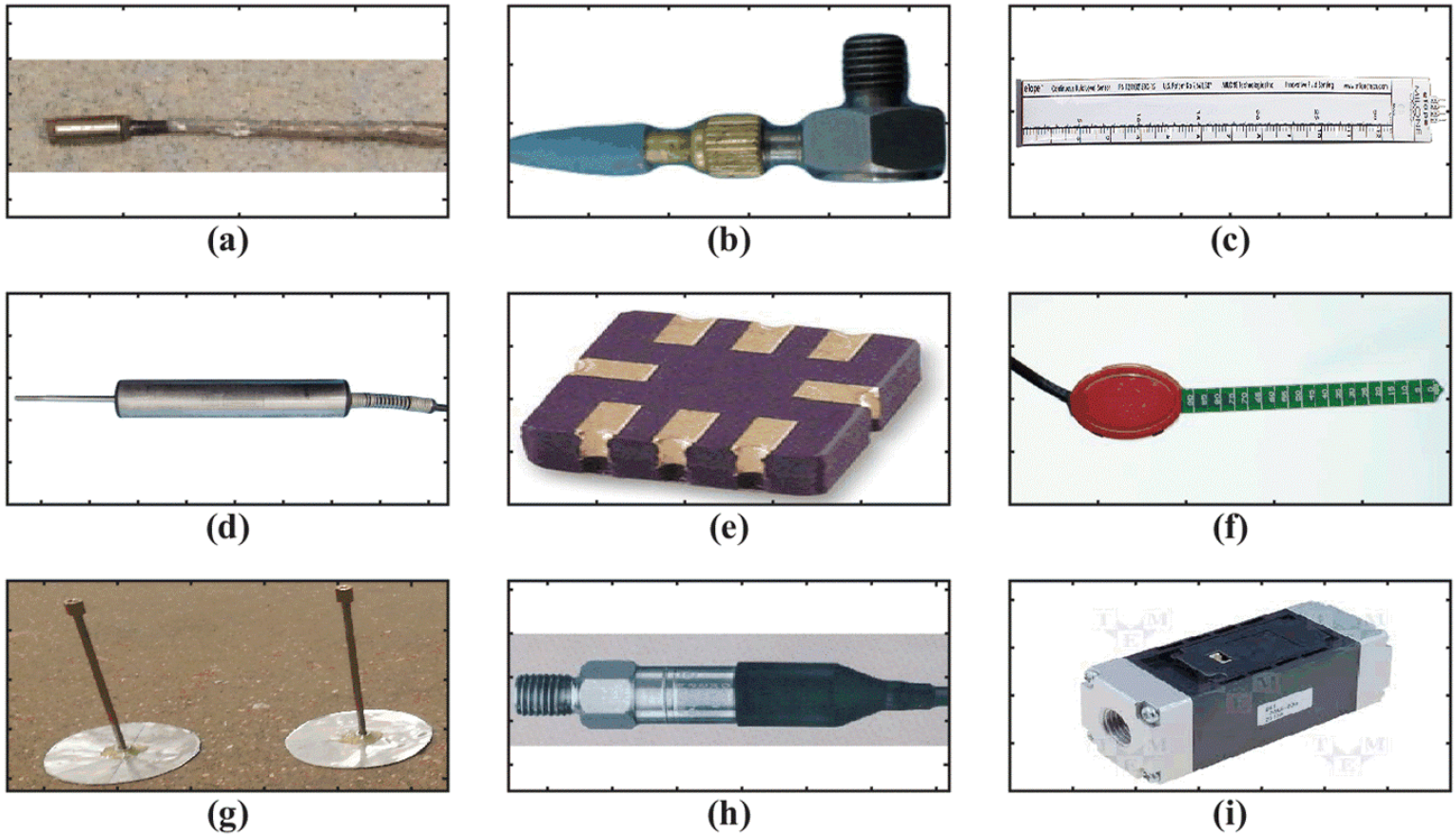

Figure 3.4– A view of the instruments used during the experiments.

The illustrated in the figure are (a) 7 bar PDCR-81 pore pressure transducer (PPT), (b) miniature piezoelectric accelerometer, (c) liquid level sensor (eTape), (d) linear variable displacement transducer (LVDT), (e) micro-electrical mechanical systems (MEMS) accelerometer, (f) soil moisture sensor (VH400), (g) LVDT plates, (h) 7 bar PDCR-810 PPT and (i) flow sensor.

Table 3.2 – Typical details of the instrumentation, in model scale.

Class	Instrument	Manufacturer	Model	Full Range	Excitation Voltage	Gain	Typical Sensitivity
Pressure	Pore Pressure Transducer (PPT)	Druck Ltd	PDCR-81	1 Bar	10	100	~10 kPa/V
			PDCR-81	7 Bar	10	10	~850 kPa/V
			PDCR-810	7 Bar	10	10	~660 kPa/V
Acceleration	Piezoelectric Accelerometer	D. J. Birchall Ltd	A/23/S	-	-	-	6 - 7 g/V
			A/23/TS	-	-	-	6 - 7 g/V
	MEMS Accelerometer	Analog Devices	ADXL78	35 g	5	1	~18 g/V
			ADXL193	120 g	5	1	~55 g/V
Displacement	LVDT	Solarton Metrology	DC15	30 mm	10	1	3.5 - 4 g/V
Flow	Flow Sensor	Omron Electronic Components	D6F-20A6-000 FLOW, 0-20 LPM	-	5	1	~4.92 L/min
Water Content	Soil Moisture Probe	Vegetronix	VH400	-	5	1	-
Liquid Level	eTape Sensor	Milone Technologies	8" eTape	-	5	1	~422 mm/V

3.2.5.1 Pore Pressure Transducers (PPTs)

Miniature 1-bar and 7-bar-range PDCR-81 PPTs were used to measure hydrostatic and excess pore fluid pressures during the 1-g shaking table and dynamic centrifuge tests. The transducers were 6.4 mm in diameter and 11.4 mm in length. The entrance of the transducers was covered by a sintered bronze stone to protect the strain-gauged silicon diaphragm from direct soil contact. The miniature PPTs were calibrated in an air pressure chamber before and after each test, subjecting the PPTs to known water pressures and recording their corresponding electric (voltage) output. The changes in electric output were recorded during a cycle of loading (0 to 500 kPa) and unloading (500 to 0 kPa). The calibration factors were attained from the slope of the best linear fit to the corresponding data points. The response of PPTs during the pre-test and post-test calibration process was practically linear. The resulting pre-test and post-test calibration factors were found to be off by approximately $\pm 6\%$ at the most.

The porous stone in front of the diagram needs to be fully saturated since air bubbles that are potentially trapped in front of the diagram may cause erroneous results. During the air injection process, air bubbles may travel inside the bronze stone and interfere with the pressure exerted on the diaphragm. This may raise some concerns regarding the accuracy of the PPT readings for partially saturated soil tests where air injection method is used. This issue was investigated, and solutions for the potential sources of error were sought, as discussed below.

To minimise the possible air entrapment inside the porous stone or in the gap between the stone and diaphragm, the PDCR-81 PPTs were kept saturated with the de-aired water until they were installed in the soil models. In addition, the air entrapment that might have occurred during the air injection process was investigated. For this purpose, the PPTs were taken out of the partially saturated soil model at the end of the test and were placed in a vacuum chamber. They were left under vacuum up to -50 kPa. It was observed that only a small amount of air bubbles came out of the PPTs. In fact, the possible air entrapment could be completely prevented by wrapping the PPTs with a flexible and very thin membrane. Nevertheless, as the pore fluid, the pressure of which is measured by the PPTs, could not freely travel inside the porous stone, this option was not followed in this research. The readings of the PPTs were checked carefully during each dynamic test. It was observed that the vast majority of the PPTs placed in both saturated and partially saturated soils provided adequately accurate hydrostatic and dynamic variation of pore fluid pressures at the corresponding locations.

A PDCR-810 PPT was installed in an air injection system to measure the air pressure applied (see figure 3.11). In a similar way to the miniature PPTs, it was calibrated by applying known air pressures and measuring the corresponding voltage output. This PPT was found to be capable of measuring the rapid changes in air pressure during the air injection process.

3.2.5.2 Piezoelectric and MEMS Accelerometers

Measurement of acceleration was made by miniature piezoelectric and MEMS accelerometers.

Piezoelectric accelerometers were used to record the acceleration in the soil and input motion. They are capable of recording only dynamic acceleration. Pre-test and post-test calibration of these instruments were performed using a calibrator manufactured by Brüel & Kjaer. This calibrator excites the accelerometers at $\pm 1\ g$ sinusoidal motion. When the correct mass of the instrument is given, the voltage corresponding to this excitation is recorded.

MEMS accelerometers were used to record the accelerations at different locations of shallow foundations and shallow soil layers. MEMS accelerometers are capable of measuring both inertial and dynamic accelerations. They were calibrated by rotating them at different angles and recording the corresponding voltage output. The use of MEMS accelerometers on the model foundations allowed for minimising the interference with the foundation response owing to their small size and mass. It is worth mentioning that accelerometers were waterproofed either by dipping them into hot wax (piezoelectric) or covering with water-proof silicon sealant (MEMS) to protect the electrical connections from the conductive environment (pore fluid). More information about the use of piezoelectric and MEMS accelerometers in the saturated, loose soil deposits can be found in Stringer et al. (2010).

3.2.5.3 Linear Variable Displacement Transducers (LVDTs)

Miniature LVDTs were utilised during the centrifuge and 1-g shaking table tests to record the cumulative settlement of shallow foundation and ground surface in the free-field. They are less effective at measuring the high-frequency displacements (over 15 Hz) yet very successful at capturing the cumulative displacements. The LVDTs were calibrated by applying known displacements (by a micrometer) and measuring the corresponding voltage output. During the tests, a metal spindle was used to extend the LVDTs. In addition, a 50 mm diameter circular bearing pad, made of a thin light aluminium plate, was placed underneath the spindle to prevent

it from sinking into the liquefied soil under the high gravity (see figure 3.4g). The LVDTs were held in place using a gantry connected to the model containers.

3.2.5.4 Flow Sensor

A MEMS-based flow sensor was used to measure the rate of air flow during the air injection process. The calibration factors provided by the manufacturer were used to convert the output data (voltage) to litres per minutes. It was found that this sensor was incapable of operating at high g-levels. Therefore, it could only be reliably used for the experiments conducted at 1-g.

3.2.5.5 Soil Moisture Sensors

Some of the tests in this research required the use of soil moisture sensor probes (VH400) to measure the volumetric water contents, which were then converted to degrees of saturation. These moisture sensors are dielectric constant based and can offer a rapid response time. They are sensitive to the change in water content and can measure the full range of volumetric water contents (from dry to fully saturated soil). The probe part of the VH400 is about 100 mm in length and 8 mm in width. The probe essentially returns an average reading over the entire length and provides readings only for the medium with which it is in direct contact.
The sensors were calibrated by inserting into Hostun sand samples prepared in small containers with varying water contents and recording the voltage reading for each of the samples.

3.2.5.6 Liquid Level Sensor

Liquid level sensor, eTape, was used during the 1-g soil column tests to monitor the variation of water level during and after the air injection process and to indirectly compute the change in degree of saturation using mass-volume relationships (see chapter 5). It is essentially a solid-state sensor with a resistive output that varies with the level of fluid. The hydrostatic pressure of the water compresses the envelope of the sensor and leads to change in resistance. The resistivity output of the sensor is inversely proportional to the height of the water.

3.2.6 Data Acquisition

The selection of the data acquisition system is important in physical modelling to ensure the quality of experimental data. In this research, the data acquisition system used for all the tests was DASYLab (Data Acquisition System Laboratory). This software was very easy to use and

provided continuous logging to the hard drive. It allowed for sampling data at high sampling frequencies, such as 6 kHz in model scale during the earthquake events. This system also enabled many data channels to be sampled simultaneously at high sampling rates during the dynamic centrifuge tests (e.g. 64 channels). Since it provided real-time displays, the readings and traces of the instruments could be viewed during the tests. It was also possible with this system to capture the data for a long period of time after the earthquakes cease, such as 150 s in model scale. This feature was important to scrutinise the post-earthquake excess pore pressure dissipation and settlement behaviour.

3.3 Centrifuge Tests

A series of ten centrifuge tests were carried out in this research. Each test involved the design of model foundations and model preparation. All the centrifuge models were prepared in the same way. Dry sand was poured into the model boxes, and the monitoring instruments were installed at the pre-determined locations. This was followed by the saturation of the dry sand models. The centrifuge experiments that required liquefaction treatment involved an additional phase: the desaturation of the saturated sand models via air injection. Phases of the centrifuge tests and the test procedure are detailed in the ensuing sections.

3.3.1 Model Foundations

In centrifuge modelling, it is of great significance to accurately model the structures. However, the exact replication of the prototype structures might be difficult due to the small-scale nature of the centrifuge models, which thus entails certain simplifications to be made. It is known that the presence of superstructures on the shallow foundations complicates the geotechnical problems due to the dynamic interaction between the superstructures and the foundations. Since the problem investigated as part of this research is already complex, simple bars with no superstructure were chosen for the model foundation (see figure 3.5). The model foundations may represent the strip foundation of a typical residential building. The key properties of the prototype replicated within the shallow foundation models were the bearing pressure and bearing area. The model foundations had a very low centre of gravity, and thus their rocking response was insignificant. They were also very rigid, and therefore no deformations within the foundations were expected.

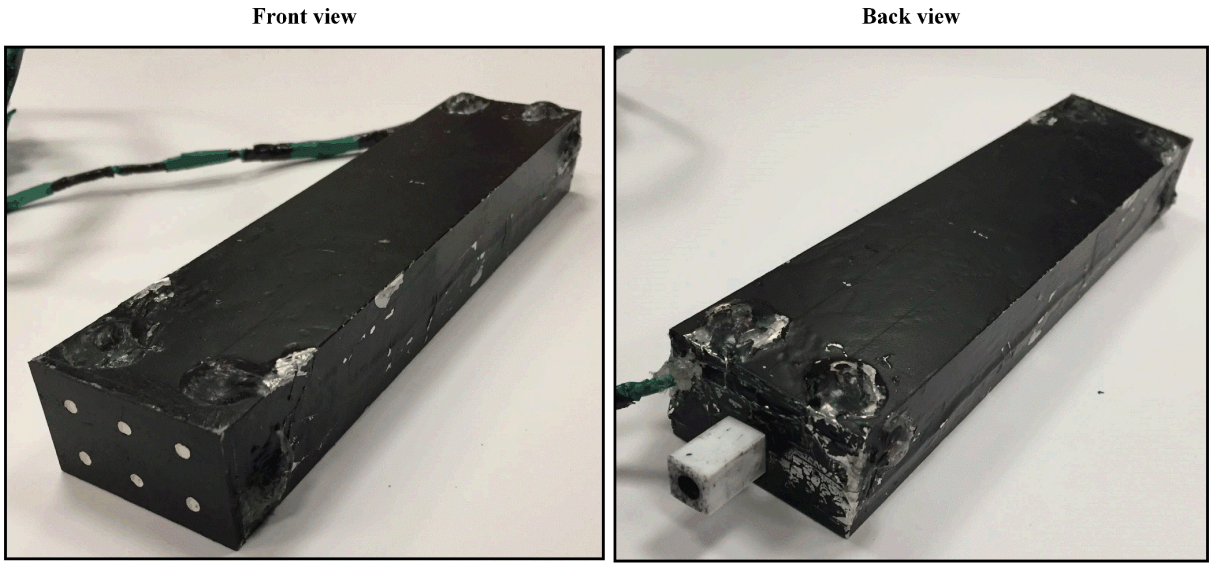

Figure 3.5– A view of the model foundation used in the centrifuge experiments.

The majority of the centrifuge experiments were carried out in the window box to acquire the images for the particle image velocimetry (PIV) analysis. The set up for the PIV technique will be described in section 3.3.5. In order to ensure high-quality data for the PIV, the front end of the foundations had to be in touch with the Perspex window, along with a limited friction at the contact area. Due to the configuration of the SAM earthquake actuator and the high-speed camera, the model foundations would be pulled away from the Perspex window towards the rear wall of the window box by the Earth's gravity when the in-flight position was reached. Therefore, a spring support system was attached at the back end of the foundations to prevent this from happening. The cross-section and plan view of this system can be seen in figure 3.6. This system was designed in a way that it held the foundations directly against the Perspex window without any additional force that might lead to an increased friction. Moreover, it allowed for the free rotation of foundations. In order to limit the friction between the support system and back wall, the support system was made of polytetrafluoroethylene (PTFE), in white colour, with low friction. In addition, a layer of low friction high-density polyethylene (HDPE), in black colour, was fixed to the rear wall of the box. Similarly, the front end of the foundations was covered with HDPE to further minimise the friction at the interface between the foundations and Perspex window. White markers were added on the front HDPE to accurately track the movement of the foundations using PIV. It is worth noting that the foundations were painted black so that the glare on the acquired images was reduced.

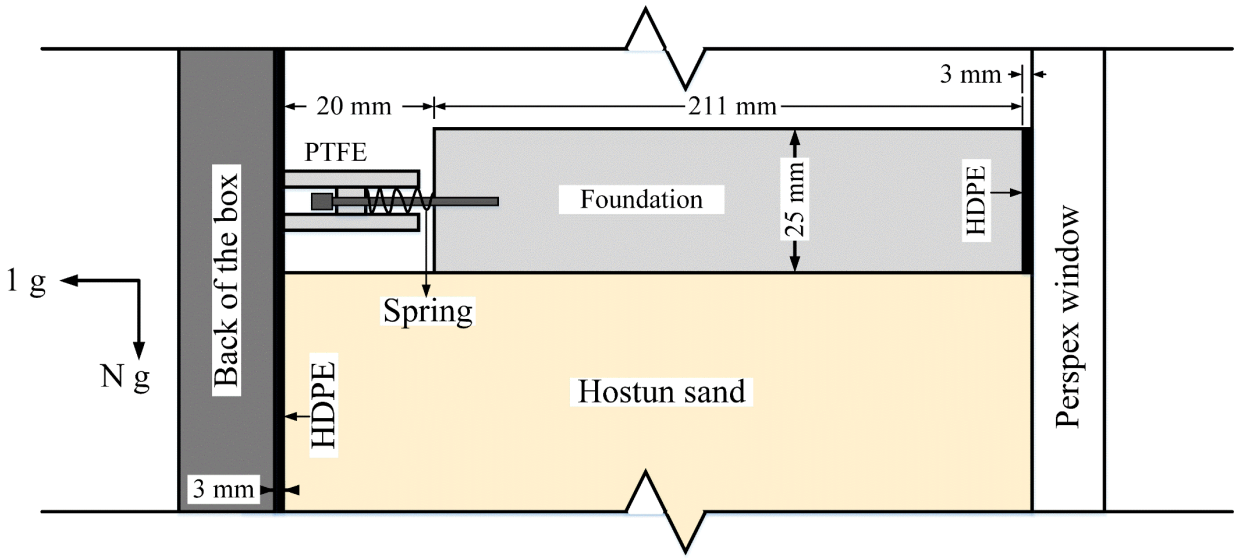

a) Cross-section

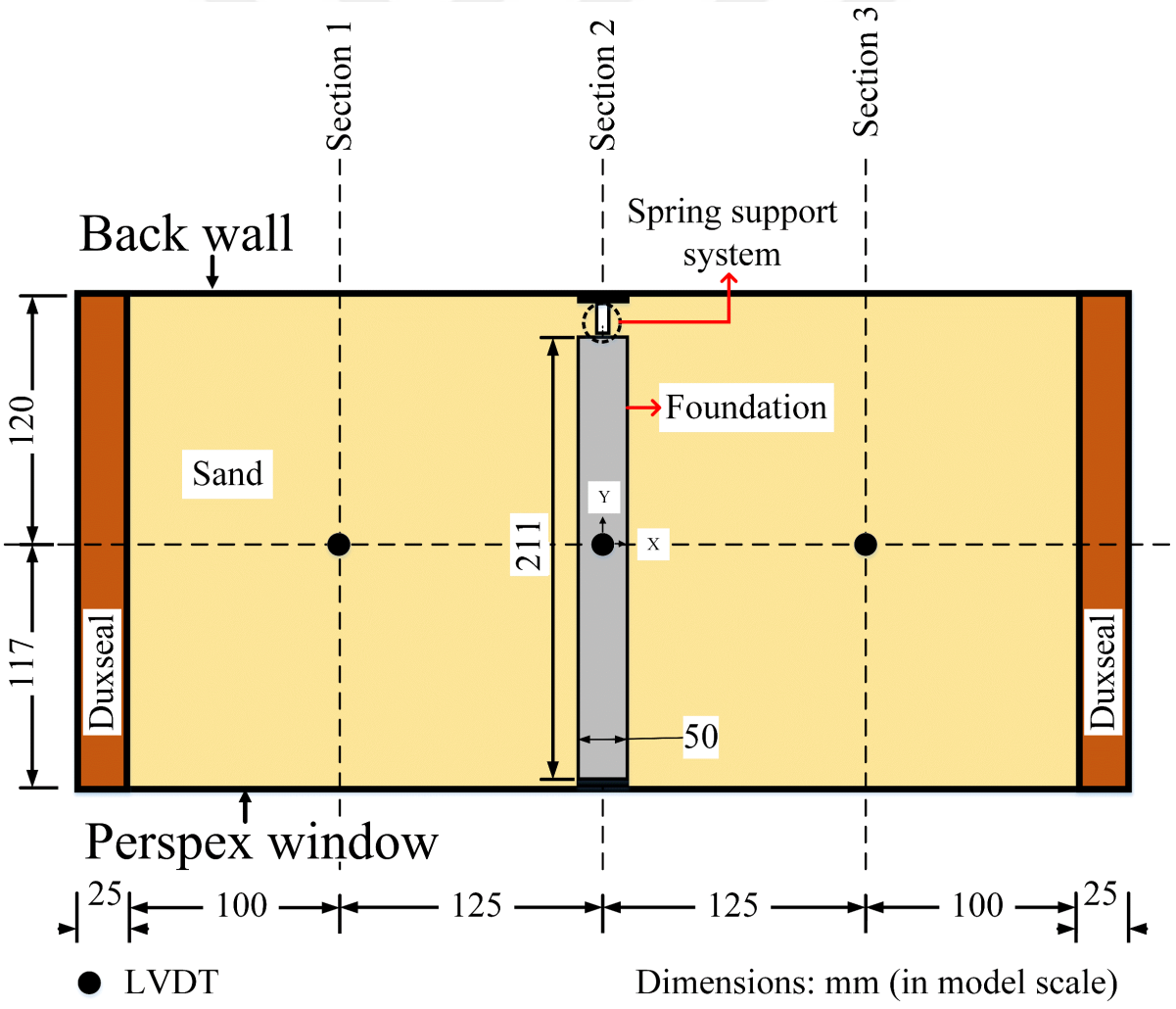

b) Plan view

Figure 3.6– The spring support system attached to the foundation.

Three different model foundations were tested during the dynamic centrifuge experiments. The characteristics of the model foundations are summarised in table 3.3. The foundations were instrumented with MEMS accelerometers, as shown in figure 3.7. The length of the foundations was to be, almost, the full width of the model boxes. The soil beneath the model foundations was only allowed to displace vertically downwards and sideways. Consequently, plane strain requirements were successfully satisfied. The foundation models were designed with the same dimensions in model scale (50 mm in width, 25 mm in height and 211 mm in length). However, their characteristics differed according to the g-level they were subjected to and the material they were made of, as follows:

Foundation MF1

- represent a strip footing of a typical heavy residential building
- made with brass
- exert a bearing pressure of 135 kPa at 70-g

Foundation MF2

- represent a strip footing of a light residential building
- made of duralumin
- apply a bearing pressure of 50 kPa at 70-g

Foundation MF3

- represent a strip footing of a light residential building
- made with the layers of duralumin and brass
- exert a bearing pressure of 50 kPa at 40-g

It is noted that the model foundations were designed to have two different values of bearing pressure, namely, 135 kPa and 50 kPa. The rationale beyond this selection was to investigate the dynamic behaviour of *heavy* and *light* shallow foundations resting on the saturated and partially saturated soils. Another purpose was to scrutinise the influence of bearing pressure on the deformation mechanisms that govern the settlement of shallow foundations. Since the model foundations had the same (low) aspect ratio in each case, the influence of this parameter remained insignificant. The reason for selecting different g-levels, namely, 40-g and 70-g, was to examine the effectiveness of the air injection technique under different levels of centrifugal acceleration and therefore confining (or vertical) stress.

Table 3.3 – Characteristics of the model foundations, in prototype scale.

Foundation ID	MF1	MF2	MF3
g-level	70	70	40
Bearing Pressure, q (kPa)	135.0	50.0	50.0
Centre of Gravity (m)	0.875	0.875	0.45
Base Width, B (m)	3.5	3.5	2.0
Height, H (m)	1.75	1.75	1.0
Length, L (m)	14.77	14.77	8.44
Surcharge Material	Brass	Duralumin	Duralumin + Brass

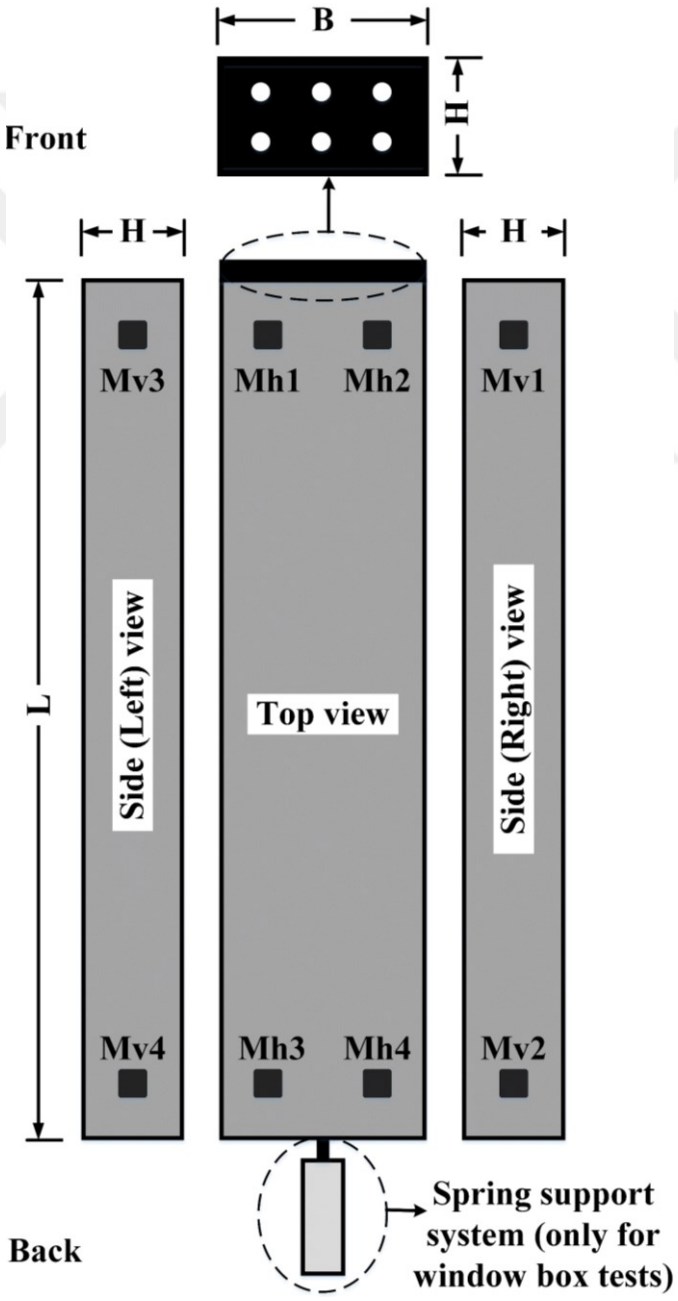

Figure 3.7– A view of the model foundations instrumented with MEMS accelerometers.

3.3.2 Model Preparation-Sand Pouring

3.3.2.1 Hostun Sand

The soil used in this research was Hostun HN31 sand (Flavigny et al. 1990). Its particle size distribution (PSD), acquired using the Single Particle Optical Sizing method (White 2002), is shown in figure 3.8. Furthermore, some of its fundamental properties are given in table 3.4.

The choice of the soil was selected according to particle size and uniformity. Hostun HN31 sand is a fine-grained siliceous sand. Since it is relatively uniform, no signification segregation is expected to occur during the sand pouring. It allows for the preparation of uniform deposits of soils, which is important for the repeatability of the models. An additional benefit of using Hostun sand is that it can liquefy, even during successive earthquakes.

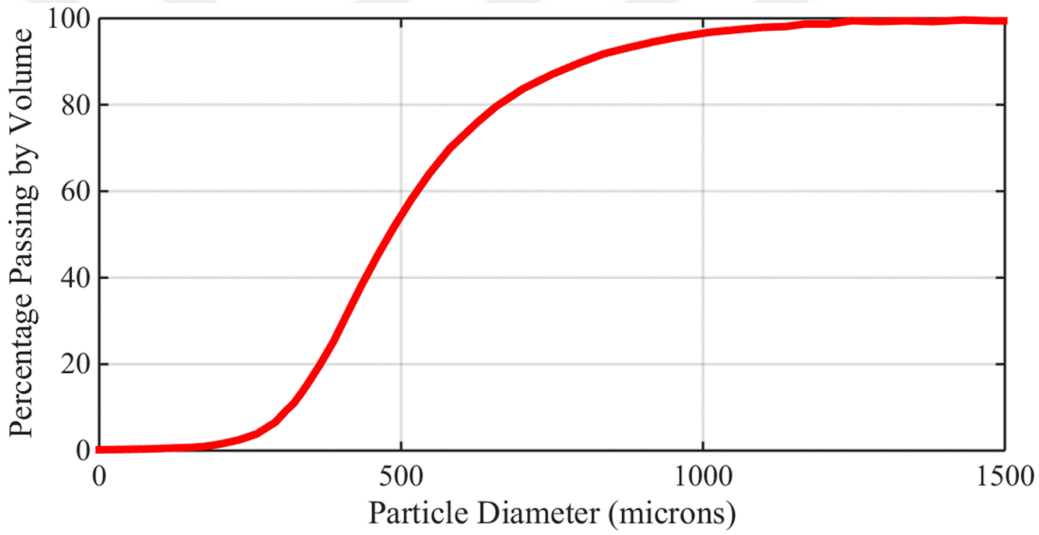

Figure 3.8– Particle size distribution for the HN31 Hostun sand.

Table 3.4 – Geotechnical properties of HN31 Hostun sand.

Property	Value	Unit
Uniformity coefficient, U_c	1.67 †	-
Specific gravity, G_s	2.65 ‡	-
Minimum void ratio, e_{min}	0.555 ‡	-
Maximum void ratio, e_{max}	1.01 ‡	-
Minimum density, ρ_{min}	1318 †	kg/m3
Maximum density, ρ_{max}	1620 †	kg/m3
Average particle size, D_{50}	0.480 †	mm

†: Heron (2013) ‡: Mitrani (2006)

3.3.2.2 Sand Pouring

For liquefaction studies, soil samples in loose conditions are preferable. In this research, sand samples were prepared using an air-pluviation technique. In this technique, the sample densities were controlled by adjusting the flow rate and the fall height. In order to produce loose sand deposits, large flow rates combined with small drop heights were chosen.

Before the actual pouring of the centrifuge models, a series of calibration pours were performed to determine the necessary parameters for the desired density. A nozzle size of 8 mm and a drop height of about 420 mm produced a relative density of approximately 40%, which confirmed the calibration results described by Chian et al. (2010). The layers of the centrifuge models were subsequently poured in pairs of steps through an automatic sand pourer, as shown in figure 3.9. The details and merits of the automatic sand pourer can be found in Madabhushi et al. (2006). With the use of automatic sand pourer, uniform layers of centrifuge models with the desired relative density (~ 40%) were successfully acquired. In addition, the automatic pourer allowed for the reproduction of the sand deposits with very similar properties. This enabled a direct and accurate comparison between the tests results.

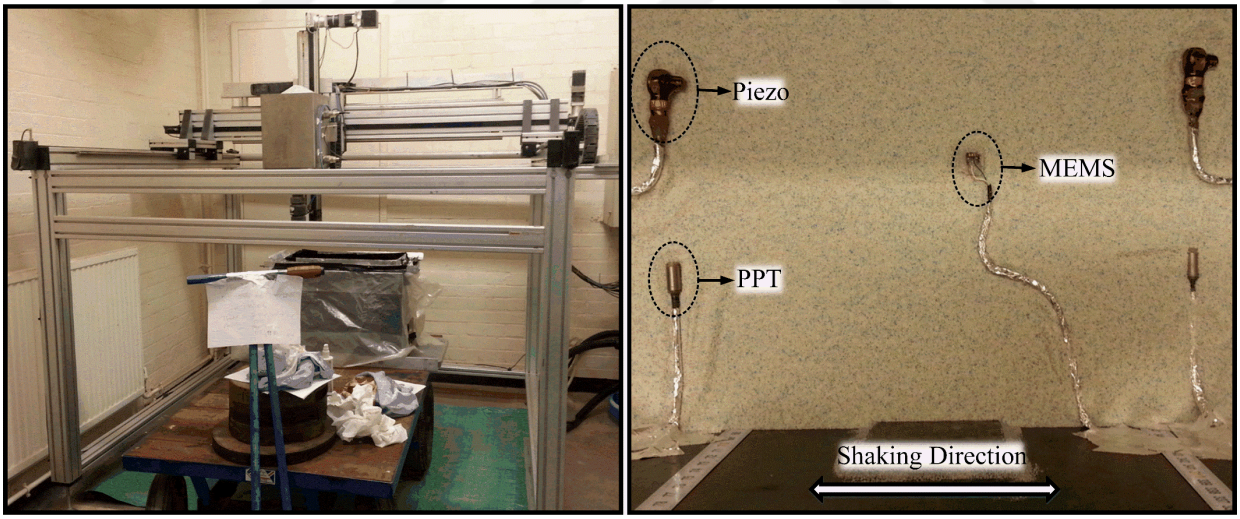

Figure 3.9– A view of the automatic sand pourer and instruments installed.

The sand pouring was periodically halted to place the instruments at the desired locations. After the instruments had been installed, it was recommenced. A typical view of the instruments installed in a centrifuge model is also presented in figure 3.9. The piezoelectric and MEMS accelerometers were orientated in the direction of shaking, whereas PPTs were placed perpendicular to the shaking. The wires of the instruments were taped to the rear wall of the model boxes to prevent the movement of the instruments from the actual '*as-placed*' location

as the sand raining continued. The locations (depth and horizontal position) of the instruments were measured very carefully after they were installed, which was of significance to prevent unreliable data from them. At the end of the sand pouring process, the surface of the models was levelled very carefully using a vacuum cleaner that was modified to use for that purpose.

3.3.3 Model Preparation-Saturation

In dynamic centrifuge testing, scaling the permeability of the soil through viscosity-scaling was necessary to correct the discrepancy between dynamic and diffusion time. For this purpose, an aquatic solution of Hydroxy-Propyl Methyl Cellulose (HPMC) was chosen as pore fluid with a viscosity of *N* (g-level) times that of water. The merits of this solution were that it was a cost-effective option and had a unit weight very close to water. Solutions of HPMC were prepared for the dynamic centrifuge tests by mixing the dry METHOCEL F50 Food Grade HPMC with boiling water. The quantity of HPMC powder for the desired viscosities was typically estimated using the empirical equation (3.1) provided by Stewart et al. (1998). With this formula, the concentration of solution, *C*, as a percentage of the entire solution by mass can be calculated for a kinematic viscosity at a temperature of 20 ℃ (υ_{20}).

$$\upsilon_{20} = 6.92 \cdot \mathrm{C}^{2.54} \tag{3.1}$$

It must be highlighted that the HPMC powder generally takes some time to dissolve in cold water. However, the duration was reduced considerably with the use of boiling water and a mechanical mixer. Pre-determined quantities of boiling water and dry HPMC powder were poured into the mixing tank and were stirred continuously under suction for a period of 4-5 days. Homogeneous and repeatable mixtures were obtained. The viscosity of the solutions was checked regularly using a viscometer device. Water or dry HPMC powder was, if necessary, added to the mixture to acquire the desired viscosity.

Once the viscous pore fluid was ready to be used, dry centrifuge models were saturated using a computer-controlled saturation system called CAM-Sat (Stringer and Madabhushi 2009). The models were enclosed with a lid or a large chamber for the window or laminar box, respectively (see figure 3.10). They were subjected to a vacuum of approximately -90 kPa to remove air within the models. The models were then flushed with CO_2 for a minimum of three times in order to ensure complete removal of air and reach the highest achievable degree of saturation, as suggested by Takahashi et al. (2006). Using the CAM-Sat system, the models were saturated very slowly by admitting the prepared viscous pore fluid at the base. Based on the upward

progression of the saturation front in the window box, it was observed that the models were saturated uniformly, and no significant disturbance of the model, such as fluidization or piping, occurred. The phreatic surface of the saturated models was kept above the ground surface. The degree of saturation of the models was determined based on the conventional mass and volume method, which will be explained later in this thesis. It is worth noting that although the masses, volumes and densities of the pore fluid and solids were meticulously determined, certain errors in the computed saturation ratios were still expected to occur due to the sensitivity of the conventional method (Kutter 2013).

Figure 3.10– Saturation of the centrifuge models through CAM-Sat system.

3.3.4 Model Preparation-Desaturation via Air Injection

In this study, the majority of the centrifuge tests involved the desaturation of models. The idea of the model desaturation was to form air-mixed zones in the saturated medium containing tiny air bubbles by feeding compressed air into the liquefiable ground. Consequently, it was aimed at causing a substantial decrease in degree of saturation of the ground. For superior results, the execution of the desaturation process needed the use of a system that could provide advantages in terms of simplicity, suitability and reliability. An air injection system equipped with different sensors was designed for this purpose.

A picture of the air injection system and a sectional view of the test setup are shown in figure 3.11 to describe a typical application of the air injection. The air injection system essentially consisted of a flow sensor, an adjustable air flow regulator, a PDCR-810 pressure transducer and two solenoid valves, which were connected to each other using a 5 mm diameter air line

tubing. The flow sensor was connected to the adjustable air flow regulator, then to the pressure transducer that was in turn connected to the solenoid valves. The fully assembled air injection system was fixed to the SAM earthquake actuator when the SAM and centrifuge models were loaded onto the centrifuge rotor arm. The adjustable air flow regulator was set manually before each test. The solenoid valves allowed to initiate and halt the air injection. The pressure transducer was used to record the actual air pressure applied to the model once the solenoid valves were switched on.

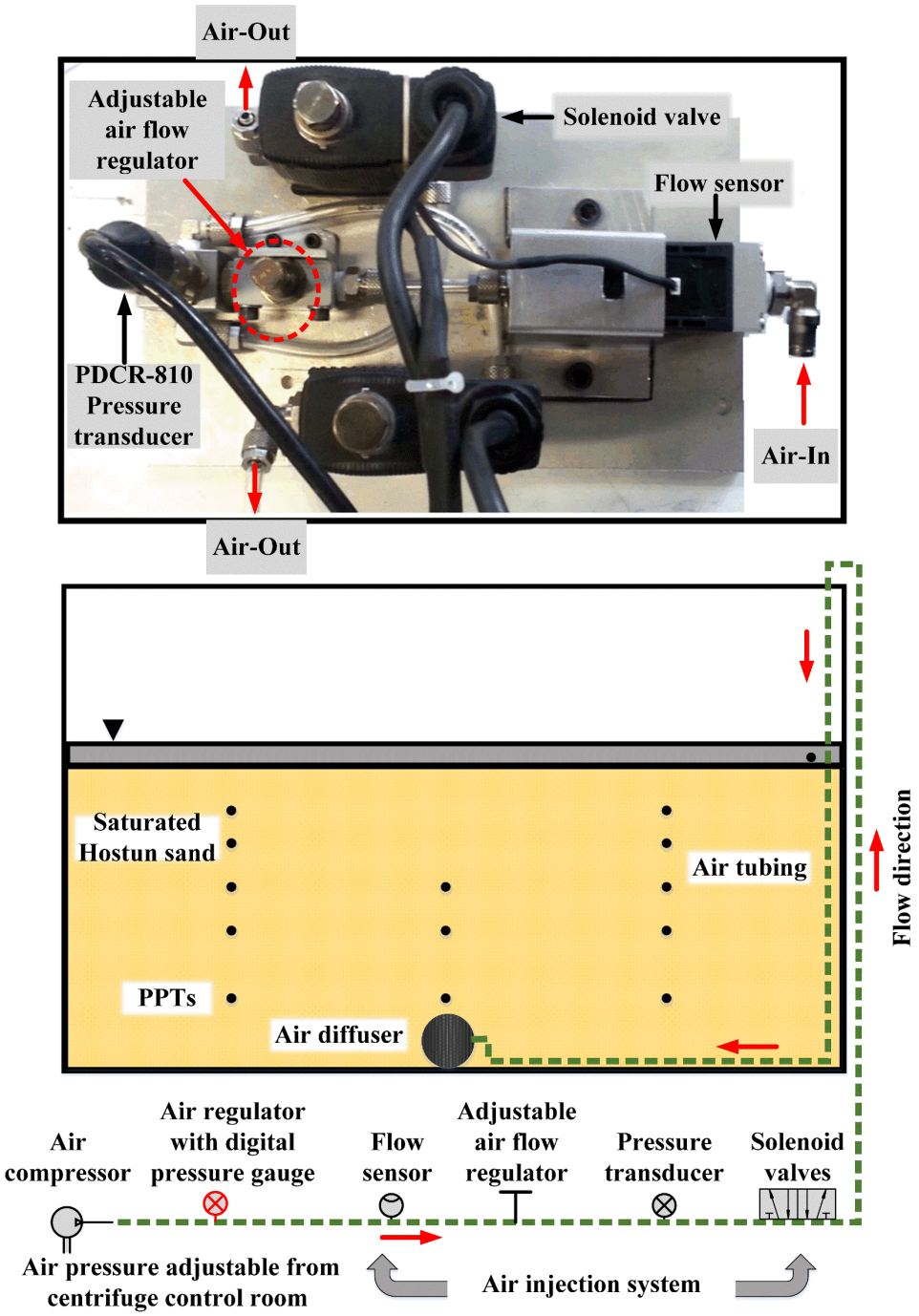

Figure 3.11– A view and sketch of the air injection control system.

The inlet of the flow sensor was connected to a supplying source of compressed air line on the beam centrifuge (see figure 3.11). The figure also shows that the outlet sides of the solenoid valves were attached to an air diffuser located on the centre-bottom of the model containers through the air tubing. The air injection pressure was adjusted through a regulator on the control panel in the centrifuge control room. With this setup, the air was successfully supplied under high pressure to the point at which air entered the model. Pore pressure transducers (PPTs) within the model ground allowed for a continuous measurement of the pore fluid pressures, which were then used to monitor the pore fluid level.

Although a well-controlled air injection system was used for the desaturation process, special care was taken to prevent significant model disturbance and maintain a fair distribution of air bubbles within the soil models. It must be noted that the use of an air injector having a large diameter of holes can potentially cause significant bubble coalescence and uneven distribution of air bubbles. Coagulated air bubbles may find a path to escape from the soil and even uplift the soil particles, resulting in considerable model disturbance (e.g. piping or boiling). Therefore, a suit of experiments was carried out in the laboratory using a Perspex tank before the actual (e.g. centrifuge) tests were conducted. The laboratory tests were aimed at selecting an appropriate air injector that can minimise the potential problems highlighted above and identifying a reasonable diameter of holes in the air injector. It was deduced from these tests that the selection of the air injector was of great importance for the quality of the desaturation process. In the preliminary laboratory tests, the use of an air injector with a large diameter of holes ($\geq$ 1 mm) led to a significant preferential flow, usually as one flow channel. Therefore, air injectors with comparatively smaller holes were tested at the later stages of the tank tests. Figure 3.12 illustrates some of the injectors (diffusers) that were tested in a water-filled tank. The PMBD (figure 3.12d), with an ultra-fine pore ceramic plate, was the most efficient diffuser to execute the desaturation process. It produced a cloud of extremely fine bubbles during the laboratory tests at the Earth's gravity. However, its use in centrifuge was found to be very hard. It did not operate well at high centrifugal accelerations and under high pore fluid pressures. This was attributed to the blockage of the extremely fine openings of the diffuser. Instead, the rubber air curtain hose (figure 3.12a), with several tiny openings of about 0.5 mm diameter and 5 mm spacing, worked well in the centrifuge and minimised the model disturbance. It was placed at the bottom of the soil beds to inject air into the saturated soils. The length of the air curtain was the full width of the model boxes, occupying the entire width of the soils beneath the model foundations and representing a two-dimensional (2-D) flow condition.

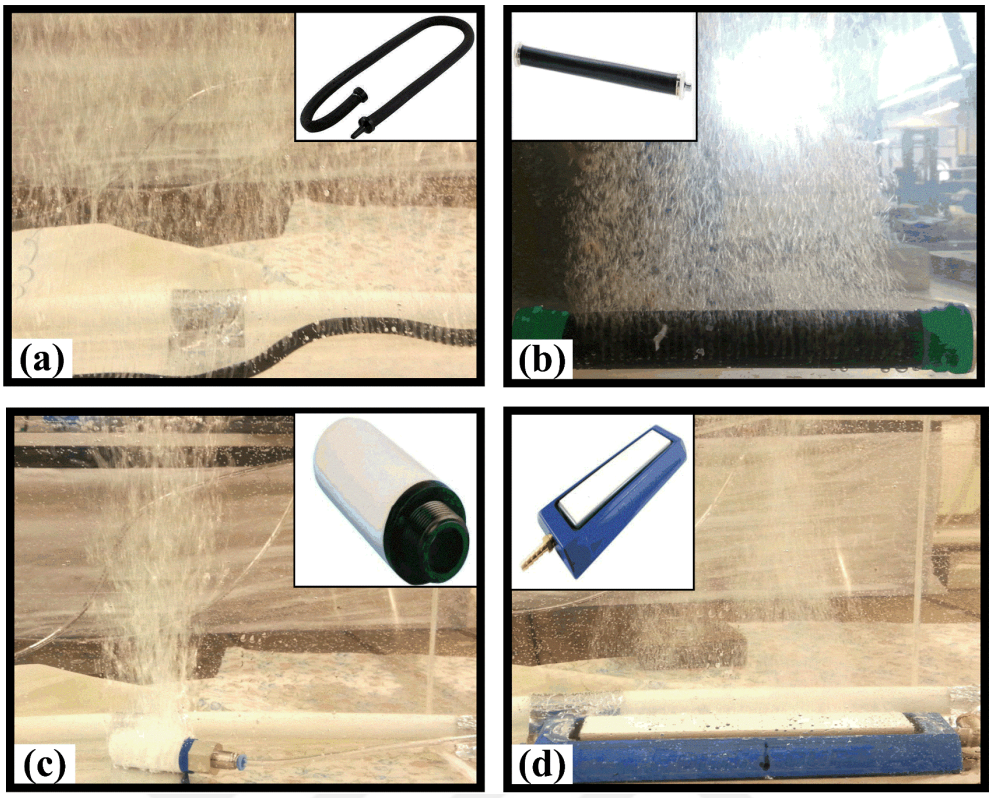

Figure 3.12– A view of the air injectors tested in a water-filled tank.
a) Rubber air curtain hose, b) rubber air bar diffuser, c) polyethylene fine flow muffler and d) point four plastic micro bubble diffuser (PMBD)

3.3.5 PIV Setup

Most of the centrifuge tests involved a high-speed photography to perform particle image velocimetry (PIV) analysis. To acquire the PIV images, a high-speed MotionBLITZ EoSens® mini2 camera along with c-mount lens with a fixed focal length of 12.5 mm were installed on the centrifuge package. This camera was capable of recording colour and high resolution of images (at 3 megapixels) at up to 523 frames per second. Moreover, the high-speed camera was connected to a trigger system on the centrifuge control panel that enabled the camera to be triggered electronically at the same time as the data acquisition. During the dynamic centrifuge tests, the frame rate for the recorded images was increased to 804 by reducing the size of the images and only viewing the zones that were of the main interest such as beneath and around the edges of the model foundations. Besides the camera, two high powered LEDs manufactured by Huey Jann Electronics were installed on the model packages. The model and PIV setup along with a typical image acquired for the PIV analysis are shown in figure 3.13. The images were recorded during the earthquakes using a short exposure time (76 μs). With the use of powerful lighting and a very short exposure time, sufficiently sharp images were obtained.

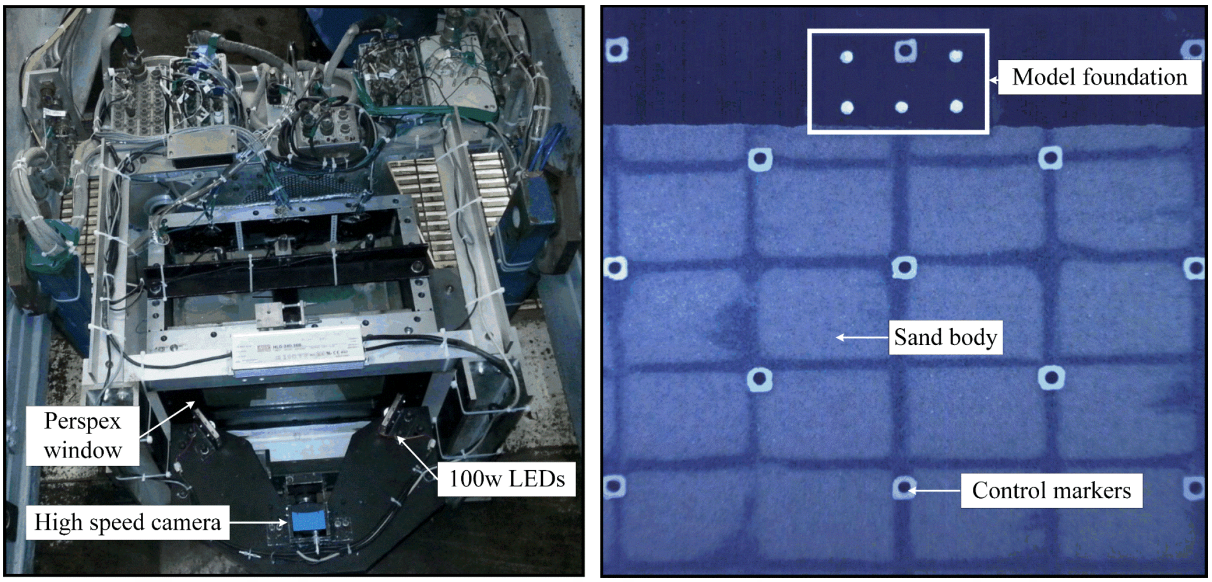

Figure 3.13– A view of the fully assembled centrifuge model loaded: PIV setup and typical PIV image.

3.3.6 Centrifuge Testing Procedure

The typical centrifuge testing procedure is as follows:

Model Package Setup

- assemble centrifuge model (saturated soil and instruments but no model foundation)
- load counterweight onto the centrifuge rotor arm (red end)
- load the SAM earthquake actuator onto the centrifuge rotor arm (blue end)
- carefully load saturated soil model onto the SAM actuator
- carefully position model foundation on the saturated soil surface (applicable to tests measuring the foundation response only)
- connect air injection system to air line supply on the beam centrifuge and soil model
- connect monitoring instruments to power supply and data acquisition system
- check response of all the instruments
- check that high-speed (PIV) camera lens is in focus and camera is operational
- check that camera trigger system works

Centrifuge Swing Up

- measure pre-test temperature and viscosity of pore fluid and record PIV image at 1-g
- swing up to desired centrifugal acceleration in increments of 10-g
- check the readings of LVDTs and PPTs in each 10-g

- take PIV image in each 10-g
- Data was logged at 100 Hz (model scale) during swing-up process. Recorded data was used to determine the initial conditions before any air injection or earthquake event.

At Desired Centrifugal Acceleration (Saturated Soil, Benchmark Tests Only)

- immediately fire earthquakes (maximum four consecutive earthquakes) and log data at 6 kHz (model scale) during shakings
- record PIV images during earthquakes (at 804 frames/second for 1.4 seconds)

At Desired Centrifugal Acceleration (Partially Saturated Soil Tests Only)

- inject air from the base of model before each earthquake (maximum four sets of air injection and associated earthquakes) and log data at 100 Hz during this process
- trigger earthquake approximately three minutes after air injection process ceases
- record PIV images before and after each air injection process and during earthquake

Once Experiment Completed

- swing down in steps of 10-g until complete stop and log data at 100 Hz (model scale)
- take PIV image in each 10-g
- measure post-test temperature and viscosity of pore fluid and soil surface level
- perform a preliminary assessment of the liquefaction effects and the performance of the applied mitigation measure based on the visual observations
- unload centrifuge model from the centrifuge rotor arm
- drain the pore fluid and carefully excavate model
- record final position of instruments (depth and horizontal distances)

Centrifuge Test Details

Each centrifuge test was undertaken in the same way: swing-up, air injection (when necessary), earthquake fire and swing-down. In some of the tests, additional test steps were followed to investigate the durability of air under simulated field conditions (see chapter 5). The different centrifuge models are summarised in table 3.5, and details of each centrifuge experiment can be found in appendix-A. The monitoring instruments were placed beneath the model foundations (Section 2) and in the free-field (Section 1 and Section 3). The locations of these instruments were consistent throughout the centrifuge test programme.

Table 3.5 – Centrifuge testing programme.

Sand Profile	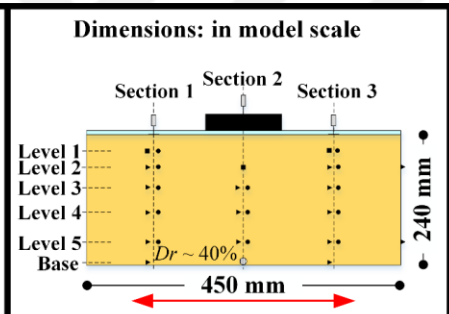			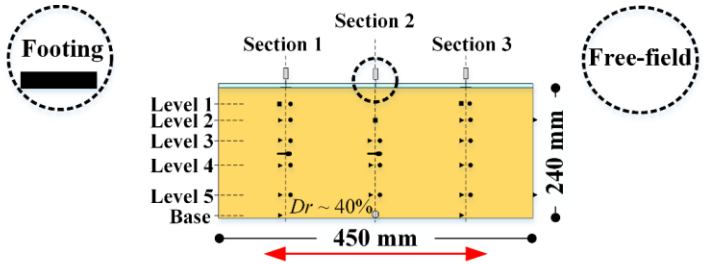				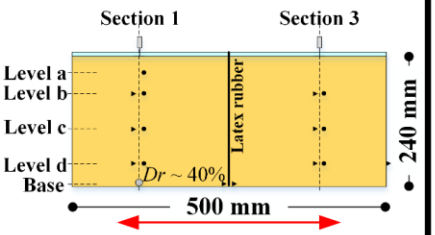	
Test ID	**CT1**	**CT2**	**CT3**	**CT4**	**CT5**	**CT6**	**CT7**	**CT8**	**CT9**	**CT10**
g-level	70			70			40	70	70	
Soil Condition	*Sat*	*Part*		*Sat*	*Part*		*Part*	*Sat & Part*	*Sat & Part*	*Sat & Part*
Footing Type	MF1			MF2			MF3	Free-Field	Free-Field	

Initial relative density of model ground is about 40% in each test. ***Sat*** and ***Part*** represent saturated soil (benchmark) and partially saturated soil (mitigated) test, respectively. The general convention for identifying the air injection and earthquake for each test is as follows: [*Centrifuge Test ID*, *Air Injection* or *Earthquake Number*]. For example, ***CT2EQ1*** represents the first earthquake event in test CT2 or ***CT2A1*** represents the first air injection process in test CT2.

Earthquakes Fired in Dynamic Centrifuge Tests

In each dynamic centrifuge test, successive earthquakes, in order of increasing amplitudes, were triggered using the stored angular momentum (SAM) actuator device. The earthquakes were parallel to the long side of models.

Typical input (horizontal) acceleration-time histories recorded during the tests can be seen in figure 3.14. The frequency of the earthquakes was kept the same during the dynamic centrifuge tests (except CT7). Peak input accelerations of approximately 0.18 g, 0.21 g and 0.23 g were acquired from the first, second and third shakings, respectively. An effort was made to fire the earthquakes with similar features to be able to make a direct comparison between the different tests. In many cases, this was accomplished, and the desired seismic motions were replicated satisfactorily. In some of the tests (CT5 and CT6), duration of the earthquakes was, however, much longer than usual (planned to last 28 seconds in prototype scale), despite the similarities in the amplitude of the earthquakes. This was due to the mechanical problems with the SAM actuator, and will be explained in section 3.5.3.1. The data from these tests allowed for the investigation of the performance of air injection during the prolonged earthquake events.

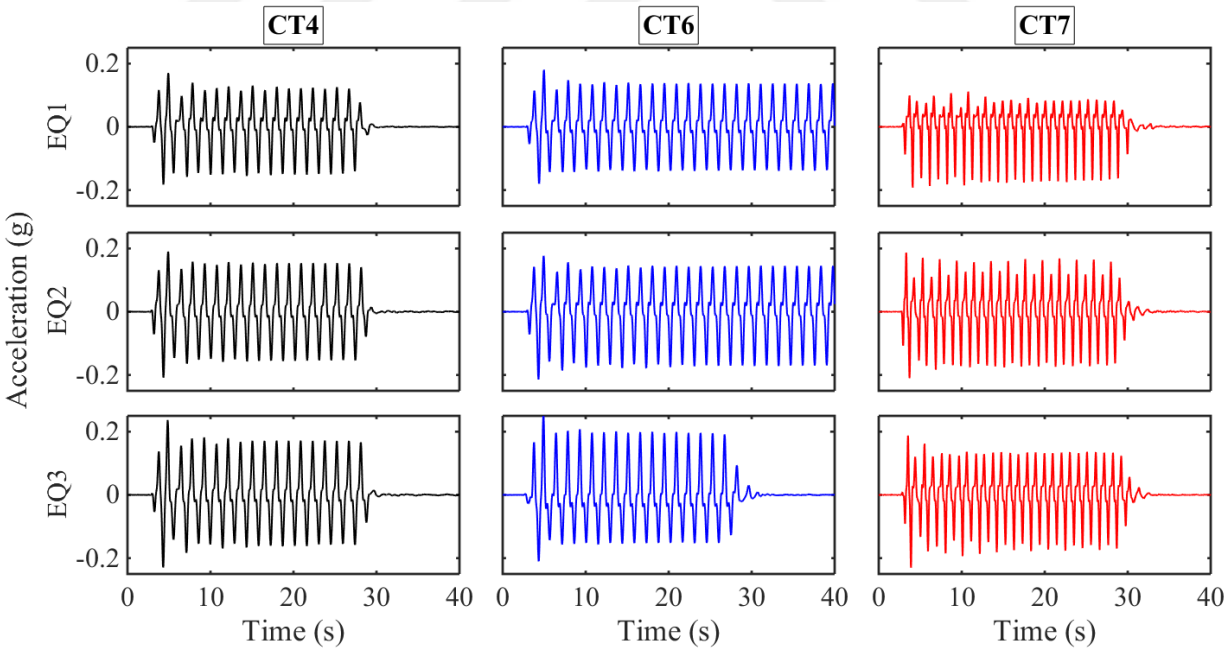

Figure 3.14– Typical input acceleration-time histories recorded in the centrifuge tests, in prototype scale.

3.4 1-g Shaking Table Tests

3.4.1 Shaking Table at the Schofield Centre

Physical modelling under the Earth's gravity is commonly used for geotechnical earthquake engineering problems since it is a less laborious, more easily accessible and economical option. Nevertheless, it cannot produce accurate prototype stress levels in small-scale models, and therefore cannot provide quantifiable data. Despite the aforementioned drawback, it offers an opportunity to gain qualitative information on the dynamic behaviour of soils and foundations. In this research, a series of three 1-g shaking table tests were undertaken. The aim of the tests was to explore the performance of air injection under low confining stresses and acquire a basic understanding on partially saturated soil behaviour beneath shallow foundations.

A shaking table available at the Schofield Centre was used to fire the earthquakes. The shaking table has an electric motor that stores angular momentum in a flywheel. This is then converted to the lateral shaking through a crank. It generates periodic simple nearly sinusoidal motion at a single frequency. A typical arrangement of the shaking table and soil model is shown in figure 3.15. PIV images were recorded during the shaking table tests using the high frame rate digital camera. The process of the PIV images allowed for the observation of the deformation mechanisms developed beneath shallow foundations.

3.4.2 Model Foundation

A strip model foundation, made of brass, was constructed for the shaking table tests. It was 50 mm wide, 30 mm high and 294 mm long. The model foundation spanned between the front viewing window and the rear wall of the model container (see figure 3.17b). The plane strain requirement was, hence, approximated in this plane. The bearing pressure exerted by the model foundation was 2.1 kPa. It was fully instrumented with MEMS to monitor accelerations at selected points of the foundation. An HDPE piece with added white markers was attached to the front face of the foundation to record the foundation movement with PIV (see figure 3.15).

3.4.3 Model Preparation-Sand Pouring and Saturation

The small-scale 1-g shaking table models were prepared in the same way as the centrifuge models. A rigid model container with a transparent Perspex viewing front was employed. Two

porous plastic tubes, connected to fittings available on the side walls of the model container, were laid on the base of the model container for the saturation of the models. An air diffuser was positioned at the base to perform the air injection, as shown in figure 3.16. Hostun HN31 sand was dry pluviated into the container using a manual overhead hopper to prepare 351 mm deep liquefiable soil beds at a relative density of about 40%. The instruments, including PPT, MEMS and piezoelectric accelerometers, were placed at the pre-determined locations in the shaking table models during sand pouring (see figure 3.16). It is worth mentioning that a series of ridges occurred in the sand due to the nature of the manual overhead hopper, which raised some doubts about the uniformity of the small-scale models for the 1-g shaking table tests.

Subsequently, the dry sand models were saturated very slowly by applying a gravity head and infiltrating de-aired water from the base. For the saturation process, a header tank filled with de-aired water was situated near the model container. The height of the water in the tank and rate of the water flow were carefully controlled to prevent model disturbance, such as boiling and piping effects. Following the saturation, the model foundation was carefully placed on the saturated soil surface. The instruments including LVDTs were connected to the data acquisition system. The lights and high-speed camera were set up accordingly to acquire PIV images.

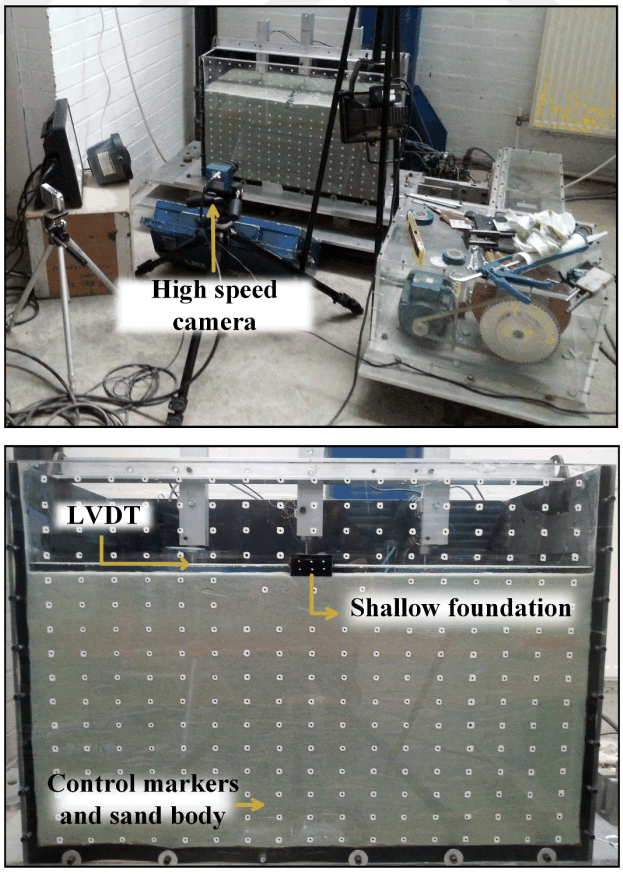

Figure 3.15– A view of the shaking table and model setup.

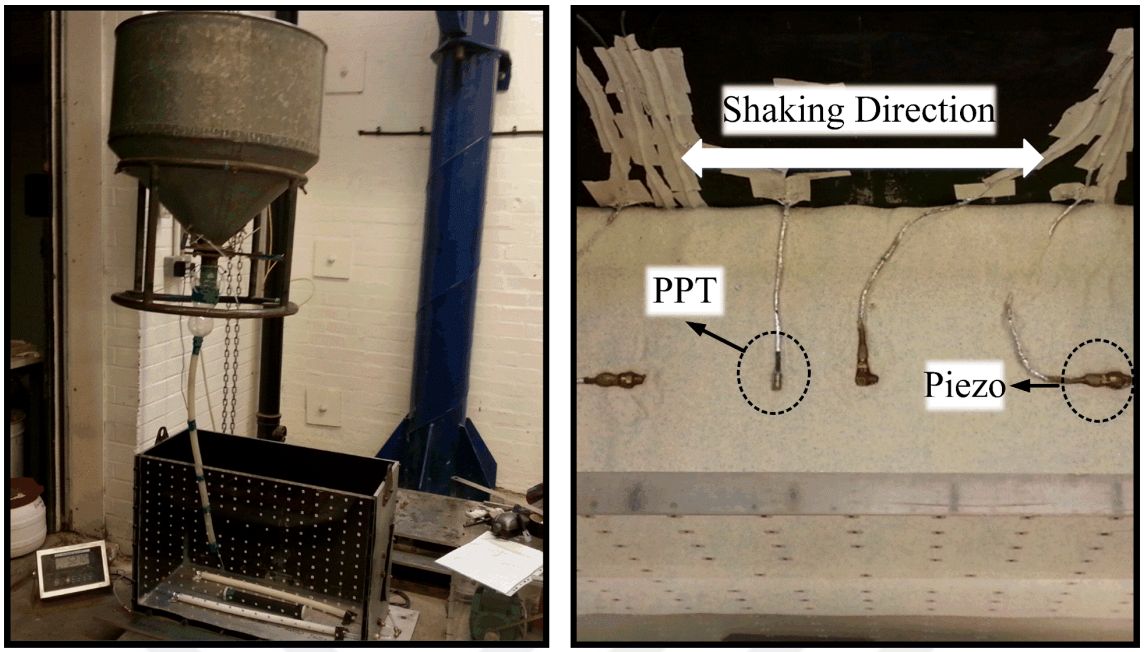

Figure 3.16– A view of the overhead hopper and instruments installed during sand pouring.

3.4.4 Model Preparation-Desaturation via Air Injection & Chemical

The saturated soil specimens were desaturated for two of the three shaking table tests. This was achieved by generating air/gas in ground using two different approaches, for comparison.

In one test, pressurised air was pumped into the saturated soil at a controlled pressure and flow rate in a similar way to the procedure described in section 3.3.4. In the other test, small gas bubbles were formed in a saturated soil through the reaction between a chemical compound, sodium perborate monohydrate (Efferdent tablets), and water. Prior to the sand pouring, Efferdent tablets were powdered and mixed with the dry Hostun sand at the pre-determined proportions. The prepared mixture was dry-pluviated into the model container. As the model was saturated, the reaction of the corresponding chemical compound with water occurred. This created oxygen bubbles within the soil model, which displaced the pore water upwards. Further information regarding this technique can be found in Gokyer (2009).

3.4.5 Shaking Table Testing Procedure

Three shaking table tests were conducted to assess the seismic response of shallow foundations resting on saturated and partially saturated soil deposits at 1-g. The test details are summarised in table 3.6. A cross-section and plan view of the 1-g shaking table models are also shown in figure 3.17.

The typical shaking table testing procedure is as follows:

Model Setup

- assemble shaking table model
- connect air injection system to air line supply and soil model
- set up high-speed camera and lights for PIV
- connect instruments to data acquisition system
- check response of all the instruments
- check that high-speed camera works and camera lens is in focus
- carefully position model foundation on the saturated soil

Desaturation

- inject air from base of model (SST2 only)
- allow one day for reaction to happen between chemical and water (STT3 only)
- log data at 100 Hz
- take PIV images before and after desaturation

Earthquake

- immediately trigger earthquake (STT1 only)
- trigger earthquake after desaturation (STT2 and STT3 only)
- record PIV images during earthquake
- allow sufficient time for excess pore pressures to dissipate once earthquake ceases
- log data at 1 kHz

Table 3.6 – 1-g shaking table testing programme.

Test ID	**STT1**	**STT2**	**STT3**
D_r **(%)**	43.2	39.1	40.7
Soil Condition	Saturated Soil (Benchmark or Unimproved)	Partially Saturated Soil (Improved via Air Injection Technique)	Partially Saturated Soil (Improved via Chemical Technique)
S_r **(%)**	96.8	90.2	89.8
Earthquake Parameters	**Frequency:** 3.5 Hz, **Amplitude:** 3.5 mm, **Duration:** 10 seconds (0.18 g Peak Input Acceleration)		

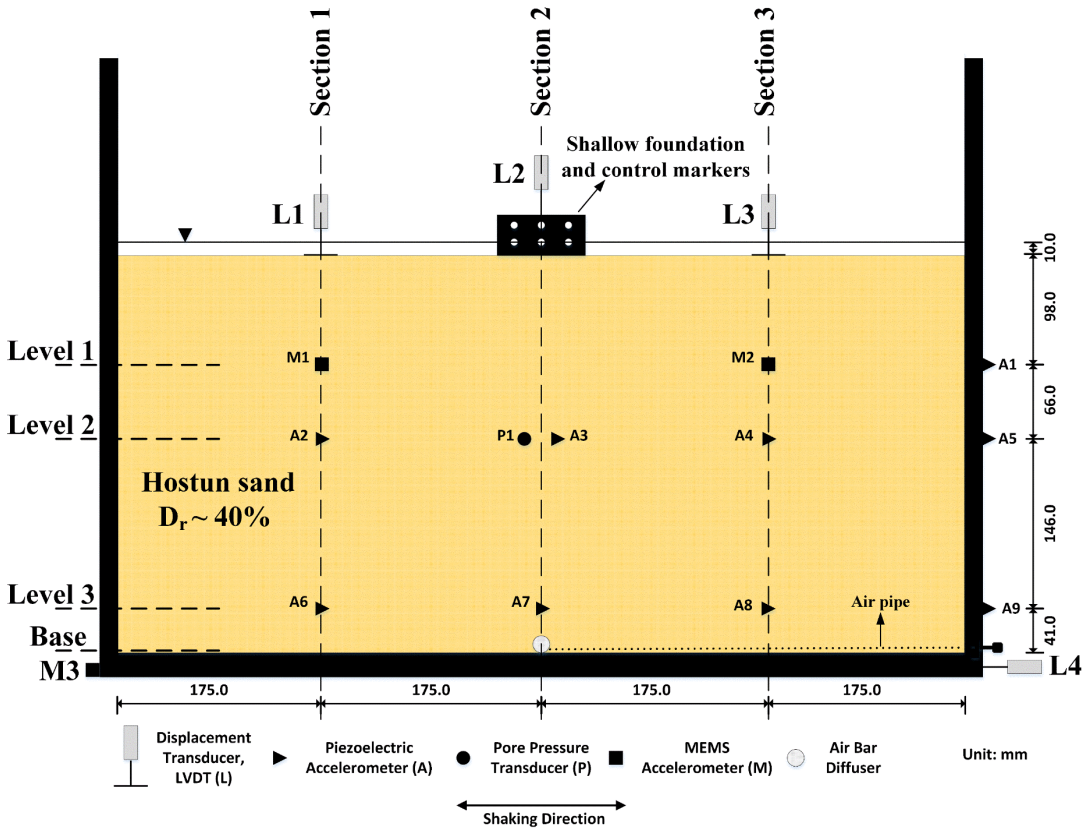

a) Cross section

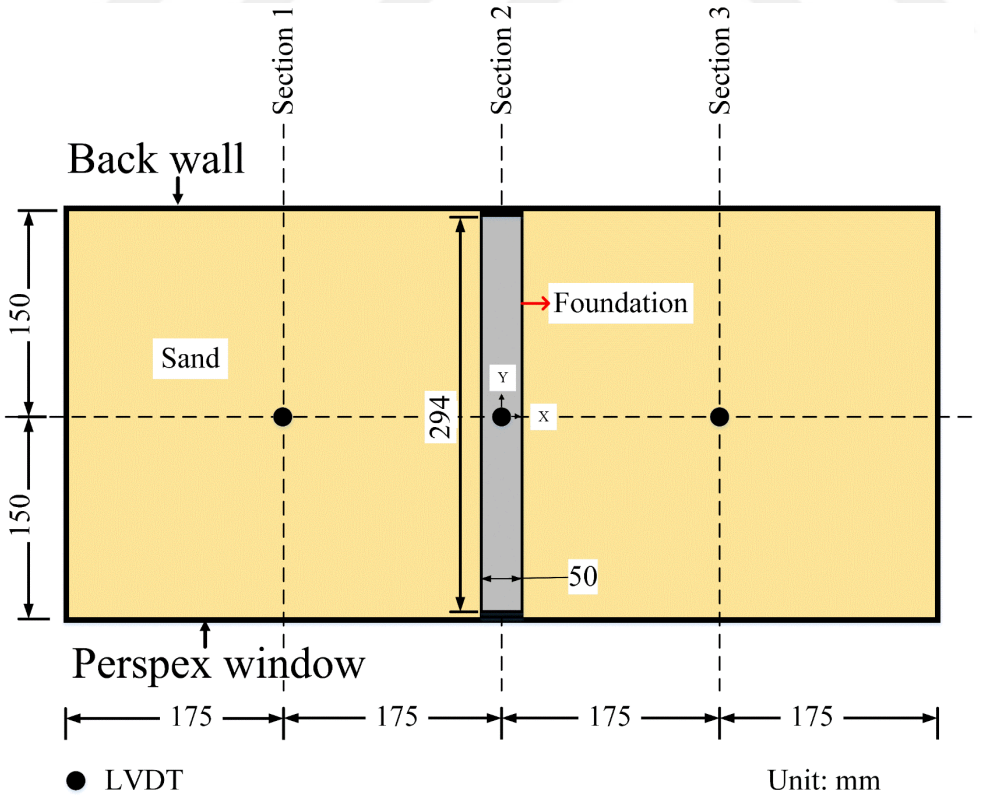

b) Plan view

Figure 3.17– Model layout for 1-g shaking table models.

3.5 Analysis Techniques

3.5.1 Data Processing and Data Presentation

The electrical voltage (signals) output from the monitoring instruments was recorded through the data acquisition system. MATLAB was used later to process the recorded data and produce the figures presented in this thesis. During the data processing, the data was filtered using a 4th order low-pass Butterworth filter with a cut-off frequency of 400 Hz. This was necessary to reduce high-frequency components in the signals due to electrical noise. Since the frequency of the earthquakes, usually 50 Hz in model scale, was substantially lower than the applied cut-off frequency, no significant information from the recorded data was removed. A '*filtfilt'* command available in MATLAB was utilised. Filtfilt is a zero-phase filtering method and filters the data twice, processing the data in forward and reverse directions. With this approach, it was ensured that the filtering process caused no permanent change in phase.
Once the recorded data was filtered and calibrated, the analysed data was presented in different forms, such as using the time domain. Unless otherwise indicated, all measurements presented in the result chapters (4-9) are in prototype scale. The analysed data, in fact, represents only a small portion of the analyses carried out but is representative of the larger data set.

3.5.2 Geo-PIV Analysis

Soil displacements beneath the shallow foundations were produced using the particle image velocimetry (PIV) technique. The analysis method and further details about the Geo-PIV software are given by White et al. (2003). Digital images were obtained using the high-speed camera. The images were processed, and the resulting displacements during the air injection and earthquake events were obtained in image space (pixels). These displacements were then converted to physical units (mm) using a series of black control markers at precisely known positions on the Perspex window. It must be highlighted that 10% of the Hostun sand in each model was dyed blue to increase the texture contrast in the images and to maintain a better tracking of the soil by PIV analysis. It was assumed that the dye had a negligible effect, if any, on the particle size distribution. In addition, in some of the tests, the concentrated blue sand was added horizontally and vertically in the front window to gain a visual indication of the accumulated displacement mechanisms. As indicated earlier, the model foundations, model containers and LVDT gantries were all painted matt black to minimise the glare from the lights.

Heron (2013) indicated that in order to acquire reliable results with the high-speed camera used, PIV analysis should only be performed on the green colour channel. Therefore, PIV analyses were performed using the green channel only. The displacement plots presented in this thesis were obtained using meshes with a patch size of 25 pixels and spacing of 20 pixels. With these selections, an accurate tracking and a higher density of displacement information were acquired. The search zone was selected to be 100 pixels. The search was always performed relative to the first images taken in order to minimise the accumulated errors.

3.5.3 Potential Errors

In this research, certain errors are expected to occur while acquiring and analysing the test data. The limitations, potential sources of errors and the problems faced during the 1-g shaking table and centrifuge-based experimental work are discussed briefly in this section.

3.5.3.1 Earthquake Events

During the dynamic centrifuge experiments, attempts were made to fire a sequence of earthquakes having a consistent frequency, size and duration. However, certain issues that took place with the SAM earthquake actuator rendered this difficult. The clutch that plays a major role in starting and stopping the earthquake loading did not work properly in tests CT5-CT7. During the first earthquake of CT5 and CT6, the electronic timer did not disengage the clutch automatically once the desired length of the earthquake was reached (0.4 s in model scale). Therefore, the earthquake had to be stopped manually. This produced earthquakes much longer than anticipated. During the first shaking of CT7, as the clutch centring mechanism did not operate correctly, the clutch was not centralised accurately, which produced an asymmetrical earthquake loading.

3.5.3.2 Model Layouts

The model layouts presented in this thesis represent ideal dimensions. The actual positions of some instruments may be marginally different due to the experimental difficulties encountered: pouring the sand to the precise depths or placing the instruments at the exact positions were hard. The nature of the tests may also contribute to this, wherein the positions of the instruments change while spinning-up the centrifuge and firing the earthquake motion. In addition, the actual properties of the soil models such as relative density may be slightly different from the

computed values. Careful handling and measurement of the position of each instrument, before and after the tests, were undertaken to minimise the potential errors stemming from these factors. In each case, the depths of the instruments were reassessed based on the hydrostatic pore fluid pressure measurements to enhance the reliability of the recorded data. It is, however, necessary to keep these pertinent issues in mind for the evaluation of the test results.

3.5.3.3 Instrument Readings

Some of the instruments used in the experiments caused erroneous data.

The MEMS and piezoelectric accelerometers measured the acceleration along their sensitive axis, which was parallel to the axis of shaking. Liquefaction of soil layers caused misalignment of certain accelerometers, leading to a reduction in the instrument output (applicable to a few tests only).

The LVDTs were used along with an extension spindle and a light circular plate. During the dynamic centrifuge tests, the plate was observed to settle into the soil due to its own and spindle's weight, resulting in some LVDT measurements being of slightly larger than the actual surface settlements. This particularly held true during the reconsolidation process in which the surface of the soil layer remained liquefied for longer. The centrifuge test CT8 provided PIV-based and LVDT-based displacement data for the soil response without shallow foundations. With the aids of such data, the shortcomings of the LVDT measurements are discussed below.

A comparison of the surface settlement captured by LVDT-L2 and PIV at the centre-top of the model ground is presented in figure 3.18. PIV data was available only for a short duration since the internal storage capacity of the camera was limited. The final PIV-based free-field settlements could, however, be estimated based on the analysis of the digital images recorded after the reconsolidation process, allowing approximately 2500 seconds in prototype scale from the end of the earthquakes. These settlements are indicated by the horizontal lines in the last time window of the figure.

It is obvious that the rate of co-seismic settlements, particularly during the first 11 cycles, was marginally different for the two methods of measurement. The maximum LVDT-based free-surface settlements at the end of the reconsolidation process were, however, found to be consistently greater than the PIV-based total surface settlements for all cases. For instance, the PIV-based total surface settlement of saturated soil in the first event of CT8 was approximately

86.7 percent of the LVDT-based total surface settlement, revealing a 13.3% error in the LVDT measurement. Figure 3.18 shows that despite some errors, LVDT measurements are not far off the actual surface settlements.

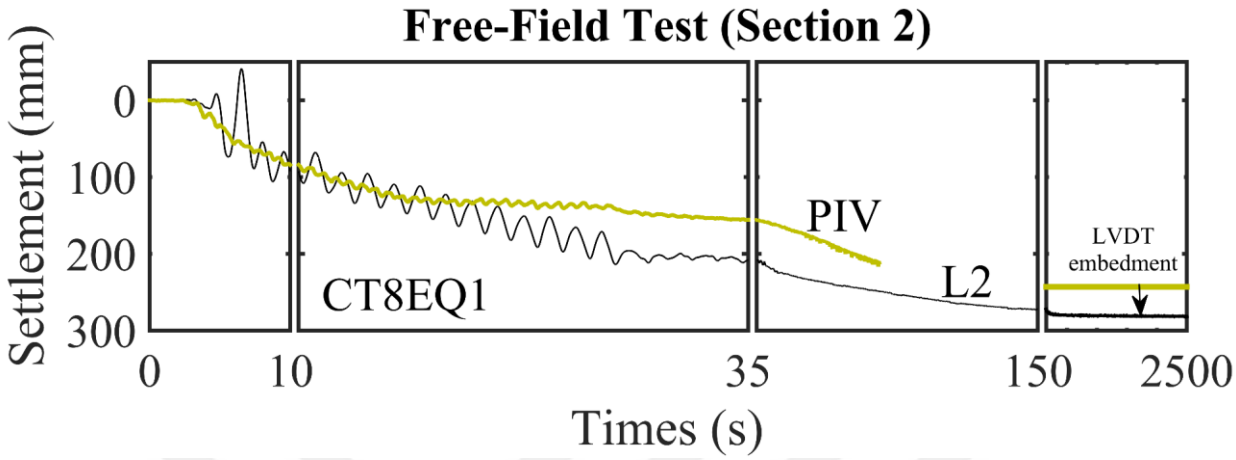

Figure 3.18– Co-seismic and post-seismic settlements based on PIV and LVDT.

3.5.3.4 Measured and Calculated Soil Properties

The measurements of the mass and volume of soil models may be subjected to certain errors. This was particularly relevant to the volume of soil specimens determined based on the soil height measurement. Any small inaccuracies in the soil height measurement would influence the computed soil volume and consequently the assessment of the dry and saturated density of the soil models. This, in turn, would affect the relative density of the soil deposits and the initial effective stresses calculated at varying depths. It was also within the realms of possibility that the errors in these model properties would ultimately contribute to the errors in the computed degree of saturation values.

In this research, the height of the centrifuge models was measured to an accuracy of ± 1 mm in model scale, which corresponded to a 0.41% error in the measured height values. Similarly, the mass of the soil models was measured to an accuracy of ± 0.2 kg, suggesting that the error in the measured mass of the specimens was 0.41%. Table 3.7 highlights the sensitivity of the density, ρ, degree of saturation, S_r, and relative density, D_r, of soils to the measurement errors. A saturated centrifuge specimen with ρ: 1900 kg/m^3, D_r: 41% and S_r: 99% was considered for this basic sensitivity study.

It is seen that for the conventional method of determining the relative density, a 0.41% error in the measured height and mass of the soil causes an error of ± 2 ($\sim$5% error) in computed D_r.

In the same way, 0.41% errors in the measured soil height and mass would lead to 1% and 2% estimated error in calculated S_r, respectively.

Table 3.7 – Sensitivity of basic soil parameters to measurement errors.

	$\pm 0.41\%$ Error		
Source of Error	ρ (kg/m^3)	D_r (%)	S_r (%)
Soil Height	1892-1908	39-43	98-100
Mass	1892-1908	39-43	97-101

3.5.3.5 Limitations on use of 1-g Shaking Table

Unlike in undrained element tests, the mechanism of partial drainage can be represented in small-scale 1-g shaking table tests, permitting the occurrence of drainage in the event of an earthquake loading. In addition, the deformation mechanisms that develop beneath the shallow foundations can be observed combining the 1-g shaking table tests with PIV analysis (Knappett et al. 2006).

Despite the wealth of information that 1-g shaking table tests can provide, they are incapable of replicating the correct stress state in the field, and therefore are unable to present accurate stress-strain conditions in the soil. Given the nature of 1-g testing, it should therefore provide qualitative answers to the problems under consideration only.

Chapter 4

Physical Modelling of Air Injection

4.1 Introduction

Some in situ tests have been conducted to examine the technical feasibility of air injection as a way of reducing degree of saturation of the free-field soil deposits (Okamura et al. 2011). At present, only a few effective guidelines are available to engineers for its application and performance. In particular, the way that air should be injected appropriately in the presence of structures has not been thoroughly examined. The distribution of entrapped air and its effects on the seismic response of soils also need further investigation.

The aim of this chapter is to provide insights into the effective way of executing air injection in the centrifuge and to examine the distribution of air bubbles trapped in soil deposits. This chapter also aims to briefly discuss the methods used for the assessment of degree of saturation. The results from centrifuge tests are presented along with a background for each subject. Some of the results presented in this chapter can be found in Zeybek and Madabhushi (2017c).

4.2 The Execution of Air Injection

Okamura and Teraoka (2005) carried out a series of 1-g shaking table experiments at different atmospheric pressures to examine the effectiveness of air injection in mitigating liquefaction in level ground and beneath rigid foundations. For the same purpose, a series of two centrifuge experiments were performed by Marasini and Okamura (2015). For the centrifuge tests, the air was injected into saturated, loose sand deposits at 50-g using an injector placed in a bottom layer of dense sand. It was reported that shallow foundations resting on the loose sand deposits settled approximately 2.5 mm (prototype scale) during the air injection process.

In fact, the effective use of air injection technique in engineering practice may require a thorough understanding on the magnitudes and rates of the applied air injection pressure. Published experimental results suggest that air injection pressure is an important parameter for this technique since an excessive air injection pressure may disturb the soil structure and cause cracking and fissuring, particularly near the air injection point. Some theoretical relationships were proposed for the maximum air injection pressure. For instance, Ogata and Okamura (2006) postulated the theoretical maximum air injection pressure above which soil can be disturbed, as given by equation (4.1).

$$(P_{inj})_{max} = P_{hyd} + 0.5 \cdot \sigma'_{v0} \tag{4.1}$$

where $(P_{inj})_{\max}$, P_{hyd}, σ'_{v0} represent the maximum air injection pressure, hydrostatic pressure and initial vertical effective stress at the injection point, respectively.

The main issue regarding the implementation of air injection beneath existing structures is the settlement of foundations that they are founded on. The above experiments, while establishing the success of the air injection technique in reducing the liquefaction risks, do not focus on the soil deformations and settlements that shallow foundations can suffer during its application, which is vital for the safety of the superstructures. The results from centrifuge tests are expected to shed light on this problem.

4.2.1 Air Injection Pressure versus Settlement

In the air injection phase of the centrifuge tests, air was supplied into the soil through the air bubble curtain located on the centre-bottom of the model (see section 3.3.4). This air curtain extended along the plane strain direction and represented a two-dimensional air flow condition. The air injection pressures were measured at a point right before the air curtain, as shown in figure 3.11. It was found that the successful application of this technique depends on the way that it was performed in the laboratory.

Figure 4.1 presents typical examples of pressure-time and foundation settlement-time histories recorded during the air injection process. In the same figure, the change in the height of the pore fluid calculated using the pore fluid pressure recorded above the soil surface (P14) is also depicted. The time axis is split into four parts to discuss the main features of the observed trend within each part. It is apparent in figure 4.1 that air bubbles can be trapped in the saturated specimens only when the air injection pressure reached the sum of hydrostatic pressure, P_{hyd},

at the injection point and air entry value, *AEV*, of soil. The pressure required to initiate air flow in the saturated medium refers to the minimum air injection pressure, $(P_{inj})_{min}$. The published studies on Hostun sand showed that this type of clean sand has an air entry value of 1.3 kPa, as presented in figure 2.11.

In figure 4.1, two different air injection approaches are compared. In CT2A1, air injection pressure was increased rapidly until air bubbles became apparent on the ground surface. This caused a foundation settlement of 2.57 mm in model (180 mm in prototype) scale, which would not ideally be acceptable if this technique was applied to a field structure. In CT3A1, a different approach was taken in which air injection pressure was increased gradually, and the response of the foundation was scrupulously monitored. In this case, the maximum air injection pressure, $(P_{inj})_{\max}$, was lower. In addition, air (injection)-induced foundation settlement was only 0.2 mm in model (14 mm in prototype) scale, which is much smaller and acceptable.

To provide a better understanding, a detailed discussion of the time history of figure 4.1 is given. For CT2A1, the first time window shows that air injection pressure increased rapidly. Air flow into the soil did not start until air injection pressure increased beyond the minimum air injection pressure, $(P_{inj})_{min}$. When air started to enter the soil, pore fluid began to move upwards, which in turn increased the pore fluid height. The initial increase of pore fluid height occurred at 57 s. Air injection pressure increased further and reached its highest amplitude (~211 kPa) at 64 s. This corresponded to the time when the foundation started to settle. A possible explanation for the foundation settlement is the upward migration of pore fluid that gradually reduced effective stresses and caused localised soil-softening below the foundation (see section 7.2.2). As the pore fluid continued to flow upwards during the next 20 s, more of the foundation soil got softer, which caused a complete bearing capacity type of failure. At this moment, the rate of settlement that foundation suffered increased significantly. At the endpoint of the third time window, the settlement of foundation almost ceased, which coincided with the time when air started to flow more along the rear wall of the model box (see section 4.4.1).

For CT3A1, air injection pressure gradually increased and reached its maximum value (~183 kPa) after 133 s. The peak air injection pressure was corresponding to the beginning of the foundation settlement. Pore fluid height started to increase after reaching $(P_{inj})_{min}$. Once air injection halted, the pore fluid height reduced to a residual value, which was primarily ascribed to excess/free air that escaped to the atmosphere. The soil below the foundation did not soften enough for a complete bearing capacity failure to form, minimising the foundation settlements.

The results above suggest that the amplitude of air injection pressure and the rate of air injection have a significant effect, but the former seem to dominate the settlement that the foundations suffered during the air injection process.

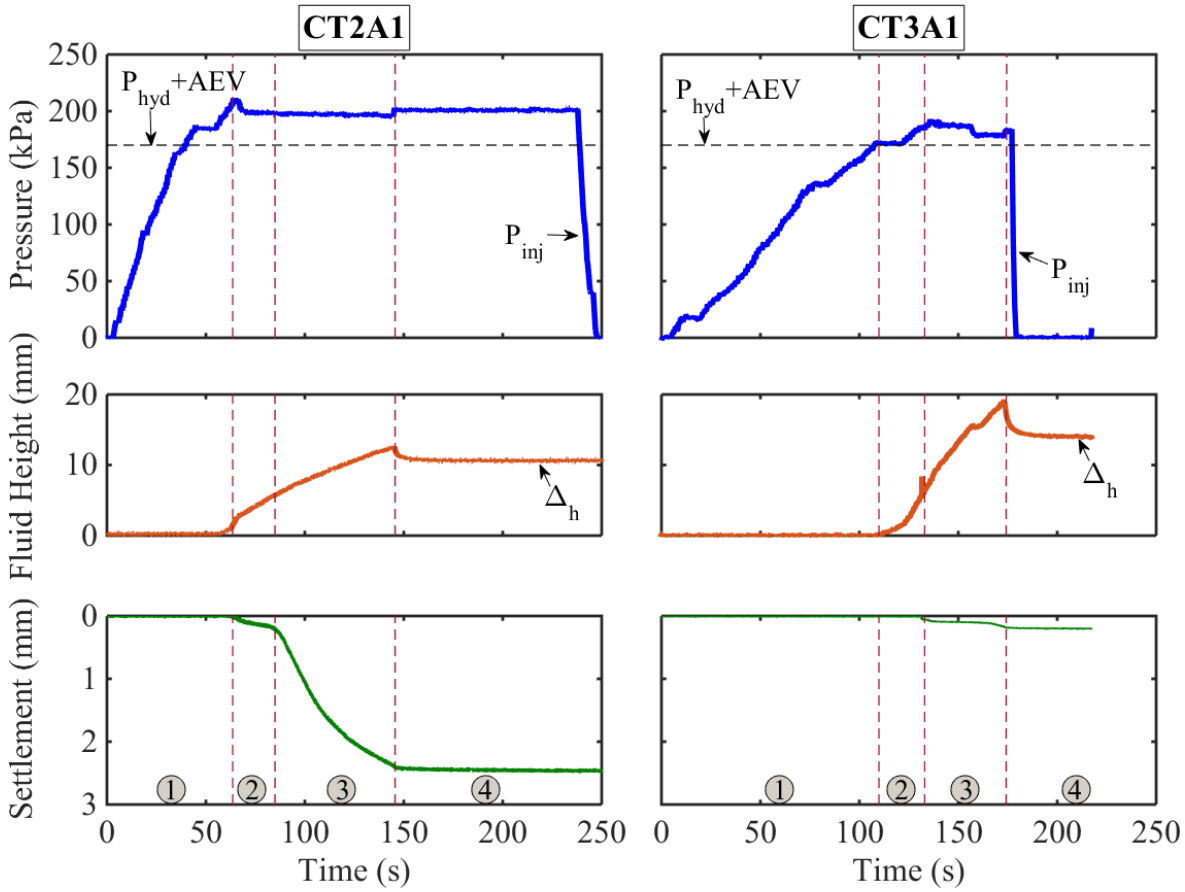

Figure 4.1– Time histories of pressure, change in fluid height and foundation settlement recorded during the air injection process, in model scale.

4.2.2 Air Injection Pressure versus Soil Deformations

Figure 4.2 shows typical examples of the soil deformations that developed beneath the shallow foundation (CT6A1) and in the free-field (CT8A1) during the air injection process. It is noted that details regarding the mechanisms that govern the soil deformations during the air injection process can be found in section 7.2.2.

For CT6A1, the maximum air injection pressure was equal to the sum of the hydrostatic pressure and about 0.12 times of the initial vertical effective stress (σ'_{v0}) at the injection point. In this case, the foundation settled approximately 21 mm in prototype scale (see figure 4.2a).

For CT8A1, the maximum air injection pressure was equal to the sum of the hydrostatic pressure and approximately 0.1 times of σ'_{v0}. This led to vertically downwards displacements in the free-field and an average settlement of 15 mm in prototype scale (see figure 4.2b).

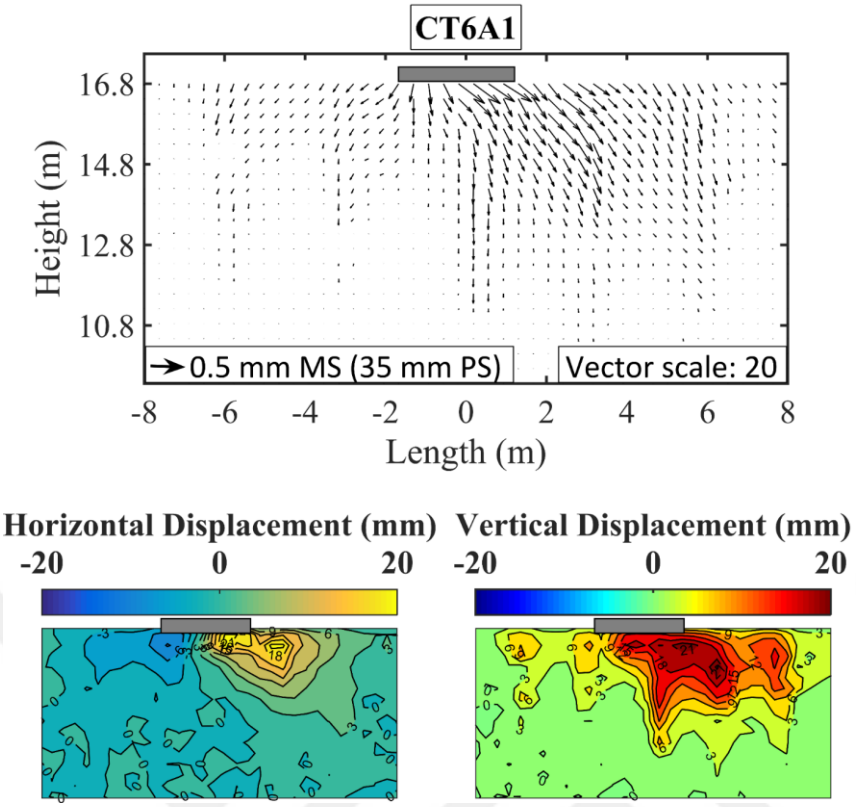

a) CT6 (beneath shallow foundation)

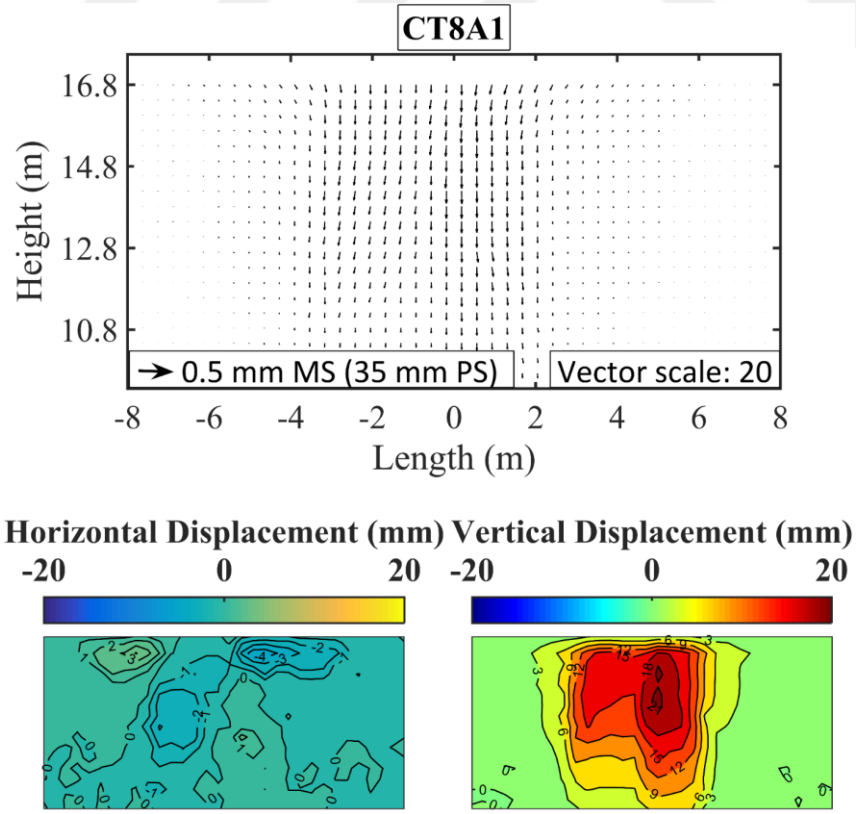

b) CT8 (in level ground)

Figure 4.2– Typical air injection-induced soil deformations.

4.2.3 Control of Air (Injection)-Induced Foundation Settlement

Typical test results corresponding to the air injection process are summarised in table 4.1. It can be clearly seen that air (injection)-induced settlements were inevitable, irrespective of the air injection pressure. This is due to the compressible nature of partially saturated soils and effective stress drop during the air flow (see section 7.2.2). However, based on the findings presented here and observations made during the tests, it can be suggested that the magnitude of air-induced settlements can be considerably minimised if

- A well-controlled test procedure is rigorously maintained (e.g. increasing the air injection pressure in a controlled manner and carefully monitoring of the foundation response). Gradual application of air injection (with a low air injection rate) is proven to be a necessary step towards limiting the possible foundation settlements.
- The applied net air injection pressure, $(P_{inj})_{\text{net}}$, given in equation 4.2 is kept small (ideally maximum 10 percent of σ'_{v0} such as in test CT6A1).

$$(P_{inj})_{net} = (P_{inj})_{max} - (P_{inj})_{min} \leq 0.1 \cdot \sigma'_{v0} \tag{4.2}$$

Air (injection)-induced settlements can remain within acceptable limits for a real structure in the field if a small net air injection pressure is applied. However, applying small air injection pressures may impact on the area and distribution of partially saturated zones. This will be examined in section 4.4.

Table 4.1 – Typical settlement data corresponding to the air injection phase.

	Test data			
Test ID	**Foundation bearing pressure q (kPa)**	**Maximum air injection pressure $(P_{inj})_{max}$ (kPa)**	**Net air injection pressure $(P_{inj})_{net}$ (kPa)**	**Settlement in prototype scale S (mm)**
CT2A1	135	210.5	40.5	180.0
CT3A1	135	183.1	13.1	14.0
CT5A1	50	170.5	0.5	9.6
CT6A1	50	185.6	15.6	21.3
CT8A1	Free-field	180.4	10.4	15.0

4.3 Assessment of Degree of Saturation, S_r

In geotechnical earthquake engineering, the presence of air bubbles in soils, and hence S_r, is important since it affects the compressibility of the pore fluid that fills the pores between soil

grains. This, in turn, influences the liquefaction resistance and permeability, k, of soils. An inaccurate measurement of S_r can lead to an overestimation or underestimation of the cyclic strength of soils. For element testing and physical modelling, an accurate assessment of S_r is, therefore, particularly important. Various ways are available to the engineers for its assessment, such as measuring the electrical resistivity; P-wave velocity; weights and volumes of solids, water and air; dielectric constant and estimating the Skempton's pore pressure parameter.

Conventionally, S_r is determined in the laboratory by comparing the weights of saturated soil samples before and after drying so that the amount of water in soil samples can be calculated (Luthin and Miller 1953). In cyclic triaxial testing, the Skempton's B-value is typically used to check S_r of the specimens. This approach is, however, hard to use for the 1-g shaking table and centrifuge tests. Similarly, P-wave velocity measurement (V_p) is widely used as an indicator of S_r. Naesgaard et al. (2007) showed that this technique is a good indicator of S_r if the air bubbles are small in size, and well-distributed among all the pore spaces. This technique was, however, found to be less successful when the size of air bubbles is large, and the bubbles are scattered non-uniformly. Furthermore, for partially saturated soils (typically $S_r \leq$98%), the use of V_p was shown to be unrealistic (e.g. Okamura et al. 2006). This was ascribed to the fact that V_p in soils gets closer to the velocity of the sound in the air and becomes insensitive to changes in the lower ranges of S_r. This was later confirmed by Eseller-Bayat (2009), suggesting that this technique has some limitations in capturing the changes in degree of saturation of the soils, particularly for S_r <95%.

With recent developments in technology, various methods are recommended to determine S_r, including electrical resistivity tomography (Consentini and Foti 2014) and time domain reflectometer (Robinson et al. 2003). A major limitation of such techniques is that they are capable of measuring S_r only at discrete points. Therefore, alternative methods are proposed to evaluate S_r of a continuous region, such as digital imaging technique (Yoshimi et al. 2011) and high-resolution measurement (Okamura and Inoue 2012).

Researchers, who investigate the air injection technique, often use conventional mass-volume relationships to assess S_r of the soil models (e.g. Marasini and Okamura 2015). In these studies, it is a common assumption that the volume of air bubbles trapped inside the soil is equal to the volume of pore fluid replaced by the entrapped air bubbles. In this thesis, S_r of the specimens was evaluated using two different approaches: mass-volume relationships and soil moisture sensors (Vegetronix). Each method will be briefly discussed next.

4.3.1 Degree of Saturation Based on Mass-Volume Relationships

Degree of saturation of saturated specimens was calculated using the known mass and volume of dry soil & pore fluid. It was found that initial (pre-test) S_r of all the centrifuge specimens was consistently above 99% across the soil models. For the partially saturated soil tests, S_r was computed based on the volume of residual air bubbles that were trapped in the specimens.

Figure 4.3 shows the pressure-time and degree of saturation-time histories recorded during the air injection process in CT5A1 and CT6A1. In these tests, air injection was performed in a controlled manner, as explained in section 4.2.3. Air bubbles started to enter the saturated soil when the minimum air injection pressure, $(P_{inj})_{min}$, was reached. The net air injection period, $(T_{inj})_{net}$, is the time from the initiation of air flow to the cessation of air flow in the soil. The pore pressure transducer installed above the ground level (P14) continuously provided data on the evaluation of fluid level. As seen in figure 4.3, the fluid level, therefore pore fluid pressure, increased due to the volume of air bubbles trapped in the soil. The change in average S_r of the soils across the model ground with time was evaluated using the soil phase (mass-volume) relationships and equation (4.3).

$$S_r(t) = S_{r0} - \frac{\Delta h(t)}{H_s \cdot n} \tag{4.3}$$

where S_{r0}, Δh, H_s and n are the initial degree of saturation, change in the fluid level, the height of soil and porosity, respectively. It is noted that n was assumed to remain constant with time.

It is worth noting that in addition to pore pressure transducers, the variation of the fluid level was monitored using a metre scale on the Perspex window. The comparison of the results from the two approaches indicated that the shallowest transducer (P14) provided very similar results with the metre scale readings. The average degree of saturation of partially saturated soils was, therefore, reliably quantified based on the readings from this instrument.

It is evident from figure 4.3 that in CT5A1, the applied air injection pressure was kept almost same as the minimum air injection pressure. The air injection pressure was reduced as soon as air bubbles began to enter the saturated medium, and it was halted following a 103.2 s (in model scale) of net air injection. This led to an average S_r of 93.1% across the soil layer. Nevertheless, in CT6A1, air injection pressure was kept reasonably above the minimum air injection pressure. Air injection was halted after approximately 80.4 s from the initiation of air flow in the soil, resulting in an average S_r of 79.5%.

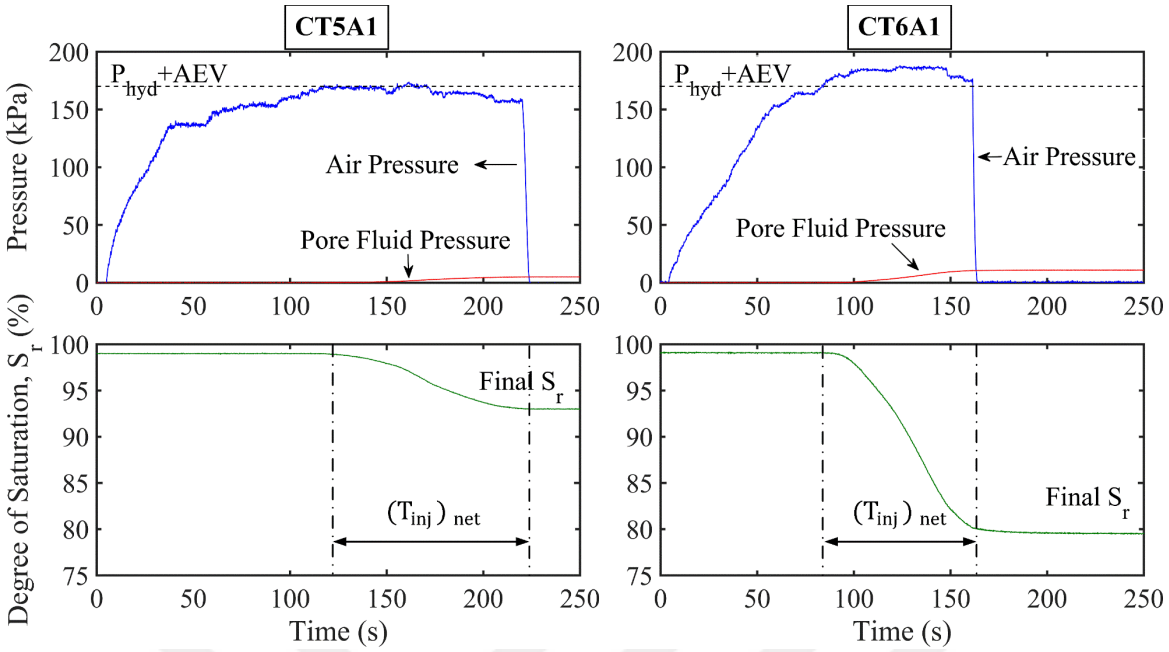

Figure 4.3– Time histories of pressure and degree of saturation in the air injection phase, in model scale.

Table 4.2 provides a summary of the test data relevant to S_r of the specimens following the air injection process. It is seen that final volume of the air trapped in the soils was a function of air injection pressure. The average S_r values usually decreased with increasing air injection pressure. The experimental data in CT2A1 was, however, out of trend. This was ascribed to the preferential flow paths that formed during the air injection process (see section 4.4.1).

It is worth mentioning that air injection pressure and time were primarily decided based on the need to desaturate the soils under controlled conditions. Observational and experimental findings were combined with an engineering judgement for this purpose. In all the tests except CT2A1, the amplitude of maximum air injection pressure was selected so that it would not cause significant foundation settlement. The total duration of air injection was defined based on the change of soil colour and pore fluid height that determines the change in S_r of the soil.

Table 4.2 – Typical degree of saturation data corresponding to the air injection phase.

	Test data			
Test ID	**Foundation bearing pressure q (kPa)**	**Maximum air injection pressure $(P_{inj})_{max}$ (kPa)**	**Net air injection period $(T_{inj})_{net}$ (s)***	**Average final degree of saturation S_r (%)**
CT2A1	135	210.5	200.2	89.0
CT3A1	135	183.1	60.1	86.0
CT5A1	50	170.5	103.2	93.1
CT6A1	50	185.6	80.4	79.5
CT8A1	Free-field	180.4	79.6	86.58

*: unit in model scale (MS)

4.3.2 Degree of Saturation Based on Soil Moisture Sensors

For the soil column experiments and some centrifuge tests, VH400 soil moisture sensor probes (Vegetronix) were used to assess S_r, along with the conventional mass-volume relationships.

Figure 4.4 depicts time histories of the degree of saturation recorded during the first and second air injection phases in centrifuge tests CT7 and CT8. It can be seen that S_r of the soil specimens was approximately 99.0% before the desaturation of models. This was verified by both mass-volume relationships and moisture sensor readings. As air was injected into the saturated soils, readings of the moisture sensors notably changed.

Comparison of the results in figure 4.4 indicates that similar final S_r values were achieved from both approaches, but the pattern of the variation of S_r with time differed. There was some delay in the response of soil moisture sensors, which was ascribed to the nature of these sensors that could provide a localised measurement of S_r only.

The entrapment of air bubbles started from the bottom up. This led to an earlier variation in average global S_r across the soils, calculated based on the conventional mass-volume method. The soil moisture sensors were located at the mid-depth of the centrifuge specimens, and the readings from these sensors changed only when they interacted with air bubbles, which caused a delayed variation in S_r. In fact, the readings from the soil moisture sensors provided further evidence of the presence of air bubbles trapped in the partially saturated soils. They also gave confidence over the reliability of S_r values computed based on mass-volume relationships.

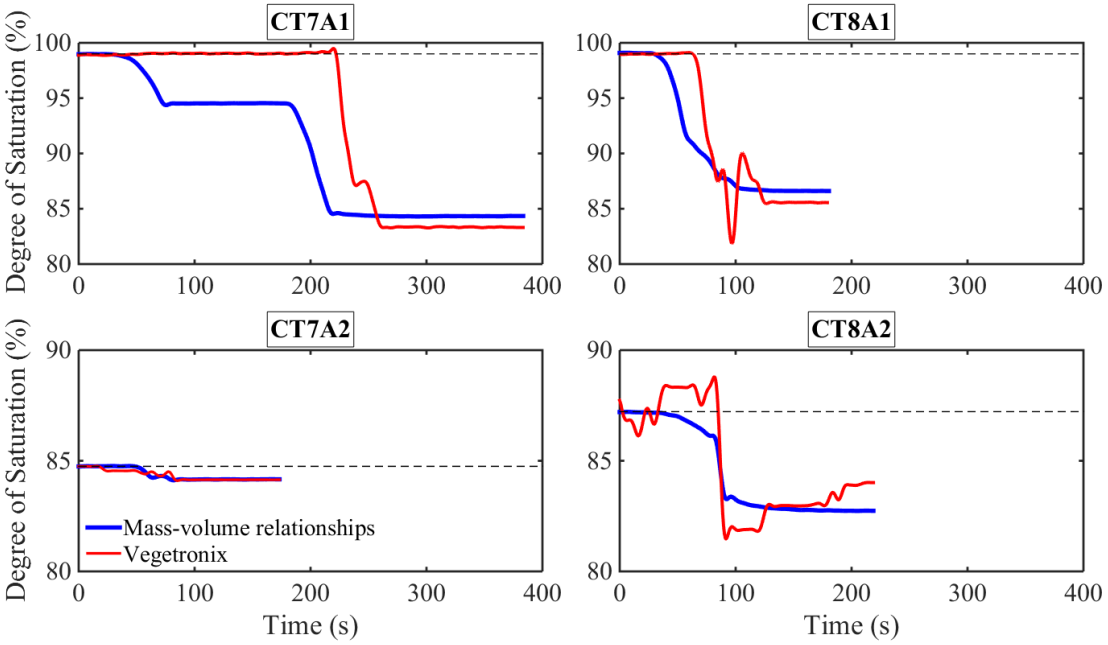

Figure 4.4– Time histories of degree of saturation, in model scale.

4.4 Distribution of Entrapped Air Bubbles

The zone of influence and distribution of air bubbles retained in soil deposits are of significance for the effectiveness of air injection technique in reducing liquefaction risks. The liquefaction resistance may vary at discrete points of the soils when entrapped air bubbles are distributed heterogeneously. The efficacy of air injection technique may also remain limited at locations away from the air injection points.

Air sparging techniques (injection of gas) are widely used in the field to remediate groundwater contaminated by volatile organic compounds (Marulanda et al. 2000). An interesting aspect of published air sparging studies is the prediction of air flow pattern and assessment of the zone of influence. These studies indicate that the effects of micro/pore scale parameters such as grain size and soil heterogeneity determine the air flow pattern. Zone of influence is, however, governed by the macro scale parameters that include the type of soil, air injection pressure, air flow rate, air injection depth and mode of air injection. Reddy and Adams (2001), for instance, demonstrated that air injected during air sparging process travels through the surface along a path of less resistance. Injected air in a heterogeneous soil tends to bypass the regions with lower permeability and flow directly towards the regions with higher permeability.

Similarly, the zone of influence was studied experimentally or through numerical simulations. Semer et al. (1998) observed that injected air travels laterally and vertically through the homogeneous porous media by increasing the radius of influence zone. The shape of the air plume was either a parabolic U or a conical V shape, and was usually symmetrical. The air saturation in oil reduced with increasing radial distance from the injection point. The zone of influence increased with increasing injection depth until a limiting depth was reached.

The objective of this section is to examine whether the liquefiable soils can be homogeneously desaturated and to what extent the air-entrapped zone affects the seismic behaviour of soils.

4.4.1 Effective Air-Entrapped Zones

The injection of air into the saturated soils was observed to change the colour of soils in the centrifuge tests. The colour of the desaturated (partially saturated) zones was much brighter compared with the saturated zones, and this was clearly visible in the front window. Two-dimensional (2-D) digital images and digital videos were recorded before, during and after the air injection process. The digital images were processed with the image processing toolbox of MATLAB. Image subtraction was used to calculate the difference between each corresponding

pixel in the two images recorded before and after the air injection process. Subtracting one image from another allowed to identify the effective air-entrapped zones (zone of influence). Figure 4.5 addresses the distribution of entrapped air bubbles in the partially saturated soils, approximately defined based on the colour change.

Figure 4.5a provides an example of the estimated shape of the effective air-entrapped zone for CT7A1. This approximate effective air-entrapped zone is highlighted by the broken curve. The area that can be monitored on the Perspex window did not cover the entire soil model. Thus, the actual position of the air injector was below the image. It is evident that the shape of the air-entrapped zone was virtually symmetrical and an almost U, engulfing the majority of the instruments placed.

Figure 4.5b shows the approximate effective air-entrapped zones for the other centrifuge tests. It is seen that the colour of the soil varied within the effective air-entrapped zones (e.g. CT3A1). This indicates that air bubbles were retained non-uniformly within these zones. The comparison of CT5A1 with CT6A1 shows that S_r of soil was much lower, and a much wider air-entrapped zone was observed in the latter. The distribution of air bubbles in this zone was also more uniform, creating a relatively more homogeneous partially saturated soil layer in CT6A1.

The different observations in the tests are attributable to air injection pressure and preferential flow paths in the saturated medium. It was found that the higher the air injection pressure, the wider and the more uniform the effective air-entrapped zone that was attained, which seems to be consistent with the published experimental data (Yasuhara et al. 2008). With a smaller net air injection pressure, it was, however, found very challenging to achieve uniformly distributed air-entrapped zones. Furthermore, the injected air had a tendency to flow through the surface along a path of less resistance (preferential flow pathways), particularly during CT8A1.

Most of the experimental results were in accordance with these findings, except CT2A1. The different behaviour in CT2A1 was attributed to preferential flow pathway that formed along the back wall of the model box. As indicated in section 4.2.1, relatively high air injection pressure was applied in this test. Visual observations, based on the digital videos taken during the course of this test, revealed that injected air started to flow mostly through the back wall of the model box after approximately 80 s from the initiation of air flow in the soil model.

It is worth mentioning that the 2-D image analysis performed here can provide no more than a rough estimate of the distribution of air bubbles. This is believed to be satisfactory for the scope of this study. However, such estimate ought to be considered with caution if the researchers want to more precisely identify the interaction between the desaturated and saturated soil zones.

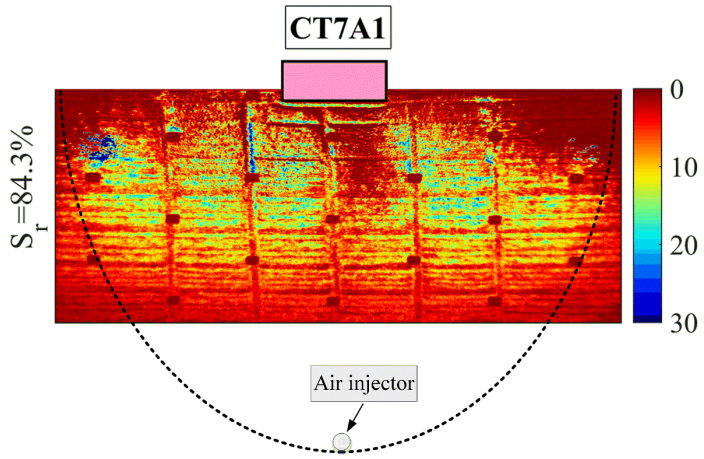

a) Estimated shape of the air-entrapped zone

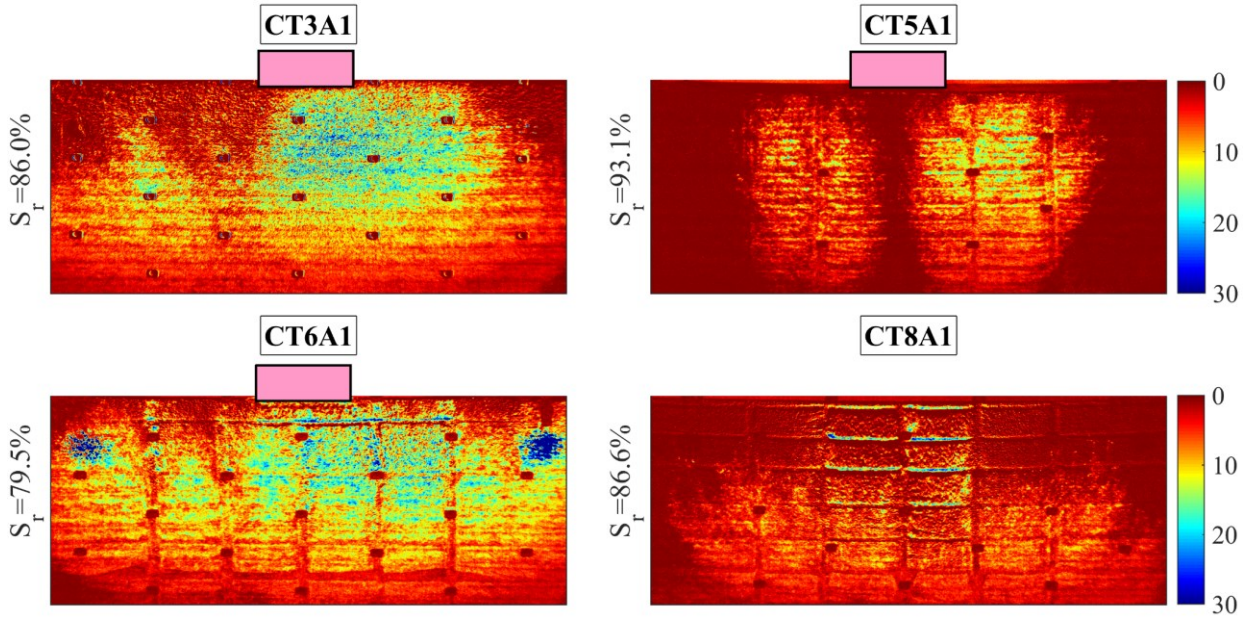

b) Effective air-entrapped zones

Figure 4.5– Distribution of air bubbles. The brighter colour is indicative of air bubbles.

To explore the size and state of the entrapped air bubbles in the partially saturated soils, high-quality images were taken using a set of high-resolution digital camera, special lens and LED lights. Enlarged digital images of the soil specimens at different locations were obtained. Figure 4.6 presents a typical example of the soil conditions after air injection and the state of the air bubbles in the soil. The identification of the pore fluid was hard to discern due to its colourless nature, but the dark colour of the soil specimen indicated that the soil outside of the effective air-entrapped zone was virtually saturated. On the other hand, the soil within the effective air-entrapped zone was partially saturated. The entrapped air bubbles were clearly identifiable as the shiny particles reflecting the LED lights. The size of the air bubbles was usually smaller or same order than the size of the soil particles. In this research, air bubbles

were below the phreatic surface where the hydrostatic pore fluid pressures were positive. The average degree of saturation of partially saturated soils was in the range of $79.5\% \leq S_r \leq 95.6\%$, and pore fluid was usually continuous with the occluded air bubbles. The occluded air bubbles in equilibrium with the surrounding pore fluid maintained the reduction in degree of saturation. It was assumed that occluded air bubbles did not significantly interact with the soil structure, and the effect of matric suction was small. In fact, this assumption was quite reasonable and in accordance with the findings presented in section 2.6.1.

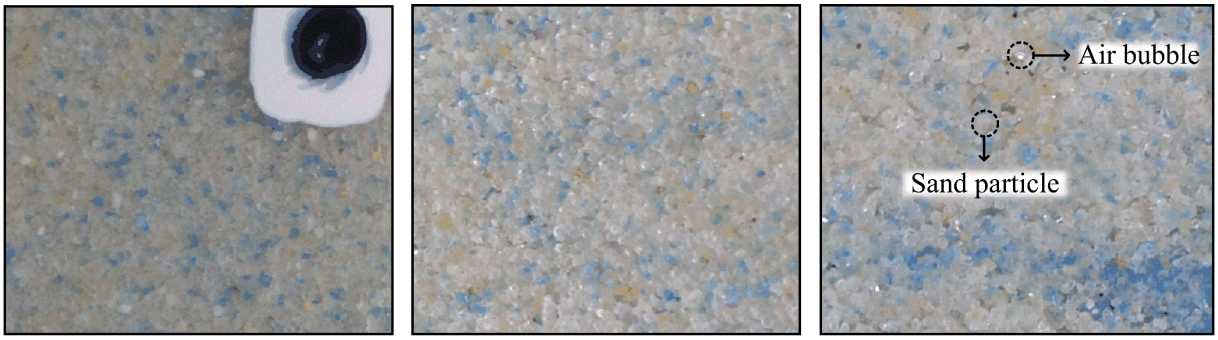

Figure 4.6– Digital image of soil specimen a) well outside of the effective air-entrapped zone, b) at the boundary and c) within the effective air-entrapped zone.

4.4.2 Impact of Distribution of Air Bubbles on the Seismic Response

The non-uniform distribution of air bubbles and narrower air-entrapped zones may potentially have some implications for the seismic response of soil. To examine this, the variation of excess pore pressure ratios, r_u, with distance from the air injector is shown in figure 4.7. It must be noted that r_u is the ratio of maximum excess pore pressure generated during the earthquake to the initial vertical effective stress computed by neglecting the foundation-induced stresses. In addition, since the excess pore pressure ratio contours could only be drawn at the locations of pore pressure transducers (PPTs), an interpolation was necessary for the rest of the soil layers.

As evident from figure 4.7, air injection significantly increased the resistance of soil to pore pressure generation. Compared with the saturated soil (CT8EQ1), much smaller excess pore pressures developed in the partially saturated soils (CT5EQ1 and CT6EQ1). The more the reduction in S_r, the less the r_u values that were observed. However, the effectiveness of air injection in reducing r_u decreased with radial distance from the air injection point. The positive impact of air injection was less apparent in the shallow soil layers. The liquefaction resistance seems to vary at discrete points of the deposits due to the non-uniformity of the desaturation.

It is worth noting that excess pore pressure ratios recorded at some measurement locations were greater than unity (r_u >1). This was ascribed to the large dilation and contraction cycles due to cyclic shearing at these locations, causing an increase and a decrease of excess pore pressures in each cycle. The r_u values were calculated based on the peaks of excess pore pressure cycles that were larger than the initial effective stresses at the corresponding depths. For the sake of simplicity, the effect of foundation-imposed stresses was also not taken into account here (see section 6.2.3.1). This also contributed to the larger values of r_u.

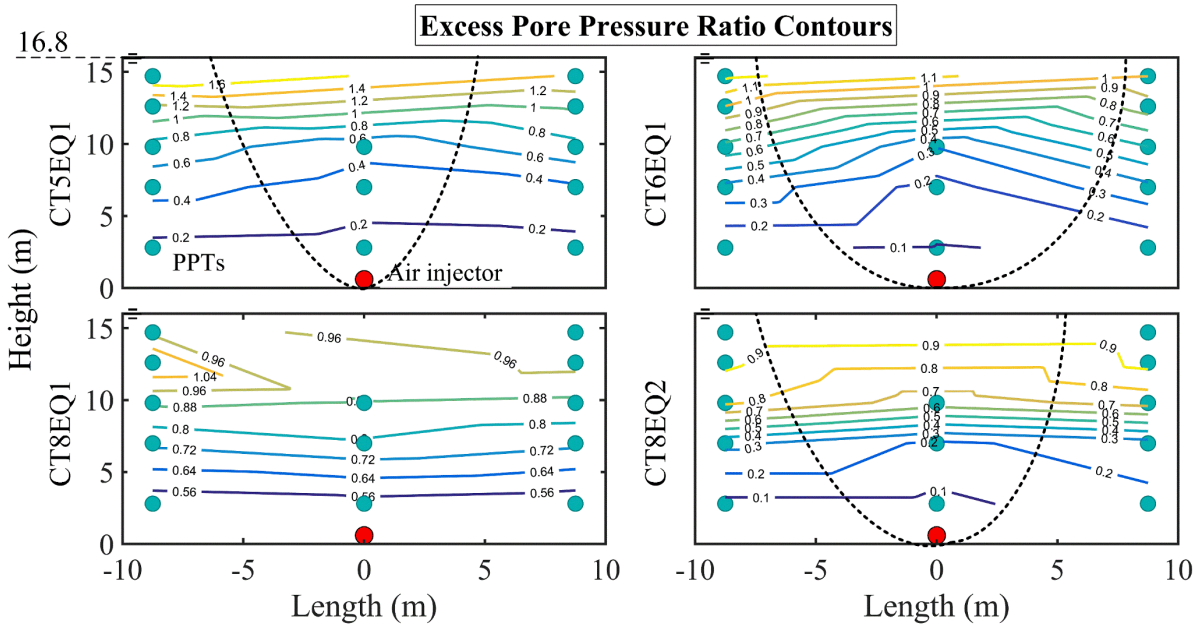

Figure 4.7– Variation of excess pore pressure ratios with distance from the air injector.

The distribution of air bubbles trapped in the partially saturated specimens was usually found to be non-uniform. Okamura and Noguchi (2009) stated that partially saturated soils with the uniformly distributed air bubbles (homogeneous specimens) would have the same liquefaction resistance as the partially saturated soils with the non-uniformly distributed air bubbles (heterogeneous specimens) if sufficient time was allowed for pore water to flow towards air bubbles. However, this finding could not be verified in this thesis. The liquefaction resistance (shown in terms of excess pore pressure ratios) varied at discrete points of the soil deposits due to the non-uniformity of the desaturation. It is thought that migration of the pore fluid from saturated to partially saturated zone will be difficult. The air in a trapped bubble will be compressible. However, if the bubble is compressed, it will increase its air pressure according to the Boyle's gas law. Therefore, it cannot be like a drainage boundary. Moreover, pore fluid flow will be very difficult since the air bubbles act as a blockage and decrease the hydraulic conductivity of the soils, which will be explained in the following chapter.

4.5 Summary

Although air injection technique might offer an economic solution for liquefaction problems, its use in practice is not prevalent. To the author's knowledge, only a few researchers have devoted their efforts to the air injection technique. Therefore, guidelines that can be reliably utilised in practice remain elusive. The objective of this chapter was to offer novel insights into the effective use of air injection technique and to investigate associated important parameters. Of particular interest was to show that the successful application and performance of air injection beneath existing structures with shallow foundations requires a well-controlled air injection process and consideration of crucial parameters such as the distribution of entrapped air bubbles in soil deposits.

Considering the results presented in this chapter, it was obvious that settlement of an existing shallow foundation may be inevitable during the application of air injection due to increased compressibility of the soil mass and airflow-induced deformations. However, the magnitude of this settlement can be reduced to an acceptable limit if the applied net air injection pressure is kept small, and air pressure is increased in a controlled manner (with low air injection rates).

Air injection pressure was also found to have some implications on the distribution of air bubbles and extent of the air-entrapped zone, which consequently influenced the seismic response of partially saturated soils. Low air injection pressures resulted in great heterogeneity within the air-entrapped zone, causing the liquefaction resistance to vary across it. Moreover, with a low air injection pressure, it was difficult to lower the degree of saturation to the targeted level. In the event of low air injection pressures, the desaturated zone extended laterally but to a certain degree. The zone of influence remained very limited, resulting in an inadequate lateral extension of improvement made.

Degree of saturation of the specimens, S_r, was estimated using (1) mass-volume relationships and (2) soil moisture sensors (Vegetronix). Air injection into the saturated medium caused the entrapment of air bubbles and significant changes in S_r. Both approaches provided relatively consistent S_r values. Readings from soil moisture sensors were considered further evidence for the presence of entrapped air bubbles in the partially saturated soils.

Chapter 5

Durability of Partial Saturation

5.1 Introduction

For liquefaction-based studies, complete saturation of the specimens in element and physical modelling tests is essential to prevent the overestimation of the liquefaction resistance of soils. It is often reported that significant amount of air entrapment may occur during the saturation process (Kutter 2013). Therefore, research efforts have been devoted towards the development of techniques that can facilitate a complete saturation in the laboratory. The main thrust of these studies is to minimise the volume of entrapped air/gas bubbles in soil models through different mechanisms such as dissolving one fluid into another, changing the pressure, displacing the bubbles. On the other hand, the interest of the present chapter is the reverse case.

Although the air injection technique holds promise for use as a way of mitigating liquefaction damage, its use in practical applications is not prevalent. This can be primarily ascribed to the concerns of practising engineers about its reliability on a long-term basis. It is known that the location of a groundwater table in the field is subjected to variations according to the climate and region. The seasonal change of the water table may increase the risk of air bubbles losing their function over time. Air bubbles may escape from the partially saturated soils, gradually dissolve in groundwater or diffuse under different field conditions, which may subsequently cause an increase in S_r and reduction in the liquefaction resistance of the ground.

The durability of undissolved air bubbles introduced during the application of sand compaction pile was investigated by Okamura et al. (2006). They showed that air trapped in natural soil deposits survived for nearly 26 years. The durability of partial saturation under hydrostatic conditions was investigated experimentally by Eseller-Bayat et al. (2013). They concluded that S_r of specimens increased by only 2% in 115 weeks. Gokyer (2009) examined the solubility of oxygen gases in water as a function of pressure. She showed that within a 20 m thick deposit,

a 1 m increase of water depth caused 3% and 6% increase in S_r for initial values of S_r: 80% and S_r: 50%, respectively.

It can be inferred from previous research that gas/air bubbles may persist in soil deposits for a significant period of time. However, these studies have not accounted for the effects of different field conditions. Moreover, very little research is available on the investigation of the potential influence of air durability on the seismic performance of partially saturated soils. Furthermore, no such studies have been undertaken to date using centrifuge testing. These facts point out the need for further research in this area.

In this study, the durability of air was investigated under a range of possible field scenarios in order to reinforce and build on the previous research by performing multiple series of one-dimensional (1-D) vertical soil column and centrifuge experiments. It is hoped that the insights offered in this section will assist to set off a major interest in the use of air injection technique, and it will be widely applied in real engineering projects. It should be noted that some of the findings presented in this chapter were published in Zeybek and Madabhushi (2017d).

5.2 Possible Field Conditions and Simplifications

In the field, partially saturated soils are exposed to different field conditions that can potentially cause the dissolution, diffusion, compression or escape of air. The field conditions specified in table 5.1 were selected as the critical parameters for evaluating the durability of air bubbles. The possible effects of these simplified field conditions were simulated and experimentally studied in the laboratory. A summary of the testing programme and typical test results are given in table 5.1. It is noted that the data for this particular study was acquired from a combination of centrifuge and soil column tests. The source of the data is explicitly indicated in table 5.1.

Existing studies into the mechanisms and physics of air/gas bubbles indicate that such parameters as absolute pressure, temperature, volume and shape of air bubbles are important for the formation, dissolution, diffusion and compression of air bubbles. The assessment of the pressure, shape and volume of individual air bubbles in soils would therefore be necessary to investigate the durability of air bubbles. However, this is quite difficult due to the complexity of the problem. In this research, the simplifications listed below are made to examine the durability of air.

- This study is restricted to partially saturated soils with high S_r (usually ≥80%). Moreover, it is solely concerned with soils having low fines content (e.g. clean sands). Under these conditions, air bubbles trapped in soils are expected to exist in the occluded form, and pore-air ought to be in equilibrium with the surrounding pore-fluid (see section 4.4.1).

- The durability of air bubbles in soil deposits is known to depend on such parameters as solubility of air, buoyant forces on air bubbles, gravitational acceleration (g-level), water flow, air and fluid pressure, degree of saturation and permeability of soils. Ideally, the derivation of the time scaling law for the longevity of air bubbles should include the combined effects of these parameters. This is, however, difficult due to the complex nature of such analysis, and this is beyond the scope of this thesis. In this chapter, the centrifuge test results are presented in model scale for the sake of simplicity.

5.3 1-D Vertical Soil Column Tests

5.3.1 Design of 1-D Vertical Soil Column Apparatus

As part of this research, the durability of air was investigated under a range of simulated field scenarios by conducting a series of 1-D vertical soil column experiments at 1-g. This section briefly explains the design of the soil column test setup.

A novel 1-D vertical soil column apparatus was constructed, as seen in figure 5.1. For this purpose, a 1200 mm clear acrylic tube with an inner diameter of 200 mm was fixed to a rigid column. Two fittings connected to an overhead tank were available for the saturation of the models. A porous plastic plate was positioned at the bottom to maintain a uniform distribution of infiltrated water. A rubber air curtain hose was connected to the system for air injection. One fitting at the top was connected to a 1-D flow muffler that was used during the flow tests. A liquid level sensor (eTape) was attached to achieve continuous monitoring of the water level, along with a metre scale. It is noted that the tube was sealed to eliminate any loss of water.

A peristaltic pump (Watson-Marlow 520S IP31 type) along with a compressible tube was used in the tests that involved vertical upward or downward flow. This pump is capable of providing a constant flow rate up to 40 millilitre/second. The use of this pump also allows the user to control and calibrate the desired flow rate manually.

Table 5.1 – Testing programme for the durability of air and typical test results.

Testing methodology	Test ID	Possible field conditions	Features of laboratory simulation	Testing procedure	Test results		
					Initial S_r (%)	Final S_r (%)	Change in S_r (%)
1-D Vertical Soil Column Tests at 1-g	SCT1	Shallow layer of soil deposit under hydrostatic condition	0.84 m soil deposit under stagnant water (low pressure)	Observation of air bubbles for 100 days	89.30	91.40	2.10
	SCT2				88.50	91.05	2.55
	SCT3	Shallow layer of soil deposit exposed to upward and downward water flow	Driving water across the specimen through pump	Upward flow (i=0.43)	92.35	93.48	1.13
	SCT4			Downward flow (i=0.47)	89.53	91.5	1.97
Centrifuge Tests at 70-g (Window Box)	CT6A4	Deep layer of soil deposit under hydrostatic condition	16.8 m soil deposit under stagnant fluid (high pressure)	25 minutes flight	78.53	79.07	0.54
	CT10A1			30 minutes flight	95.65	96.19	0.54
	CT6A4	Pore water pressure increase (e.g. rise in river, dam level)	Increasing fluid pressure through increasing g-level	Centrifugal acceleration (70-g → 90-g)	79.07	80.56	1.49
	CT8A3				82.12	83.14	1.02
Exceptions: CT7: at 40-g CT9: (Laminar Box)	CT3A4	Pore water pressure decrease (e.g. fall in river, dam level)	Decreasing fluid pressure through decreasing g-level	Centrifugal acceleration (70-g → 1-g)	-	-	-
	CT6A4				-	-	-
	CT7EQ1	Cyclic loading (e.g. earthquake, traffic, machine vibration)	Applying lateral excitation to the specimens	Shaking with *PIA*: 0.18g	84.34	84.75	0.41
	CT8EQ2			Shaking with *PIA*: 0.21g	86.58	87.22	0.64
	CT9EQ1/2	Soil layer exposed to multiple scenarios	Combination of selected cases	Settlement of level bed	-	-	-

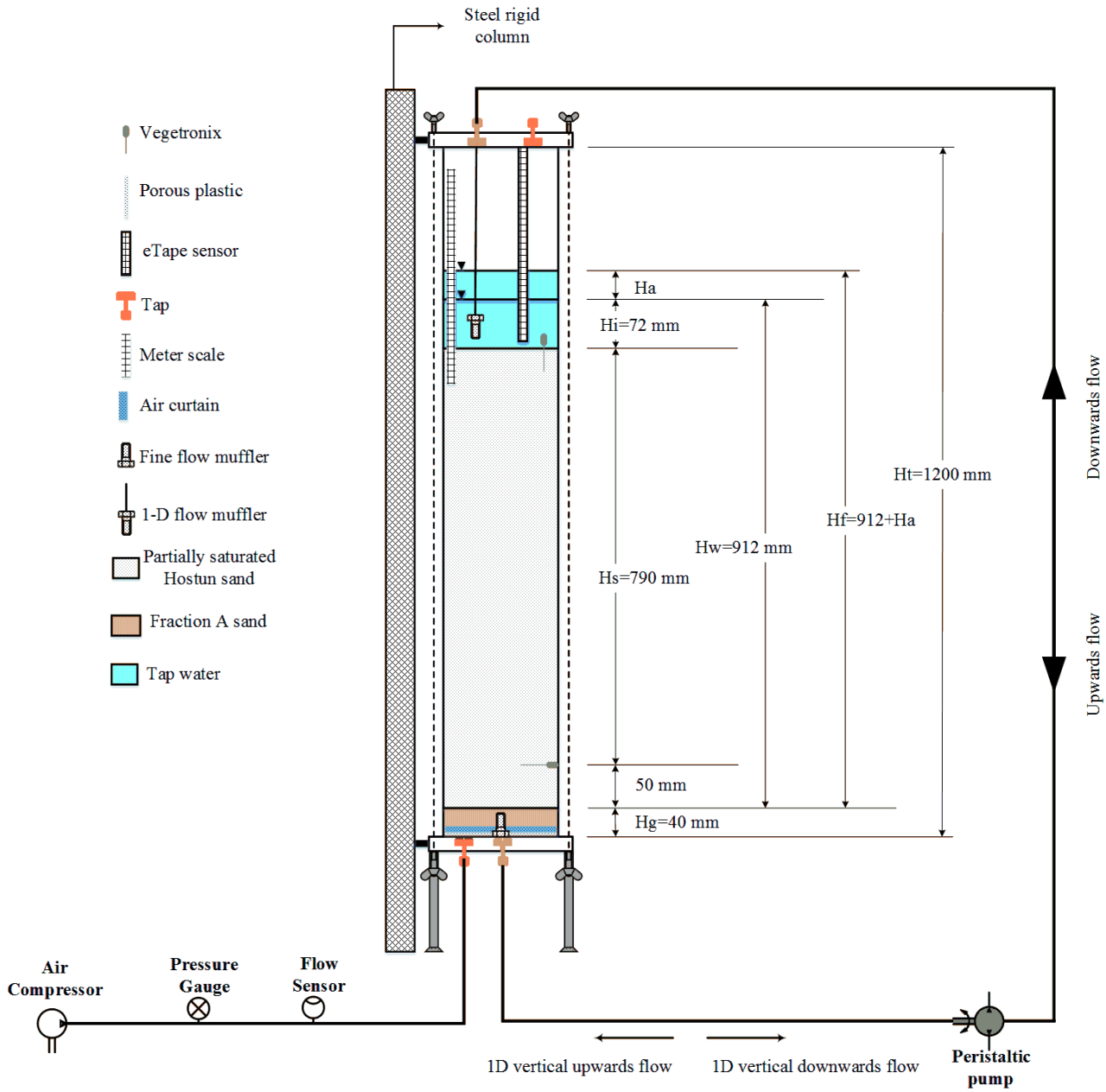

Figure 5.1– Schematic illustration of the 1-D vertical soil column test apparatus.

5.3.2 Model Preparation

A 40 mm thick drainage layer of Fraction A sand was dry pluviated into the tube to obtain 1-D flow. Two soil moisture sensors (VH400) were installed at the pre-determined locations. Dry-pluviated Hostun sand with a relative density of ~40% was situated on the Fraction A sand. An effort was made to keep the sand flow rate and fall height constant during the sand pouring to achieve uniform specimens. Dry specimens were then saturated through the infiltration of de-aired water from the bottom up. The saturation continued until a water level of 72 mm was attained above the soil surface. Subsequently, air was injected into the saturated specimens in a controlled way, which resulted in an increase in the height of the water table. The data from the VH400 and eTape sensors was collected during the saturation and air injection process. A typical setup for the 1-D vertical soil column tests is presented in figure 5.2.

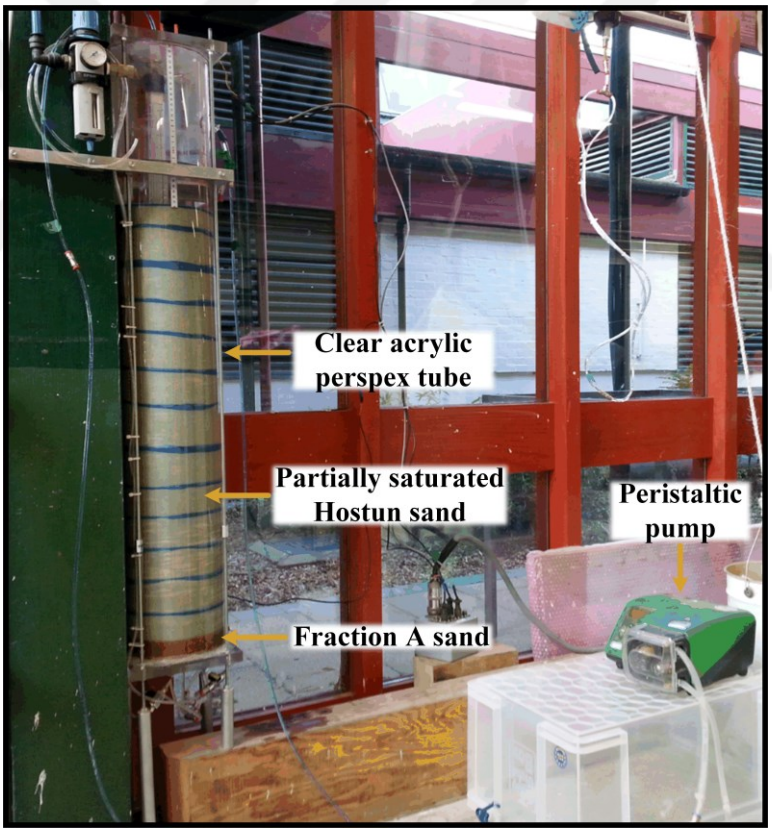

Figure 5.2– Typical test setup for the vertical soil column tests.

5.3.3 De/Saturation of 1-D Vertical Soil Column Specimens

As indicated, 840 mm thick dry Hostun sand specimens were prepared in the fabricated soil column apparatus at ~40% relative density. Following saturation of the specimens, they were desaturated in a controlled fashion. Figure 5.3 illustrates a typical example of the assessment

of S_r during the saturation and air injection process in SCT1. Both mass-volume relationships and soil moisture sensors (Vegetronix) were used for this purpose. It can be seen that S_r of the saturated specimen was ~96%. As air was injected, the free-water level increased due to the volume of pore fluid replaced by the volume of air bubbles that entered into the soil. After air injection had been halted, the water level dropped to a residual value due to excess/free air that escaped from the voids of soil. The volume of residual air bubbles in occluded form was considered when calculating the final S_r of partially saturated soils.

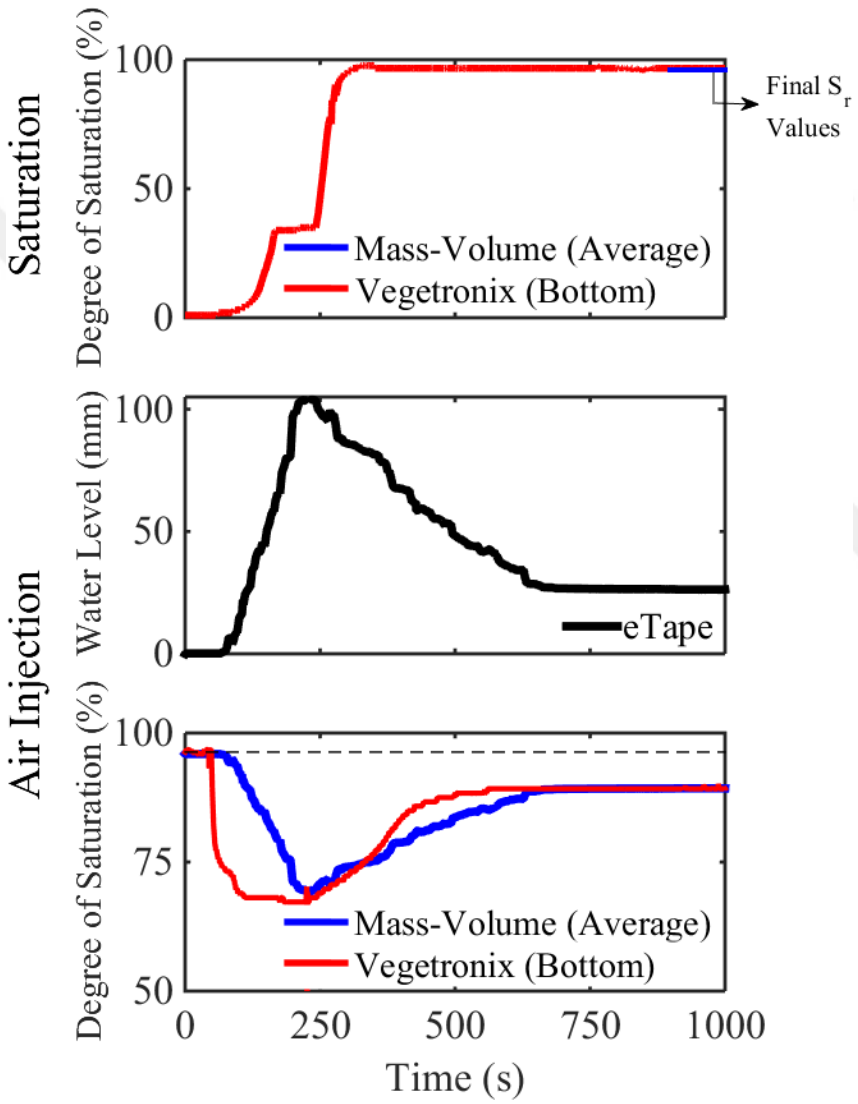

Figure 5.3– Typical test data corresponding to de/saturation of the soil column specimens.

The computed S_r of saturated soils was found to be around 96% for the soil column specimens. Following the air injection process, initial S_r of partially saturated samples was 89.3%, 88.5%, 92.35% and 89.53% for SCT1, SCT2, SCT3 and SCT4, respectively. It is noted that analogous final S_r values were achieved from both approaches, but the pattern of the variation of S_r with time differed. This was explained by the entrapment of air bubbles that started from the bottom,

leading to an earlier variation in the readings of the moisture sensor. Besides the liquid level sensor (eTape), the variation of the free-water level was monitored using a metre scale on the soil column apparatus. The readings of this sensor appeared to correlate well with the readings from the metre scale. Consequently, it is believed that a reasonable estimate of the free-water level, and therefore S_r, was accomplished during the course of vertical soil column tests.

5.4 Durability of Entrapped Air

5.4.1 Durability under Hydrostatic Conditions

The durability of entrapped air under hydrostatic conditions (stagnant fluid) was explored at 1-g. Following the air injection, free water accumulated above the soil surface and readings of the soil moisture sensors were regularly monitored for a short-term and long-term basis. Daily measurements were taken initially. It was found that the change in the water level principally occurred due to evaporation and condensation process at varying room temperature within the day. Thus, weekly measurements were made for the rest of data. It must be highlighted that the acrylic tube was tightly sealed with caps. The loss of water due to evaporation process was therefore strictly prevented.

Figure 5.4 demonstrates the change in S_r of partially saturated soils over a short and long period of time. In the short term, the increase in average S_r was ~1.4% and 2% for soil column tests SCT1 and SCT2, respectively. The final S_r values recorded by the moisture sensor (bottom) were marginally smaller than those of mass-volume relationships. This may suggest that the majority of the entrapped air bubbles escaped from the shallow depth of the specimens, and the change in S_r was much greater in the shallow soil layers. In the long term, average S_r of the specimens increased by 2.1% and 2.55% in 100 days for SCT1 and SCT2, respectively.

It is worth highlighting that a relatively rapid increase of S_r was observed up to 21 days after which a small variation of S_r was recorded only. The trend for days between 21 and 100 was used to predict the time required for partially saturated soils to reach S_r: 100%. Full saturation was extrapolated to occur after 1395 and 1560 days for SCT1 and SCT2, respectively.

The findings in figure 5.4 indicate that the majority of the air bubbles can remain entrapped in the voids of specimens under hydrostatic conditions. The soil column tests, however, involved about a 1 m column of water. For a deep layer of natural soil deposit, the water pressure will

be significantly higher, and such pressure might potentially affect the longevity of air bubbles. High-g geotechnical centrifuge offers an opportunity to recreate the high water pressures in a small-scale model. To evaluate the durability of air bubbles under larger pore fluid pressures, S_r of partially saturated soils was monitored at a centrifugal acceleration of 70 over a period of 20-25 minutes in model scale (MS). The larger pore fluid pressures and larger buoyancy forces acting on the air bubbles were the corollaries of 16.8 m deep soil deposits in prototype scale. Figure 5.5 shows the change in S_r under hydrostatic conditions in centrifuge tests CT6A4 and CT10A1. It can be seen that the change in S_r was only about 0.5%. Even at larger pore fluid pressures, it was very difficult for air bubbles to find a path and escape through a deep soil layer. The small change in S_r was therefore mainly attributed to the escape of air bubbles from the shallow soil layers.

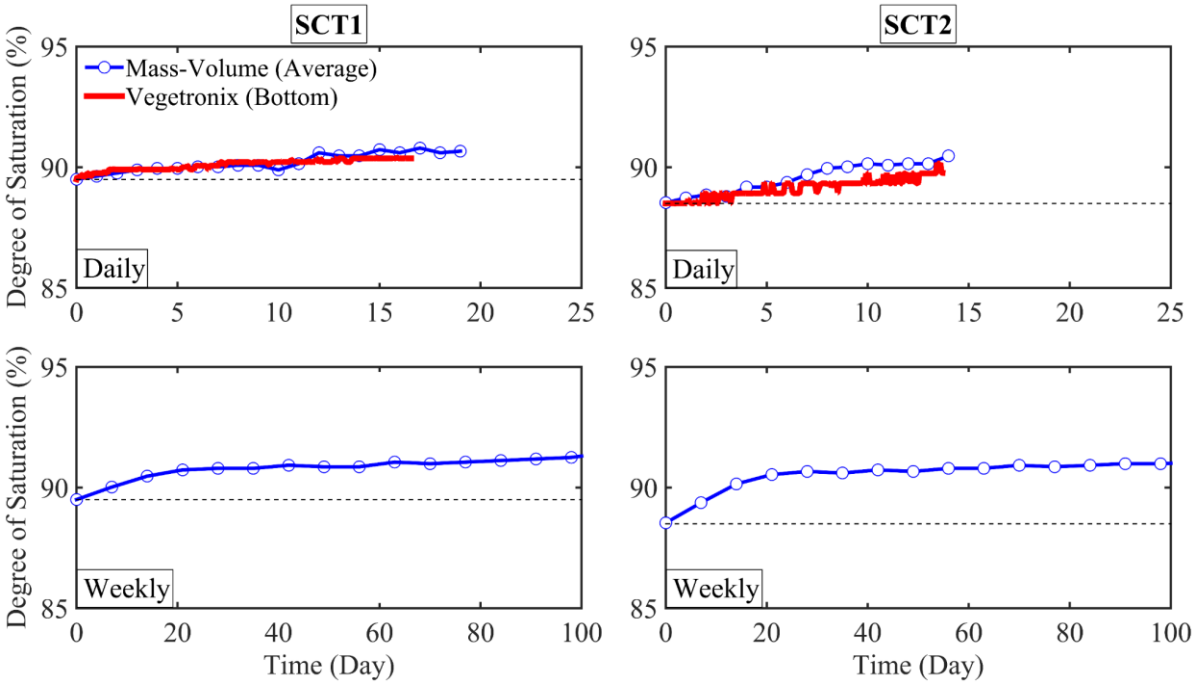

Figure 5.4– Variation of degree of saturation under hydrostatic condition at 1-g, on a short and long-term basis.

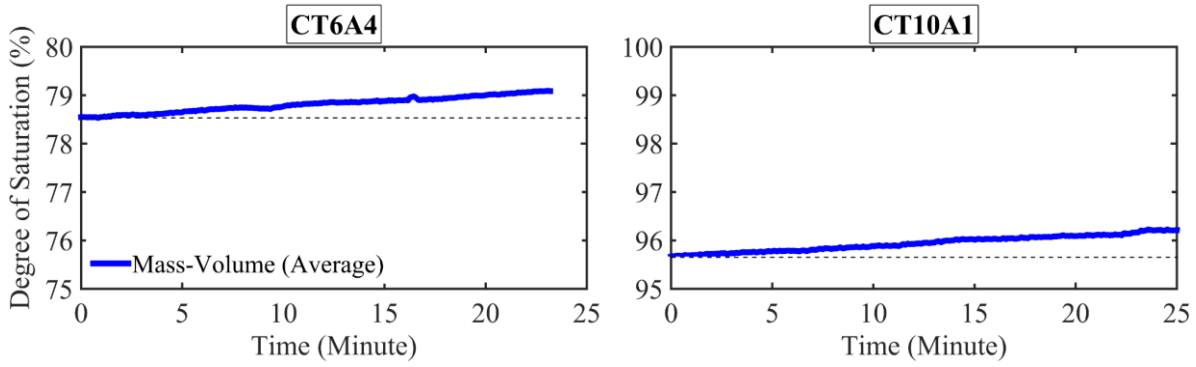

Figure 5.5– Variation of degree of saturation under hydrostatic condition at 70-g.

5.4.2 Durability under Hydraulic Flow

The durability of entrapped air bubbles under 1-D upward and downward vertical flow was investigated in soil column tests SCT3 and SCT4, respectively. In the tests, water was driven through the partially saturated specimens using the peristaltic pump, with flow continuing for approximately 30 hours. The approximate hydraulic gradients, i, applied during the tests were 0.43 and 0.47 for SCT3 and SCT4, respectively. Figure 5.6 shows the change of S_r with time during the upward and downward flow. It is evident that S_r of specimens increased about 1.1% and 2% in SCT3 and SCT4, respectively. The change in S_r took place mostly in the first few hours, and it remained almost unchanged afterwards. This reveals that the volume of occluded air bubbles being carried along by a flow of water through the soil matrix was small, and most of the air bubbles successfully remained entrapped in the voids of soils. In fact, these results seem to be in accordance with the existing literature (e.g. Eseller-Bayat et al. 2013). It is well known that in saturated soils, water flows through the pore space filled with water. However, the permeability of partially saturated soils is lower owing to the presence of air bubbles that form a barrier to the water flow. Therefore, instead of travelling with water, the majority of the air bubbles are expected to act as a blockage in the flow path.

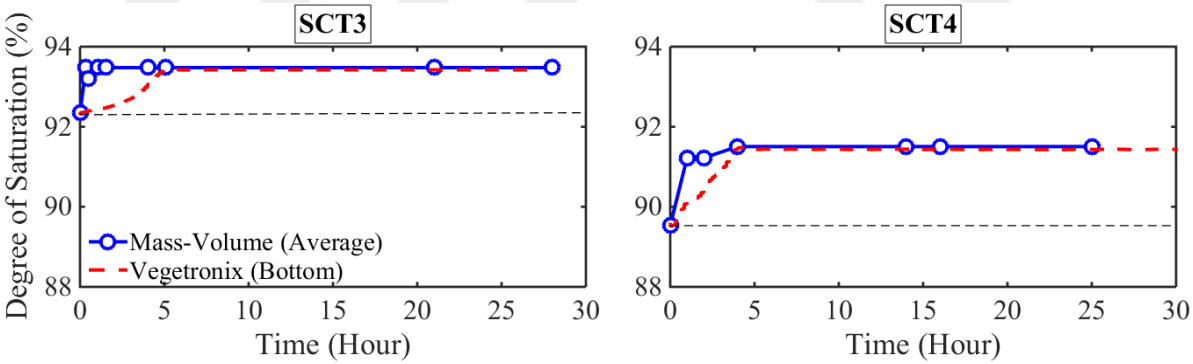

Figure 5.6– Variation of degree of saturation under upward (Test3) and downward water flow (Test4).

5.4.3 Durability under Varying Pressure

The durability of entrapped air in the field can be affected by the pressure change that might be potentially induced by the fluctuation of the water level. As stated in section 4.4.1, entrapped air bubbles were in equilibrium with the surrounding pore fluid. Intuitively, it may be expected that changing the g-level, therefore pore fluid pressure, would alter the equilibrium condition. This would change the volume of entrapped air bubbles and consequently alter the final S_r of the specimens. To investigate this hypothesis, a series of four centrifuge tests were conducted.

5.4.3.1 Increasing Centrifugal Acceleration

The change in S_r as a function of g-level-time history is shown in figure 5.7. The centrifugal acceleration was increased from 70-g to 90-g in CT6A4 and CT8A3. This increase corresponds to a 4.8 m change in the pore fluid depth. During this process, the variations in the pore fluid pressures enhanced by the centrifugal acceleration and changes in the ground surface and phreatic surface level were carefully monitored. The final S_r of the specimens was re-calculated based on the final volume of free fluid collected above the ground surface. The surface of the pore fluid was also monitored through a webcam to observe the potential air bubbles that might escape from the soil due to increased buoyancy forces on them. It is evident that within a 16.8 m partially saturated soil profile, an increase of 4.8 m pore fluid depth caused only 1.49% and 1.02% increase of S_r in CT6A4 and CT8A3, respectively.

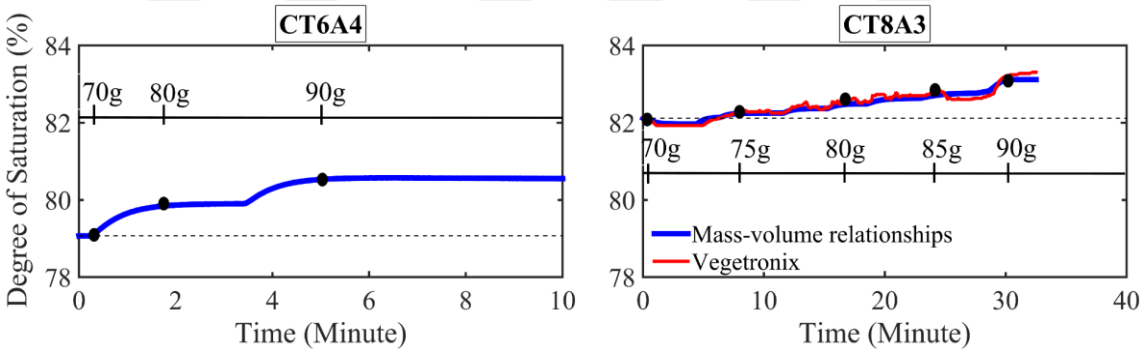

Figure 5.7– Variation of degree of saturation under increasing g-level, in model scale.

5.4.3.2 Decreasing Centrifugal Acceleration

The durability of air bubbles under decreasing g-level, therefore decreasing pore fluid pressure, was investigated in CT3A4 and CT6A4. The centrifugal acceleration was gradually reduced from 70-g to 1-g. A series of images were recorded during this process.

Figure 5.8 shows the images recorded at 70-g and 1-g. The upper images show the equilibrium condition at which pore-air and pore-fluid had approximately equal pressure at 70-g. Once the centrifugal acceleration reduced to 1-g, the shallow soil layers did heave. Some large air-filled cavities became apparent at the mid-depth of the soil layers (lower images in figure 5.8).

It was observed that entrapped air bubbles in equilibrium with surrounding pore fluid began to move upwards and escaped from the soil surface as the g-level reduced. Due to the decrease in the surrounding pore fluid pressure, the volume of air bubbles increased. Air bubbles growing in size tended to coagulate, forming larger bubbles. The formation of air-filled cavities was a direct consequence of the coagulation of relatively smaller air bubbles.

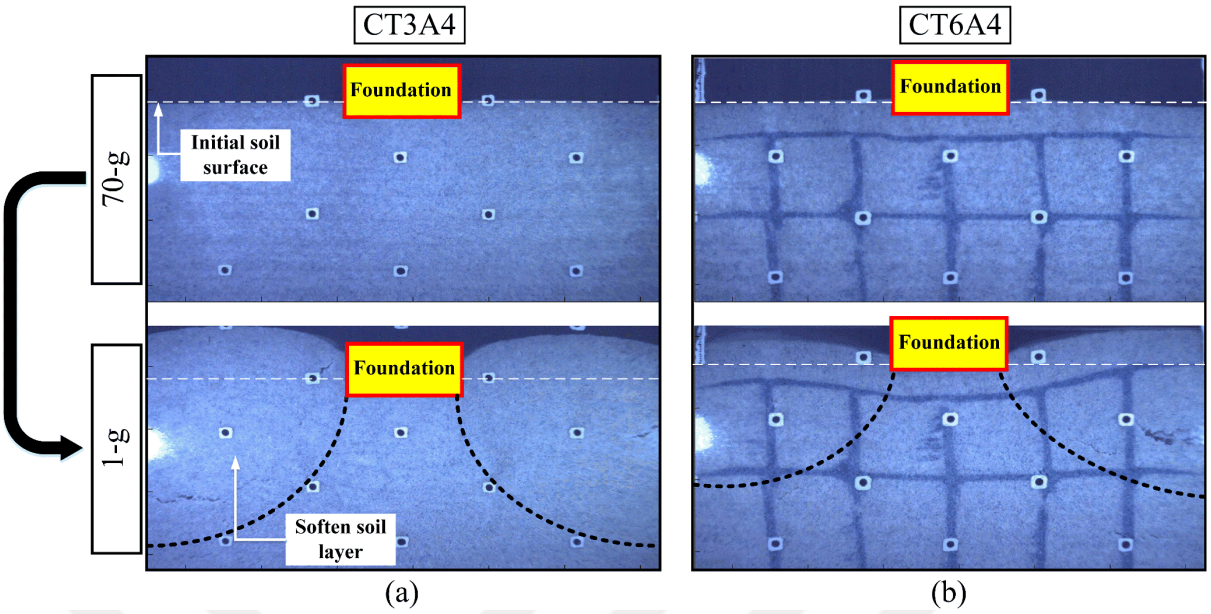

Figure 5.8– Photos of model cross-sections recorded during centrifuge swing-down.

The importance of the findings presented here was that any change in the pore fluid pressure affected the air bubble stability at the corresponding soil layers and led to the escape of air bubbles. In addition, it directly affected the soil behaviour: significant volume change and softening of soil happened, particularly at the shallow layers.

Figure 5.9 presents the horizontal and vertical displacements of the soil particles that took place during this process. It is obvious that the soil particles moved laterally and vertically upwards (negative vertical displacement indicates the heave). The movement of soil particles under the shallow foundations was small due to the bearing pressure of the foundations. However, the soil particles further away from the edges of the foundations were pushed vertically upwards.

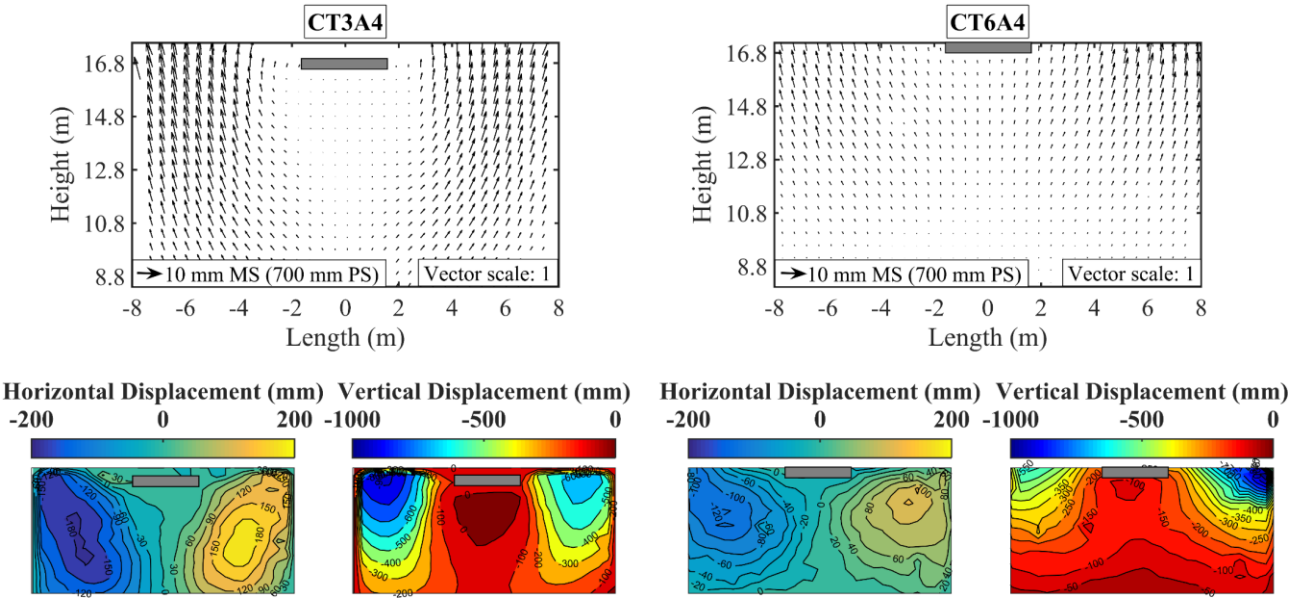

Figure 5.9– Soil deformations during centrifuge swing-down, in prototype scale.

5.4.4 Durability under Earthquake Loading

The durability of entrapped air bubbles was investigated under the earthquake loadings. Figure 5.10 shows the time histories of input motion and degree of saturation, S_r, recorded during the centrifuge experiments CT7EQ1 and CT8EQ2 . The variation of S_r was evaluated based on the readings of soil moisture sensors (Vegetronix) located within the mid-depth of the soil models.

By vibrating the partially saturated soils, S_r was found to increase by 0.41% in CT7EQ1 and 0.64% in CT8EQ2. The increase in S_r can be principally attributed to the compression of air bubbles during the earthquake events owing to their compressible nature, as suggested by Hsu and Vucetic (2004). Another source of the corresponding increase in S_r may be pore-fluid flow. It was separately reported by Zeybek and Madabhushi (2017a) that earthquake-induced excess pore pressure gradients caused pore-fluid flow during and after the earthquakes. The flow of pore fluid continued until the pore pressures reached the equilibrium in the soil. It is possible that the pore-fluid flow may lead to transport and escape of the air bubbles, particularly from the upper part of the soil deposits. This mechanism is, however, expected to be of secondary importance, based on the findings presented in section 5.4.2.

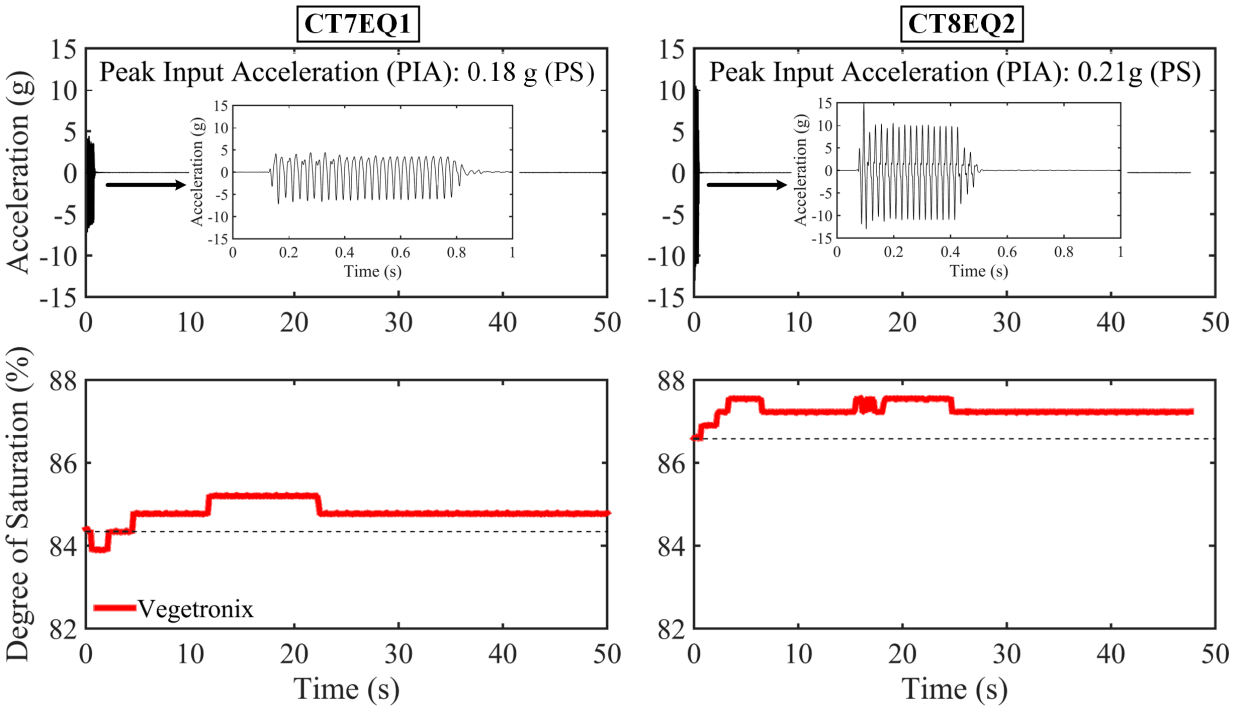

Figure 5.10– Variation of degree of saturation under horizontal shaking, in model scale.

5.4.5 Seismic Response under the Combined Field Conditions

In the first and second earthquake of CT9, the settlement of the free-field was examined under the combined effects of the simulated field conditions using the geotechnical centrifuge.

For this test, initially two columns of saturated soil with the same D_r were prepared within the laminar container. The soil columns were separated by an impermeable and flexible membrane at the centre of the model container. The partially saturated soil created using the air injection technique was tested in Section 1, whereas the saturated soil was examined in Section 3 (see figure A.4 in appendix-A). This centrifuge experiment consisted of two earthquakes:

- The first earthquake event was to investigate the settlement of a level bed of saturated and partially saturated soil under such simulated field conditions as hydrostatic and earthquake loading.
- The second earthquake was to examine the seismic settlement of the same model ground that was additionally subjected to an increased centrifugal acceleration, and therefore an increased pore fluid pressure.

Centrifuge models were subjected to consecutive earthquakes. Peak base accelerations of 0.18 and 0.21 g were applied during the first and second earthquake events, respectively (see table A.9).

Figure 5.11 shows the settlement-time histories recorded at different stages of the experiment, which are detailed below.

- Air was injected into the saturated soil in Section 1 once the centrifugal acceleration of 70-g was reached. The injection of air caused a 14% reduction of S_r (from 99% to 85%).

The maximum air injection pressure applied was equal to the sum of the hydrostatic pressure and approximately 0.23 times of the vertical effective stress at the injection point. This resulted in a free-field settlement of about 15.3 mm in prototype scale. The air (injection)-induced settlement was indicated by a horizontal dashed line.

- The first earthquake was fired after 30 minutes (model scale) of centrifugal flight. It is seen that the rate of co-seismic and post-seismic free-field settlement of partially saturated soil was much smaller than that of saturated soil. Consequently, partially saturated soil suffered a considerably smaller magnitude of total free-field settlement.

- The second earthquake on the same soil model was applied after increasing the centrifugal acceleration from 70-g to 90-g and 30 minutes (model scale) of centrifugal flight at 90-g. Similarly, partially saturated soil in the free-field settled less than its saturated counterpart. These findings may suggest that air injection technique was still very effective at reducing the liquefaction-induced settlement although the model ground was subjected to different simulated field conditions.

- Following the second earthquake, the model was swung down to 1-g. During the swing-down process, the partially saturated soil, particularly at the shallow depths, softened due to the soil disturbance, as reported in section 5.4.3.2. This highlighted the importance of the equilibrium between the entrapped air bubbles and surrounding pore fluid.

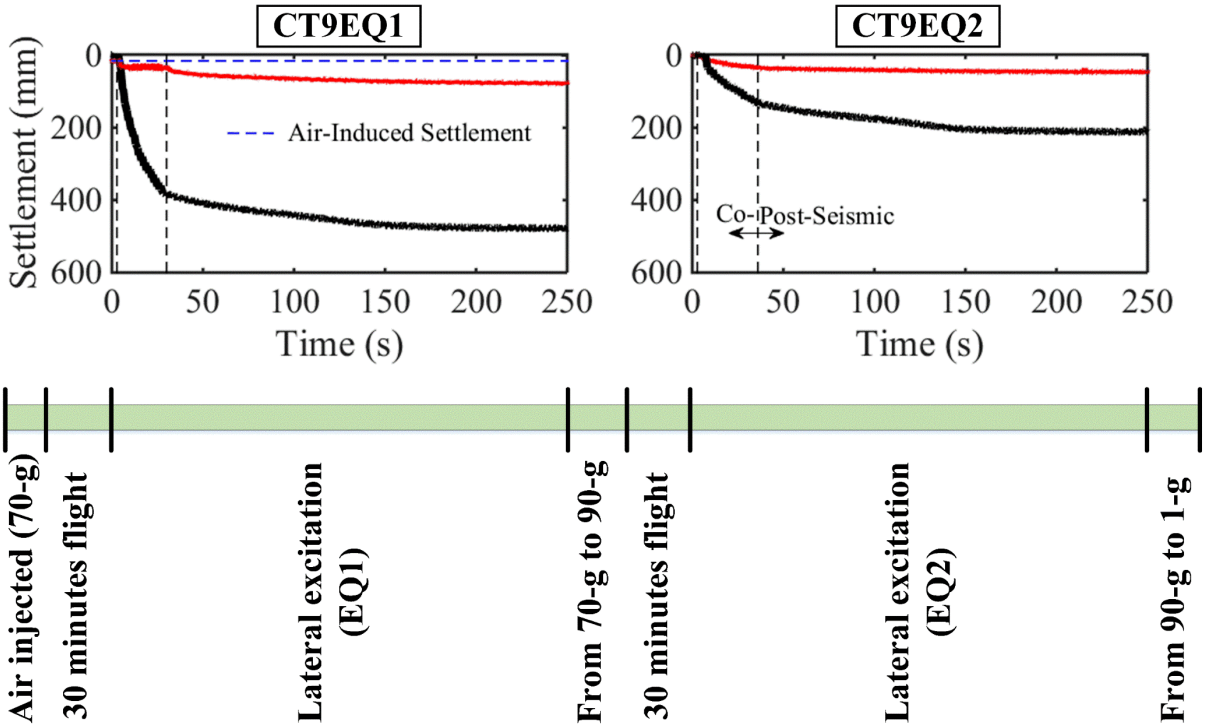

Figure 5.11– Seismic settlement of a level bed deposit at different stages of centrifuge test, in prototype scale.

5.5 Summary

The objective of this chapter was to provide insights into the possible effects of different field conditions on the durability of entrapped air bubbles. The seismic performance of a level bed of partially saturated soils which were subjected to the combination of various field conditions was also discussed.

The field scenarios were simplified and simulated in the laboratory. With the simulated field conditions, the durability of air bubbles in the partially saturated specimens was examined under hydrostatic condition at low and high pore-fluid pressure; upward and downward vertical flow; varying pore-fluid pressure and lateral excitation. Analysis of the experimental results suggested that some of the entrapped air bubbles lost their function under these conditions, which brought about an increase in degree of saturation of the partially saturated specimens. The corresponding increase was however minor for almost all conditions, except decreasing g-level and hence pore-fluid pressure. This condition caused unstable air bubbles and an upward movement of soil particles, which resulted in significant volume change and deformations in the soil models. This finding highlighted the importance of the state of equilibrium between entrapped air bubbles and surrounding pore fluid. The movement of air bubbles in soils would be possible if the soil or water pressures reduced significantly.

The seismic settlement of the free-field was examined under the combined effects of simulated field conditions. The test results confirmed that air injection was still an effective method of reducing the liquefaction-induced settlement in the free-field although the partially saturated soil was subjected to many of the simulated field conditions.

Although only the simplified version of real field circumstances is considered in this research, it offers valuable insights into the long-term reliability of the air injection technique. These insights might be of interest to practising engineers working on liquefaction remediation techniques, and they might begin the frequent use of this technique in real engineering projects worldwide.

Chapter 6

Dynamic Behaviour of Partially Saturated Soils

6.1 Introduction

Due to the insufficient number of field and experimental studies available on the air injection technique, the key parameters that affect the dynamic response of partially saturated soils, remediated with this technique, have not been explicitly identified. The response of shallow foundations resting on these soil deposits has also not been studied extensively. Similarly, much uncertainty has remained even regarding the basic understanding on the dynamic behaviour of level deposits of partially saturated soils, particularly in terms of the settlement response.

In this research, the key parameters were investigated through physical model tests. The selected testing parameters were degree of saturation (S_r), confining stress, foundation bearing pressure (q) and characteristics of input motions applied. The results from 1-g shaking table and centrifuge tests offer insights into the relative importance of each of these parameters in the dynamic response of soils and foundations.

In this chapter, the impact that each testing parameter has on the shallow foundation and free-field settlements will be discussed. It will provide insights into the influence of each parameter on the acceleration and excess pore pressure generation. The importance of the incorporation of these parameters in engineering practice will be highlighted. Later section of this chapter will also discuss the co-seismic and post-seismic behaviour of level deposits of saturated and partially saturated soils separately, in terms of the build-up and dissipation of excess pore pressures and ground surface settlements. It is intended that the findings will be useful for a rational design and execution of air injection technique in practice. Some of the results presented in this chapter can be found in Zeybek and Madabhushi (2017a).

6.2 Important Parameters for the Dynamic Response of Partially Saturated Soils

6.2.1 Degree of Saturation

Degree of saturation, S_r, is perhaps the most important parameter in examining the liquefaction resistance of partially saturated soils. The influence of S_r on the liquefaction resistance of soils is well-documented using element tests. The enhanced cyclic liquefaction resistance of soils as S_r is reduced by only a few percent was previously highlighted in section 2.4.1. The primary thrust of the researchers was to show the importance of accomplishing 100% saturation in the specimens to inhibit the undesirable partially saturated condition and prevent an overestimation of the liquefaction resistance of specimens.

The main objective of the air injection-based studies is, on the other hand, to reduce S_r of the saturated soils and maintain an increase in the liquefaction resistance. Published physical model tests investigating the behaviour of shallow foundations resting on the partially saturated soils indicate that in accordance with the laboratory test data, the liquefaction potential of liquefiable soils and relevant foundation settlements significantly decrease as S_r reduces (Marasini and Okamura 2015). Most of this research is, however, qualitative in nature. A comprehensive understanding on how and more importantly why the co-seismic and post-seismic response of shallow foundations resting upon these soils change with varying S_r is required.

The intent of this section is to offer novel insights into the behaviour of partially saturated soils providing physical explanations of the observed trends. The particular interest is to show that the magnitude and rate of excess pore pressure generation & dissipation, the consequent liquefaction-induced foundation & soil surface settlements and soil & foundation accelerations are a strong function of S_r. Only the first earthquake data from the centrifuge experiments CT4 (S_r: 99.0%), CT5 (S_r: 93.1%) and CT6 (S_r: 79.5%) are presented. In fact, they are the most useful data to derive main conclusions regarding the effect of S_r but are representative of the larger database that contains data from multiple earthquakes.

6.2.1.1 Settlement Behaviour

Time histories for the settlement of shallow foundations resting on the soil layers with different S_r, ranging from 99.0 to 79.5%, are plotted in figure 6.1. Settlements that occurred during each

air injection process are indicated concurrently by the horizontal dashed lines to highlight their relative contributions to the total foundation settlements. In this figure, positive displacements represent the settlement of foundations. In addition, the time histories of the input motion recorded during the tests are presented. The amplitude and frequency of the earthquakes were kept the same, and a peak base acceleration of around 0.18 g was accomplished for all the tests. In CT5 and CT6, the duration of the first earthquakes was, however, much longer than desired due to problems with SAM shaker, as reported in section 3.5.3.1. Despite these problems, general patterns of behaviour were successfully compared by conducting the analysis on a cycle-by-cycle basis. In fact, the longer duration of the earthquakes enabled the behaviour of partially saturated soils during the prolonged shakings to be investigated (see section 6.2.4).

It is evident in figure 6.1 that the total settlement of the shallow foundations, applying a bearing pressure of 50 kPa, reduced substantially when air was injected into the deposits of saturated soils. After an equivalent number of acceleration cycles (17), the foundation on the saturated soil settled by 978.6 mm in CT4 (S_r: 99.0%). On the other hand, the sum of air-induced and earthquake-induced foundation settlements recorded for the partially saturated soils was 423.3 mm in CT5 (S_r: 93.1%) and 242.8 mm in CT6 (S_r: 79.5%). This indicates that following the mitigation of liquefiable soils using the air injection technique, the total foundation settlements reduced by approximately 57% and 75% in these soil deposits.

The cumulative foundation settlements over 17 acceleration cycles against degree of saturation are presented separately in figure 6.1 to elucidate the influence of S_r on the trends of foundation settlement. It appears that a reduction in the foundation settlement did follow a reduction in S_r. The cumulative foundation settlements reduced with decreasing S_r values but exhibited a non-linear trend (explained later in section 6.2.3.2).

For a structure resting on a liquefiable soil deposit, the major concern of design engineers is to restrict the foundation settlements in order to prevent the total or partial collapse of the structure during an earthquake. It is evident air injection provided a sizeable reduction in the foundation settlement and prevented overall failure of the system, indubitably establishing its benefits as a way of mitigating liquefaction damage. Although this was an encouraging finding, even such reduced foundation settlements would be outside the realms of those that may be acceptable for a real structure in practice.

It should be noted that the effectiveness of the air injection technique may have been affected by the insufficient geometry of the improved (desaturated) zone and non-uniform distribution

of air within this zone, as mentioned in section 4.4.1. However, on the basis of the trends shown by the centrifuge test results, it can be suggested that the foundation settlements may be reduced to reasonable limits with wider and more uniformly desaturated zones than those tested.

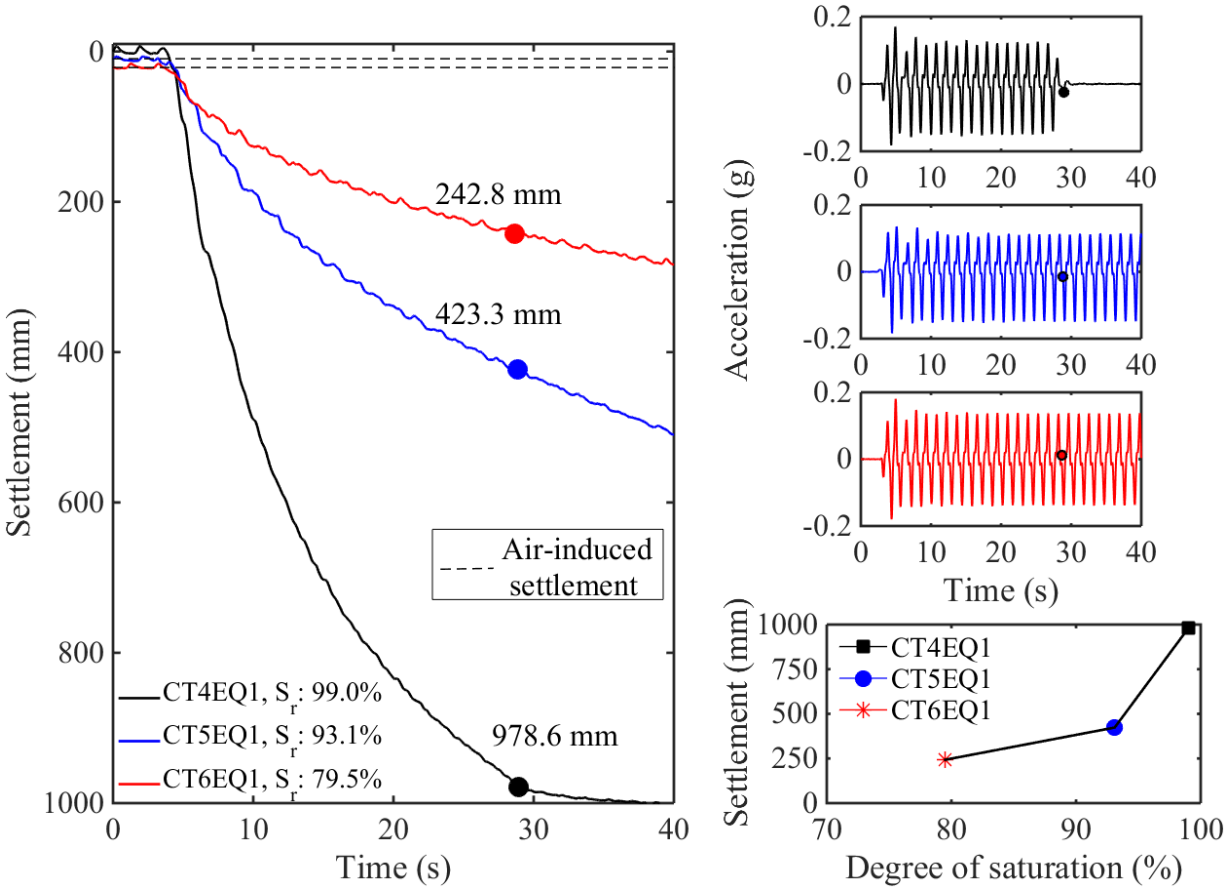

Figure 6.1– Typical foundation settlement-time, acceleration-time and settlement-degree of saturation histories.

Differential Settlement

It is known that in the case of large differential settlements between the foundation and the soil surface, the overlying structures can be unusable although they remain undamaged by rotation or earthquake. The relative settlements between the foundation and the soil right next to it can be particularly hazardous to lifeline connections. In order to investigate the effect of air injection on the differential settlements between the foundation and the soil surface, the free-field settlement-time histories were examined, and a typical example of the analysed data is presented in figure 6.2a. Air-induced settlements are indicated by the horizontal dashed lines. Positive displacements represent the vertical settlement of the soil surface, whereas negative displacements represent heave in this figure. In addition, the differential settlements at the end of 17 cycles of acceleration are depicted in figure 6.2b to explicitly show the variation of differential settlements with degree of saturation.

As shown in figure 6.1, the foundation settlement that developed in the saturated soil (CT4) was 978.6 mm. Therefore, the differential settlement between the foundation (Section 2) and the soil surface (Section 1) was more than 1100 mm in this case. The differential settlements were observed to reduce with the injection of air. The foundation appeared to settle 84 mm more than the soil surface in the partially saturated soil (CT5). This result gives a clue as to the effectiveness of the air injection in minimising the differential settlements. Further reduction in S_r resulted in even less relative settlement in the partially saturated soil (CT6), with a differential settlement of 17 mm between the soil and the foundation. This also highlights the effect of S_r on this trend.

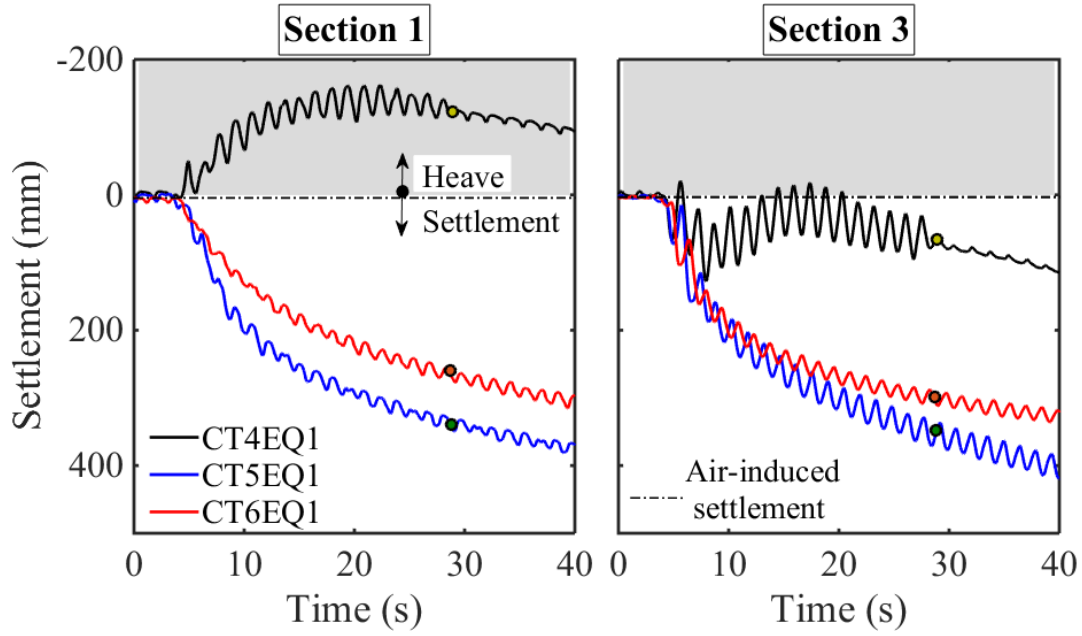

a) Typical time-histories of the free-field settlement

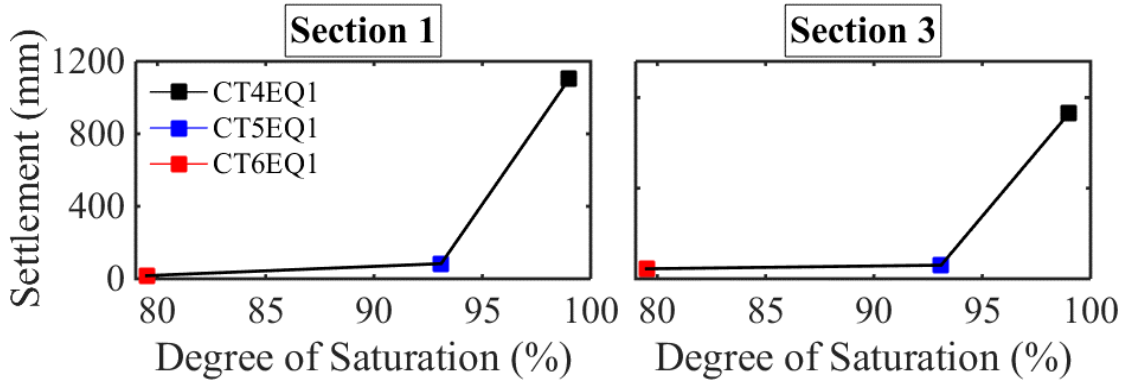

b) Differential settlement versus degree of saturation

Figure 6.2– Differential settlements between the foundation and the soil surface.

Structural and Boundary Effects

It must be pointed out that the free-surface responses should ideally be recorded at locations away from the foundations and container end walls to ensure that structural and boundary effects are negligible. As described in section 3.2.4, a soft putty-like material (Duxseal) was used at the container end walls to minimise the boundary effects such as stress wave reflections in the direction of earthquake loading. However, this Duxseal boundary does not remove the lateral constraint on the monotonic movement of soil due to failure mechanisms. The responses underneath the foundation were achieved in Section 2, whereas the free-field responses were recorded in Section 1 and Section 3 (see figure A.2 in appendix-A). The total length of the model container in the shaking direction was ten times of the foundation width, B. The horizontal distance from each edge of the foundation to the boundaries was $4B$. Moreover, the LVDT measurements were made at a distance of $2B$ from the edges of the foundations.

It was observed that in the saturated soils, the deformation mechanisms mobilised by the foundations were large. This behaviour will be discussed further in section 7.2.1. Despite the small width of the foundation used in this test, the upward displacements in figure 6.2a might have been somewhat affected by the large extent of the deformation mechanism and proximity of the boundaries. It is worth stating that the aforementioned issue was of insignificance for the partially saturated soils since the displacements in these soils were relatively small, limiting the extent of the deformation mechanisms developed in the horizontal and vertical direction. The measurements in Section 1 and Section 3 were, therefore, unambiguously corresponding to the free-field response in these soil deposits.

6.2.1.2 Generation of Excess Pore Pressures

The above settlement data reinforced the benefit of air injection in reducing the settlement of shallow foundations atop liquefiable ground. To ascertain in detail the way that air injection produced such improvement, the information retrieved from pore pressure transducers are analysed. Of particular interest is to assess the effect of reducing S_r on the excess pore pressure generation.

The traces of excess pore pressures measured at the mid-depth of the soil layers beneath the central axis of the foundations are depicted in figure 6.3. The peak values of excess pore pressures at the end of 17 acceleration cycles are also plotted against the depths of the corresponding transducers below the soil surface. The initial liquefaction at which excess pore

pressures generated during the dynamic excitations are equal to the initial vertical effective stresses ($r_u = 1$) is indicated by the continuous solid and dashed lines for the two different cases. $r_u = 1$ (foundation) and $r_u = 1$ (free-field) were computed by accounting for or neglecting the effects of foundation-induced stresses on the vertical effective stresses, respectively.
It is worth indicating that the foundation-induced stresses were calculated using the Boussinesq stress distribution method. This is an elasticity-based method and has some limitations for the assessment of the true stress distribution within the deposits of liquefiable soils, which will be discussed in section 6.2.3.1.

In figure 6.3, it is apparent from the first time window that in the saturated soil for CT4, excess pore pressures were generated very quickly at 7-m and 9.8-m depths after the earthquake loading commenced. They built up and became equal to the initial effective stresses in the free-field. The soil layers reached complete liquefaction particularly at the shallow depths, and they remained liquefied throughout the duration of shaking. The magnitude of excess pore pressure developed at 14-m depth was unexpectedly smaller than that generated at 9.8-m depth. This might be ascribed to a calibration error for the corresponding pore pressure transducer. In accordance with the observed trend in the saturated soil, after the earthquakes started, excess pore pressures, in particular at the shallow layers, developed very quickly in the partially saturated soils for CT5 and CT6. On the contrary, the magnitude of the maximum excess pore pressures was significantly smaller for each of the two partially saturated soils. The initial liquefaction was not reached in any case.

The comparison of the excess pore pressures that developed within the saturated and partially saturated soils also indicates that the resistance to excess pore pressure generation increased as S_r reduced. Decreasing S_r of soils slowed down the rate of excess pore pressure generation and reduced its magnitude further. Further reduction in S_r led to the development of lower excess pore pressures. These findings correlated well with the previous settlement data.

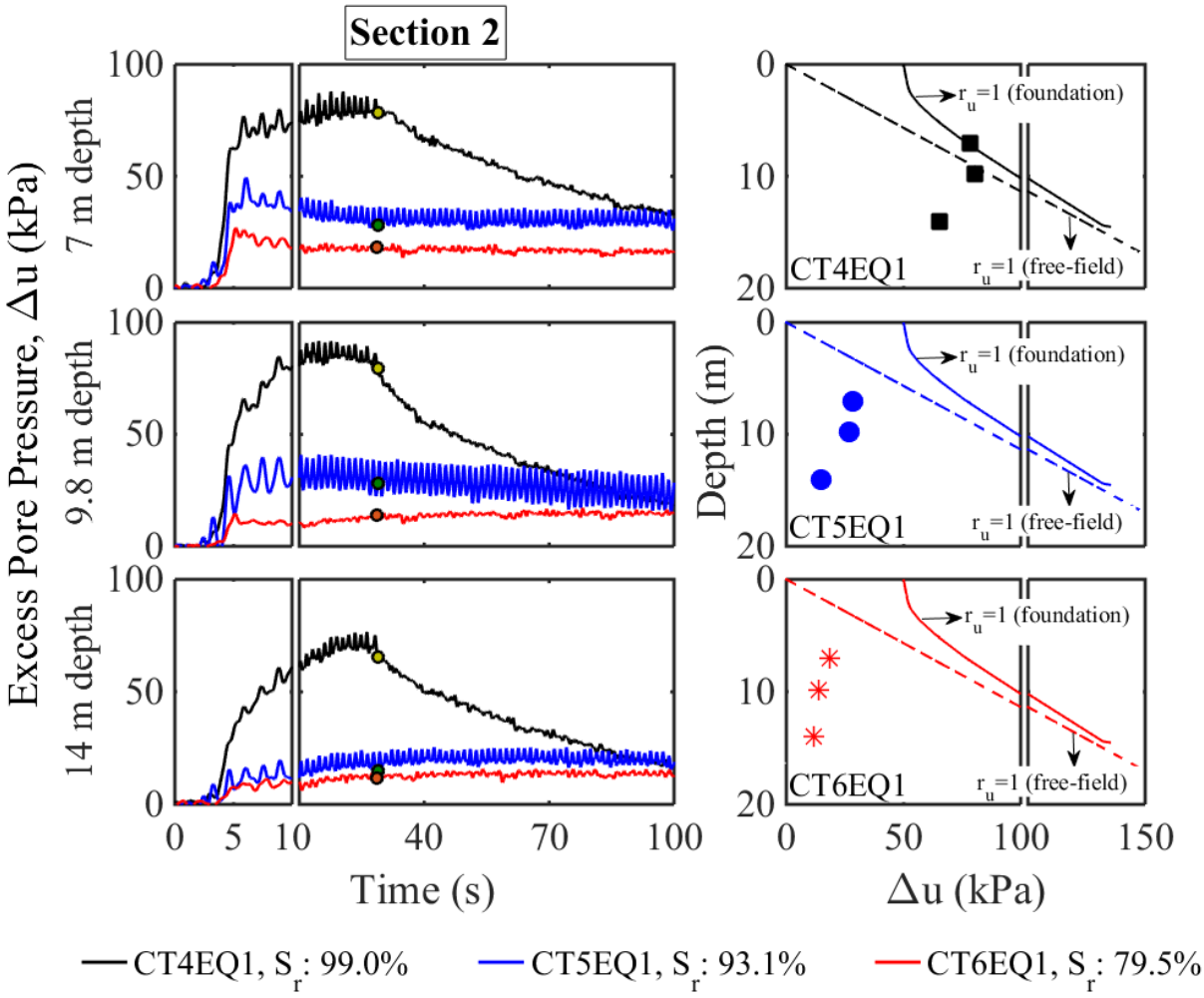

Figure 6.3– Typical excess pore pressure-time and depth-excess pore pressure histories beneath foundations.

Figure 6.4 demonstrates the excess pore pressures that developed in the free-field during the first earthquakes of CT4, CT5 and CT6. Unfortunately, pore pressure transducer at a depth of 4.2 m in Section 3 malfunctioned for the saturated soil (CT4). The remainder of the pressure transducers provided significant information for comparison.

It can be seen from the first time window that at the shallow layers of saturated soil (namely 2.1-m and 4.2-m depths) excess pore pressures built up almost immediately, and complete liquefaction was reached after approximately 2 to 3 seconds of the earthquake. Similarly, excess pore pressure at the mid-depth of the soil deposit (7-m depth) reached full liquefaction after about 4 seconds of the seismic event. Although initial vertical effective stresses were not lost completely, r_u of approximately 0.9 was reached at the relatively deeper layer (9.8-m depth), which indicated that significant soil-softening occurred even within the deeper layers of the saturated soil. The rate of excess pore pressure generation also reduced with depth.

Examining the excess pore pressures generated in the partially saturated soils, it can be seen that excess pore pressures completely reached (CT5) or virtually reached (CT6) the value of initial vertical effective stresses at the shallow layers. This behaviour was in accordance with the observed response in their saturated counterpart. However, unlike for the saturated soil, the magnitude of build-up excess pore pressures was significantly smaller in the deeper layers for each of the partially saturated soils. Excess pore pressures generated at depths of 7 and 9.8 m did not reach the initial vertical effective stresses. In addition, the rate of excess pore pressure generation slowed down slightly, particularly at the deepest soil layer.
It should be emphasised that excess pore pressures that developed in the deeper layers of both partially saturated soils exhibited an interesting behaviour. They increased rapidly and reached a peak value at the early stage of earthquakes. However, such peak value could not be retained, and the magnitude of excess pore pressures exhibited a decreasing trend with each cycle even while the earthquakes continued. This response will be examined further in section 6.2.1.3.

From the aforementioned results, it seems that air injection significantly minimised the excess pore pressure generation. Furthermore, in agreement with the observed trend beneath shallow foundation, free-field excess pore pressures generally reduced as S_r of soil deposits decreased. It is worth noticing that the positive influence of air injection on the soil's resistance to pore pressure generation and impact of S_r on this trend appeared to decrease, under lower confining stresses, at shallow soil layers (usually 2.1 m) and at locations away from the air injector. These findings justified the importance of confining stresses for the liquefaction resistance of partially saturated soils and emphasised the significance of the extent of the air-entrapped zone. The effects of confining stresses will be discussed in depth in section 6.2.2.

Excess pore pressure-time histories in figure 6.4 also show that smaller transient pore pressures were generated in each cycle, and a cyclic response of pore pressures was present at almost all depths. The cyclic response can be attributed to a large amount of cyclic shearing that took place in these regions during the earthquake loading. The cyclic shearing resulted in dilation and contraction during each seismic cycle. This, in turn, caused a decrease and an increase in excess pore pressures. This phenomenon is widely reported in many independent centrifuge tests, and it is ascribed to the butterfly loops in $q - p'$ space (Coelho et al. 2007).

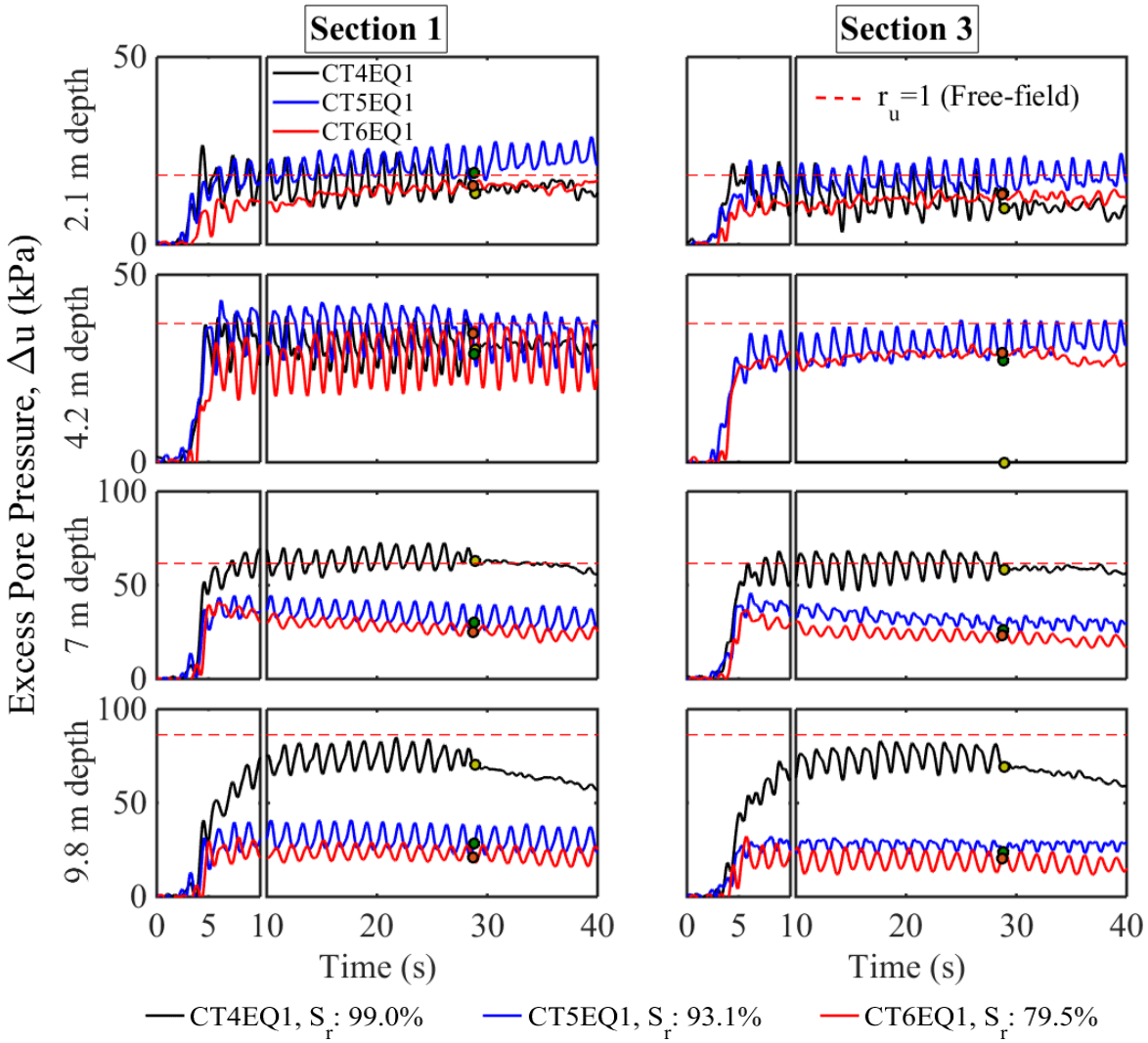

Figure 6.4– Typical excess pore pressure-time histories in the free-field.

6.2.1.3 Dissipation of Excess Pore Pressures

The above data revealed that S_r has a significant impact on the generation of excess pore pressures during the dynamic loading. In addition to the co-seismic response, the investigation of the influence of S_r on the dissipation of excess pore pressures and pore fluid flow in the soil layers is of equally importance. Hydraulic gradients, i, generated between different depths can be plotted to examine the pore fluid flow.

Hydraulic gradient between any two points is given by the ratio of change in total head between the two points to the distance between them. Total head is the sum of pressure and elevation head at each point. In the initial hydrostatic condition, total heads at all locations of the soil models are the same. As a result, no flow of pore fluid is present. Hydraulic gradients develop during and after earthquakes owing to the differences in excess pore pressures. Therefore,

excess pressure heads, which can be obtained by dividing the excess pore pressures to the specific unit weight of pore fluid, are sufficient to compute the hydraulic gradients.

The test data from the first earthquakes of CT4, CT5 and CT6 were analysed. The hydraulic gradients recorded in the free-field during and after the earthquakes are presented in figure 6.5. A positive hydraulic gradient denotes upward flow in this figure. In the presentation of the results, the co-seismic behaviour was separated from the post-seismic dissipation behaviour by two vertical dashed lines, as seen in the first time window. The boundary between co-seismic and post-seismic behaviour was simply determined based on the duration of the earthquake in the saturated soil (CT4). Although the duration of the earthquakes was longer than normal for the partially saturated soils (CT5 and CT6), the corresponding boundaries were deemed practical for these soils as well. In fact, this simplification enables a direct comparison between the tests and comparison of the general patterns of behaviour.

The results from the saturated soil (CT4) demonstrated that very high excess pore pressure gradients were generated during the earthquake event. The dissipation of excess pore pressures started from the base where excess pore pressures had nowhere to dissipate, and the dissipation was only permitted from the soil surface. Therefore, the flow of pore fluid was always upwards in all locations after the earthquake ceased. The pore fluid flow continued until the pore pressures reached equilibrium throughout the soil. The hydraulic gradients due to excess pressure heads began to reduce just before or immediately after the earthquake ceased for soil layers at the depths of 7-9.8 m and 4.2-7 m. At the shallow layers (namely depths 2.1-4.2 m), the reduction in hydraulic gradients started much later than the end of shaking. The soil, under low effective stresses, near the surface remained in a weakened state for longer.

In the partially saturated soils (CT5 and CT6), at the shallow layers, high excess pore pressure gradients developed during the earthquake. At this level, excess pore pressures remained higher for a long period of time, and they were the last to dissipate. This behaviour was analogous to the observed response in their saturated counterpart. At the deeper layers, unlike for the saturated soil, comparatively much smaller excess pore pressure gradients were generated during the earthquake for each of the two partially saturated soils. Downward flows became apparent in some layers, particularly at 7-9.8 m depths. The hydraulic gradients were generally very small when the earthquakes ceased. Moreover, despite the profoundly longer duration of earthquakes, the hydraulic gradients in the partially saturated soils began to decline quickly and dropped to a negligible level much earlier or at the same time as their saturated counterpart.

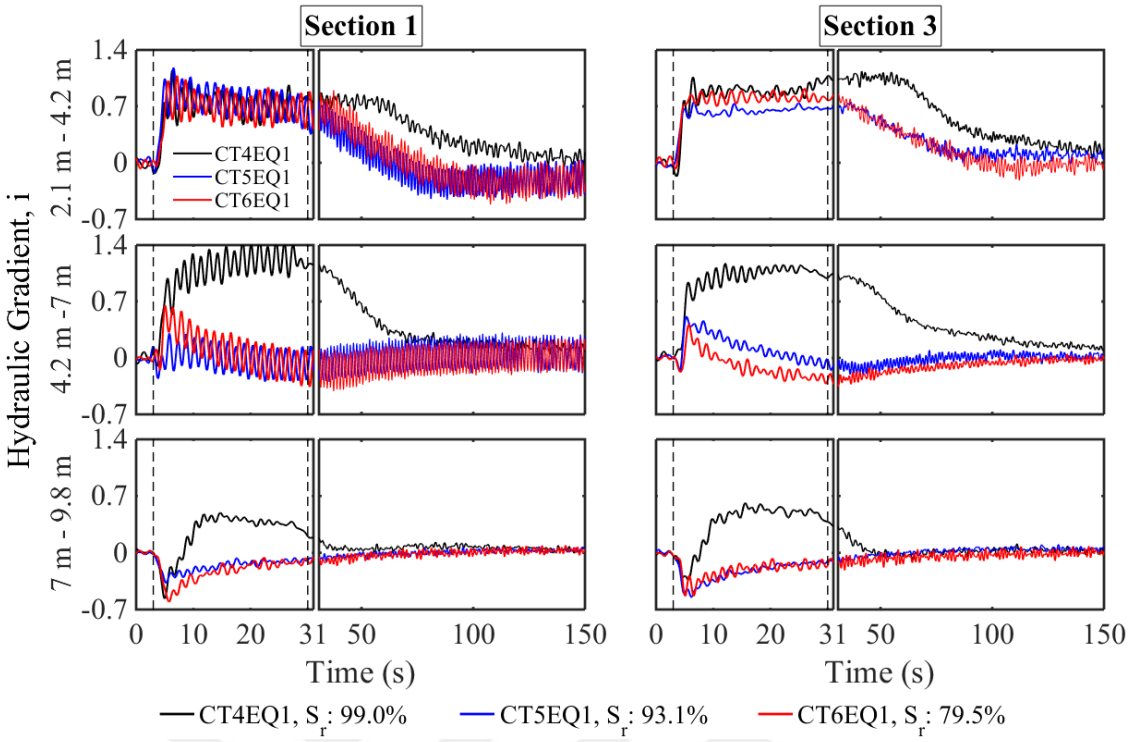

Figure 6.5– Time histories of hydraulic gradients recorded in the free-field during and after earthquakes.

Depth of Liquefaction

The isochrones of excess pore pressure head recorded in Section 1 are plotted in figure 6.6 to show the direction and magnitude of hydraulic gradients that formed at different times and depths. The r_u =1 line displayed in this figure indicates the limit excess pressure head where the corresponding soil layer reached complete liquefaction. The isochrones of excess pressure heads were presented at the time intervals of 4 s, 17 s and 28 s, which corresponded to the first 2, 11 and 17 cycles of acceleration from the start of earthquake, respectively. The remainder of the time intervals, after 28 s, corresponded to the post-earthquake reconsolidation process in a short and long-term for the saturated case.

In the saturated soil for CT4 (S_r: 99.0%), excess pore pressure profile did completely touch the r_u = 1 line at a depth of 7 m and almost touch it at a depth of 9.8 m, revealing a very deep layer of the liquefied soil layer. Large hydraulic gradients formed vertically upwards after few seconds of the earthquake. While the liquefaction of soil started from the surface and propagated downwards, the dissipation of excess pore pressures commenced from the base and moved upwards. The deepest PPT at 14 m depicted slightly lower excess pore pressure than expected probably owing to its calibration that was at fault. However, partially saturated soil layers liquefied until 4.2 m for CT5 (S_r: 93.1%) and 2.1 m for CT6 (S_r: 79.5%). As far as the pore fluid flow within the soil layers is concerned, despite the prolonged shakings in the

partially saturated soils, pore fluid flow due to excess pore pressure gradients almost ceased at the end of 300 s, and the equilibrium of pore pressures throughout the soil layers maintained. These findings justify that there is an apparent link between S_r and depth of liquefied soil layer. The depth of free-field soil layer that reached liquefaction decreased as S_r of soil deposits was reduced through the air injection. The increased liquefaction depth may explain the relatively larger post-seismic settlements in the saturated soil than in the partially saturated soils. Further insights into the post-seismic settlement response in such soil layers can be found section 6.3.1.

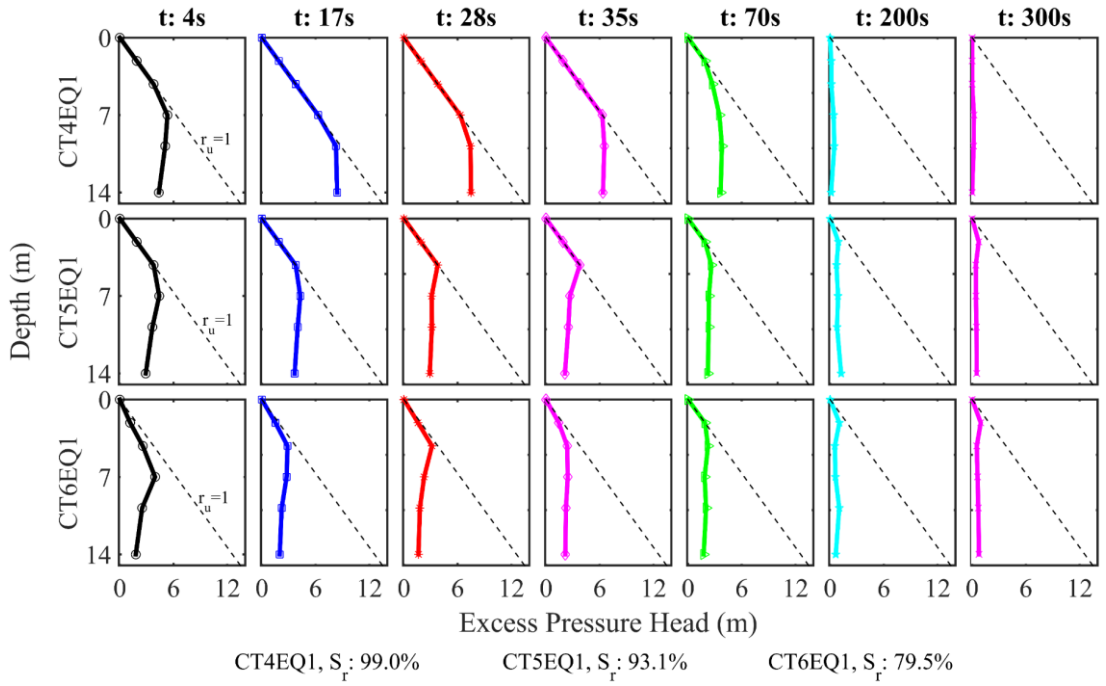

Figure 6.6– Variation of excess pore pressure head with depth and time.

Discussion of Excess Pore Pressure Dissipation

The results above show that the mechanisms of excess pore pressure generation and dissipation in the saturated and partially saturated soils were different from each other, but the second phenomenon was particularly complicated. It is known that excess pore pressures can only be generated in a soil deposit where the voids are filled with pore fluid. The presence of occluded air in the pore fluid can either prevent or reduce the build-up of excess pore pressure, depending on degree of saturation of soil and initial pressure of air bubbles. The observed trends, described in section 6.2.1.2, showed that high excess pore pressures were generated in the saturated soil, and they usually retained their peaks throughout the earthquake while oscillating vigorously at that level. At the deepest soil layer, excess pore pressure started to dissipate just before the end of the earthquake. This is ascribed to the insufficiency of the small magnitude of acceleration cycles towards the end of the earthquake to maintain such a high level of excess pore pressures.

In the partially saturated soils, comparatively much smaller excess pore pressures developed particularly at the deeper soil layers under high confining stresses. After they reached their peak, a rapid drop in the excess pore pressures seemed to happen even while the earthquake continued. Relatively smaller magnitude of excess pore pressure generation can be attributed to occluded air bubbles that contracted during the dynamic loading and reduced the build-up of excess pore pressures. It was reasonable to expect that air bubbles would influence the dissipation of excess pore pressures since they could potentially decrease the hydraulic conductivity of soils. The non-uniform distribution of air bubbles within the soil layers (see section 4.4.1) was also expected to add to the complexity of the dissipation behaviour in these soils. Further study of the phenomena under consideration may be necessary to garner a comprehensive understanding of the dissipation behaviour in the partially saturated soils.

6.2.1.4 Acceleration Amplification/Attenuation Behaviour

As far as the trend in figure 6.3 is concerned, any change in S_r of soils affected the pore pressure behaviour beneath the shallow foundations. This, in turn, influenced the acceleration-time histories measured within the soil columns and foundations. To visualise the aforementioned, the histories of amplification/attenuation ratio-cycle number recorded beneath the light shallow foundation during the first earthquakes of CT4, CT5 and CT6 are presented in figure 6.7. The measured horizontal accelerations were explicitly investigated, and amplification/attenuation ratios were calculated on a cycle-by-cycle basis. Starting from the first quarter cycle of the earthquakes, these ratios were found by dividing the maximum positive and negative acceleration of a given accelerometer in each cycle by the maximum positive and negative acceleration of the corresponding input accelerometer in the corresponding cycle. It must be noted that the soils examined here were subjected to earthquakes of the same input acceleration amplitude (0.18 g), and S_r of soil deposits was the only variable in each case.

The acceleration records in the saturated soil (CT4) showed that as the soil liquefied, significant deamplification of the input motion occurred. The amplitude of foundation acceleration and soil acceleration in both positive and negative direction significantly reduced with each cycle. For instance, the amplitude of horizontal acceleration close to the soil surface (at 4.2 m) became only 0.18 of the input motion in the positive direction around cycle 3. At a depth below 9.8 m, an attenuation occurred until the first five cycles. There was some amplification afterwards, which was suggestive of the dilation of soil and regaining some strength.

Unlike in the saturated soil, the deposits at similar depths (namely 4.2 m and 9.8 m) remained unliquefied in the partially saturated soils (CT5 and CT6). Therefore, a notable attenuation of foundation and soil acceleration did not happen. For CT5, a slight attenuation and amplification of the foundation acceleration were apparent in positive and negative direction, respectively. A further reduction in S_r entirely prevented the attenuation in the amplitude of oscillation associated with the occurrence of liquefaction (CT6). On the contrary, it led to the amplification of the acceleration of foundation soil. Larger amplitude of accelerations was transmitted to the foundation through this unliquefied soil zone. This finding indicates that reducing S_r of the soil deposits might play a role of intensifying the dynamic loads experienced by foundations and increasing the dynamic demand on them.

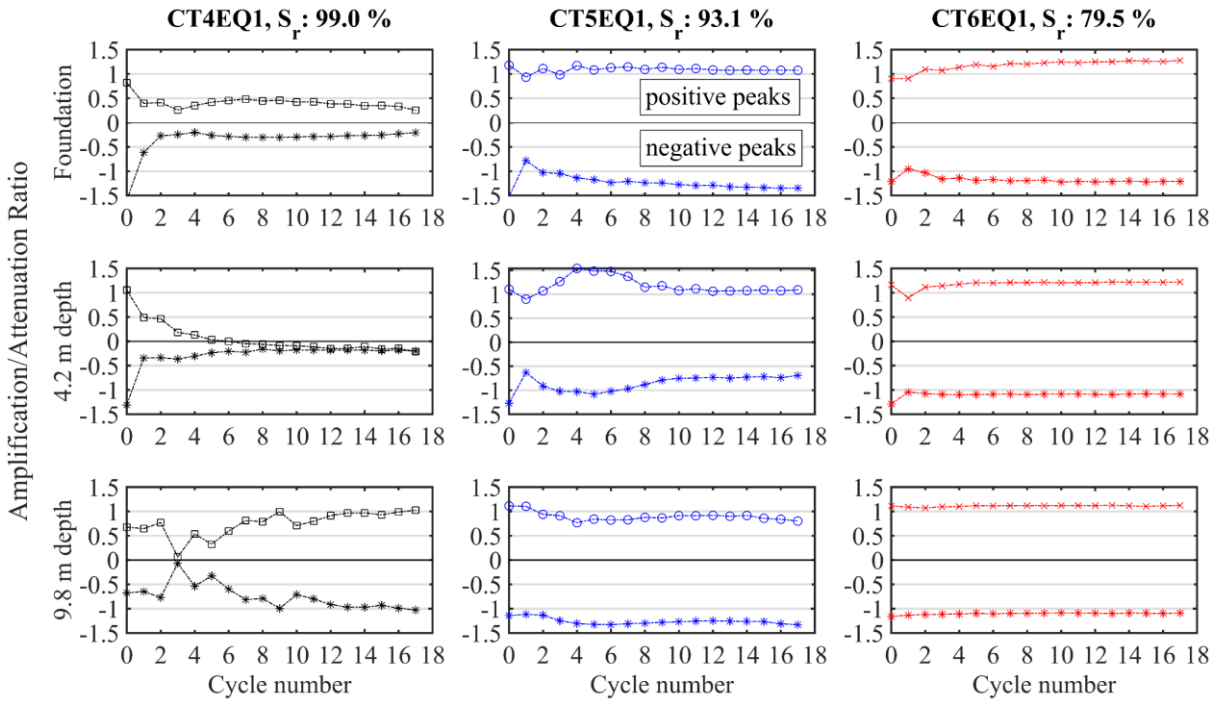

Figure 6.7– Typical amplification/attenuation ratios for foundation and foundation soil.

6.2.1.5 Shear Stress-Strain Loops

The dynamic shear stress-strain response was calculated to examine how air injection affects the shear stiffness of soils. Figure 6.8 presents typical excess pore pressure, input acceleration, shear stress & strain time histories in tandem with the shear stress-strain loops recorded at a depth of 4.2 m below the ground surface for the saturated (CT4) and partially saturated soil (CT6). The shear stresses and strains were calculated using the vertical array of acceleration data and following the methodology proposed by Elgamal et al. (1996). Filtering of horizontal acceleration data was carefully performed, as recommended by Brennan et al. (2005).

It is seen in figure 6.8 that excess pore pressure built up during the first 1-2 cycles of the earthquake in the saturated soil, and it reached liquefaction. Later in the earthquake, the magnitude of shear stresses dropped significantly since the liquefied soil was unable to transmit such shear stresses. In general, it experienced large shear strains and small shear stresses, showing a softened shear stress-strain (τ-γ) loop. Nevertheless, despite displaying shear strains of just slightly smaller amplitude, the partially saturated soil at the equivalent soil layer experienced relatively larger shear stresses during the pore pressure build-up, which was suggestive of a stiffer response. Later in the earthquake, the drop in the shear stiffness of soil was very limited in this case. Overall, the aforementioned trend indicates that a reduction in S_r of liquefiable soils with the aid of air injection plays a significant role in minimising the generation of excess pore pressures and consequent softening of soil at the relevant locations. It affects the shear stress-strain response of a given soil layer, enabling a partially saturated soil to display a much stiffer response than its saturated counterpart.

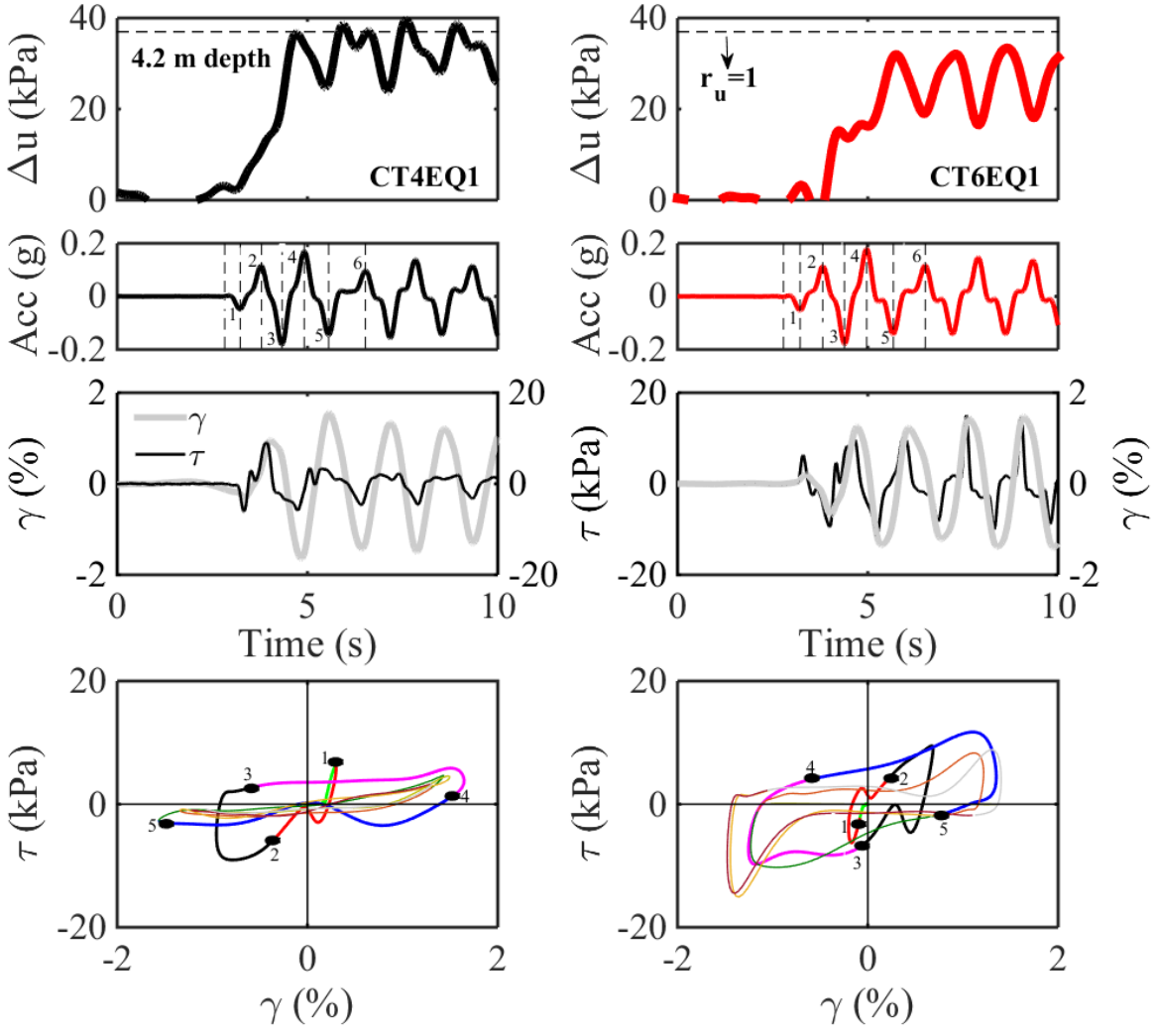

Figure 6.8– Typical shear stress-strain loops recorded in the free-field (Section 1).

6.2.2 Confining Stress Level (Vertical Stress)

Published liquefaction studies often report that confining stress is an important parameter to describe the liquefaction behaviour of soils. The cyclic liquefaction resistance of saturated soils varies according to their density, the amplitude of static shear stress (if present) and confining stress level (Vaid and Chern 1983). For a given saturated soil at a given relative density, there is a non-linear relationship between the liquefaction resistance and the confining stress (Seed and Harder 1990). The compressibility of the soils further complicates this behaviour.

The published data based on triaxial testing revealed an increasing trend in the liquefaction resistance of partially saturated soils with decreasing S_r, as shown in figure 2.8. However, S_r alone is deficient in a more comprehensive explanation of the partially saturated soil response and in assessing its cyclic liquefaction resistance. Okamura and Soga (2006) compiled an array of laboratory test data from the literature and reported a wide range of liquefaction resistance for the same S_r. The authors concluded that S_r is not the only factor that affects the liquefaction resistance of partially saturated soils, but also the effects of initial confining stress and initial hydrostatic pore pressure play a predominant role in their resistance to liquefaction. The vast majority of the research that forms the basis for the confining stress dependency of liquefaction resistance of soils is based on the element testing in the laboratory. Despite the great virtues of element tests for the basic understanding of the phenomena, it is not very convenient for the investigation of the effects that confining stress has on the response of shallow foundations resting on the saturated and partially saturated soils. Although this issue can be simply resolved by using physical model experiments, very little research is available on this particular topic.

The stress level of a free-field soil at any depth is dependent on the self-weight of the overlaying soil deposit. Therefore, the stress level that can be reproduced in a small-scale 1-g shaking table test will be markedly smaller than that in the field. Since soil liquefaction is a stress-dependent phenomenon, this stress dissimilarity may cause the results of 1-g shaking table tests to be somewhat sceptical. In the field of geotechnical earthquake engineering, despite the limitations of 1-g shaking table tests concerning the quantitative values, they can still provide significant (qualitative) information on the deformation mechanisms that drive the liquefaction-induced settlement of shallow foundations and on the partially saturated soil behaviour. Geotechnical centrifuge modelling can be used to overcome the limitations of 1-g small-scale tests. In this approach, the self-weight of the soil itself is increased with increasing centrifugal accelerations, and the stress level in the small-scale model becomes equivalent to that in the field (prototype).

This section presents a systematic investigation of the combined influence of S_r and initial confining stress on the seismic liquefaction behaviour of saturated and partially saturated soils and on the response of shallow foundations resting on such soil deposits. Of particular interest is to explore the effectiveness of air injection in reducing the liquefaction risks, under different confining stresses, at varying g-levels and soil depths. The main intent is to reinforce and build on the previous research with the aids of the findings from the first earthquakes of shaking table tests (STT1, STT2 and STT3) and high-g centrifuge tests (CT4, CT5 and CT7).

6.2.2.1 Settlement and Excess Pore Pressure Response (1-g Testing)

Figure 6.9 shows the first earthquake time histories of settlement, excess pore pressure ratios and input motion for the 1-g shaking table tests. The preparation of the specimens and initial test conditions were already summarised in section 3.4.

It is clearly seen that the magnitude of foundation settlement and excess pore pressure ratio was the largest for the unimproved soil deposit having a pre-earthquake S_r of 96.8% (STT1). The remediation of liquefiable soil layers via air injection (STT2) and chemical compound of sodium perborate monohydrate (STT3) affected the settlement and excess pore pressure behaviour to a certain extent. Despite their beneficial effects, approximately 7% reduction of S_r provided only 22% (SST1) and 11% (SST3) decrease of the foundation settlement.

As far as the excess pore pressures generated at the mid-depth of the soil layers are concerned, they increased quickly and reached a peak value at the early stages of the earthquake. The shakings, with low frequencies, were unable to retain the build-up excess pore pressures at this level, and they started to drop while the earthquakes continued. Air injection or chemical compound caused only a minor reduction of excess pore pressures. Overall, under the Earth's gravity, a deep layer of soil liquefied during the build-up of excess pore pressure, irrespective of the presence of air/gas bubbles within the specimens. For all cases, the shallow foundations suffered extensive seismic settlement, sinking deep into the liquefied soil.

It is worthy of notice that partially saturated soils responded differently in the tests SST2 and SST3. Although pre-earthquake S_r of the specimens was very similar in each case, air-injected partially saturated soil performed better than the chemically treated soil. The different response of the two soils was more likely related to the different size and distribution of air bubbles. Particularly for the chemical method, the segregation of Efferdent powder may occur during the sand pouring process, leading to non-uniform distribution of air bubbles.

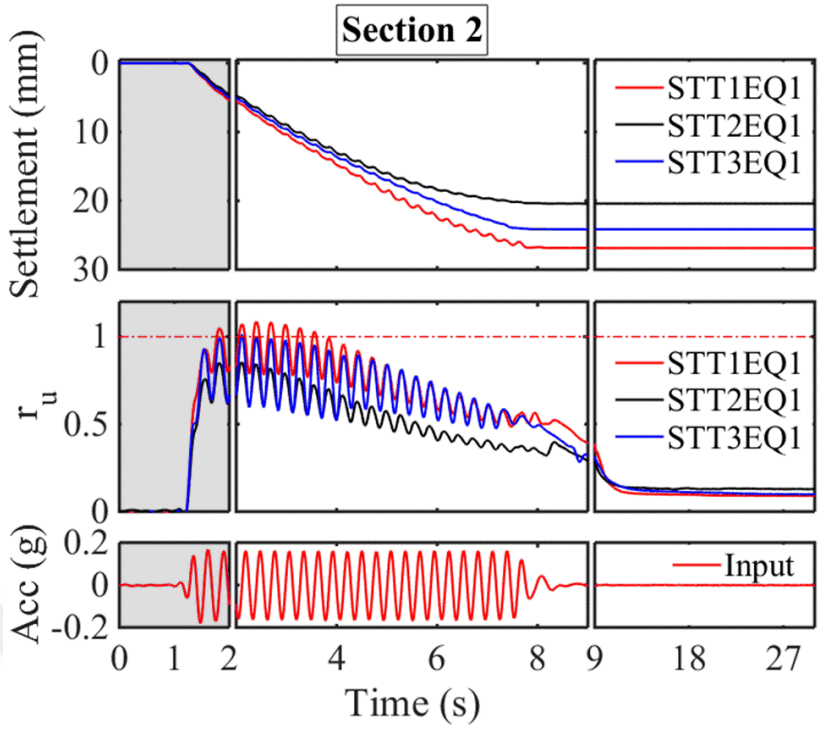

Figure 6.9– Time histories of foundation settlement and excess pore pressure ratios (1-g testing).

6.2.2.2 Settlement and Excess Pore Pressure Response under High-g

The results from centrifuge tests conducted at 70-g already justified the significance of the confining stress for the general patterns of excess pore pressure behaviour (see section 6.2.1.2). The manner in which confining stress affects the seismic performance of air injection method was explored further by subjecting the partially saturated model to the centrifugal acceleration of 40-g in CT7. The representative settlement and excess pore pressure ratio traces are presented below, with a particular focus on the impact of g-level and soil depth on the observed trends. No centrifuge test was undertaken at 40-g for the saturated soil case. Results from the saturated soil test conducted at 70-g (CT4) are, therefore, used for comparison.

The first earthquake time histories of average foundation settlement recorded for the saturated soil in CT4 (S_r: ~99%) and for the partially saturated soil in CT7 (S_r: ~84%) are plotted in figure 6.10. The settlement traces show that in contrast to the shaking table tests at 1-g, air injection technique was successful at minimising the liquefaction-induced shallow foundation settlements, under the higher confining stresses, at the increased gravitational field.

Figure 6.10 also presents the time histories of excess pore pressure ratios that built up beneath shallow foundation (Section 2) during the first earthquakes of CT4 and CT7. It is evident that significant excess pore pressures were generated in the saturated soil (CT4), and a deep layer

of soil experienced a significant soil-softening associated with liquefaction. On the other hand, air injection minimised the magnitude of the build-up excess pore pressures, subsequently reducing the depth of liquefaction and soil-softening in the partially saturated soil (CT7).

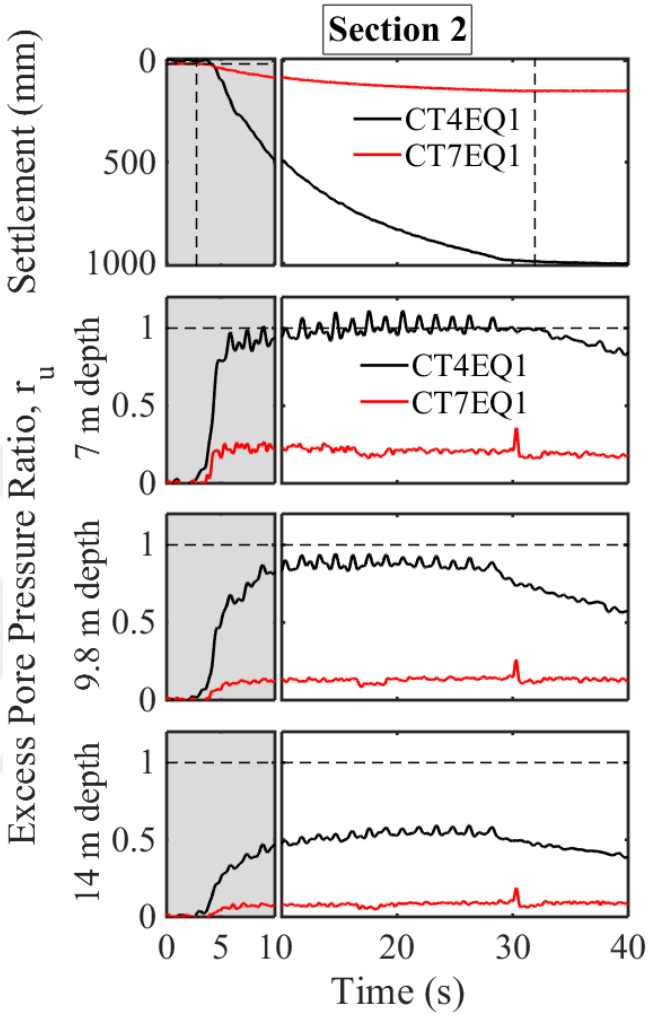

Figure 6.10– Time histories of foundation settlement and excess pore pressure ratios (high-g testing).

Free-Field Response

To offer further insights into the corresponding problem, representative time histories of excess pore pressure ratios recorded in the free-field and during the first earthquakes of CT4 and CT7 are compared in figure 6.11. The maximum excess pore pressure ratios (r_u =1) are shown by the horizontal dashed lines. It is apparent that large excess pore pressure ratios were generated in the saturated soil (CT4). Significant soil-softening associated with liquefaction occurred at almost every depth, up to 9.8 m. The build-up of excess pore pressures, under lower confining stress, at the shallow depths of the partially saturated soil (CT7) showed the similarities to the observed trend in the saturated case. Excess pore pressure ratios generally became equal to unity at the depths of 2.1 and 4.2 m. The magnitude of excess pore pressure ratios generated in

the deeper soil layers was, however, much smaller in the partially saturated soil than in the saturated soil, and r_u =1 was not reached in any case.

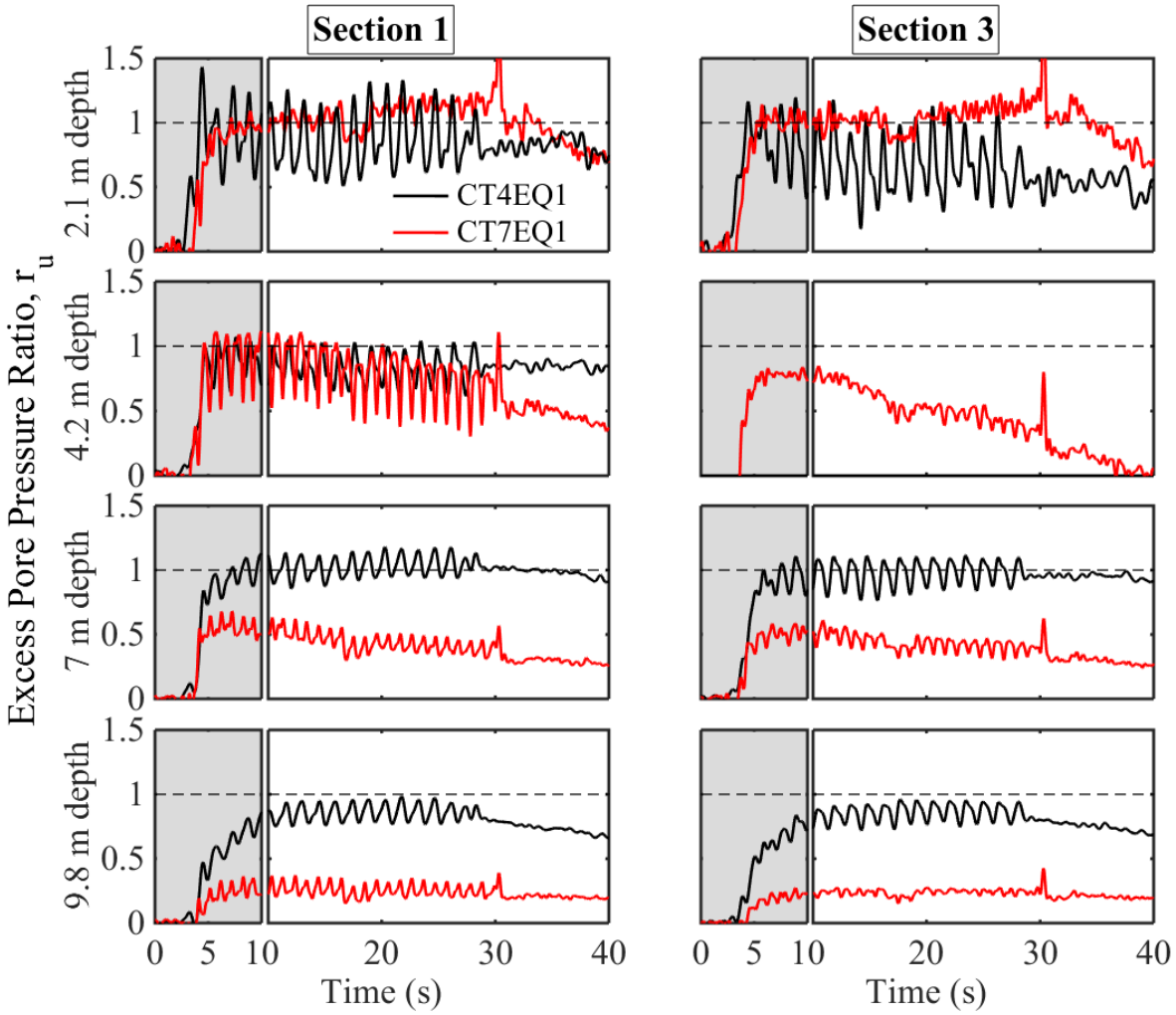

Figure 6.11– Time histories of excess pore pressure ratios in the free-field (high-g testing).

With the aids of the observed trends, it can be said that the effectiveness of air injection as a remediation method increases with increasing confining stress. The efficiency with which air injection improves the liquefaction strength of soils, currently shown in terms of excess pore pressure ratios, often reduced considerably at the shallower depths where the confining stresses are smaller, whereas it increased profoundly, under the higher confining stresses, at the greater depths. These results correlated very well with the experimental findings of Okamura and Soga (2006). Based on the cyclic triaxial tests, the authors showed that under a very low confining stress the liquefaction resistance of the partially saturated soils, irrespective of their S_r, was almost same as the liquefaction resistance of the saturated soils. However, partially saturated soils displayed significantly higher liquefaction resistance than their saturated counterparts as initial confining stresses increased.

6.2.2.3 Shear Stress-Strain Loops

Figure 6.12 depicts the typical shear stress-strain histories calculated along the right-hand side of the centrifuge models (Section 3) with and without air injection. They were computed using the horizontal acceleration-time histories recorded at different depths of the soil models.

It is seen in figure 6.12 that initial small-strain shear stiffness increased with depth in all cases. The increase in the confining stress of soil caused a corresponding increase in the soil's shear stiffness, which correlated well with many published data. In the saturated soil (CT4), the shallow and deeper soil layers liquefied after a few cycles of earthquake loading, showing softened shear stress-strain (τ-γ) loops. In comparison, in the partially saturated soil (CT5) the equivalent stress-strain loops demonstrated that while the soil at the shallow depth with lower confining stress behaved in a similar way to that in CT4, it showed significant shear stiffness in the deeper level. This suggest that air injection enables the soil to resist the full liquefaction at the higher confining stresses, whereas it is less effective at the lower confining stresses.

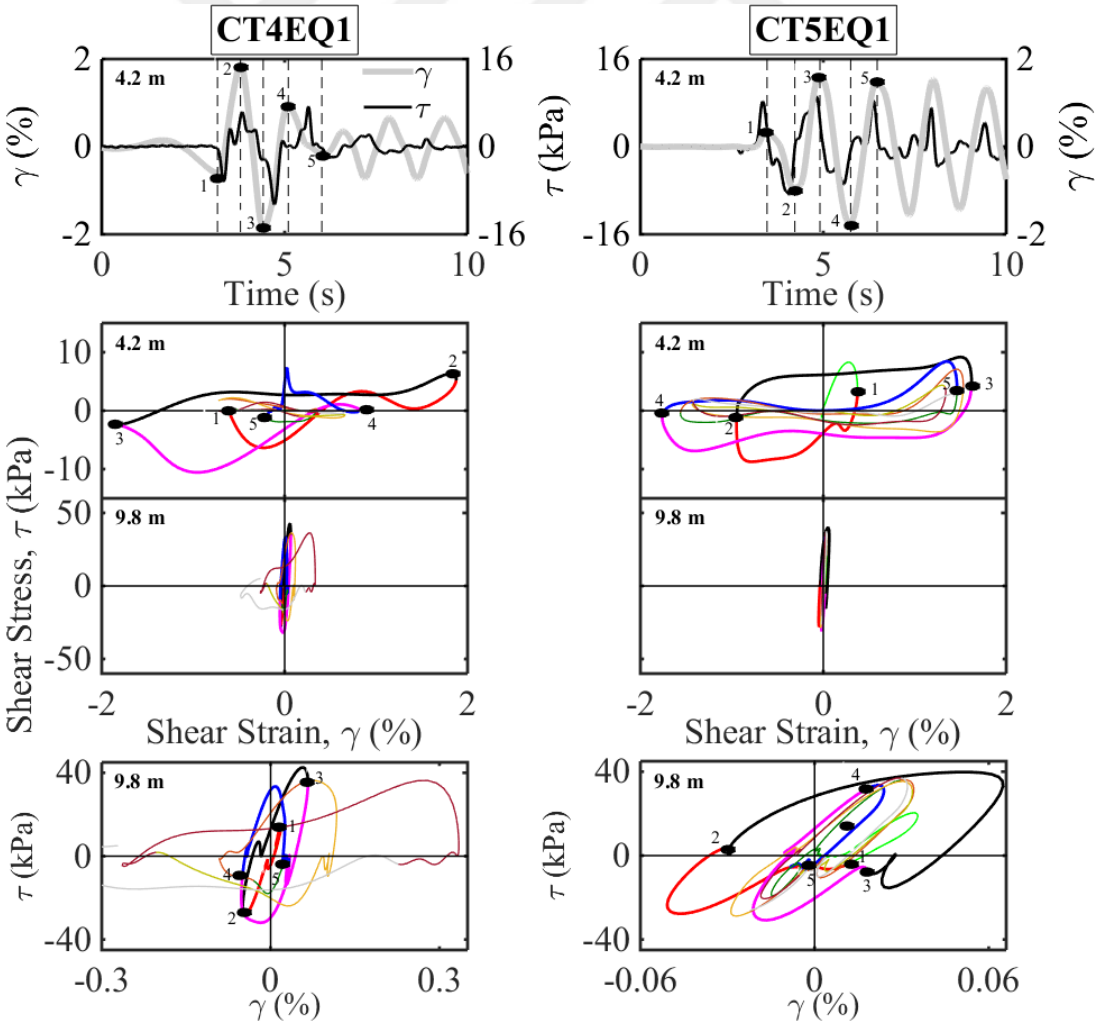

Figure 6.12– Typical shear stress-strain loops recorded in the free-field (Section 3).

6.2.3 Bearing Pressure

The field and experimental evidence described in the literature shows that bearing pressure, q, is an important parameter that affects the settlement of structures with shallow foundations built on liquefiable ground. It is documented that the presence of shallow foundations imposes additional stresses on soils. The increased stresses in the foundation soil, in turn, act towards reducing the liquefaction susceptibility of the corresponding soil layers. However, the impact of this effect on the seismic liquefaction response is shown to depend on not only the properties of structure but also the properties of soil and ground motion. For instance, based on centrifuge tests, Dashti et al. (2010) demonstrated that during a moderate earthquake, much smaller excess pore pressures built up beneath a structure with a foundation bearing pressure of 130 kPa than those having a foundation bearing pressure of 80 kPa. In comparison, the heavier structure was observed to settle less on the same soil type. During a much stronger earthquake, the assessment of the influence of bearing pressure on the soil and foundation performance, however, became relatively more complicated. Based on the case histories from the 2010 Maule earthquake in Chile, Bertalot et al. (2013) observed a threshold value for the bearing pressure of shallow foundations. An increasing trend in the settlement of buildings with shallow foundations was observed as the bearing pressure increased up to 80 kPa. Nevertheless, this was followed by a decreasing trend above that level. Using the centrifuge test results, the decreasing settlement of shallow foundations with increasing bearing pressure was later ascribed to the limited excess pore pressure generation around the edges of the foundations owing to the large initial shear stresses in the soil and lack of dynamic shear stress reversal (Bertalot and Brennan 2015).

Overall, these observations stress the significance of the bearing pressure for the interpretation of the seismic response of shallow foundations on the liquefiable soil deposits. They may also point to the need for a consideration of this parameter in the study of air injection technique.

It is of interest in this section to discover the possible impact of foundation bearing pressure on the dynamic behaviour of saturated and partially saturated soils. For this purpose, the data from centrifuge tests examining the response of the *heavy* and *light* foundations are compared. The *heavy* foundations applied a bearing pressure of 135 kPa in CT1, CT2 and CT3. The *light* foundations exerted a bearing pressure of 50 kPa in CT4, CT5 and CT6. The width and aspect ratio of the shallow foundations remained the same. The effect of bearing pressure was isolated by increasing the weight of the foundations (see section 3.3.1).

6.2.3.1 Foundation-Induced Stress Distribution

In the event of an earthquake loading, effective stress, a measure of contact forces between the soil grains, varies considerably in a liquefiable deposit, owing to the build-up of excess pore pressures. This causes a consequent degradation of the shear stiffness and strength of soil. Once the earthquake event is over, the contact forces are re-established during the reconsolidation of liquefied soil, in which total stress remains constant. Damage to soil and foundation occurs both during and after the earthquake. This indicates that deformations that develop within a liquefiable ground can be accurately evaluated when the true stress distribution is known.
In the presence of foundation on the level ground, the total stress is no longer the geostatic vertical stress, and affected by the bearing pressure of the foundation. The stress distribution due to foundation, however, changes with the onset of liquefaction. Soil-softening during an in/complete liquefaction and related redistribution of foundation-induced stress render the determination of the true stress distribution in soils a more complex task. This problem may be solved using a well-developed finite element method of analysis, which is however not widely available to engineers. The relevant problem is also deemed beyond the scope of this thesis.

In this thesis, the models represented plane strain problems, and model foundations represented strip footings. Despite its scientific limitations, the contribution of foundation-induced stresses to the total stresses was calculated using the elasticity-based Boussinesq stress distribution method. It was mainly for the ease of the performed analyses and interpretation of the results.

6.2.3.2 Settlement Behaviour

Figure 6.13 shows the first earthquake time histories of the settlement that the *heavy* and *light* foundations experienced and of input acceleration. It is worth noting that the test conditions and initial soil properties were almost the same for each experiment. Furthermore, for all cases, applied input motions were very similar, with the exception of the prolonged earthquakes in CT5 and CT6. The data for the *light* foundation was already discussed in section 6.2.1.1.

It does appear in figure 6.13 that similar to the *light* foundation, the total settlement of the *heavy* foundation drastically decreased with reducing S_r, leaving no doubt about the effectiveness of air injection as a remediation treatment. Approximately 62% and 91% of the total foundation settlements reduced in CT2 and CT3, respectively. The settlement traces also demonstrate that the *heavy* foundation started to settle after the first cycle of the earthquakes, and the settlement accumulation mainly developed during the earthquake events in each case.

In comparison, the rate of co-seismic settlement was much larger under the *light* foundation than the *heavy* foundation, irrespective of the treatment of soils. In the saturated soils, the rate of settlement for the *heavy* foundation was almost linear in CT1, whilst the trace of the *light* foundation followed a comparatively less linear trend in CT4. The introduction of air bubbles resulted in a dramatic decrease in the rate of co-seismic foundation settlement, but this effect was much greater under the *heavy* foundation.

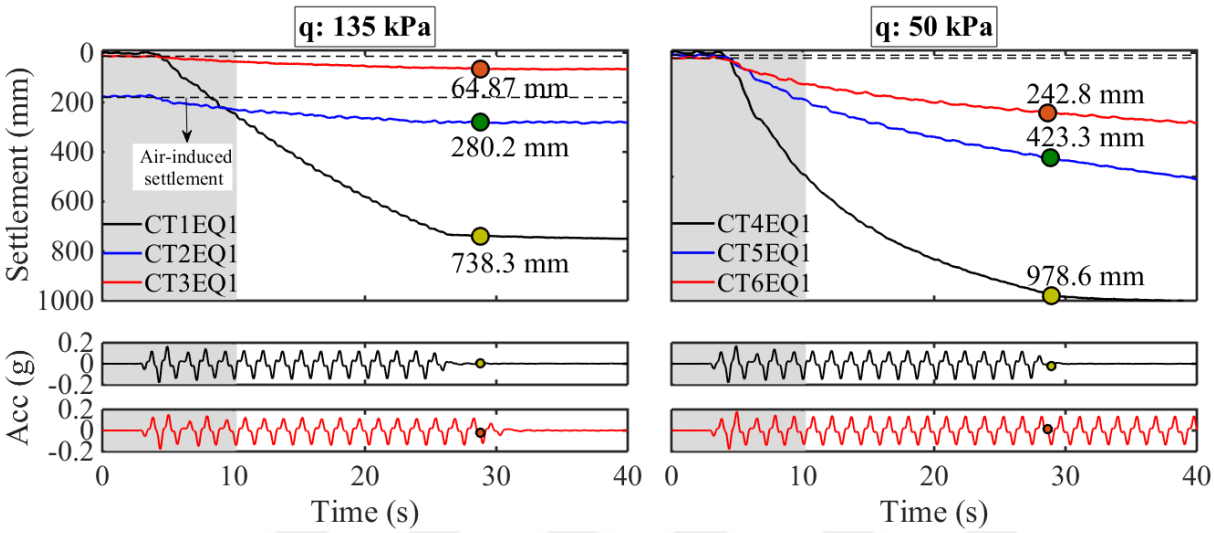

Figure 6.13– Time histories of heavy and light footing settlement and input acceleration.

Degree of saturation of the soil models varied in the centrifuge tests. The cumulative foundation settlements over an equivalent number of acceleration cycles (17) against S_r are presented separately in figure 6.14. This figure shows the influence of air injection, and hence S_r, on the settlement trends of foundations with different contact pressures. For the *light* foundation, the cumulative settlements appear to substantially decrease with a reduction in S_r. Nevertheless, it can be inferred from the observed trends that the corresponding reduction in the foundation settlements may be insignificant below certain S_r values, such as 80%. In other words, a further reduction in S_r may not cause a marked decrease of foundation settlement, and the relative gain in performance may probably be minor. For the *heavy* foundation, the settlements continued to reduce up to a degree of saturation of 86 %. Since the *heavy* foundation experiences very small settlement at this saturation level, no further data points are required to establish the lower threshold of degree of saturation, below which partial saturation will have little or no benefit.

In figure 6.14, settlement response of the *heavy* and *light* foundations resting on the saturated soils indicated a decreasing settlement trend with increasing bearing pressure. This behaviour can be linked to the increased stress field and variation in the excess pore pressure response beneath the foundations. The foundation-induced stresses that causes high stress concentration

over a large area probably increased the cyclic resistance of the foundation soil, affecting the excess pore pressure behaviour (see figure 6.15). In parallel with this observation, it is evident that the benefit of air injection (or reducing S_r) was notably greater for the highly confined partially saturated soils. In fact, this was consistent with the aforementioned findings in section 6.2.2. Accordingly, it should be expected that the success of air injection technique in reducing the liquefaction-induced foundation settlements will be higher beneath a *heavy* structure than a *light* structure on the same soil type and under the similar ground motion characteristics.

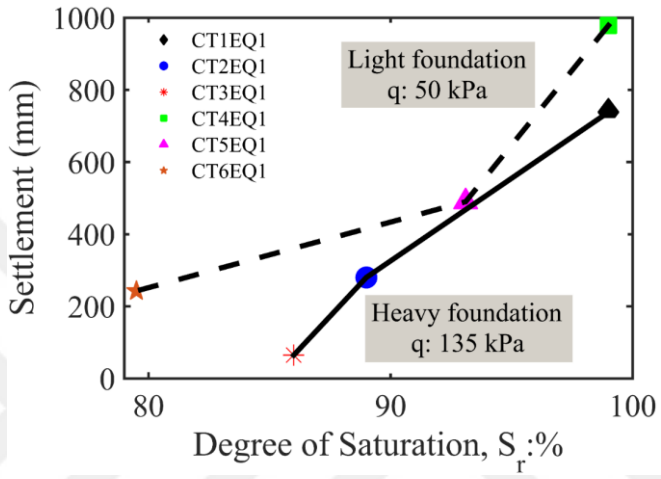

Figure 6.14– Foundation settlement versus degree of saturation.

6.2.3.3 Generation of Excess Pore Pressures

This section discusses the impact of bearing pressure on the excess pore pressure response at the equivalent cycles of earthquakes and equivalent soil depths. Figure 6.15 presents the first earthquake time histories of excess pore pressures recorded at the mid-depth of the soil layers and under the axis of the shallow foundations during the centrifuge tests CT1 to CT6. The first earthquake input acceleration-time histories from CT1 and CT4 are also shown for a reference.

The comparison of the excess pore pressures developed within the saturated soil layers at 7-m depth indicated that relatively smaller excess pore pressures were generated under the *heavy* foundation (CT1) than the *light* foundation (CT4). Moreover, at this depth, the generation of excess pore pressures to maximum was more gradual and slower under the *heavy* foundation. In fact, the observed trends agreed with the results of many independent centrifuge tests on the response of shallow foundations (e.g. Liu and Dobry (1997) and Dashti et al. (2010)). It is suggested that although a soil deposit under a higher confining stress is capable of generating higher excess pore pressures for a given excess pore pressure ratio, r_u, it requires larger cyclic shear stresses to develop such excess pore pressures. Under the applied input motions being of

same amplitude and duration, the resistance of the soil to the excess pore pressure generation is expected to be higher under the *heavy* foundation that imposes larger confining stresses. In figure 6.15, the decreasing trend in the magnitude of excess pore pressures as bearing pressure increased may suggest that for each of the two experiments, the applied earthquakes were not strong enough to overcome the higher capacity of the soils for increased excess pore pressures. It is noted that the impact of bearing pressure on the pore pressure behaviour varied at different soil depths. For instance, unlike at 7-m depth, the magnitude and pattern of excess pore pressure development were similar at 9.8-m for each of the two tests. This may indicate that the effect of foundation-induced confining is localised to the soil beneath it, and its influence on the excess pore pressure generation became relatively small at locations away from the foundation. It is also evident in figure 6.15 that air injection hindered the development of high excess pore pressures in the soil layers. As a result, the magnitude and rate of excess pore pressures became considerably smaller in the partially saturated soils than in their saturated counterparts. The comparison of the excess pore pressures generated beneath the *heavy* and *light* foundations also shows that the increased resistance of partially saturated soils to pore pressure generation was more pronounced under the higher confining pressures of foundations and in the deeper layers.

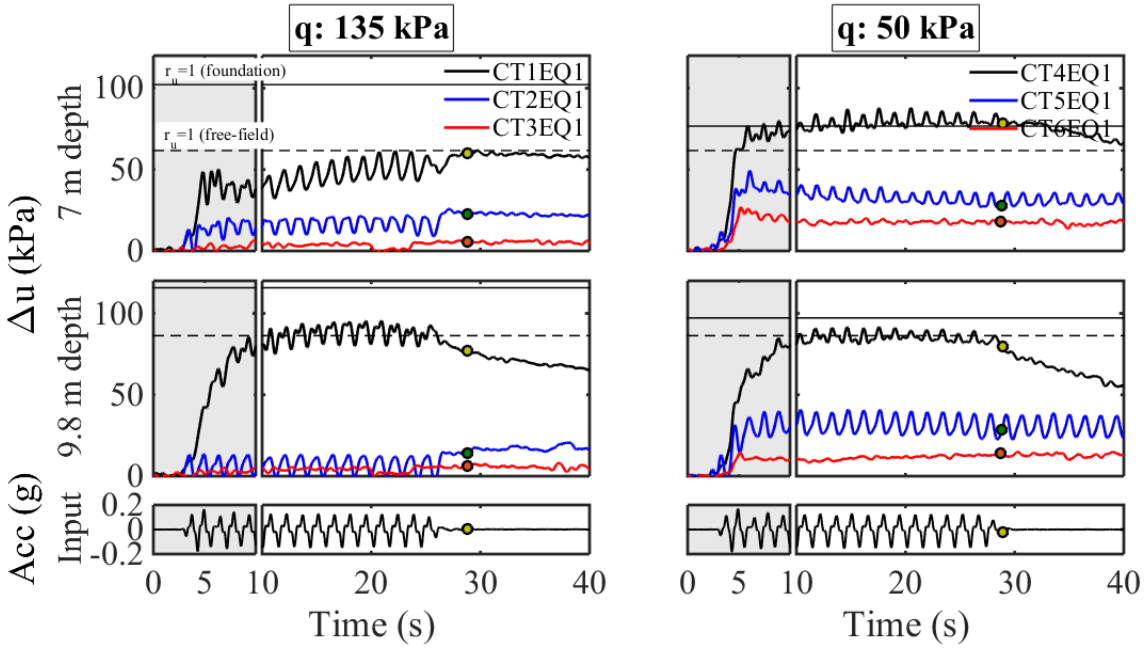

Figure 6.15– Time histories of excess pore pressures beneath heavy and light foundations.

6.2.3.4 Acceleration Amplification/Attenuation Behaviour

Section 6.2.1.4 already justified the predominant role of S_r in minimising or preventing the attenuation of the amplitude of oscillation, associated with the occurrence of liquefaction. It

was shown that reducing S_r led to larger amplitude of accelerations being transmitted to the *light* foundations through the soil column below its centre line. Here, effects of the foundation bearing pressure are investigated to offer further insights into the problem.

Figure 6.16 compares the amplification/attenuation ratios of the *heavy* and *light* shallow foundations. It is apparent that the *heavy* foundation suffered less deamplification of the input motion than the *light* foundation for each of the two saturated soils. Similarly, larger accelerations were transferred to the *heavy* foundation than the *light* foundation for the partially saturated soils. The observed trends may suggest there is an apparent link between the level of accelerations transferred to the foundations and the bearing pressure. The increasing level of foundation accelerations with increasing bearing pressures can be attributed to the formation of an area of increased stiffness beneath the shallow foundations. Balakrishnan and Kutter (1999) explained how the natural period of the soil deposits changes when the stiffness of soils alters. They claimed that increasing the stiffness of deposits may increase the ground motion amplification, depending on the predominant period of ground motions.

With the aids of the aforementioned test results, it can be suggested that a decrease of S_r and presence of shallow foundations allow an area of increased stress and stiffness to be formed beneath the foundations. This inhibits the soil-softening associated with earthquake-induced liquefaction. In comparison with the *light* foundation, the extent of such area is expected to be larger beneath the *heavy* foundation due to the level of foundation-imposed confining stresses. Consequently, much larger accelerations get transmitted from this bearing stratum to the *heavy* foundation. It is worth to emphasise that the impact of this effect is expected to be the greatest when the area of increased stiffness reaches the base of the soil models.

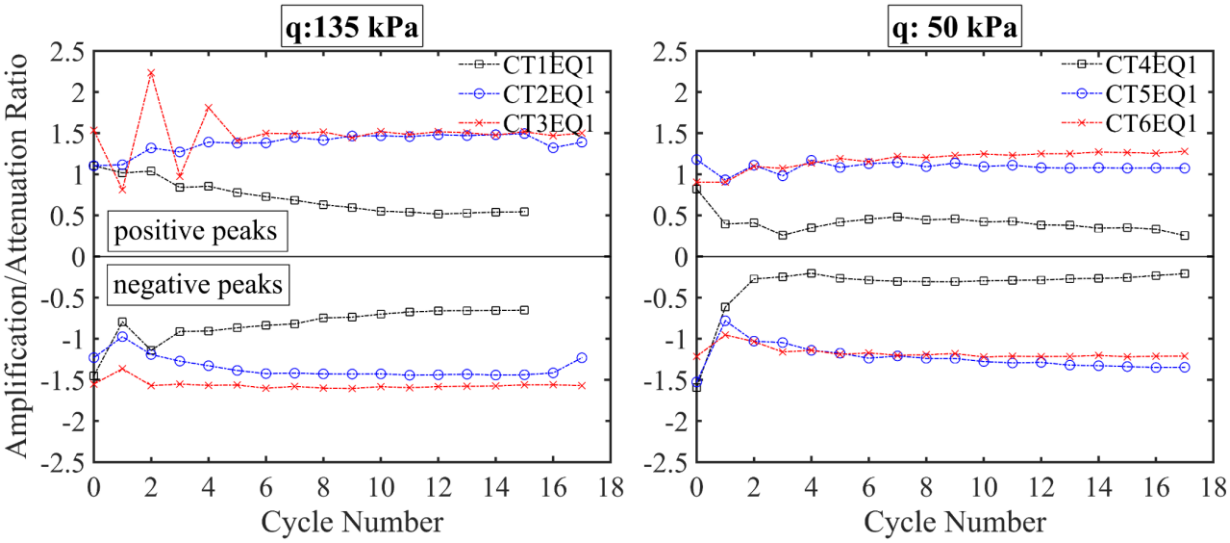

Figure 6.16– Amplification/attenuation ratios for the heavy and light foundations.

6.2.4 Earthquake Motion Characteristics

The characteristics of an earthquake loading (e.g. peak ground acceleration and duration) are of engineering significance since they notably affect the liquefaction response of soils. The amplitude of cyclic shear stresses and number of their applications are the main factors for the seismic liquefaction (Seed 1979). These factors are related to the amplitude (peak acceleration) and duration of strong shaking. The duration of a strong ground motion can significantly affect liquefaction-induced deformations as the generation of excess pore pressures and degradation of soil stiffness correlate well with the number of cyclic loadings or stress reversals.

In this study, centrifuge models were subjected to a series of earthquakes to explore the effects of earthquake amplitude on the dynamic behaviour of soils. There are, however, some doubts about the acceptability of firing multiple earthquakes on the same soil model. Despite an insignificant change in the soil density, the liquefaction resistance of soil deposits may increase even when subjected to earthquakes whose magnitudes are insufficient to cause liquefaction (Seed et al. 1977). Furthermore, firing the second earthquake may be inadequate to trigger liquefaction if the first earthquake causes significant liquefaction. An entirely different soil and foundation response may develop for the succeeding events, which increases the complexities in assessing the soil-foundation interaction mechanisms (Adamidis and Madabhushi 2016a).

The incorporation of the relative density, D_r, into the problem also becomes important if each successive event causes large settlement and subsequent densification of the soil models. Published element tests often show that loose soils exhibit a higher tendency for the volumetric strains and are more susceptible to liquefaction than their dense counterparts. Based on the centrifuge experiments on the uniform deposits of saturated soils, Coelho (2007) observed that dense soils performed better than loose soils. The free-field settlements were consistently reduced as D_r increased. The dense soils exhibited much stiffer post-liquefaction stress-strain response than the loose ones. Similarly, Adalier and Elgamal (2005) observed that the tendency for the volumetric strains and the potential for the liquefaction dramatically reduced with increasing D_r. Furthermore, an increase of D_r, and hence stiffness, was observed to increase the factor of safety against the bearing failure of the foundations, but this was found to amplify the dynamic demand on them (Dashti et al. 2010).

This section discusses the response of saturated and partially saturated soil deposits beneath the *heavy* and *light* shallow foundations under different amplitude and duration of earthquakes.

6.2.4.1 Settlement Behaviour

The time histories of the foundation settlement recorded during the consecutive earthquakes, having similar frequency contents but different peak input accelerations (*PIA*) and durations, are depicted in figure 6.17. The estimated relative densities of each specimen were simply recalculated after each subsequent air injection and earthquake event based on the new height of the specimens. An indication of the changes in soil density due to successive earthquakes is given in table 6.1. It must be pointed out that this, basic, analysis considers the maximum soil surface settlements measured within the centrifuge models. The densities are just simplified approximations and average values over the entire soil layers, owing to the nature of non-linear change of relative density with depth. It is likely that the shallow soil layers will densify more than the deeper soil layers. Furthermore, the soil column in certain areas will contract, whereas certain soil columns will experience intense shearing that causes dilation.

In figure 6.17, although the previous earthquake caused a significant densification of the model ground, both the *heavy* and *light* shallow foundation on the saturated soils settled excessively during the next earthquake (CT1 and CT4). For each case, very high excess pore pressure ratios developed and led to significant softening of foundation soil (see figure 6.18). This indicates that the amplitude of the applied earthquakes was large enough to cause liquefaction multiple times in the same model ground. This, in fact, supports the acceptability of firing multiple earthquakes in order of increasing size. The presented data itself is, however, not sufficient to reach a conclusion about the deformation mechanisms that produced such settlements in each event. This will be discussed further in section 7.4.4.

Air injection provided a considerable reduction of the foundation settlement during the first earthquakes, as shown in figure 6.13. It seems that the beneficial effect of air injection increased further during the second and third events (see figure 6.17). This trend was most identifiable for the partially saturated soils under the *light* foundation (CT5 and CT6). The cumulative foundation settlements over an equivalent number of 17 acceleration cycles are summarised in table 6.2. It is clearly seen that the percentage reduction of the foundation settlement (relative gain in performance) increased during the successive events. It must be acknowledged that the soil densification after each event must have played a predominant role in the observed trend (decreasing foundation settlement). This may point out the need for the isolation of D_r effects on the partially saturated soil behaviour and on the performance of air injection technique.

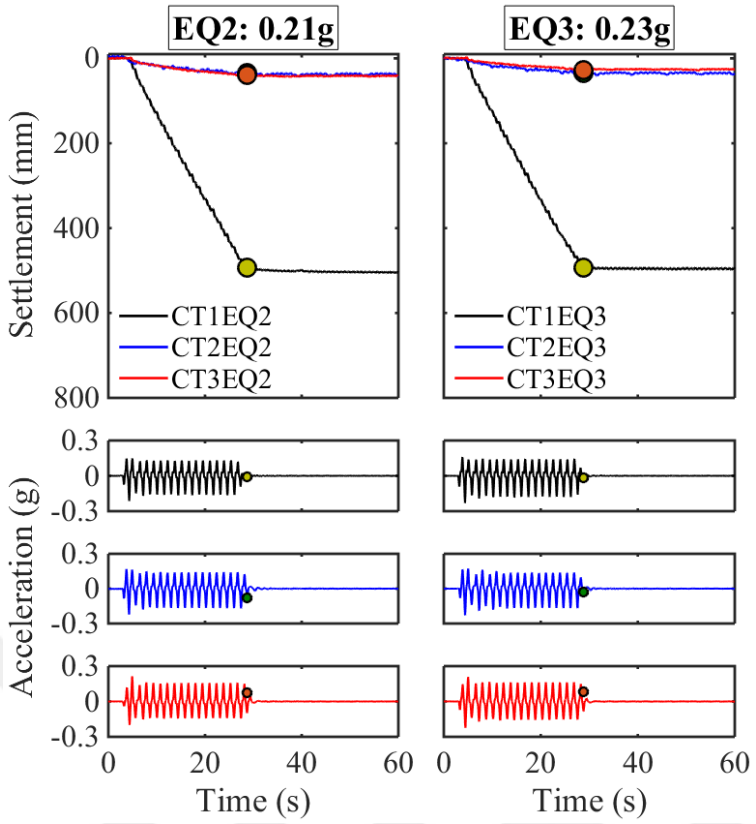

a) Heavy foundation

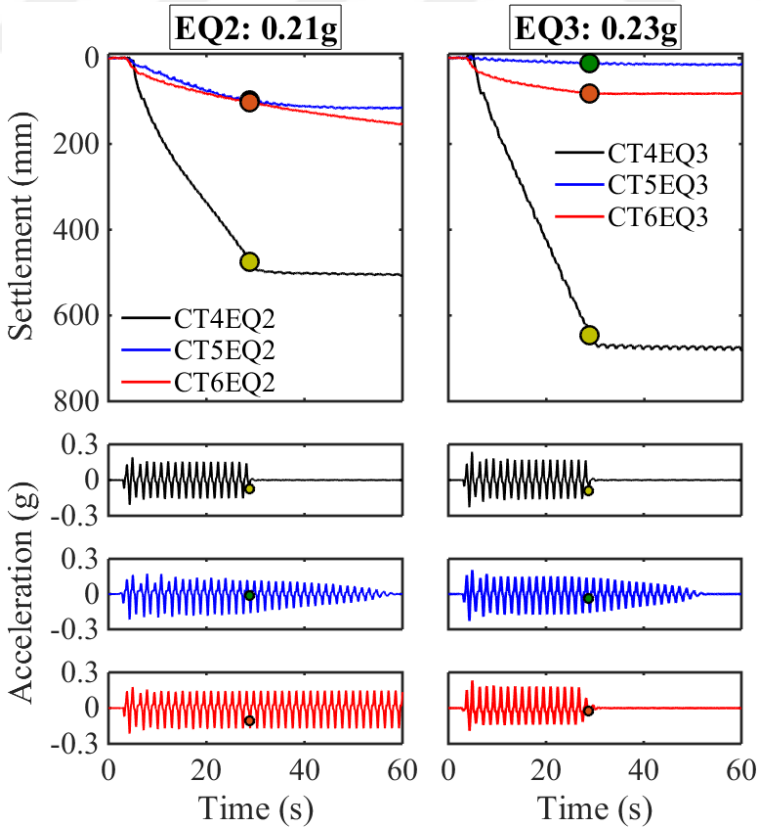

b) Light foundation

Figure 6.17– Time histories of settlement and acceleration recorded during the successive earthquakes.

Table 6.1 – Approximate relative densities during the successive events.

TEST ID	Relative Density, D_r (%)					
	Air1+EQ1		Air2+EQ2		Air3+EQ3	
	Initial D_r (%)	*Final* D_r (%)	*Initial* D_r (%)	*Final* D_r (%)	*Initial* D_r (%)	*Final* D_r (%)
CT1	40.8	53.1	53.1	64.4	64.4	75.4
CT2	40.0	46.1	46.1	47.8	47.8	48.2
CT3	39.9	42.8	42.8	44.4	44.4	44.9
CT4	40.2	58.7	58.7	70.1	70.1	85.0
CT5	39.9	56.7	56.7	60.0	60.0	60.3
CT6	40.1	56.2	56.2	61.1	61.1	61.4

Table 6.2 – Percentage reduction in the cumulative foundation settlement during the successive events.

TEST ID	Reduction in Settlement (%)					
	Air1+EQ1		Air2+EQ2		Air3+EQ3	
	Settlement (mm)	*Reduction (%)*	*Settlement (mm)*	*Reduction (%)*	*Settlement (mm)*	*Reduction (%)*
CT1	738.3	-	492.2	-	492.2	-
CT2	280.2	**62.0**	34.9	**92.9**	34.5	**93.0**
CT3	64.87	**91.2**	38.7	**92.1**	26.9	**94.5**
CT4	978.6	**-**	474.8	**-**	646.9	**-**
CT5	423.3	**56.7**	99.4	**79.1**	12.0	**98.1**
CT6	242.8	**75.2**	103.0	**78.3**	80.0	**87.6**

The performance of air injection technique during the prolonged earthquake loadings is also discussed briefly in this section. Based on the centrifuge test data, air injection was found to be very effective technique in decreasing the liquefaction-induced foundation settlements even under the moderate and strong amplitudes of earthquakes that lasted for an unrealistically long period of time.

For instance, a foundation settlement of 511.4 mm, including co-seismic and post-seismic settlements, was recorded during the second earthquake event for the saturated soil in CT4 where the earthquake ceased after 28 s. Nevertheless, the measured foundation settlement was only 259 mm for the partially saturated soil in CT6 where the earthquake lasted for about 300 s. This indicates that nearly half of the foundation settlement reduced although the partially saturated soil layer was subjected to an earthquake ~11 times as long as the earthquake in its saturated counterpart. This observation may be important for the rational design of the air injection technique in the field.

6.2.4.2 Generation of Excess Pore Pressures

The time histories of excess pore pressure ratios, r_u, recorded during the first, second and third earthquakes are presented for the saturated and partially saturated soils underneath the *light* foundation (figure 6.18). It can be seen that for the saturated soil (CT4), firing earthquakes in increasing amplitudes overcame the increased liquefaction resistance owing to the previous earthquake, and significant excess pore pressures were generated at a depth of 7 m. A complete loss of effective stress and full liquefaction occurred for the first two shakings. Moreover, significant soil-softening happened during the third event, approaching a state of full liquefaction. In the deeper layers (namely at the depths of 9.8 and 14 m), the second and third earthquakes did not produce complete liquefaction of the saturated soil although they were of larger amplitude than the first event. It seems that much larger amplitude of earthquakes was needed to generate sufficient excess pore pressures to cause full liquefaction at these locations. In contrast to the saturated soil, much smaller excess pore pressures built up in the partially saturated soils during each successive earthquake event (CT5 and CT6). There was no sign of significant soil-softening at any soil layer.

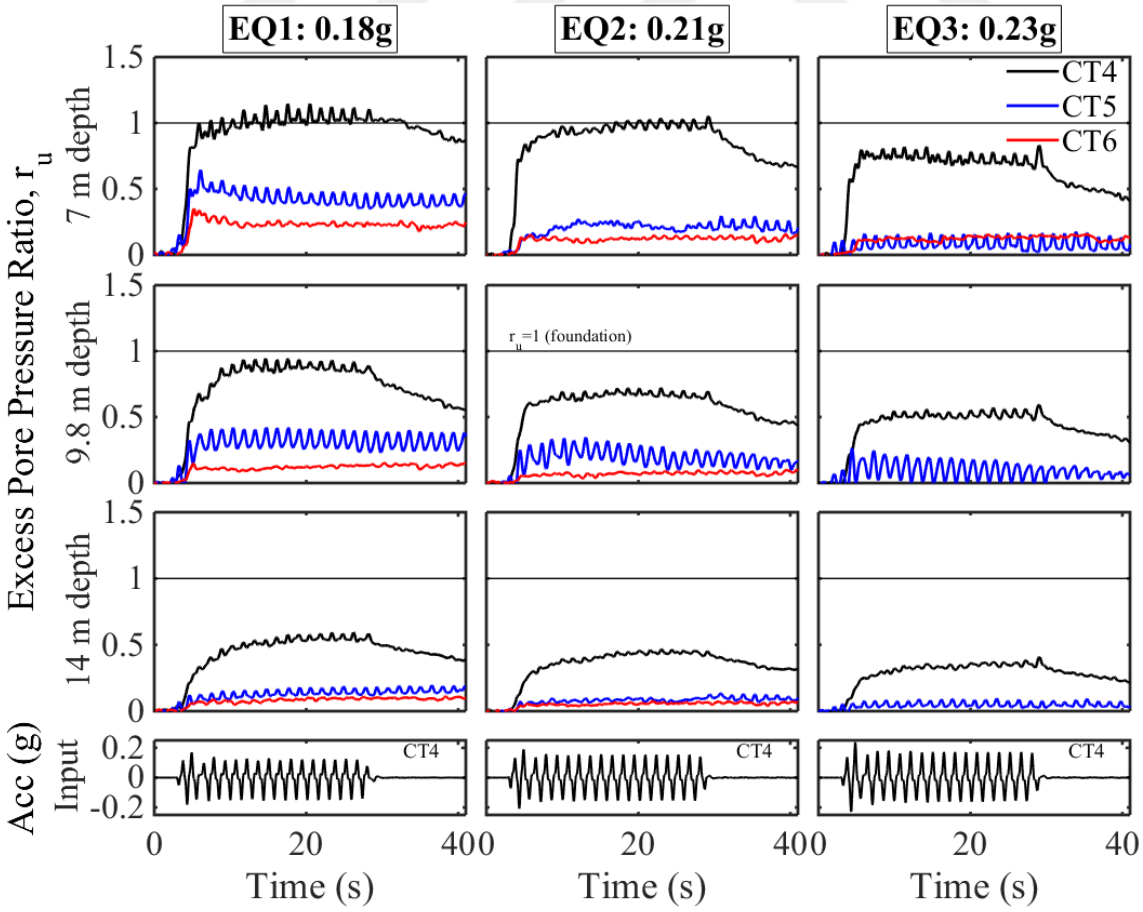

Figure 6.18– Time histories of excess pore pressure ratios beneath the light foundation.

A stronger earthquake was expected to produce larger excess pore pressures. On the contrary, for both saturated and partially saturated soils, consistently much smaller excess pore pressures developed during the successive earthquakes with increasing amplitudes. In addition, the rate of excess pore pressure generation usually slowed down in each consecutive earthquake (see figure 6.18). These observations may justify the influence of successive events, and therefore increased D_r, on the magnitude and rate of excess pore pressure generation.

The relationships between peak input accelerations, *PIA*, and excess pore pressure ratios, r_u, measured beneath the *heavy* and *light* foundations are depicted in figure 6.19. It is seen that for saturated soils (CT1 and CT4), r_u values reduced with increasing *PIA* values. The decreasing trend in r_u values with increasing amplitude of earthquakes was attributed to the densification of soil layers. As the dense soil layers were expected to exhibit less-contractive or dilative behaviour, the pore pressure regime during each consecutive earthquake displayed relatively smaller build-up of the excess pore pressure. Partially saturated soils showed significant similarities to the saturated soil behaviour: a decreasing trend in r_u values was observed with increasing *PIA* values.

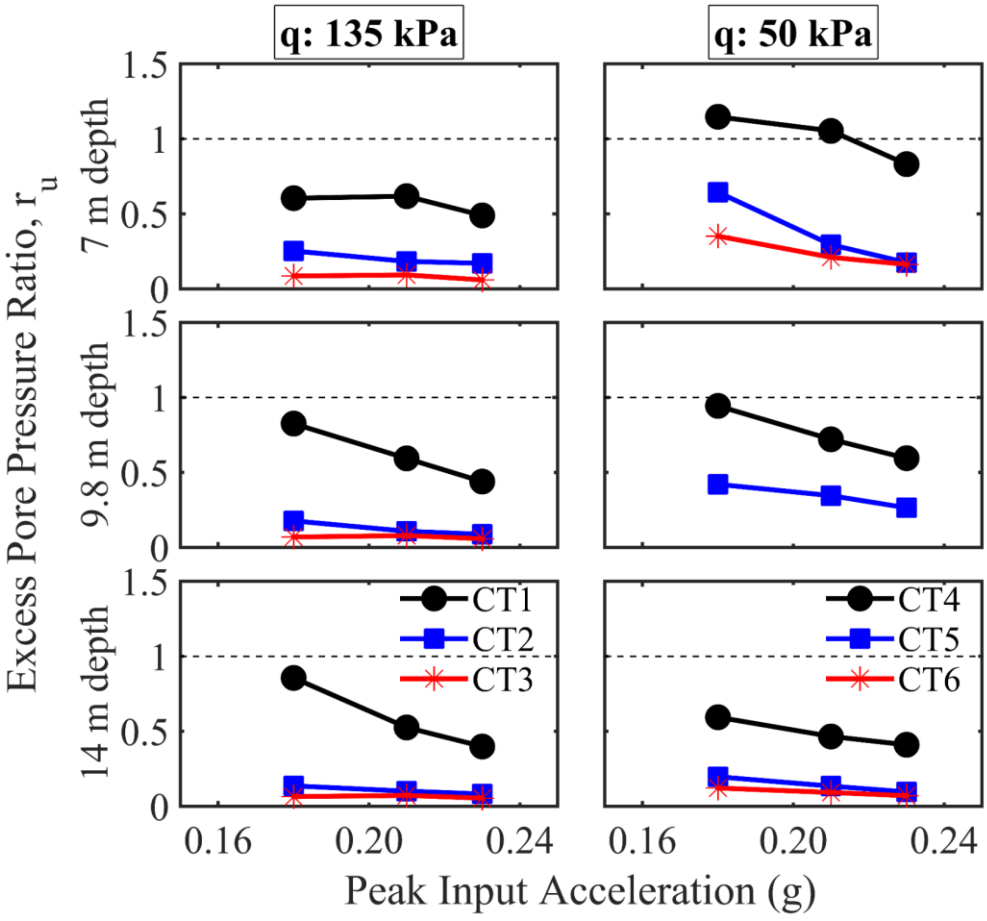

Figure 6.19– Excess pore pressure ratios recorded beneath the foundations versus peak input accelerations.

6.2.4.3 Acceleration Behaviour

The FFTs of horizontal input and foundation accelerations were computed from the horizontal acceleration-time histories recorded during the centrifuge tests. The magnitudes of the FFTs from the consecutive earthquakes with increasing amplitudes were compared to assess the seismic response of shallow foundations resting on the saturated and partially saturated soils. Figure 6. 20 shows the FFTs calculated at the level of *heavy* and *light* shallow foundations for the first 17 cycles of acceleration. Moreover, the FFTs were computed for short successive periods to examine the variation of the FFTs at different stages of the earthquakes (figure 6.21). As figure 6.20 shows, the dominant frequency of the earthquakes was observed at 0.6783 Hz. There was a second peak around 2.07 Hz due to the harmonics of the horizontal earthquake motions. For all cases, the response of the foundations was influenced by the amplitude of the earthquakes. The stronger motion of earthquake usually produced a larger magnitude of FFTs. A significant modification of the input motion (amplification or attenuation) took place as it propagated through the saturated and partially saturated soils. Even if the input motion was very similar, the level of such modification was found to be different for each of the two foundations, emphasising the effects of bearing pressure on the soil and foundation behaviour. The magnitude of the FFTs of foundation accelerations was also observed to vary from cycle to cycle, particularly for the saturated soil (see figure 6.21). This highlighted the effects of the number of cycles on the observed behaviour.

For the saturated model of CT4, the motion reaching the *light* foundation exhibited a significant attenuation in relation to the input motion for each of the three different earthquake amplitudes. A large attenuation of the harmonics and the predominant frequency occurred in this case. Nevertheless, the horizontal acceleration of the *heavy* foundation resting on the saturated soil (CT1) just marginally deamplified during the moderate motion (0.18 g) and showed enormous amplification during the stronger earthquakes. The different response of the *heavy* and *light* foundation was attributed to the level of additional stresses imposed by foundations on the soil underneath (see section 6.2.3).

The comparison of the performance of saturated and partially saturated soil layers shows that the magnitude of the FFTs of foundation accelerations increased following the liquefaction treatment of soil layers, intensifying the dynamic loads experienced by the foundations. The increased stiffness of underlying soil deposits was responsible for this behaviour (see section 6.2.1.5). It is worth noting that the increased relative density of the underlying soil layers due

to the first moderate earthquake event must have played certain roles in the increased shallow foundation accelerations during the larger events. Therefore, the consideration of this factor is also equally important for the evaluation of the dynamic demand on the shallow foundations.

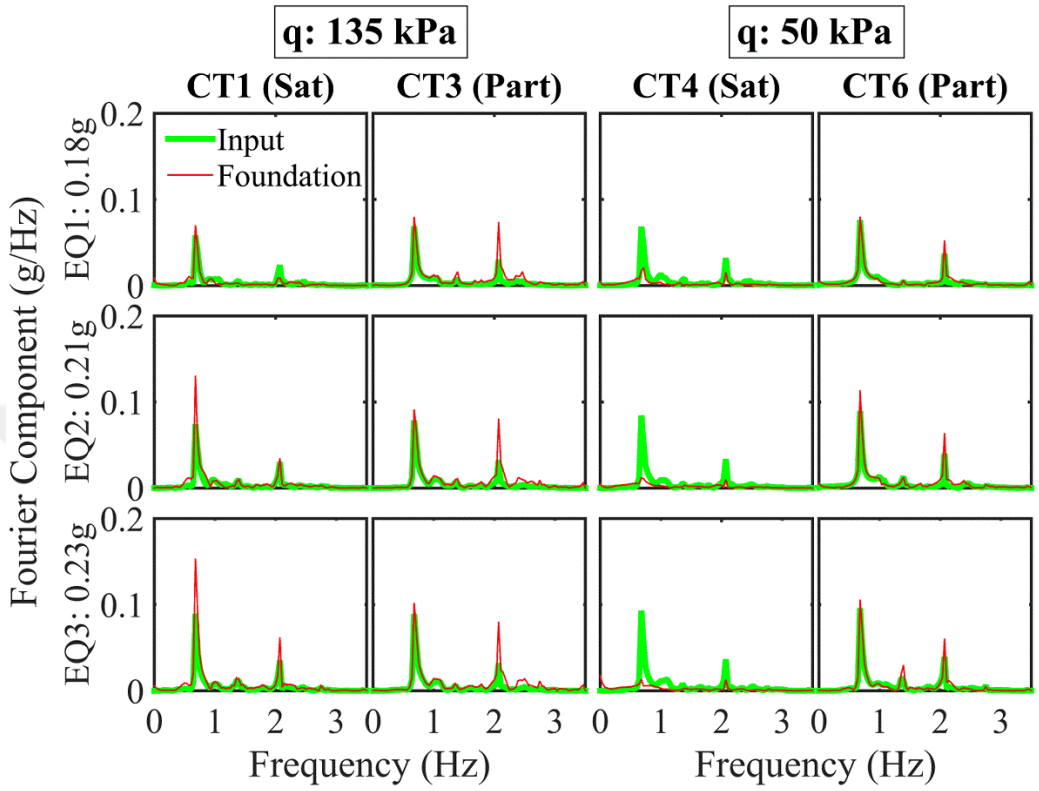

Figure 6.20– FFTs of the horizontal input and foundation accelerations recorded for the first 17 cycles.

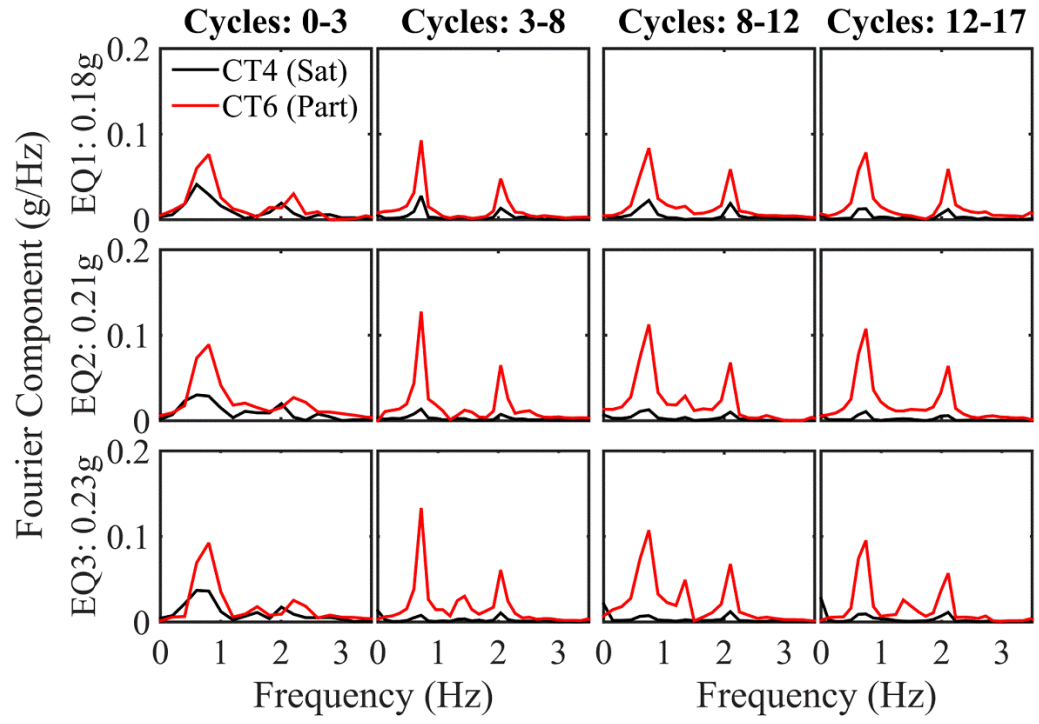

Figure 6.21– FFTs of the horizontal foundation accelerations recorded at varying cycles of the earthquake event.

6.3 Dynamic Response of Level Bed of Partially Saturated Soils

The primary aim of this section is to offer insights into the main mechanisms that generate the total ground surface settlement of saturated and partially saturated soils. The data from the free-field centrifuge experiments, namely, CT8, CT9 and CT10 are used for this purpose. The co-seismic and post-seismic behaviour of level deposits of saturated and partially saturated soils are deduced from the time histories of excess pore pressures and ground surface settlements.

6.3.1 Co-Seismic and Post-Seismic Behaviour

Figure 6.22 presents typical time histories of settlement, excess pore pressures and input acceleration recorded during the first and second earthquake of CT8. These results correspond to data attained from Section 1, as shown in figure A.3 (see appendix-A). The time axis is split into four windows in different scales to separately investigate the co-seismic response in the initial and following cycles as well as the post-seismic response in the short-term and long-term, respectively. The excess pore pressures, Δu, are those recorded at two different depths of soil deposits.

It is apparent that a very different response was observed for the saturated soil (CT8EQ1) and partially saturated soil (CT8EQ2). The reduction in degree of saturation of the soil substantially influenced the rate and extent of soil-softening as well as timing of liquefaction and excess pore pressure dissipation. Excess pore pressures generated within each soil deposit touched the r_u=1 line, leading to significant strength loss at the shallower depth (2.1 m). Although the initial liquefaction was not reached in any case under the higher confining stresses at a depth of 9.8 m, relatively greater excess pore pressure developed in the saturated soil as compared to its counterpart. This indicates that the extent of soil-softening at this layer was relatively larger in the saturated case. While both soil deposits displayed a very similar initial rate of excess pore pressure at the shallow layer, excess pore pressure generation was observed to slow down in the deeper layer of the partially saturated soil. Once the earthquake ceased, the dissipation of excess pore pressures started from the base and propagated towards the ground surface. The shallow soil layer remained liquefied for longer, retaining the elevated excess pore pressures. This trend was observable for both cases. Nevertheless, the build-up of excess pore pressures started to drop relatively fast in the partially saturated soil (as less fluid is transmitting upwards from the deeper layers), revealing its different dissipation time response.

In the free-field tests, co-seismic ground surface settlements took place in each of the two soil deposits, with a slightly decreasing rate towards the end of the earthquakes.

- The rate of co-seismic and post-seismic ground surface settlements was much greater in the case of saturated soil, resulting in larger total surface settlements. In particular, the contribution of post-seismic surface settlements, due to reconsolidation associated with the dissipation of excess pore pressures, was relatively major in the saturated case in comparison with its partially saturated counterpart. The increased rate of co-seismic settlement in the saturated soil can be ascribed to the partial drainage that allows pore fluid flow during the earthquake (Coelho 2007).
- Since the excess pore pressure gradients that were generated and loss in the shear stiffness were comparatively limited in the partially saturated soil, a decreasing trend in the post-seismic settlement was observed. The surface settlement predominantly stemmed from the increased compressibility of the soil mass due to air bubbles that contracted during the dynamic loading.

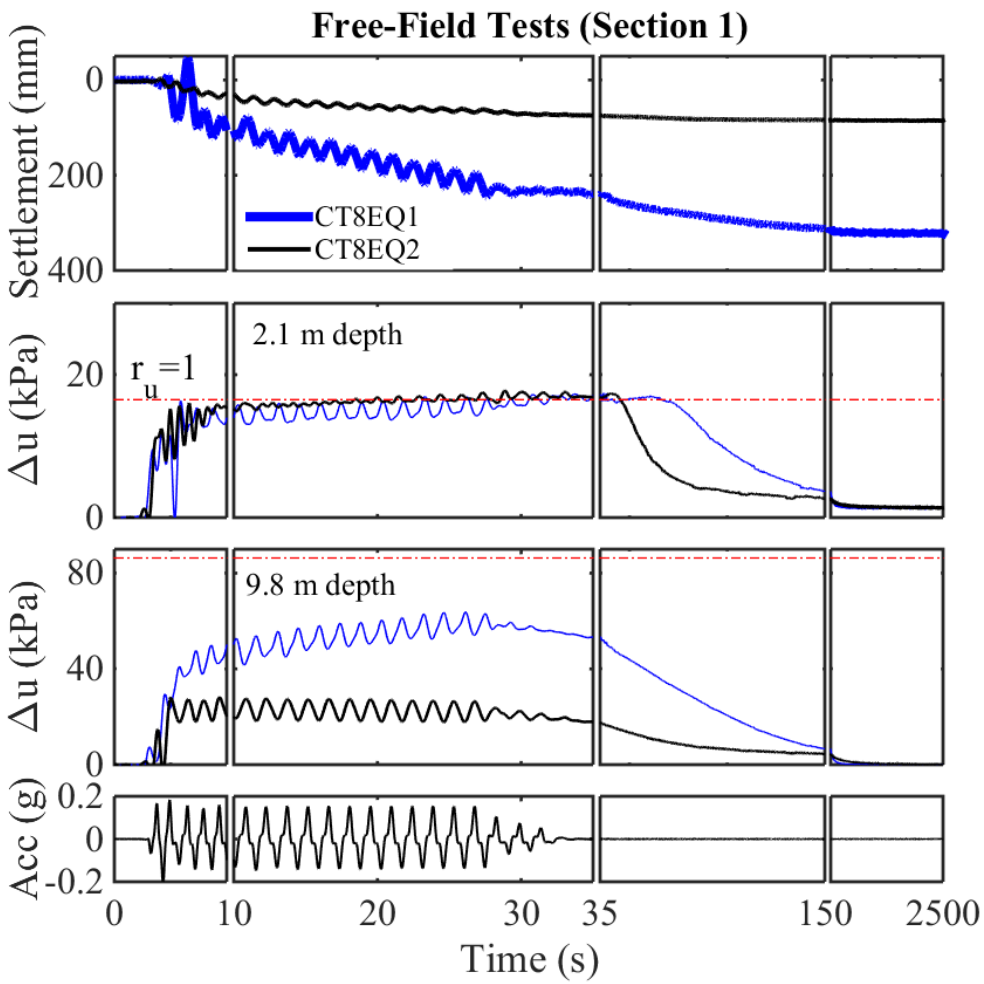

Figure 6.22– Free-field settlement, excess pore pressure and input motion time histories.

The response of soil deposits to successive earthquakes depends on the densification that occurs in each event. Despite this, the data presented with the added effect of densification in figure 6.22 still offers useful insight into the typical response of saturated and partially saturated soils.

Figure 6.23 presents the time histories of settlements and excess pore pressures recorded during the first earthquake event of CT9 and CT10. The region between the two vertical dashed lines represents the co-seismic response, whereas the remaining data is indicative of the short-term post-seismic response. The short and long-term post-seismic reconsolidation settlements were plotted separately in figure 6.24 to explicitly illustrate the predominant role of S_r.

Figure 6.23 shows that the total free-field settlement of saturated soils was always larger than that of partially saturated soils. Saturated soil at the shallow layer reached full liquefaction for each of the two tests. On the other hand, at similar depths of the free-field soil, complete liquefaction was not reached in any partially saturated soil test. For both saturated and partially saturated soils, the rate of settlement during the earthquakes (co-seismic) was greater than the rate of settlement after the end of earthquakes (post-seismic).

It is evident in figures 6.23 and 6.24 that (1) the contribution of co-seismic and post- seismic settlements to total surface settlements and (2) the rate and magnitude of excess pore pressure generation/dissipation were different for each of the two tests, depending on S_r.

- In CT10, S_r of partially saturated soil was only ~3.4% lower than that of saturated soil. In this test, excess pore pressures were generated quite fast, and started to drop almost at the same time for both cases. The rate of co-seismic and post-seismic settlement in the partially saturated soil was only marginally smaller than that in the saturated soil.
- In CT9, as S_r of partially saturated soil reduced further (by ~14%), the dissipation of excess pore pressures led to settlements at different rates and magnitudes. In this case, much smaller excess pore pressures were generated in the partially saturated soil when compared to its saturated counterpart. Therefore, it experienced relatively much smaller reconsolidation settlement, which correlated well with the data presented in figure 6.22.

Overall, these results show that the relative influence of each mechanism on the settlement response was highly dependent on S_r. In the partially saturated soil with a high S_r value (e.g. ~95.6%), significant excess pore pressures were generated, causing a significant reduction in the shear stiffness of soil. Under a given amplitude and duration of earthquake loading, the improvement that air injection provided remained limited. The response of partially saturated soil became, virtually, analogous to that of its saturated counterpart.

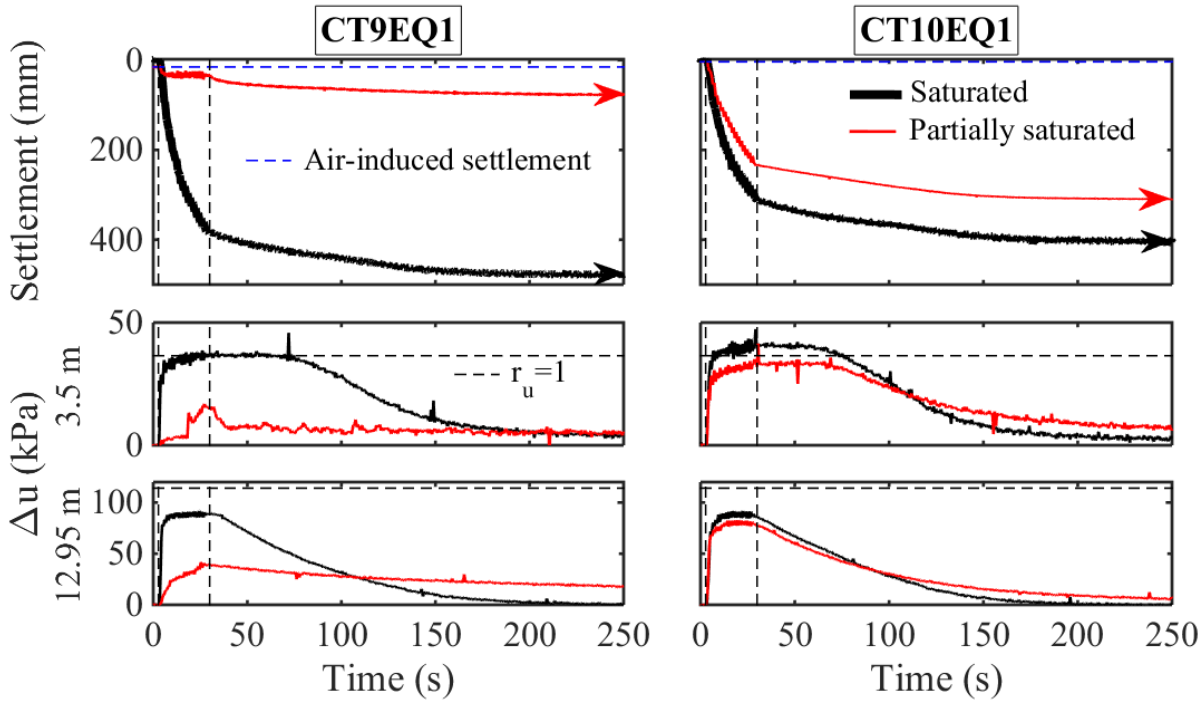

Figure 6.23– Free-field settlements and excess pore pressures.

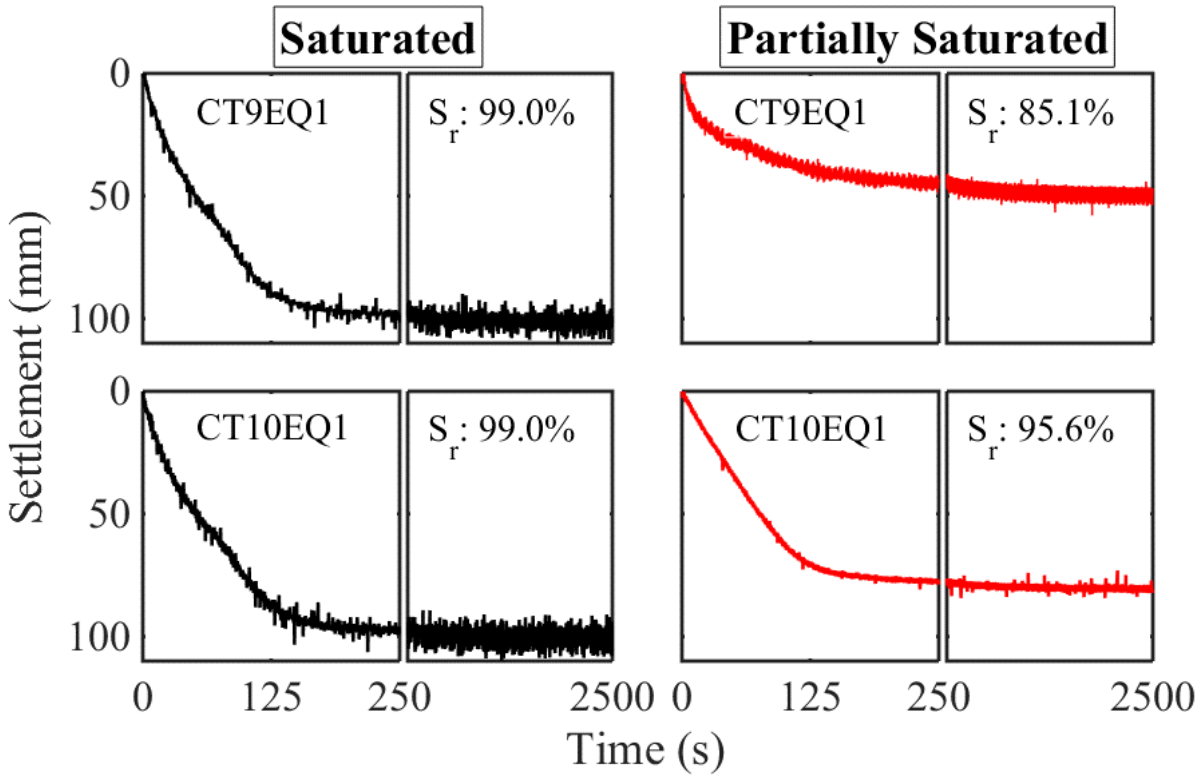

Figure 6.24– Free-field post-seismic (reconsolidation) settlements.

6.4 Summary

Early sections of this chapter examined the effects of key parameters on the dynamic response of saturated and partially saturated soil deposits on which shallow foundations rest.

The centrifuge tests showed that the settlements that shallow foundations suffered and excess pore pressures that built up during the earthquake loading were minimised as S_r reduced. The decrease in S_r also limited the depth of liquefied soil and shortened the period in which liquefied soil at the shallow layers remained in a softened state. Reducing S_r was, however, found to intensify the accelerations transmitted to the foundations through an area of soil below the foundations that remained unliquefied.

Through the centrifuge testing, it was shown that decrease of S_r (by air injection) was more effective in reducing the foundation settlements and increasing the resistance of soil to pore pressure generation under higher confining stresses. Through the 1-g shaking table testing, it was shown that reduction of S_r by air injection or chemical method did not produce sufficient improvement, irrespective of the presence of air/gas in the soil. These findings may justify that confining stress, besides S_r, is an essential consideration for practitioners and researchers, particularly those investigating the air injection technique by employing 1-g shaking table apparatus.

The impact of foundation bearing pressure on the dynamic response of saturated and partially saturated soil layers was examined. In the saturated soils, the *heavy* foundations suffered less settlements than the *light* foundations under similar earthquake motions. Excess pore pressures required to cause initial liquefaction also increased with increasing foundation bearing pressure. This behaviour was ascribed to an increased stress field that changed the excess pore pressure regime underneath the foundations. The foundations that imposed higher stresses on the foundation soil provided higher cyclic liquefaction resistance.

In the partially saturated soils, the beneficial effect of air injection on reducing the foundation settlements was more prominent beneath the *heavy* foundations than their *light* counterparts. This was again explained by the level of increased stresses that the *heavy* foundation produced. Furthermore, amplifying effect of air injection on the foundation accelerations, owing to the formation of an area of increased stiffness, was more noticeable in the partially saturated soils beneath the *heavy* foundations.

The performance of air injection technique during the prolonged shakings was examined. Air injection was shown to be an effective way of reducing liquefaction-induced deformations even during the moderate and strong amplitude of earthquakes that lasted for a long period of time.

Later section of this chapter placed emphasis on the mechanisms that produced the earthquake-induced settlement of saturated and partially saturated soils in the free-field.

The free-field settlement of saturated soil directly correlated with the generation and dissipation of excess pore pressures. The excess pore pressures generated during the earthquake loading reduced the effective stresses progressively in each cycle. This caused a significant reduction in the shear stiffness of soil (soil-softening) and subsequently large ground surface settlement. The co-seismic settlement due to partial drainage and post-seismic reconsolidation settlement during the excess pore pressure dissipation contributed to the total surface settlement.
The dominant settlement-generating mechanism changed when air was injected into the deposit of saturated soil. The magnitude of excess pore pressures that built up during the earthquake loading significantly reduced. This caused a relatively small magnitude of effective stress and shear stiffness reduction in the partially saturated soil. The contribution of reconsolidation settlement to the total soil surface settlement was small. The main mechanism that produced the settlement of the free-field was the increased compressibility of the soil mass associated with the presence of occluded air bubbles in the soil deposit.

Chapter 7

Deformation Mechanisms: Shallow Foundations

7.1 Introduction

When liquefaction happens in soil layers beneath shallow foundations, tilting or excessive settlement of such foundations can occur, severely affecting superstructures. To minimise possible liquefaction-induced deformations, ground improvement works are often carried out. The current state of practice is to estimate the depth of liquefiable soil that requires remediation and to determine the extent of liquefaction remediation (e.g. required final soil strength to limit excessive settlements). Knowledge of the soil deformation mechanism provides insights into the potential soil and foundation deformations (e.g. magnitude and rate of settlement and rotations) and enables more reliable estimates of the extent of liquefaction mitigation needed. The aim of this chapter is to identify dominant settlement mechanisms beneath foundations and to discuss the variation of such mechanisms through the application of liquefaction mitigation scheme.

In the literature, settlement of liquefiable soil layers beneath shallow foundations are shown to be an outcome of an intricate interplay between several mechanisms, and the mechanisms with a localised nature can be critical for the settlement response. For instance, Dashti et al. (2010) conceptually identified the settlement-generating mechanisms in deposits of saturated soils and categorised them into volumetric strain-induced and deviatoric strain-induced deformations. The volumetric strain-induced deformations were caused by the consolidation, localised partial drainage and a decrease in effective stresses. The deviatoric strain-induced deformations arose from partial bearing failure due to the strength loss or building ratcheting due to soil-structure interaction during an earthquake loading. Furthermore, the contribution of each deformation mechanism to the total building settlements was shown to depend on different parameters

associated with the properties of the liquefiable ground and the structure and characteristics of the ground motion.

The centrifuge test results presented in chapter 6 demonstrated that air injection can be an effective way of minimising the liquefaction-induced foundation settlements. Nevertheless, a comprehensive understanding of the way that air injection provides such improvement is still required. At present, little experimental research is available on the displacement mechanisms beneath and around the edges of shallow foundations resting on the partially saturated soils. The centrifuge test results presented in this chapter provide insights into the soil displacements that occurred during and after air injection. Of particular interest is the way that the deformation mechanisms that dominate the settlement of shallow foundations change depending on the presence of air in the soil deposits. A range of parameters that influence this phenomenon are investigated. Some of the results described in this chapter were published in Zeybek and Madabhushi (2017b).

7.2 Response beneath and around Foundation

Deformations that developed beneath and around shallow foundations were photographed in the centrifuge and 1-g shaking table tests using the high-speed camera (see section 3.3.5). The PIV derived displacement vector fields and contours are presented below and clearly show the deformation mechanisms generated during the seismic events (see section 7.2.1) and during the air injection process (see section 7.2.2).

7.2.1 Deformation Mechanisms during the Seismic Events

Figure 7.1 presents the digital images taken after an equivalent number of acceleration cycles (17) during the centrifuge tests CT1, CT3, CT4 and CT5 (see appendix-A for test details). This figure provides a visual representation of the influence of air injection on the soil deformations and overall performance of shallow foundations. This applies in particular to the tests presented on the right-hand side of the figure, whereby the horizontal and vertical lines of blue sand were poured adjacent to the Perspex window. The initial (pre-test) positions of shallow foundations are highlighted by the green dashed line rectangle, whilst their locations after 17 cycles are represented by the white solid line rectangle. Furthermore, the initial locations of the ground surface are highlighted using the horizontal dashed lines.

By examining the liquefaction-induced deformations in the saturated soils beneath shallow foundations (CT1: *heavy* foundation and CT4: *light* foundation), it is evident that a very deep layer of deformation took place in the liquefiable soil deposits, with foundations settling more than the adjacent ground and the ground adjacent to the foundations settling more than the free field. The width of the surface settlement trough (profile) was much narrower beneath the *light* foundation. Very large lateral movements of the vertical lines of coloured soil, which were evenly distributed throughout the liquefiable soil layers, were apparent in CT4. These lateral deformations increased from the bottom to the surface of the soil.

However, in the partially saturated soils (CT3: *heavy* foundation and CT5: *light* foundation), a shallow layer of deformation took place in the soil layers. The horizontal soil movements were concentrated only at the shallow depths, and their magnitude was very small indeed. A small punching settlement of the foundations was observed due to limited shear stiffness and strength loss in the foundation soil. The foundations got slightly embedded within the surrounding soil.

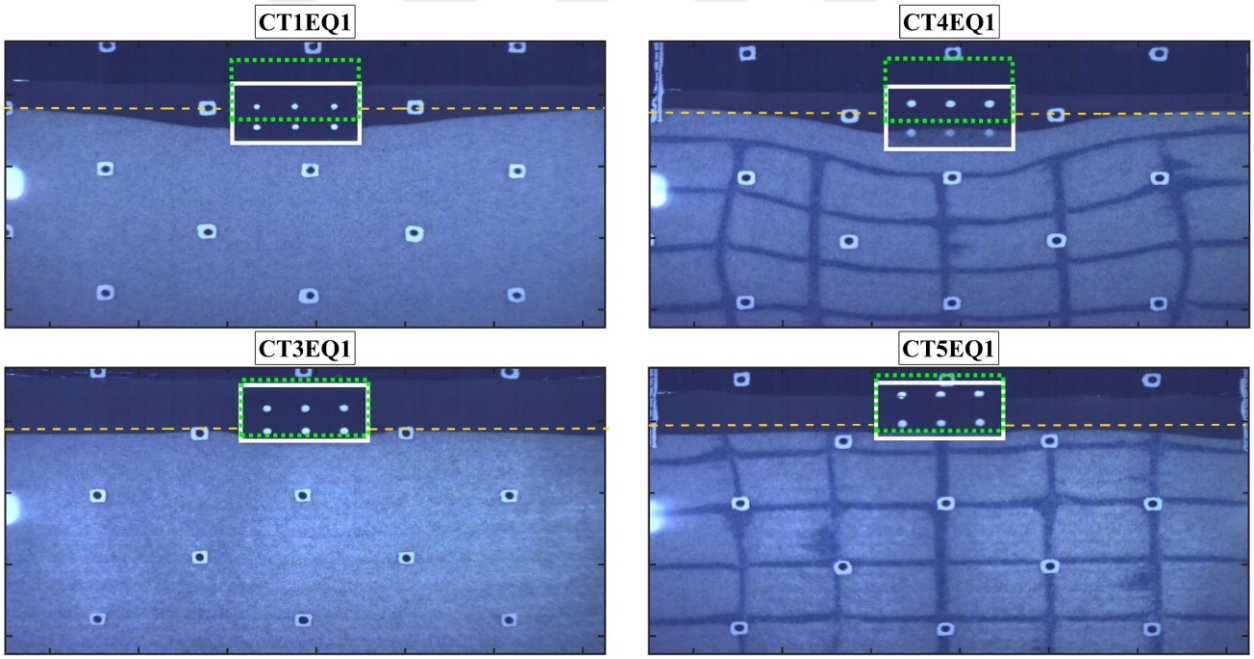

Figure 7.1– Typical photos of cross-sections of the models. Dashed lines represent the initial condition.

Figure 7.2 presents accumulated soil displacements for the tests with the *heavy* foundation. The trace for the input motion displacement, which indicates the time period for which the displacements were examined, is shown in figure 7.2d. All displacements correspond to the whole duration of seismic motion (approximately 17 acceleration cycles) and were calculated relative to the rigid base. They are indicative of overall deformation mechanisms in the tests. The displacements generated during the post-seismic reconsolidation process were not

included in these plots owing to the limited storage capacity of the camera. In fact, the displacements at the same scale (scale 1) in figures 7.2a, 7.2b and 7.2c provide a good visual comparison between the tests. These plots show that deformations in the partially saturated soils (CT2 and CT3) were markedly smaller, compared with those in their saturated counterpart (CT1). The magnitude of displacements in these tests was magnified by 20 times as shown in figures 7.2e and 7.2f in order to clearly reveal the deformation mechanisms.

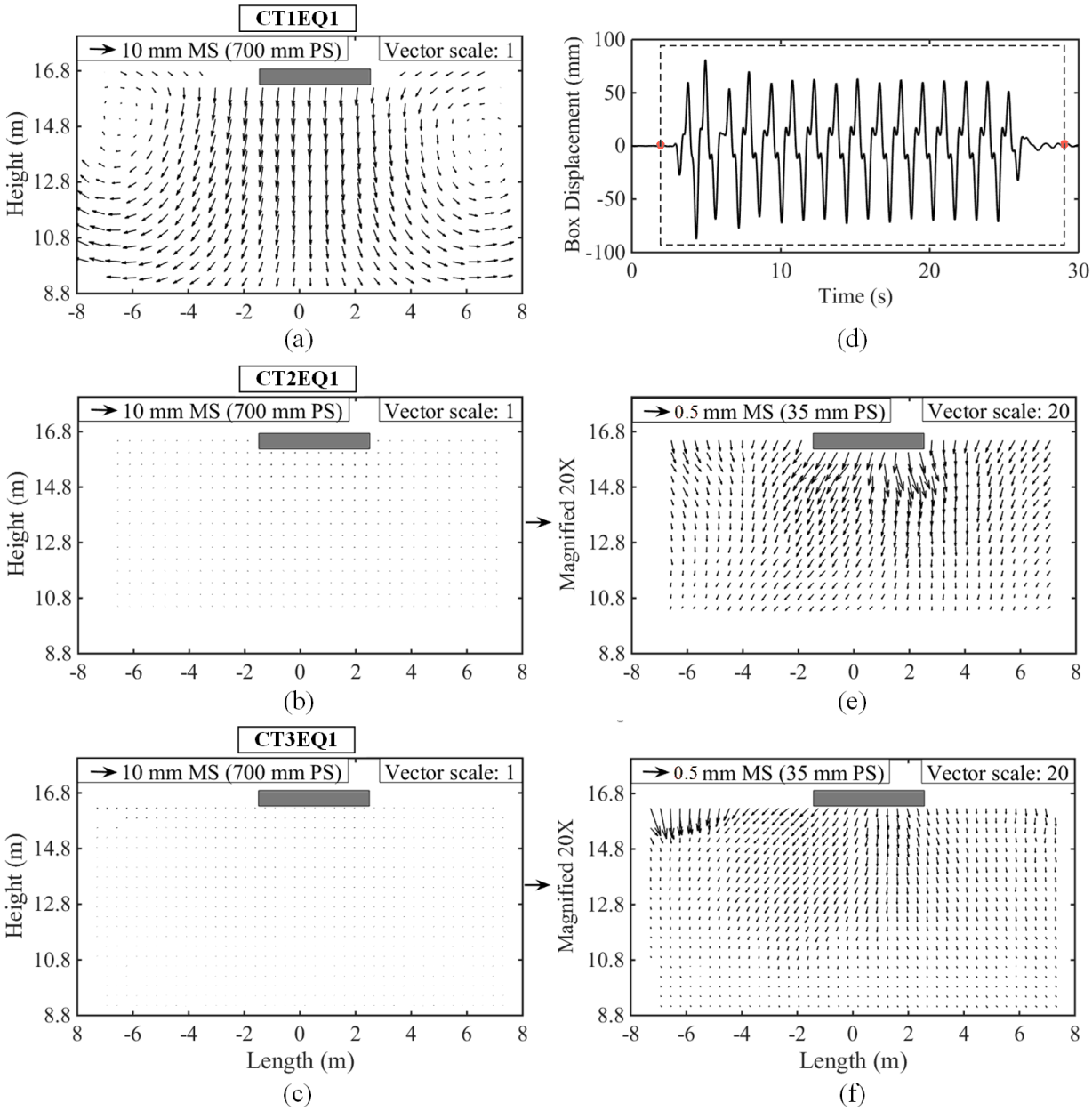

Figure 7.2– Displacement vector fields beneath heavy foundations recorded at the end of 17 acceleration cycles. The illustrated in figure 7.2d is the time history of input displacement recorded on the model container.

It is seen in figure 7.2 that a symmetric displacement mechanism occurred in the saturated soil (CT1). Significant deformations were evident beneath and around both edges of the foundation.

There was a wedge of soil that moved almost as a block vertically downwards underneath the foundation. A large extent of liquefied soil adjacent to the foundation also moved downwards, following the settlement of the foundation. The inability of the liquefied free-field soil to provide lateral confinement caused the rest of the liquefied soil layer to be displaced laterally and pushed outwards, causing the surface of the soil to heave at the free-field locations- Section 1 and Section 3 in figure A.1 (see appendix-A). The depth of liquefaction increased to a level where a bearing capacity failure mechanism did form. Relatively large vertically downward displacements around the edges of the foundation can suggest that the positive volumetric strains at locations away from the foundation were surpassed by the deviatoric strains, causing the foundation to settle more than those locations. This correlated well with the observations of such researchers as Adalier et al. (2003). Moreover, points of rotation were observable at a distance of about 4 m from the edges of foundation and 1.5 m from the soil surface, around which liquefiable soils revolved.

Zeybek and Madabhsuhi (2017b) separately showed that LVDTs captured an upward ground surface movement (heave) at the locations of L1 and L3 which were at about 7 m from the edge of the foundation. The area monitored by the camera did not engulf the entire soil zones, as shown in figure A.1 (appendix-A). The boundaries may have facilitated the upward movement of soil towards the edges of the model container as a result of the large extent of the displacement mechanism. In fact, this produced continuity between the observed trends in the saturated soils beneath shallow foundations with different bearing pressures (section 6.2.1.1).

Unlike in the saturated soil, the displacement mechanisms were relatively more localised, and mobilisation of a bearing capacity failure mechanism did not take hold in the partially saturated soils (see figure 7.2). The magnitude of soil displacements was significantly smaller in the partially saturated soils, and majority of the soil deformations occurred vertically downwards, with only little lateral movement of foundation soil into the free-field. This reveals that air injection provided a lateral confinement for foundation soil and limited the deviatoric strain-induced deformations. On the other hand, vertical soil displacements due to positive volumetric strains associated with an increased compressibility of the soil mass seemed to significantly contribute to the total settlements.

There was a lack of symmetry in CT3 in which no lateral soil movements were visible on the right-hand side of the foundation, but only vertically downward displacements were present. The asymmetric deformation mechanism in this soil can be attributed to the asymmetry in the earthquake loading and non-uniform desaturation within the soil column (see section 4.4.1).

Examination of the soil displacements on a cycle-by-cycle basis can provide a much clearer view of the size, shape and changes in the deformation mechanisms that affect the soil layers. For this purpose, the soil displacement vectors occurring during half-cycles near the beginning of earthquakes were examined for the tests, and typical results are presented in figure 7.3. Indicated on the lowest two traces are the settlement-time histories and approximate time period for which the displacements were examined.

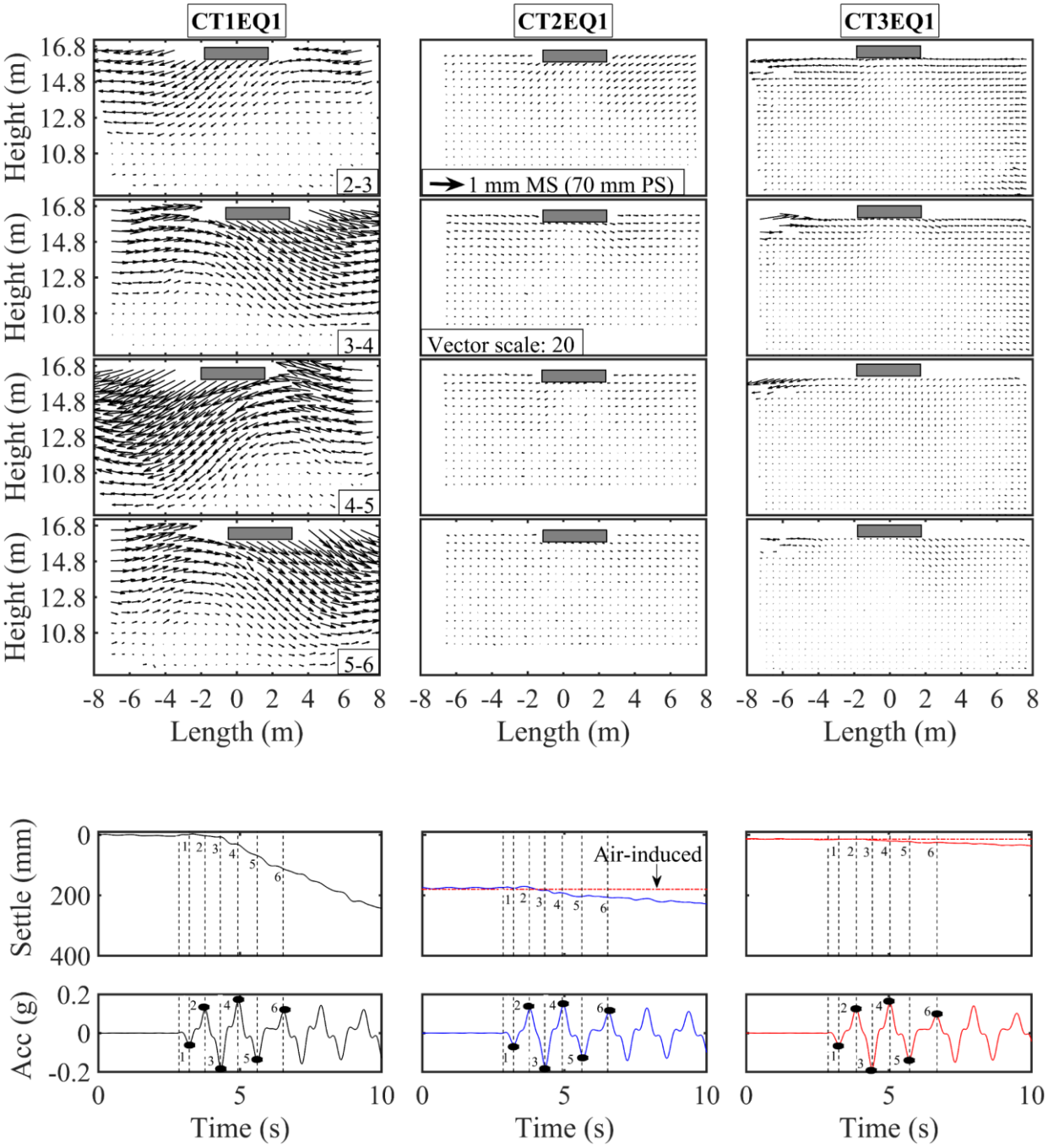

Figure 7.3– Accumulation of soil deformations beneath shallow foundations and foundation settlements during half-cycles near the beginning of the earthquake. Vector length scale is 20 for all cases.

The left column of figure 7.3 shows the displacements that occurred in the saturated soil (CT1) during each half-cycle of the first earthquake, commencing from a point when the foundation started to settle significantly. A pattern of almost linear and very large foundation settlement rate was recorded by LVDT-L2, particularly after the half-cycle (2-3). The same pattern was ascertained from the PIV displacements. Significant deformation occurred during each half-cycle, and the depth of the deformation increased up to more than twice of foundation width (7.7 m in prototype scale), specifically from phase 3-4 to 5-6. As discussed in figure 7.2, the deformation wedges moving almost as a whole were apparent, and the size of the deformation zone increased in its lateral extent due to the fully liquefied free-field soil that fell short of lateral support. One-sided deformation wedge to the right or left of the foundation took place depending on the direction of the box movement, and these movements were accompanied by the vertical settlement of foundation. This points out that deformation occurred twice during each cycle of the earthquake. The deviatoric strains that developed under shear stresses induced by the foundation and earthquake can be easily observed, especially after phase 3-4. Although it is hard to distinguish the deviatoric and volumetric strains from the overall displacements, it is clear that the accumulated deviatoric strains contributed significantly. This is evident from the large lateral deformation components in the soil layer.

The middle and right column in figure 7.3 demonstrate the soil displacements and foundation settlements occurring during each half-cycle in the partially saturated soils (CT2 and CT3). In both cases, the rate of foundation settlement was significantly smaller, as compared to that recorded in their saturated counterpart (CT1).

In CT2, rapid settlement of the foundation during the first three half-cycles (from 2-3 to 4-5) was followed by a reduced rate of settlement during the last half-cycle (phase 5-6) and the rest of the earthquake. Correspondingly, the magnitude of soil deformations was smaller and much shallower in this soil. In general, an overall movement of the sand body from side to side at the very shallow layers was apparent. There was only a small size of soil wedge that moved down and away from the foundation under both edges of the foundation, which was indicative of minor deviatoric strains. This was particularly the case for phase 2-3 and 3-4.

A very similar trend was observed in CT3. The magnitude of displacement vectors and the depth of deformation were reduced further in this soil. Despite the slight deviatoric strains under the right edge of the foundation in phase 5-6, the soil displacements underneath the foundation were generally in the downward direction, and there was almost no horizontal soil movement under the foundation in phase 4-5.

7.2.2 Deformation Mechanisms during the Air Injection Process

The injection of air can cause permeant settlement of shallow foundations, as reported in section 4.2.1. Despite its small magnitude, air (injection)-induced settlement may still be a concern of practising engineers. In an effort to gain insights into the settlement-generating mechanisms that occur during the air injection process, PIV analyses were performed using the digital images recorded during the air injection phase of centrifuge testing.

Figure 7.4 shows the typical air-induced soil displacements that developed beneath the shallow foundations (CT3, CT6 and CT7) and in the free-field (CT8). It is apparent that air injection resulted in vertically downward displacements in the free-field (implying settlement). Air injection also caused the foundation soil to displace laterally towards the free-field.

As shown in section 4.3.1, occluded air bubbles replaced pore fluid within the voids of the soil during the air injection process. This led to an upward migration of pore fluid within the soil deposits. When this process occurred rapidly, effective stresses in the upper part of soil layers, with low confining stresses, dropped significantly. Thus, ironically flow-induced liquefaction took place at these locations. The compressibility of the soil mass also considerably increased with the inclusion of air bubbles. Downward soil displacements in the free-field are, therefore, attributed to the positive volumetric strains caused by the decrease in effective stresses during the air injection process and increased compressibility of the soil mass.

The positive volumetric strains caused the free-field settlements, while the foundation-imposed static shear stresses caused an almost complete (such as in CT2) or partial & localised bearing capacity deformations (such as in CT3). They eventually led to the settlement and rotation of the shallow foundations. It must be indicated, though, that the recorded air-induced settlements and rotations were significantly small in all of the centrifuge tests (except for CT2). Therefore, they were not expected to have a significant effect on the seismic response of foundations.
It is noted that as mentioned before, an almost complete bearing capacity failure mechanism developed beneath the shallow foundation during the air injection process in CT2. Further information on the deformations and excessive settlement of the foundation observed in this test can be found in Zeybek and Madabhushi (2017b).

Observations made during the partially saturated soil experiments revealed that a small amount of entrapped air bubbles had a tendency to coagulate during the air injection process, forming temporary and localised air-filled cavities. Moreover, in some cases, excessive air bubbles

continued to move upwards until they stabilised in the soil-fluid system. Air bubbles moving upwards slightly pushed the upper soil particles at the very top, where the confining stresses are very small. These eventually led to a volumetric expansion in these regions. Nevertheless, the volumetric strains associated with the increased soil compressibility surpassed the localised volumetric expansion in these soils.

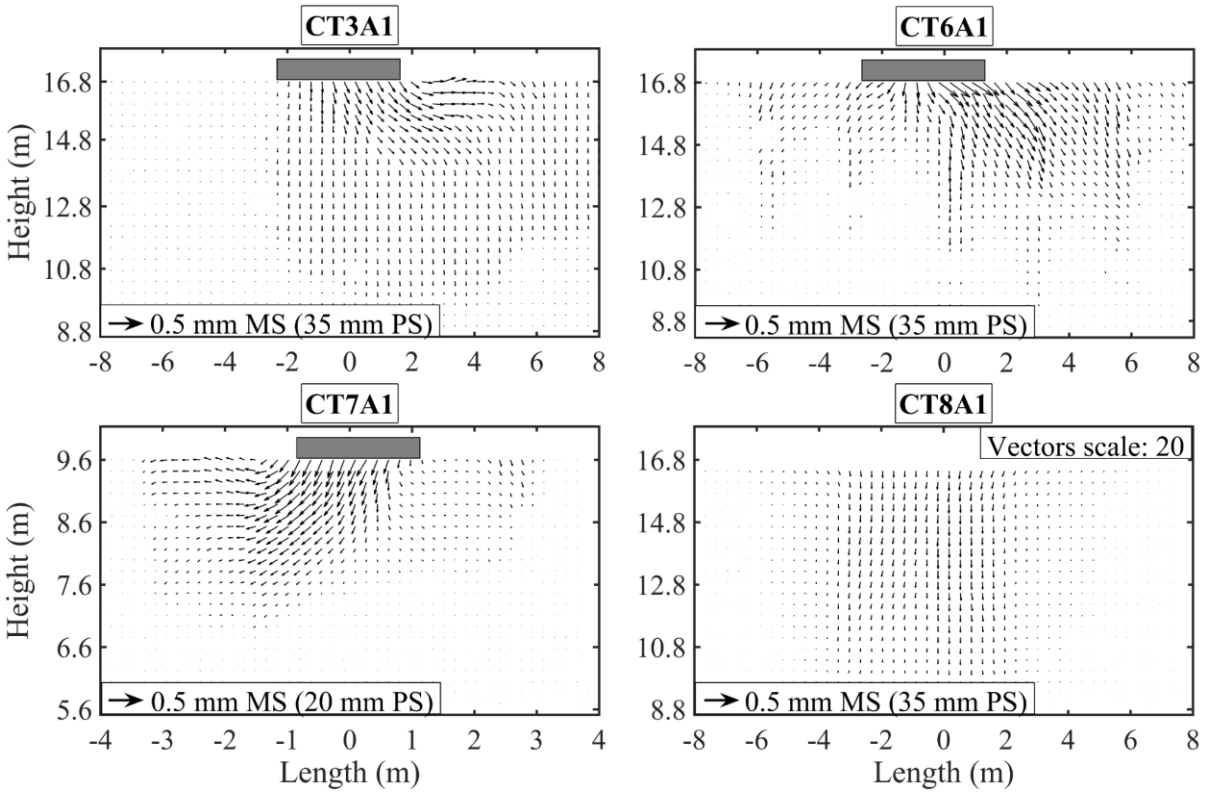

Figure 7.4– Soil displacement vectors during the air injection process. Vector length scale is 20 for all cases.

It is interesting to note that figure 7.4 shows evidence of asymmetric deformations under both sides of the foundations, with rotation being in anticlockwise or clockwise direction. This was ascribed to the non-uniform distribution of air bubbles, which produced heterogeneous partially saturated soils (see figure 4.5). The implication of this observation for design engineers is that different air injection orientations can be used to try to desaturate the soils more uniformly. In this case, the strength and compressibility of the soil body and therefore the magnitude of air-induced soil displacements can be unified across the entire contact area of the foundations, which in turn reduces the risk of differential foundation settlements. For instance, in CT3A1, the maximum soil displacements occurred on the right side of the foundation, which matches the zone of high desaturation shown in figure 4.5. Increasing the desaturation of the left side, engineers can allow the foundation to rotate anticlockwise to remove the differential settlement as long as the stability of the entire structure is maintained.

7.3 Experimentally Observed Deformation Mechanisms

The most critical deformation mechanisms at play in the saturated and partially saturated soils were identified in the previous and current chapter.

In the saturated soils, volumetric strains due to partial drainage during the seismic loading and more importantly deviatoric strains due to static and dynamic shear stresses induced by the foundation and earthquake loading led to significant deformations in the soil layers. Although majority of the free-field settlements seemed to happen during the seismic events, post-seismic reconsolidation settlements also contributed to the total settlements at the soil surface. An extended failure mechanism predominantly drove the settlement of shallow foundations. The mass of soil beneath the foundation lost its lateral support from the surrounding soil that liquefied, and it accumulated vertical settlement with each half-cycle.

Similarly, the mechanisms that control the deformations in the partially saturated soils were determined. A summary of such mechanisms is given in table 7.1. Although minor deviatoric strain-induced deformations were present, the prevailing settlement-producing mechanism was volumetric strain-induced deformations in the partially saturated soils. As degree of saturation reduced, the increased compressibility of the soil mass appeared to significantly contribute to the total settlements during the earthquake event. The contribution of post-seismic settlements to the overall surface settlements remained insignificant in this case.

Table 7.1 – Mechanisms of deformations in the partially saturated soils.

Type of Deformation	**Mechanism of Deformation**	
	During air injection	**During and after earthquake**
Volumetric	Positive volumetric strains due to the decrease in effective stresses induced by upward flow and due to the increase in the compressibility of the soil mass	Positive volumetric strains due to the increase in the compressibility of the soil mass
	Negative volumetric strains (expansion) due to the coagulation of air bubbles and upward air escape	Limited volumetric strains due to the reconsolidation during the excess pore pressures dissipation
Deviatoric	Localised and partial bearing capacity failure due to the strength loss in the foundation soil during upward flow	Limited bearing capacity failure Limited cumulative foundation settlements due to shear deformation

7.4 Effects of Key Parameters on Soil Deformations

Dynamic centrifuge and 1-g shaking table tests were used to identify the key parameters and to derive conclusions for their effect on the excess pore pressure, settlement and acceleration response of soils (see chapter 6). The evaluation of PIV-based soil displacements developed underneath and around the shallow foundations also allowed for an increased understanding on the changes of deformation mechanisms going from saturated to partially saturated case. The ensuing sections discuss the effects of degree of saturation, confining stress, bearing pressure and earthquake amplitude on the deformation mechanisms, using the displacement vector fields and their contours.

7.4.1 Degree of Saturation

Figure 7.2 previously depicted the soil displacements that developed beneath the *heavy* shallow foundation and accumulated over an equivalent number of approximately 17 acceleration cycles. In the same way, the soil displacements that developed underneath the *light* shallow foundation and accumulated over the same number of acceleration cycles are presented in figure 7.5, with a particular interest in the impact of S_r on the volumetric strain-induced and deviatoric strain-induced deformations.

Figure 7.5 reveals a mechanism of significant extent and a deep layer of liquefaction in the saturated soil during the first earthquake of CT4. An extended, bearing capacity failure mechanism was mobilised. Following settlement of the foundation, the soil under and adjacent to the foundation presented downward movement. The rest of the soil within the liquefiable deposit displaced laterally outwards. On the other hand, soil movements were considerably smaller when air was injected into the deposits of liquefiable soil. The deformation mechanisms became shallower and more localised in the partially saturated soils during the first earthquake of CT5 and CT6. A mobilisation of the bearing capacity failure mechanism was not the case in any of the two tests. It is found that shear strains and horizontal movements of soil to the free-field reduced, and the depth of liquefaction was limited substantially. The findings presented here, in fact, correlate well with the results described in figure 7.2.

The comparison of the soil displacements which developed in the partially saturated soils offers further clarification regarding the significance of S_r. The magnified displacement vectors in figures 7.5e and 7.5f reveal that a very different displacement mechanism was observed for

each of the partially saturated soils. In CT5, a localised displacement mechanism concentrated at the shallow layer was observed. The soil under both edges of the foundation and near its perimeter had a tendency to displace laterally. However, in CT6, usually vertically downward soil displacements, with only little horizontal soil movements, were apparent. The lateral soil displacements occurred only under the left edge of the foundation. The differences in behaviour can be attributed to initial S_r of the soil deposits. As S_r reduced from 99.0% (CT4) to 93.1% (CT5) and 79.5% (CT6), the shape of the displacement mechanisms changed dramatically.

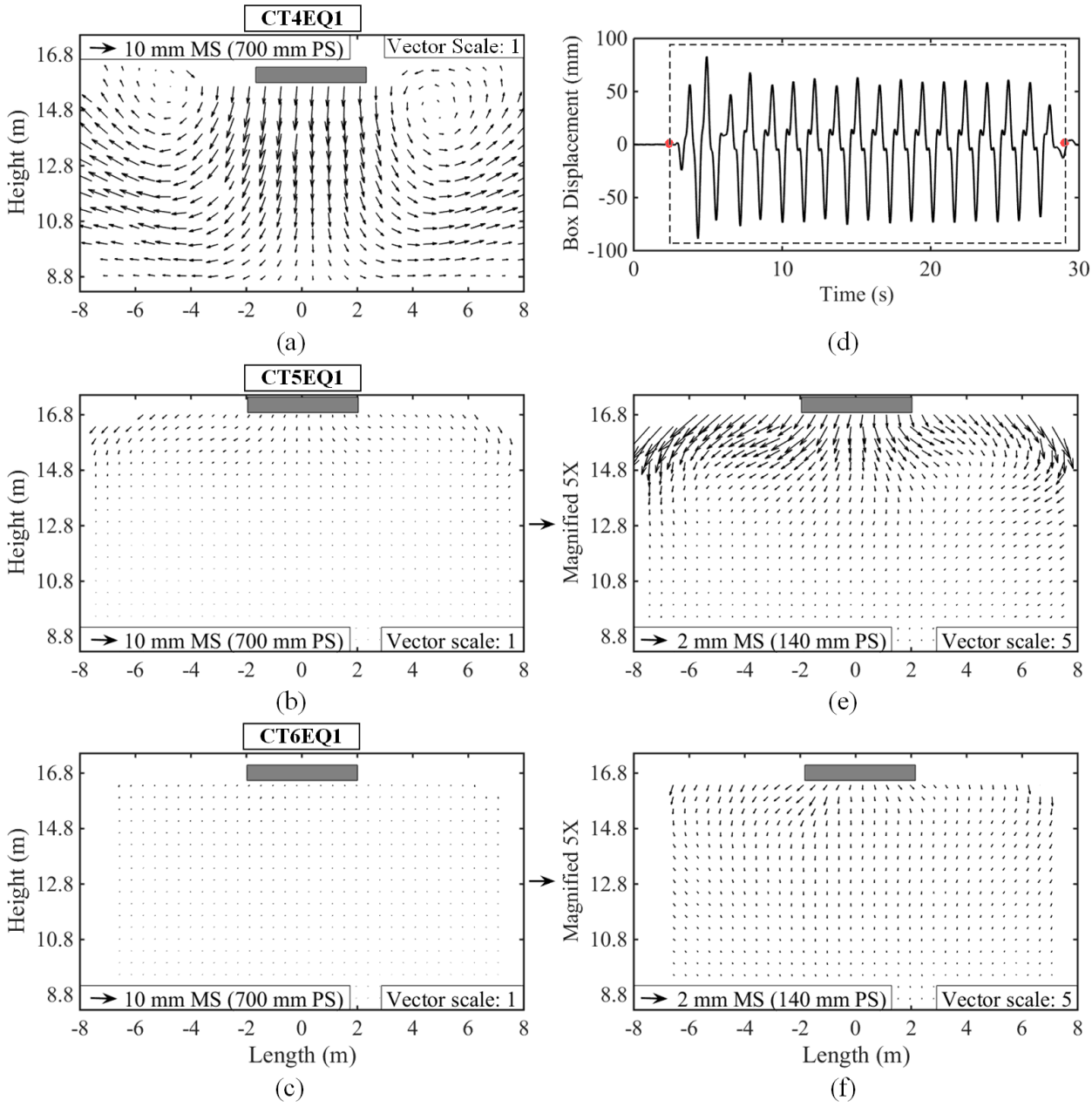

Figure 7.5– Effect of degree of saturation on deformation mechanisms. The illustrated in figure 7.5a, 7.5b, 7.5c, 7.5e and 7.5f are the soil displacement vectors beneath light foundations recorded at the end of 17 acceleration cycles. The illustrated in figure 7.5d is the time history of input displacement recorded on the model container.

A better understanding of the influence of S_r on the observed patterns can be gained with the evaluation of horizontal soil movements that developed during the seismic events. Figure 7.6 presents the typical horizontal soil displacements that accumulated over 17 acceleration cycles of the first earthquakes in CT5 and CT6.

In CT5, the soil at the shallow layers (up to a depth of approximately 4.2 m) softened substantially due to liquefaction and displaced laterally. The soil column beneath and around the edges of the foundation experienced significant horizontal displacements. Relatively larger lateral displacements developed further away from the foundation centre line towards the free-field and closer to the soil surface on both sides of the foundation.

In a similar way, some lateral displacements developed within or outside of the soil column beneath shallow foundation in CT6. In comparison with the area below the centre line of the foundation, relatively larger horizontal displacements were observed around the edges of the foundation. The magnitude of accumulated horizontal displacements for the whole soil layer in question was significantly smaller in CT6 (S_r: 79.5%) than in CT5 (S_r: 93.1%). This indicates that accumulated horizontal displacements in the partially saturated soils decreased as S_r reduced further. The displacement mechanism also became shallower with decreasing S_r.

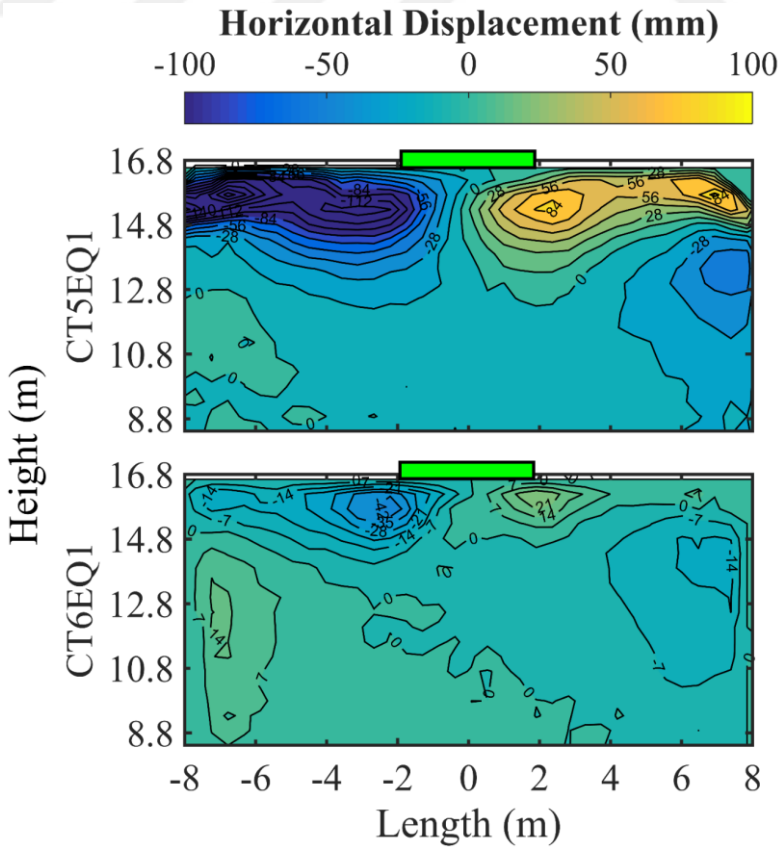

Figure 7.6– Accumulated horizontal soil displacements over 17 acceleration cycles.

7.4.2 Confining Stress (Vertical Stress)

The displacement mechanisms that developed in the 1-g shaking table and centrifuge tests can provide further insights into the impact of confining stress on the deformation mechanisms and seismic settlement of shallow foundations. This is discussed for both saturated and partially saturated soils below.

Figure 7.7 depicts the soil displacements that accumulated beneath the shallow foundations throughout the first earthquake of 1-g shaking table tests, STT1 and STT2. It is worth noting that illustrated in this figure are the final positions of the foundations, at the end of the earthquakes. It appears that an extended bearing capacity failure mechanism was mobilised for both cases. In the case of STT1 (unimproved, deposit of saturated soil), a deep layer of liquefaction occurred, and the foundation settled significantly. The soil below the centre line of the foundation moved vertically downwards, whereas the soil under both edges of the foundation also had a tendency to displace laterally. In fact, the largest displacement vectors were visible under the right edge of the foundation above which some upward soil movements were apparent as well. There, the soil moving upwards led to a large embedment of the foundation. During the first shaking of STT2 (soil deposit improved with air injection), the accumulated foundation settlement was slightly smaller, and the extent of the displacement mechanism was slightly shallower. The soil along the axis of symmetry of the foundation moved vertically downwards. The magnitude of displacement vectors below the foundation gradually decreased with depth and became relatively negligible after a depth of approximately one foundation width. The soil next to the right and the left edge of the foundation was pushed out from beneath the perimeter of the foundation and moved upwards. This again led to a large embedment of the foundation.

For comparison, figure 7.8 shows the soil displacements that developed beneath the shallow foundation during the first shaking of STT3 (soil deposit improved with chemical compound). The time history of the input displacement, which was practically analogous for the 1-g shaking table tests, is also depicted in this figure. As evident, although the magnitude of displacement vectors was slightly smaller in this soil, the extent of the soil deformation seemed to be consistent with that in its saturated counterpart, STT1. The soil, particularly under the right edge of the foundation, was seen to move outwards towards the free-field soil. An area of soil below the foundation moved vertically downwards. The upward movement of soil next to the right and the left edge of the foundation was also apparent.

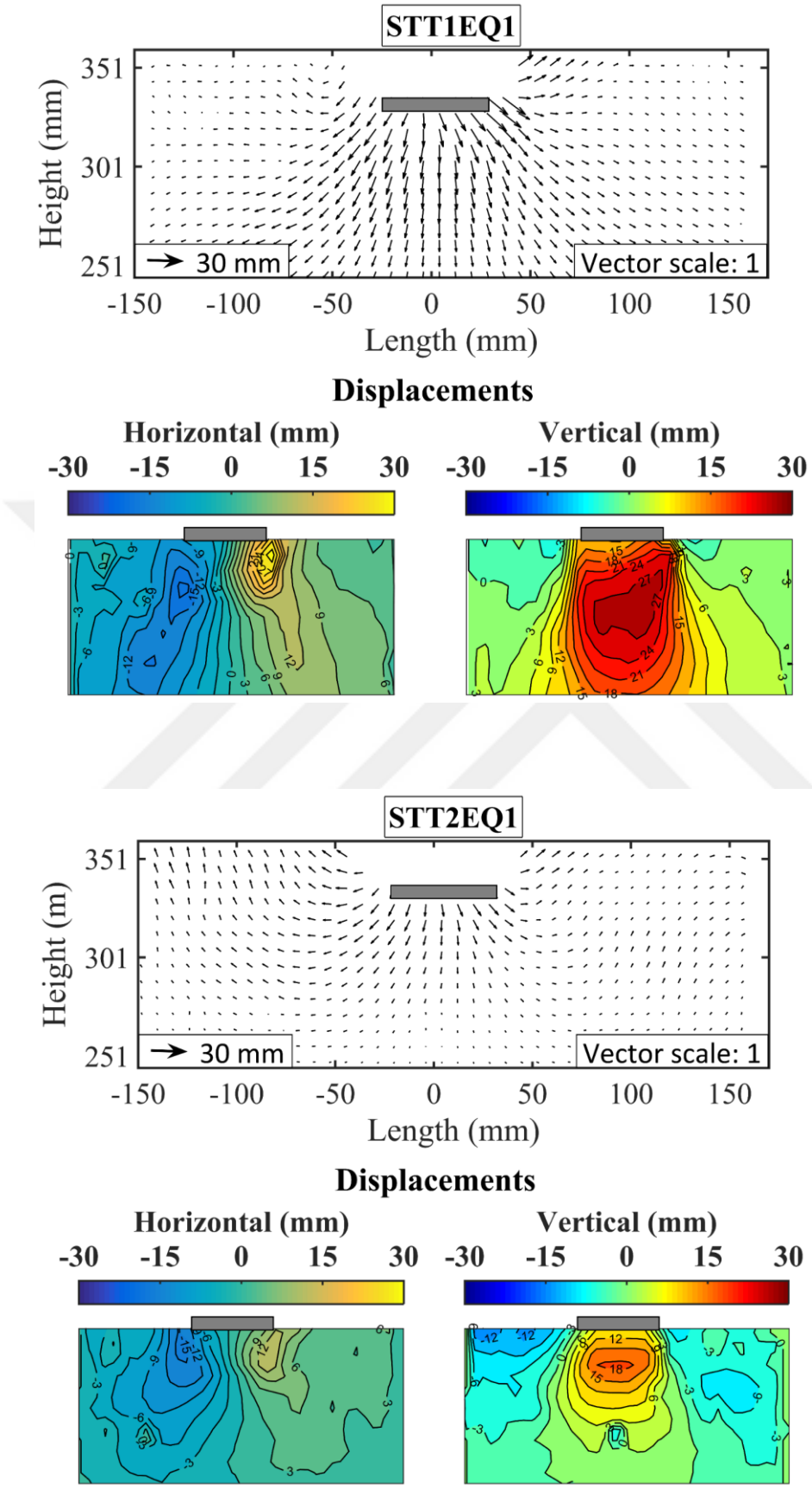

Figure 7.7– Ultimate soil displacements at 1-g shaking table tests, calculated relative to the rigid base and corresponding to the whole duration of the seismic motion.

Each of the two methods of liquefaction remediation was found to be insufficient at low-stress level (1-g) to minimise the liquefaction-induced deformations. Injection of air or using chemical compound caused only a small percentage of reduction in the total settlement of shallow foundations resting on each of the partially saturated soils. The soil displacing laterally from under the edges of the foundation towards the free-field appeared to be the case for all the tests. In addition, a significant reduction in the bearing capacity of the soil was observed to occur, leading to large foundation soil displacements.

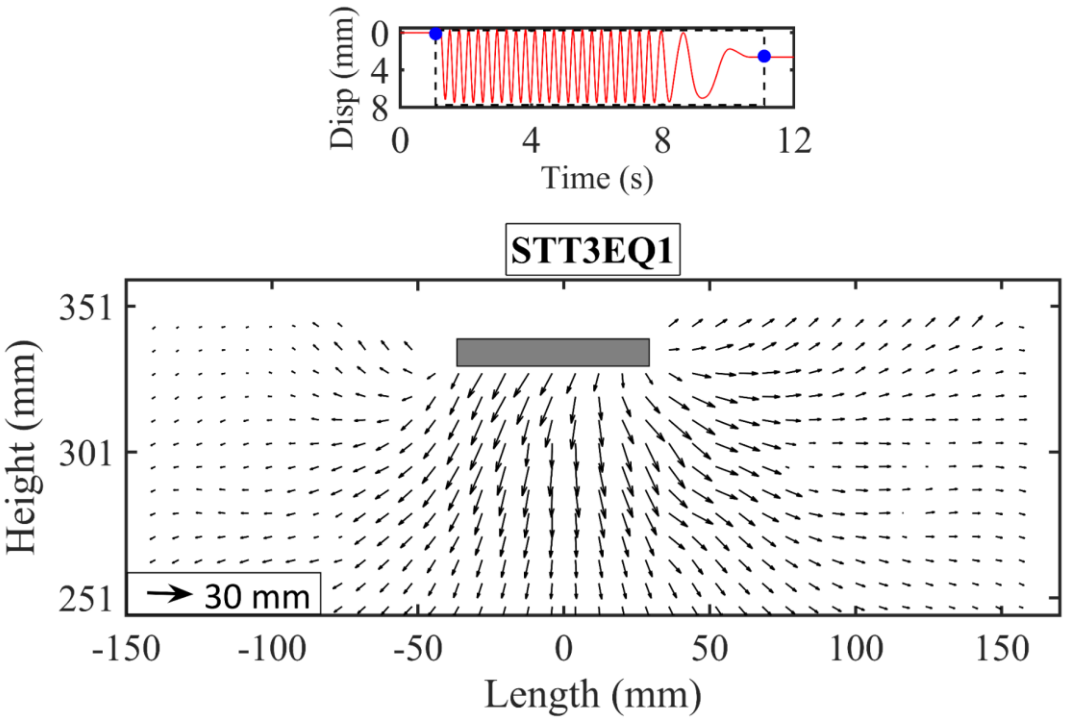

Figure 7.8– Ultimate soil displacements at 1-g shaking table test involving chemical compound treatment.

The displacement vector fields recorded during the first shaking of partially saturated soil in CT7 (tested at a centrifugal acceleration of 40) are shown in figure 7.9.

It is seen that the soil area close to the surface on the left-hand side of the foundation moved laterally. Moreover, the soil column on either side of the soil layer beneath the foundation had a tendency to displace outwards from under the footing, contributing to its embedment. However, the rest of the soil column, particularly on the right-hand side of the foundation, moved vertically downwards, which was indicative of the soil contraction. The depth of the contractive soil layers extended up to a depth approximately equal to two times the foundation width. No significant vertical soil displacement was recorded below this depth. At the very shallow layers, the contractive response was probably facilitated by the proximity to the free-field drainage boundary (short drainage paths) and low confining stresses.

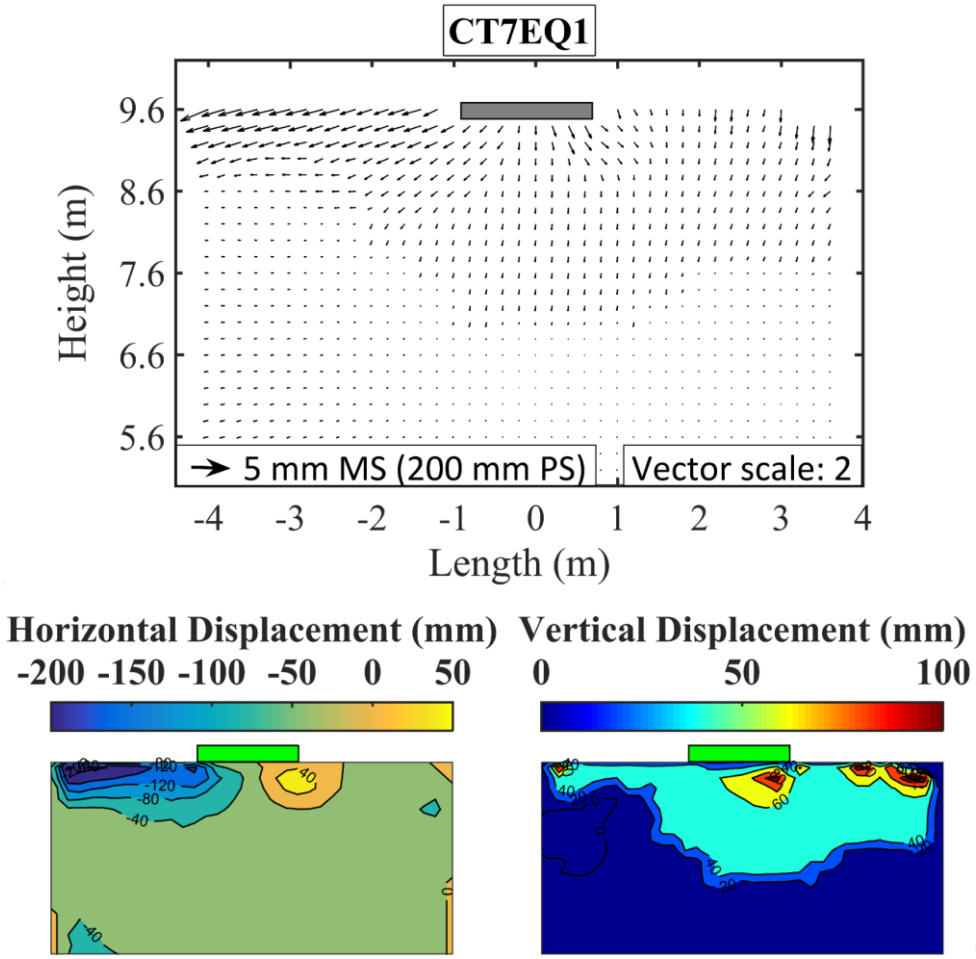

Figure 7.9– Soil displacements accumulated during 17 acceleration cycles of the first event in CT7.

Overall, in this section the performance of air injection and its influence on the deformation mechanisms were evaluated at different confining stresses. The soil displacement vectors and their contours recorded during the 1-g shaking table and centrifuge tests were used for this aim. From this assessment, a different conclusion was drawn for each case.

In contrast to the partially saturated soils examined in the 1-g shaking table apparatus, a bearing capacity failure mechanism was not mobilised in the partially saturated soils that were tested, under higher confining stresses, at an increased level of centrifugal acceleration.

It is inferred from the observed trends that confining stress is an important parameter not only for the magnitude of soil displacements but also for the size and shape of the deformation mechanism.

7.4.3 Foundation Bearing Pressure

Examination of the settlement-time histories of shallow foundations, with different weight but the same contact areas and aspect ratios, provided a qualitative assessment of the influence of bearing pressure on the overall settlement response (section 6.2.3.2). It was shown that during a moderate earthquake the foundation that exerted a higher contact pressure settled less due to higher foundation-induced stresses and smaller cyclic stress ratio beneath it. In order to offer further insights into the problem in question, the horizontal, vertical and total contours of soil displacements that accumulated in the saturated and partially saturated soils over 17 cycles of acceleration are presented in figures 7.10 and 7.11, respectively.

As indicated earlier, significant deformations occurred in the saturated soils beneath and on either side of the *heavy* and *light* foundations. A mobilisation of the bearing capacity failure mechanism was evident in both cases. Figure 7.10 presents the displacement mechanisms that developed in the saturated soils beneath the *heavy* (CT1) and *light* foundation (CT4).

It is clear that the horizontal displacement of soil below each of the two shallow foundations was relatively small, and the soil zones on either side of the foundations predominantly moved laterally. The contour of zero horizontal displacements did not reach the axis symmetry of the foundations. This was particularly obvious in the case of *heavy* foundation. In comparison, the magnitude of lateral soil movements was much larger for the *light* foundation. For the *heavy* foundation, the maximum horizontal displacements took place deep within the saturated soil. For the *light* foundation, they occurred at relatively shallow layers and a distance equal to approximately twice of the foundation width from its centre.

It is evident from the vertical displacement contours that the *heavy* foundation settled less than its *light* counterpart. An area underneath and around the edges of both foundations appeared to move downwards along with the foundations. The width of the bulb of soil extended further with increasing soil depths, but the extent of the bulb was much bigger in the case of *heavy* foundation, leading to a wider settlement profile at the surface of the soil.

Total displacement contours revealed a different displacement mechanism for the two different foundations. The maximum displacements took place beneath the shallow foundations for both cases; however, a relatively greater magnitude of displacements developed beneath the *light* foundation. In addition, the shape of the total soil displacement contour, particularly in the deep soil layers, was much flatter in this case.

The observed trends may indicate that the development of horizontal soil movements in the saturated soils is closely linked to the level of confining stresses beneath shallow foundations. Increased foundation-induced stresses owing to increased bearing pressure plays a role in reducing the horizontal soil movements. This substantially provides a reduction in the overall liquefaction-induced settlement of shallow foundations. Moreover, the observed differences in the shape of displacement mechanisms is a corollary of the increased stress field due to the bearing pressure of shallow foundations.

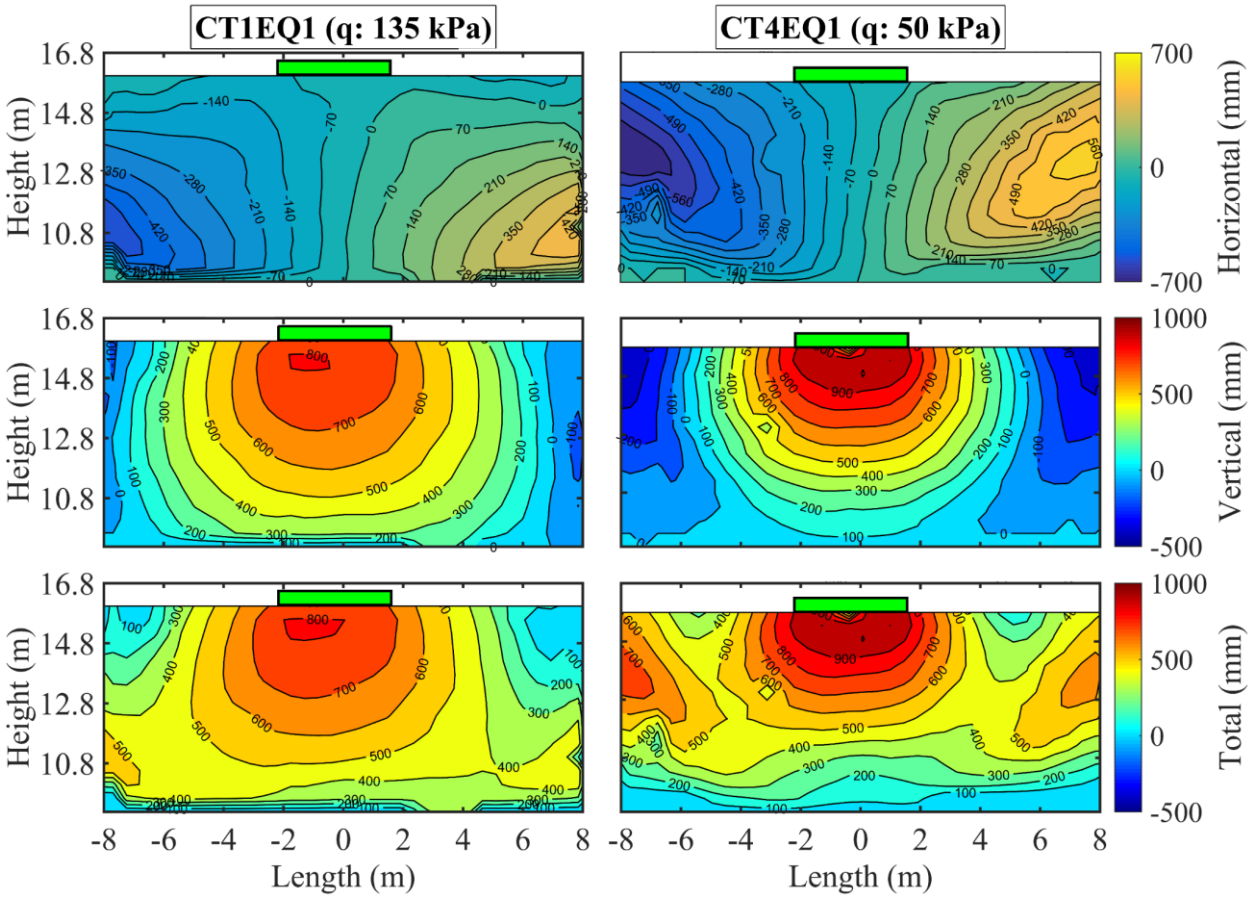

Figure 7.10– Accumulated horizontal, vertical and total displacement contours for the saturated soils.

Figure 7.11 depicts the contours of horizontal, vertical and total displacements that developed in the partially saturated soils beneath the *heavy* foundation (CT3) and *light* foundation (CT6). The comparison of the extent and magnitude of the soil displacements is expected to shed light on the influence of bearing pressure on the deformation mechanisms in these soil deposits.

The following observations were made based on figure 7.11:

Horizontal soil movements were primarily concentrated beneath the left edge of the *heavy* foundation, whereas they were observed under both left and right edge of the *light* foundation.

The magnitude of laterally outward soil movements from the edges of the shallow foundations was relatively smaller in the *heavy* foundation than the *light* foundation, although S_r of soil was relatively higher in the former. This may suggest that in addition to S_r, the increased stress regime in the ground as a result of foundation-induced stresses is important for the lateral displacement of partially saturated soils.

The maximum horizontal, vertical and total soil displacements took place at the shallow layers for both cases. In the *heavy* foundation, there was an area of large displacement close to the soil surface (at the left-hand corner). The observed localised displacement area was attributed to relatively heterogeneous desaturation of the soil in this location.

In the partially saturated soils, the vertical and total displacement contours did not have the same form of a bubble as for the saturated soils (shown in figure 7.10). They were flatter and wider at the equivalent depth of soil layers. The areas of maximum vertically downward and total soil displacements were more localised for both foundations, despite relatively smaller magnitude of displacements being observed under the *heavy* foundation.

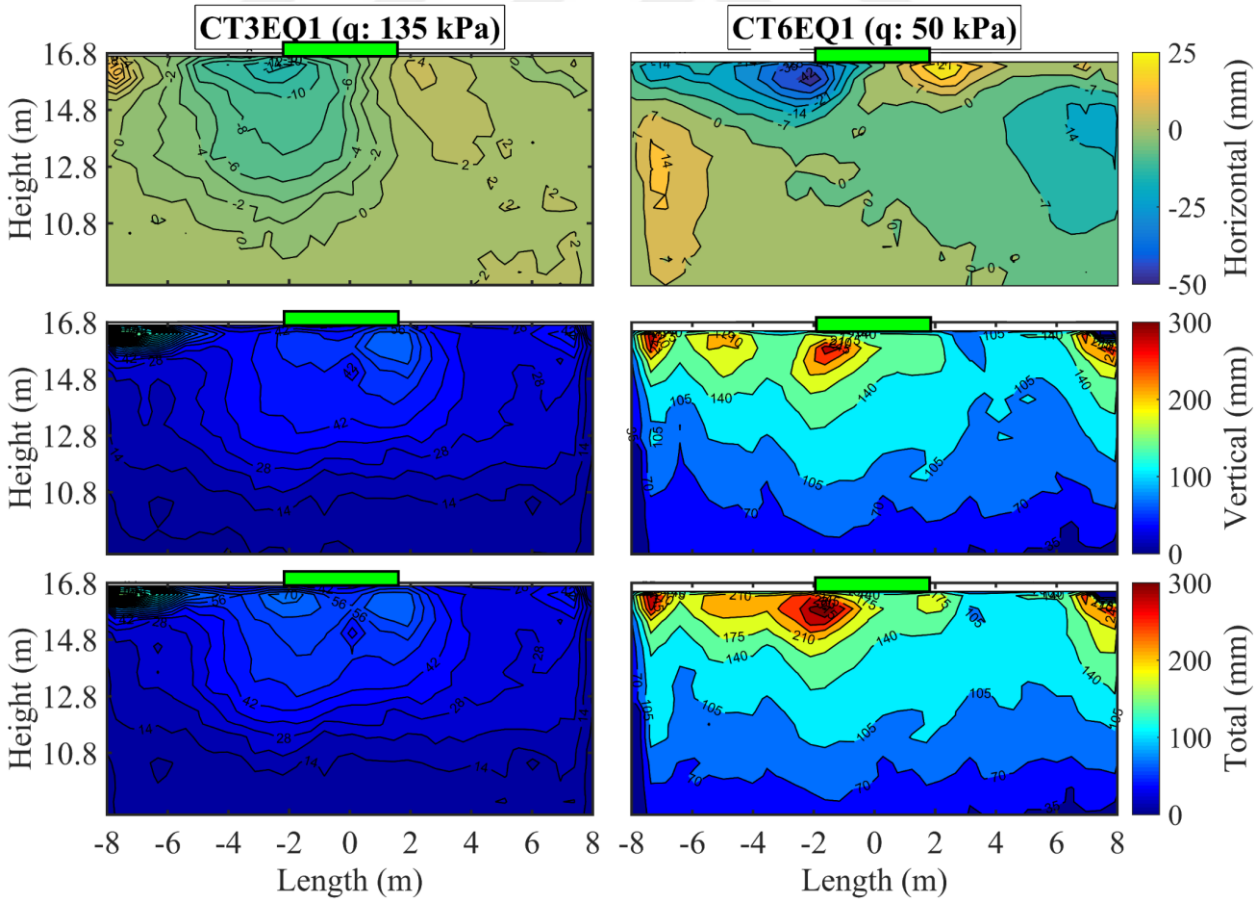

Figure 7.11– Accumulated horizontal, vertical and total displacement contours for the partially saturated soils.

7.4.4 Earthquake Amplitude

This section discusses the influence of earthquake amplitude on the deformation mechanisms. By comparing the soil displacement vectors that developed during the consecutive earthquakes with increasing amplitudes, a different soil displacement behaviour was observed for each case, as detailed below.

Figure 7.12 shows the soil displacements that accumulated over 17 cycles of acceleration in the saturated soils (CT1 and CT4). In the first earthquake, an extended failure mechanism that reached a depth of approximately 8 m was mobilised. A mass of soil underneath and around the edges of the foundation displaced exclusively vertically as the lateral support from the surrounding soil was lost. Horizontal displacements were observed further away from the edges of the foundation. During the successive earthquakes, the displacement mechanism became relatively more localised. The result was a mobilisation of a failure mechanism that extends to a depth of 6 m during the second earthquake. The area of soil under the foundation again moved vertically downwards, but the horizontal displacement of soil started from next to the edges of the foundation, leading to relatively smaller surface settlements at these locations. The failure mechanism only extended to 4 m depth during the third successive earthquake: the soil under the edges of the foundation was pushed away.

The experimental results showed that liquefaction occurred multiple times in the saturated soils, and the foundation settled further during each earthquake event. The mechanism of settlement differed in the seismic events according to the level of foundation embedment. The foundation settlement was driven by an extended failure mechanism during the first shaking where the foundation embedment was the smallest. The driving mechanism for the foundation settlement, however, became shallower and more localised during the following earthquakes as the foundation got embedded after each event.

It is worth noting that the amplitude of the earthquakes was not correlated with the magnitude of the settlements that shallow foundations suffered, as reported in section 6.2.4.1. Although a stronger earthquake would be expected to cause larger settlement of the foundations and larger deformations of soils, this was usually not the case. This may suggest that in conjunction with the level of foundation embedment, the densification of the soil layers after each consecutive earthquake should be kept in mind while the displacement mechanisms are being examined.

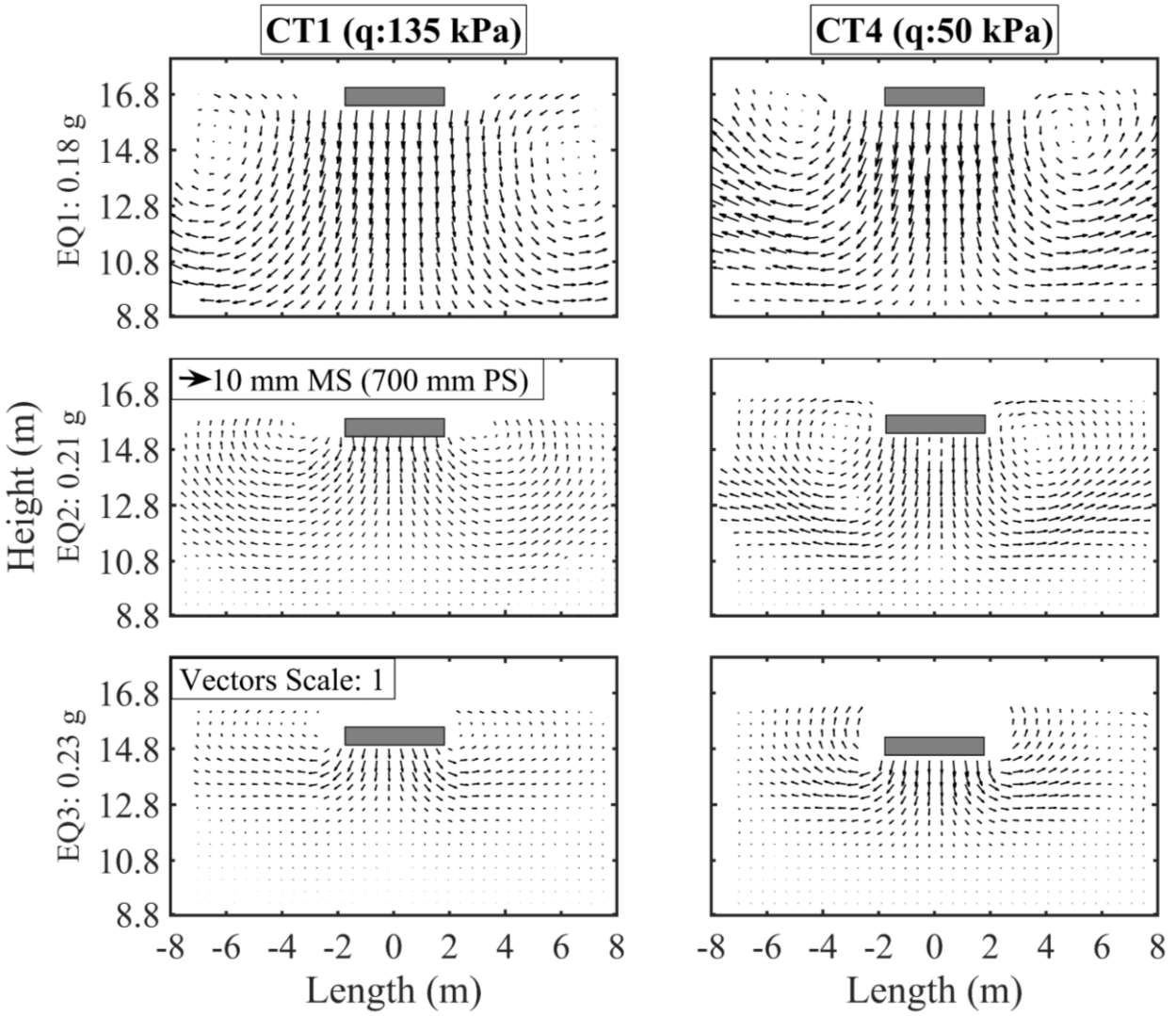

Figure 7.12– Accumulated soil displacements for the saturated soils during the successive earthquakes.

Figure 7.13 presents the soil displacements measured over 17 cycles of acceleration in the partially saturated soils (CT3 and CT6). Due to the small magnitude of deformations that were involved, the displacement vectors were magnified by 20 and ten times for CT3 and CT6, respectively.

It is seen in figure 7.13 that the displacement response of partially saturated soils was more complicated than that of saturated soils. The shape of the displacement mechanisms remained almost the same during the consecutive earthquakes in CT3, whereas different shape of displacement mechanisms were observed in CT6. Apparently, the main settlement-producing mechanism was the increased compressibility of the soil mass for all cases. This led to vertically downward movements across the soil. There were also small outward soil displacements from beneath the edges of the foundations, particularly in the case of CT3. This mechanism, however, covered only a small area that concentrated at the shallow layers.

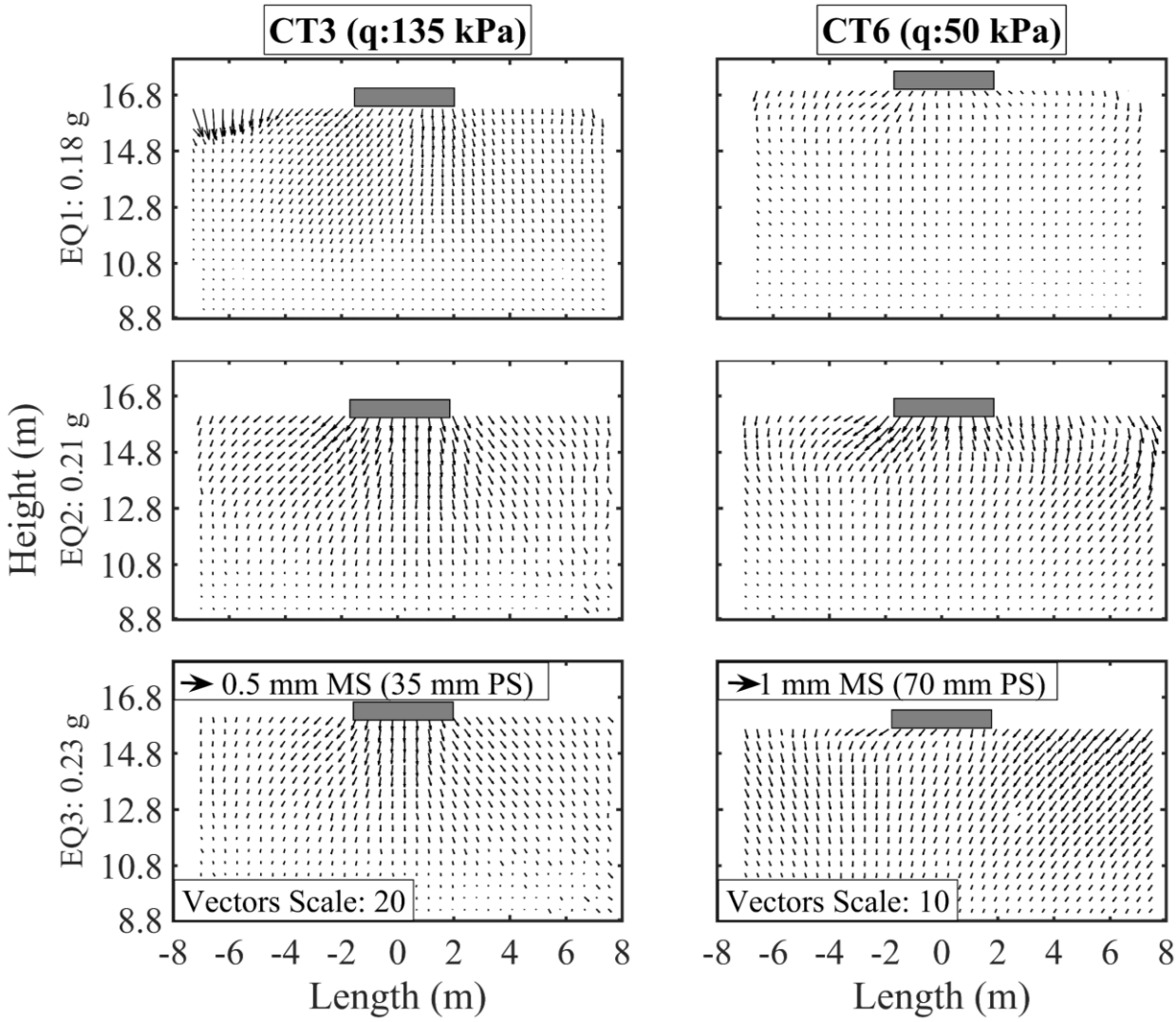

Figure 7.13– Accumulated soil displacements for the partially saturated soils during the successive earthquakes.

7.5 Summary

This chapter offered insights into the deformation mechanisms that governed the settlement of shallow foundations resting on the saturated and partially saturated soils. The deformation mechanisms were identified using the PIV-based displacement vectors and their contours.

The results emphasised that the settlement of shallow foundations resting on the saturated soils arose from (1) deviatoric strain-induced deformations associated with foundation-induced and earthquake-induced shear stresses and (2) volumetric strain-induced deformations associated with partial drainage and reconsolidation. The former appeared to dominate the settlement of shallow foundations. This was evident from the strong tendency of horizontal soil movements within the saturated soil layers and formation of extended failure mechanisms.

On the other hand, in the partially saturated soils, deviatoric strain-induced deformations under static and dynamic shear stresses were significantly minimised. The depth of liquefaction also markedly reduced, and a complete bearing capacity failure mechanism did not form under shallow foundations. In these soil deposits, volumetric strain-induced deformations associated with increased soil compressibility (in the presence of air) were found to be the main factor contributing to the total foundation settlements.

The displacement vector fields and their contours were used to elucidate the effect of S_r on the deformation mechanisms. A decreasing trend in the magnitude of horizontal and vertical soil movements was observed with decreasing S_r. The depth of liquefied soil layer also continued to reduce, and the resistance of soil to the bearing capacity failure mechanism increased further with a further reduction in S_r.

In addition to S_r, the development of horizontal and vertical soil movements was directly correlated with the stress level and soil stiffness beneath shallow foundations. The magnitude of horizontal soil movements appeared to reduce as the foundation-induced stresses beneath shallow foundations increased. Deformations that developed, under low confining stresses, at 1-g testing were large, irrespective of the presence of air/gas bubbles in the soil. It must be noted that as stress levels in the 1-g tests were substantially lower than in the prototype, use of quantitative results from these tests should be approached with caution. Unlike in the 1-g tests, the observed deformations seemed to decrease profoundly as the partially saturated soils were tested in the centrifugal environment that produced an increased gravitational field and increased level of confining stresses. In these tests, although the magnitude of horizontal and vertical soil displacements was relatively large closer to the soil surface, the areas of large soil displacements significantly decreased in the deeper layers. Consequently, air injection provided a significant reduction in the total settlement of shallow foundations.

Chapter 8

Simplified Methodology to Estimate the Settlement of Partially Saturated Soils

8.1 Introduction

The prediction of earthquake-induced settlement of a level bed of saturated soil or shallow foundation is a major issue in geotechnical earthquake engineering. Research has led to the development of several methodologies that are commonly employed in design practice, as discussed in section 2.3.4. These methodologies often assume an undrained soil behaviour. The settlement is anticipated only after the earthquake ceases and once the dissipation of excess pore pressures completes (called reconsolidation). Recent centrifuge-based studies (e.g. Coelho (2007) and Zeybek and Madabhushi (2017b)) have reported that this approach may not be true. Large ground surface settlement is shown to happen during an earthquake loading, where the soil liquefies reaching a near-zero effective stress state (σ'_{v0}~0) and a reduced stiffness.

The saturated soil condition often receives much of the attention since it is categorised as the worst case scenario for liquefaction related damage. Consequently, a meaningful prediction of the earthquake-induced settlement of partially saturated soils has remained elusive. In fact, the methodologies available in practice cannot be readily used for this purpose. In addition to their shortcomings highlighted above and in section 2.3.4, these methodologies fail to incorporate the impact of such parameters as S_r.

This chapter aims to assess the reliability of currently available state of the practice methods. It also describes an effective stress based methodology developed for the prediction of ground surface settlement of partially saturated soil layers, along with the limitations, uncertainties and possible improvements. The fundamental features of the reconsolidation of soils are discussed

separately based on an overview of the literature. The prediction of reconsolidation settlement is explained in conjunction with the scientific rationale beyond the procedure followed.

8.2 Settlement Evaluation Methods in State of Practice

The state of practice heavily relies on the free-field semi-empirical methodologies that aim to predict the liquefaction-induced settlement of shallow foundations resting on saturated deposits of liquefiable soils. The common assumption is that the foundation settlement is analogous to that of the free-field. This approach was, however, shown to have serious limitations as it fails to incorporate the influence of several additional volumetric and deviatoric strain-induced deformation mechanisms at play, as discussed in chapter 7.

The importance of the foundation width (B) and foundation bearing pressure (q) and the depth of liquefiable layer (D_L) for the average foundation settlement (S_f) is widely reported. Yoshimi and Tokimatsu (1977) introduced the normalisation of B and S_f with D_L. Based on the field data regarding the liquefaction-induced settlement of buildings in 1964 Niigata earthquake, the normalised settlements (S_f/D_L) were correlated to the normalised width (B/D_L). Liu and Dobry (1997) later developed an empirical design chart with an upper and lower boundary, using the field data from 1964 Niigata and 1990 Luzon earthquake. More recently, based on the observed settlements of buildings having shallow foundations from 2010 Maule earthquake, Bertalot et al. (2013) proposed a design chart that incorporates the influence of bearing pressure. Here, centrifuge test results are compared with the predictions of currently available and widely used semi-empirical methodologies and empirical graphs.

8.2.1 Free-Field Settlement

In table 8.1, the centrifuge measurements corresponding to the saturated soil tests are presented comparatively, along with the predictions of the three semi-empirical free-field methodologies. It is seen that the method of Wu and Seed (2004) and Tokimatsu and Seed (1987) provided the greatest and the smallest prediction of settlement, respectively. The estimates of Ishihara and Yoshimine (1992) lay between the two methods. Tokimatsu and Seed's prediction matched the free-field centrifuge measurement reasonably well in CT9. On the other hand, the other two methods overpredicted the centrifuge free-field settlement for all cases. It is also evident in table 8.1 that even the best prediction method failed to estimate the foundation settlement.

Table 8.1 – Comparison of the experimental settlement with the predictions of free-field methodologies.

Centrifuge Test ID	Free-field methodologies:			Centrifuge test data:	
	: Tokimatsu and Seed (1987) Settlement (mm)	*: Ishihara and Yoshimine (1992) Settlement (mm)*	*: Wu and Seed (2004) Settlement (mm)*	*: Foundation Total Settlement (mm)*	*: Free-field Total Settlement (mm)*
CT1	504 mm the volumetric strain of 3%	722 mm the volumetric strain of 4.3%	840 mm the volumetric strain of 5%	768.8	-
CT4				1019.0	-
CT8				-	323.2
CT9				-	495.5
CT10				-	407.4

8.2.2 Foundation Settlement

8.2.2.1 Saturated Soils

Figure 8.1 compares the normalised settlement of shallow foundations recorded during the saturated soil tests with the empirical charts of Liu and Dobry (1997) and Bertalot et al. (2013). In this figure, the width and foundation settlements were normalised by the total depth of the saturated deposit of liquefiable soil (D_L =16.8 m). The normalised values were plotted on top of these charts. For the purpose of comparison, a set of centrifuge test data were collected from the previous publications and presented along with the measured centrifuge test data.

It is evident in figure 8.1a that Liu and Dobry's boundaries failed to capture the majority of the data points. In particular, the database compiled from the most recent centrifuge tests appeared to be out of trend. The results poorly correlated with these boundaries, particularly for relatively lower and higher B/D_L ratios (e.g. very narrow foundation or a thin layer of liquefiable soil). This chart overpredicted the settlement measurements made in this thesis and reported in the literature. Dashti et al. (2010) reported that centrifuge test results from a relatively thick layer of liquefiable soil (D_L =6 m) did fit well with these limits. However, the results deviated from the Liu and Dobry's boundaries for a relatively thin layer of liquefiable soil (D_L =3 m) and therefore high normalised width ratios ($B/D_L \geq 2$). They concluded that the normalisation of B with D_L might work well only for a sufficiently thick layer of liquefiable soil.

Bertalot et al. (2013) considered the combined effect of B and q and proposed a graph to predict the maximum expected foundation settlement. Figure 8.1b compares the centrifuge data with their S_f/D_L contours. It is noted that due to the scarcity, Bertalot et al.'s data was limited to a

region shown by a rectangular in figure 8.1b, and they extrapolated the curve for the remaining region. Their boundaries were extended further here (shown as broken contour lines) since the width of the foundation used in this study fell outside of their original region. It is found that the use of this chart provided a reasonable estimate for the settlement of the *heavy* foundation (q: 135 kPa), but it overestimated the settlement of the *light* foundation (q: 50 kPa).

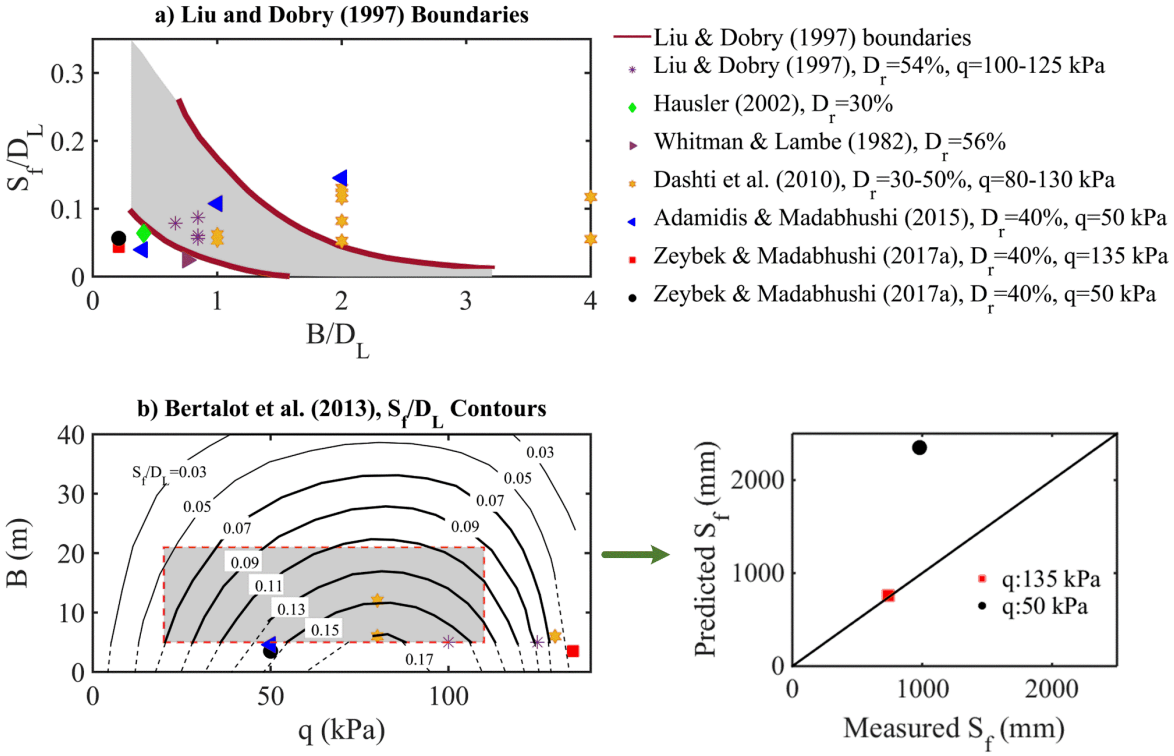

Figure 8.1– Comparison of the predicted and measured foundation settlement (saturated soils).

8.2.2.2 Partially Saturated Soils

The effects of ground motion characteristics and soil properties (e.g. relative density, fines content and degree of saturation) are not incorporated in these design charts. The normalised settlement of foundations from both saturated and partially saturated soil tests is compared with the predictions of Liu and Dobry's boundaries in figure 8.2. Furthermore, the variation of normalised settlement ratios with S_r is depicted. It is obvious that foundation settlement and hence normalised settlement ratios reduced with decreasing S_r. The centrifuge measurements were well outside the band of Liu and Dobry's graph, providing an upper bound for settlement in all cases. This points out that for engineering design, the use of this chart will be impractical to predict the settlement of shallow foundations resting on the partially saturated soils. In order to achieve adequately accurate predictions, it will be necessary to incorporate the combined effects of important variables on D_L (e.g. degree of saturation and confining stress).

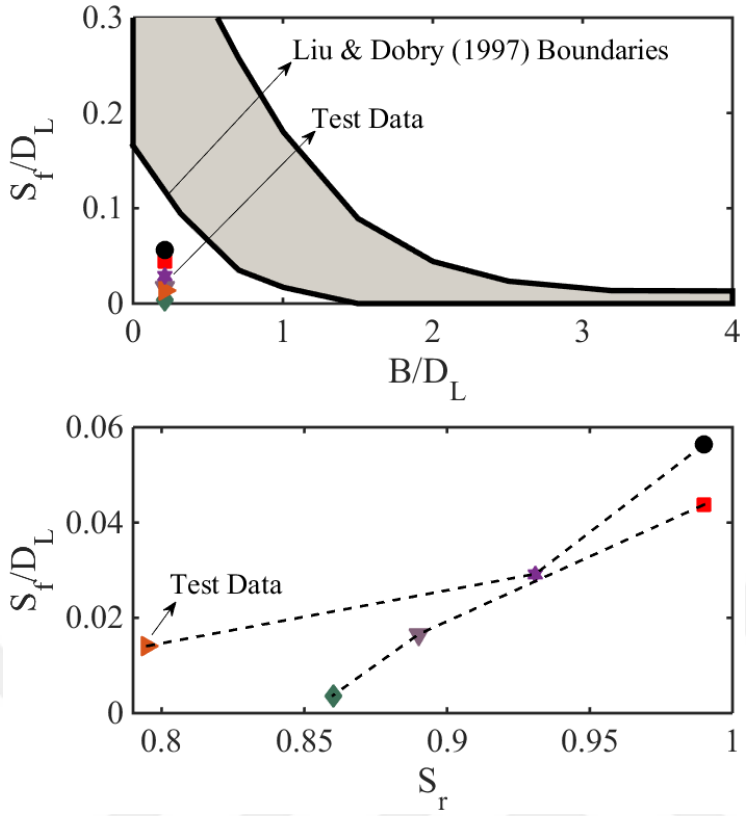

Figure 8.2– Comparison of the predicted and measured foundation settlement (partially saturated soils).

8.3 A Simple Methodology for Settlement Prediction

8.3.1 The Basis for the Methodology

Based on the experimental observations in this research, the dynamic response of saturated and partially saturated soils can be represented in a schematic way (figure 8.3).

Under an earthquake loading, air bubbles trapped in a pore fluid assist in reducing the build-up of excess pore pressures with their compression (contraction). A partially saturated soil layer, therefore, undergoes a smaller decrease of effective stress and simultaneous stiffness drop than its saturated counterpart. Although complete liquefaction is not reached, the build-up of excess pore pressures and related soil-softening still cause some vertical settlement (see chapter 6). The changes in compressibility as air is added to the soil system also contributes to the settlement. The extent of the ground surface settlement related to soil-softening and increased compressibility ought to be a function of such parameters as σ'_{v0} and S_r.

Here, inherent in the proposed methodology is the assumption that the total ground surface settlement of a partially saturated soil can be estimated as long as the total surface settlement

of the same soil in the saturated condition is known. The ground surface settlement associated with soil-softening (or reduction in soil stiffness) is expected to reduce with a decrease of S_r. However, the settlement due to compressibility should increase with decreasing S_r. It should be noted that this methodology does only consider the settlement of a level ground layer with no foundations. Moreover, it is constructed not based on the collected data itself but developed using principles and theoretical understanding on the partially saturated soil behaviour.

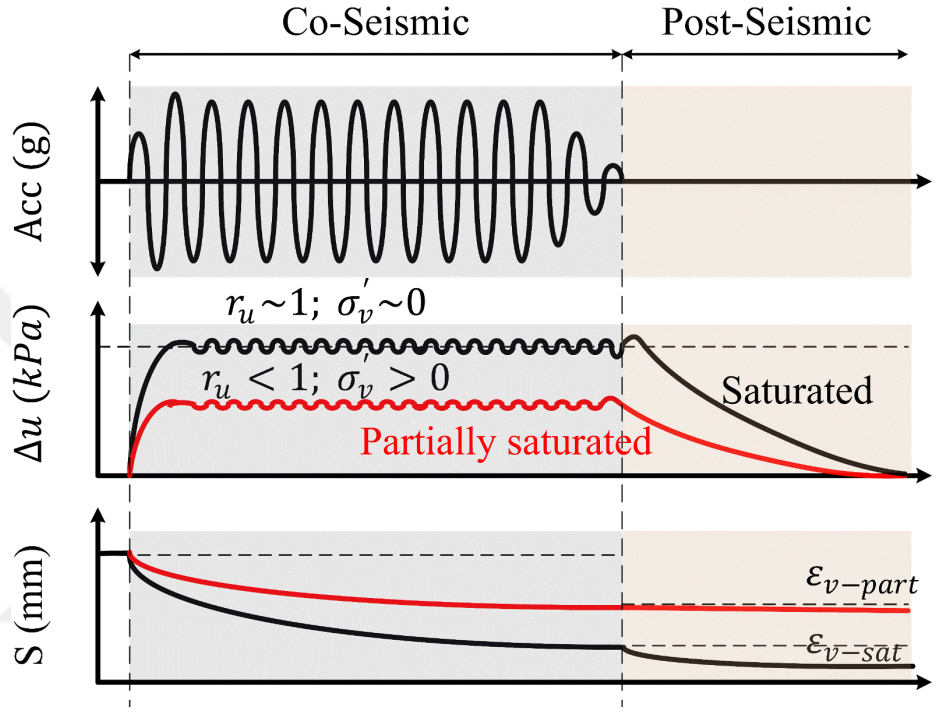

Figure 8.3– Schematic representation of saturated and partially saturated soil behaviour.

8.3.2 Framework for the Methodology

The soil deposit was divided into *n* sub-layers, as presented in figure 8.4. Material properties were assigned to each layer. Homogeneous soil layers were assumed whereby the soil properties (e.g. S_r and D_r) were constant for each layer. Compression was allowed to happen only in the vertical direction. The earthquake-induced ground surface settlement of the soil deposit was obtained by integrating the settlement of each sub-layer:

$$S = \sum_{i=1}^{n} \Delta_{z,i} = \sum_{i=1}^{n} \varepsilon_{v,i} \cdot d_{z,i} \tag{8.1}$$

where S is the total surface settlement, and $\Delta_{z,i}$, $\varepsilon_{v,i}$, $d_{z,i}$ are the partial settlement, volumetric strain and thickness of each sub-layer, respectively.

A schematic of the proposed methodology is presented in figure 8.5.

Liquefaction-induced settlement of soils during dynamic loading is a fully coupled problem. The deformation of soil matrix involves coupling between the excess pore pressure generation/dissipation and effective stress. Moreover, soil is a highly non-linear material. From the 1970's onwards, several linear and non-linear methods have been developed to compute the dynamic response of soil layers. The fully-coupled non-linear dynamic analysis methods (e.g. Muraleetharan et al. 1994) can be used for the seismic response of partially saturated soils. This approach is, however, quite complex and difficult to apply. Here, a simple but more applicable method is proposed.

Assuming the validity of the principle of superposition, reasonable approximations of the volumetric strains at the centre of each sub-layer can be accomplished by summing the volumetric strains expected from each of the two mechanisms:

$$\varepsilon_{v,i} = \varepsilon_{v,i-epp} + \varepsilon_{v,i-com} \tag{8.2}$$

where $\varepsilon_{v,i-epp}$ is the earthquake-induced volumetric strains associated with the excess pore pressure generation/dissipation, causing soil-softening (change in soil stiffness) and fluid flow. $\varepsilon_{v,i-com}$ is the volumetric strains related to the increased soil compressibility.

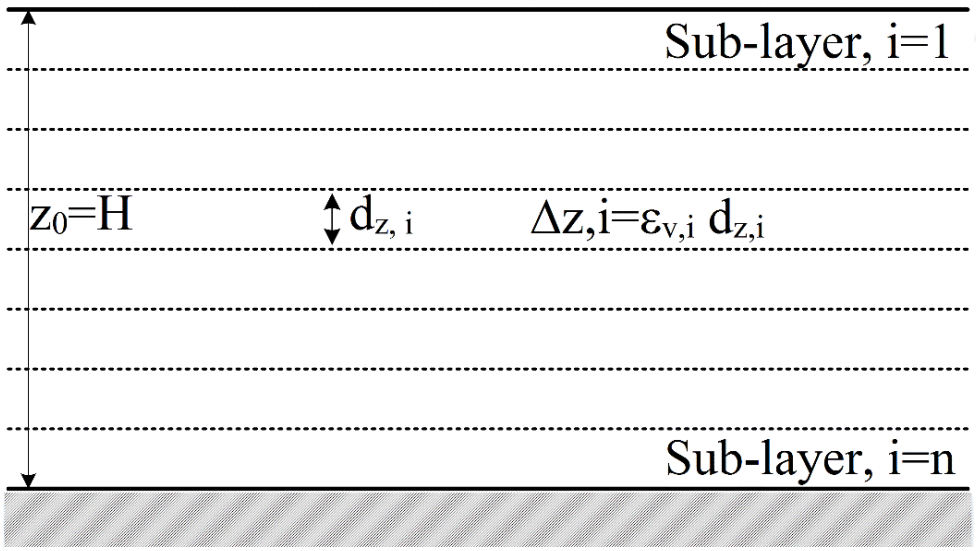

Figure 8.4– Schematic representation of a uniform soil layer divided into n sub-layers.

8.3.2.1 Volumetric strains due to excess pore pressure (epp)

The volumetric strains of a partially saturated soil due to epp, $\varepsilon_{v-epp_{(part)}}$, can be estimated as a function of volumetric strains of the same soil in a saturated condition, $\varepsilon_{v-epp_{(sat)}}$, and the magnitude of excess pore pressure ratio that develops, r_{u-part}:

$$\varepsilon_{v-epp_{(part)}} = f(\varepsilon_{v-epp_{(sat)}}, r_{u-part}) \tag{8.3}$$

In a similar way, the excess pore pressure ratio for a partially saturated soil, r_{u-part}, can be linked to that develops in its saturated counterpart, with the added parameter of S_r:

$$r_{u-part} = f(r_{u-sat}, S_r) \tag{8.4}$$

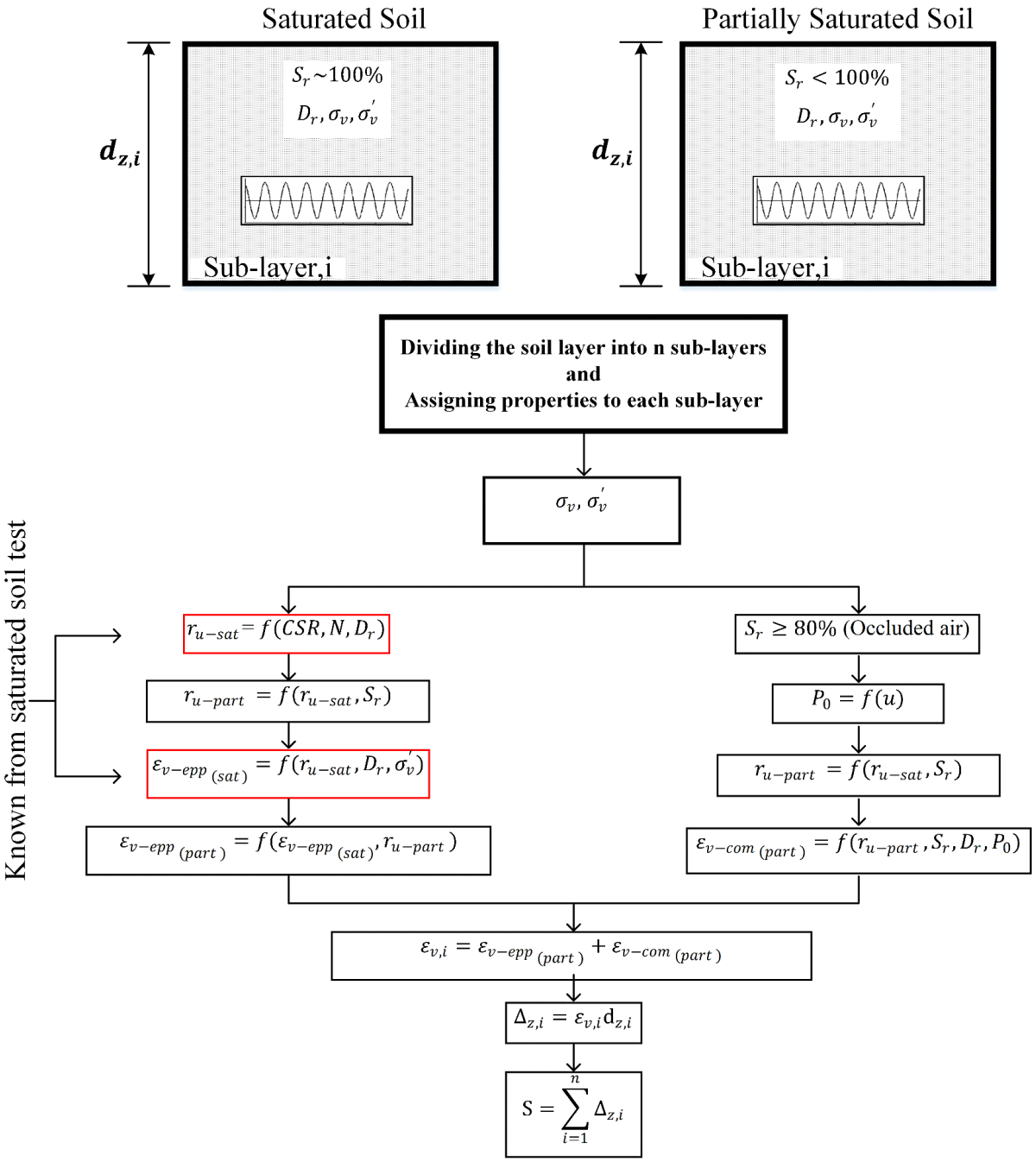

Figure 8.5– Schematic flow chart of the proposed methodology.

8.3.2.2 Volumetric strains due to compressibility

The volume of occluded air, under equilibrium with an absolute hydrostatic pore fluid pressure, P_0, reduces under an external pressure applied, as discussed in section 2.6.2. Under an earthquake loading, the external pressure is the excess pore pressure which can be simply expressed in terms of r_{u-part}. The general form of the relationship for this can be written as:

$$\varepsilon_{v-com_{(part)}} = f(r_{u-part}, S_r, D_r, P_0) \tag{8.5}$$

In fact, this approach can be more appropriate for the partially saturated soils with high S_r values, such as $S_r \geq 80\%$.

8.3.3 Evaluation of the Model Parameters

8.3.3.1 Excess Pore Pressure Ratio

The magnitude of excess pore pressures that develop in a partially saturated soil reduces significantly as S_r decreases. Based on the data collected in this research and available database in the literature, it is recommended that the reduction in r_u can be reflected by a power function that includes S_r:

$$r_{u-part} = r_{u-sat} \cdot {S_r}^{n1} \tag{8.6}$$

This approach assumes the validity of establishing a direct correlation between r_{u-sat} and r_{u-part} as a function of S_r.

Determining the power *n1* requires a number of dynamic element or physical modelling tests performed at a wide range of S_r. Thus far, only a few data set have been available in the published literature, particularly for clean sands. Okamura and Soga (2006) collected some of the available element testing data. They showed that the normalised liquefaction resistance ratio (R) increases significantly as S_r reduces, as depicted in figure 8.6.

In this thesis, it is assumed that liquefaction resistance of soil can be inversely correlated to r_u. The data set from Yoshimi et al. (1989) was used to define a relationship between r_{u-sat}, r_{u-part} and S_r. The equation 8.7 produced the best fit line for their database.

$$\frac{r_{u-part}}{r_{u-sat}} = 0.7 \cdot {S_r}^{12} + 0.3 \tag{8.7}$$

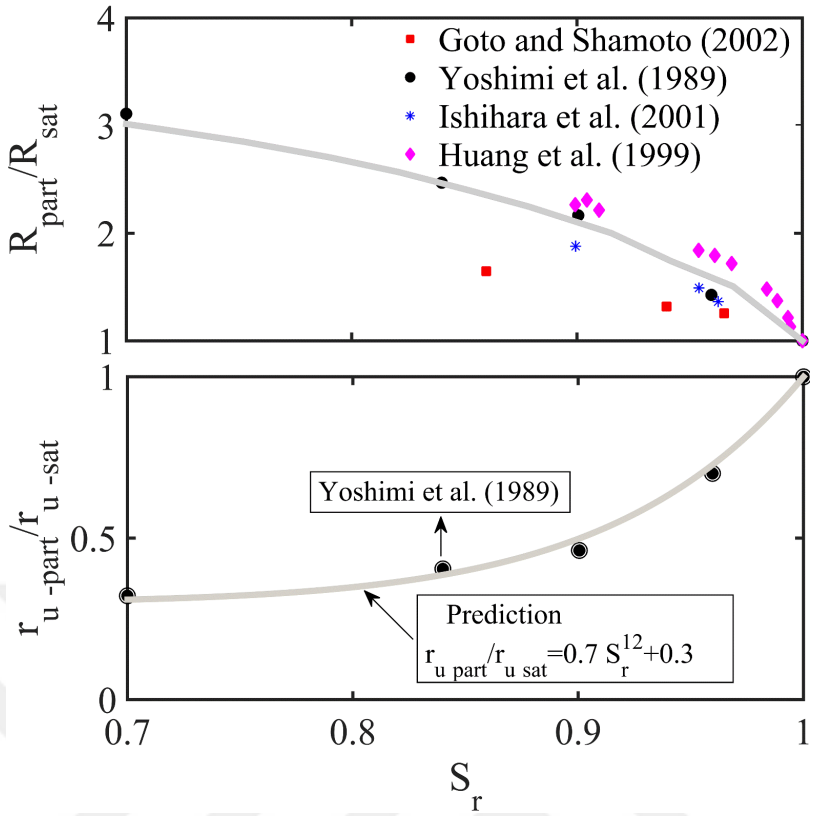

Figure 8.6– Change of liquefaction resistance and excess pore pressure ratio with degree of saturation.

In order to assess whether equation 8.7 can produce consistent results for different types of soil and testing method, its prediction is compared with the centrifuge data in figure 8.7. The excess pore pressure ratios for partially saturated soils were normalised with those of saturated soils. It is evident that the proposed relationship was capable of producing predictions with a sufficient accuracy at the middle depth of the soil deposits (7 m, $\sigma'_{v0} = 62$ kPa). However, it consistently overpredicted the normalised excess pore pressure ratios at the larger depths (14 m, $\sigma'_{v0} = 124$ kPa). In fact, this behaviour can be mainly ascribed to the stress dependency of partially saturated soils (see section 6.2.2.2). The effectiveness of air injection in reducing the excess pore pressure generation was shown to drop, under a low confining stress, at the shallow soil layers. This caused the development of very high r_u values, irrespective of S_r. Therefore, the proposed relationship provided lower bounds for r_u in such layers. On the other hand, the prediction offered upper bounds for r_u at the deeper layers where air injection worked better, and much smaller excess pore pressure ratios were generated. It can be deduced from the observed trends that the predictions of equation 8.7 are conservative for higher confining stresses and satisfactory for the mid-range of effective stresses (average for the soil deposit under consideration). The establishment of a broader range of data set is encouraged so as to increase the accuracy of the predictions.

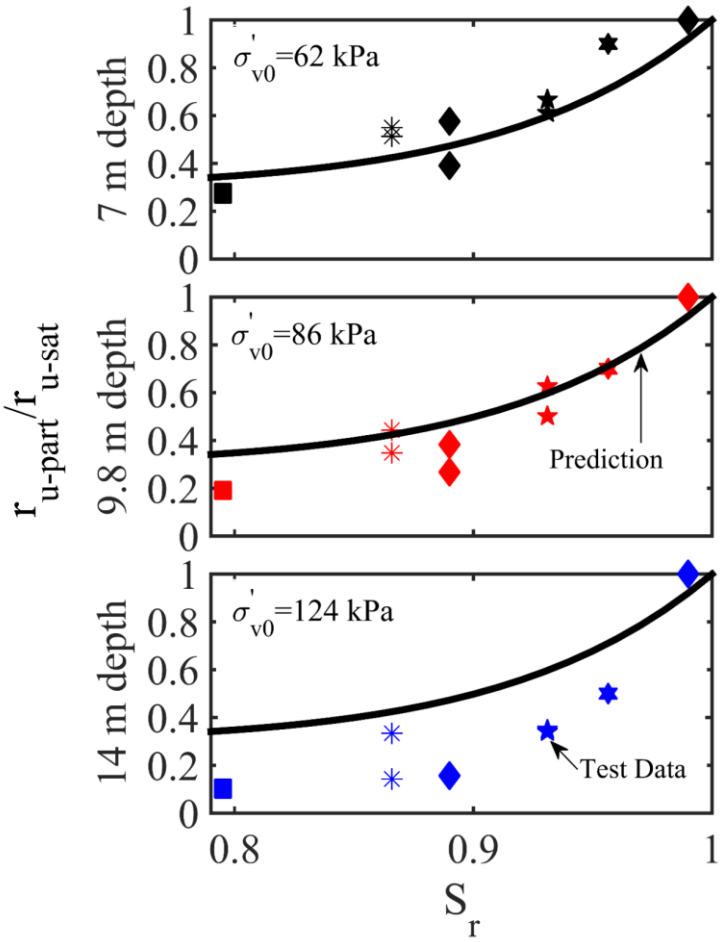

Figure 8.7– Comparison of the predicted and measured excess pore pressure ratios.

8.3.3.2 Volumetric strains due to epp

Lee and Albaisa (1974) showed that volumetric strains of saturated soils at different relative densities and confining stresses reduce with decreasing pore pressure ratios (figure 8.8). Tokimatsu and Yoshimi (1983) later suggested that although full liquefaction is not reached, excess pore pressures generated during an earthquake loading can still cause some volumetric strains of saturated soils.

These experimental findings may indicate that epp-induced volumetric strains of a saturated soil can be represented as a function of excess pore pressure ratios. In the same way, volumetric strains of a partially saturated soil caused by epp can be related to the magnitude of excess pore pressure ratios that tends to reduce with a decrease of S_r. A linear function is assumed here in order to convert this to a relationship between $\varepsilon_{v-epp_{(sat)}}$ and $\varepsilon_{v-epp_{(part)}}$:

$$\varepsilon_{v-epp_{(part)}} = \varepsilon_{v-epp_{(sat)}} \cdot \frac{r_{u-part}}{r_{u-sat}} \tag{8.8}$$

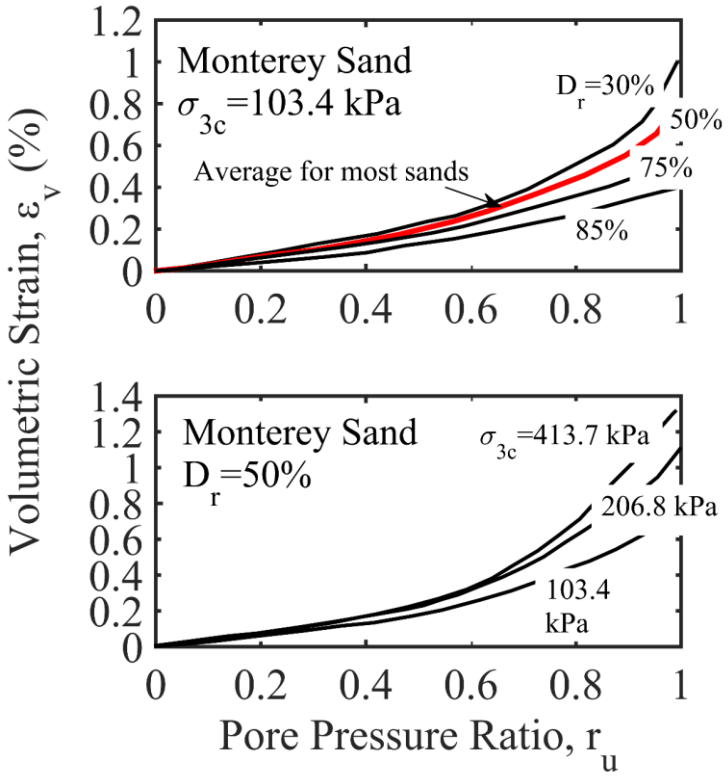

Figure 8.8– Relationship between pore pressure ratio and volumetric strain (after Lee and Albaisa 1974).

8.3.3.3 Volumetric strains due to compressibility

For a given relative density of a partially saturated soil, the volumetric strains due to increased compressibility, $\varepsilon_{v-com_{(part)}}$, can be estimated using the theoretical solution given in equation 2.10.

8.3.4 Validity of the Methodology

The total stress, σ_{v0}, and effective stress, σ'_{v0}, at the centre of each sub-layer were calculated using equation 2.3. For this case, the moist unit weight of the soil, γ_{moist}, was considered. The volumetric strains of saturated soil due to epp, $\varepsilon_{v-epp_{(sat)}}$, were calculated in each sub-layer using the ground surface settlement measured in the centrifuge and assuming that the volumetric strains were maximum at the shallowest layer and decreased linearly with depth until they became zero at the base of the soil deposit. The volumetric strains in the partially saturated soils due to epp, $\varepsilon_{v-epp_{(part)}}$, and compressibility, $\varepsilon_{v-epp_{(com)}}$, were determined using equations 8.8 and 2.10, respectively. Subsequently, the total surface settlement of partially saturated soils was computed by summing the volumetric strains for each sub-layer.

Figure 8.9 depicts the estimate of settlement based on each volumetric strain mechanism and compares the predicted settlement with the centrifuge test measurements. The validity of the proposed method was assessed through the quality of fit to the experimental data.

It is evident in figure 8.9 that despite certain uncertainties in the observed trends, the estimation of the proposed methodology was satisfactory in predicting the total ground surface settlements measured during the centrifuge tests. The uncertainties in the prediction can be attributed to the limitations of the centrifuge tests conducted and the assumptions made for the development of the methodology. For instance, the proposed methodology assumes a uniform distribution of S_r and homogenous partially saturated specimens. However, this was not accurate for the centrifuge tests where air bubbles were distributed non-uniformly across the soil deposits, as reported in section 4.4.1. Despite the uncertainties, the proposed methodology can provide a reasonable and logical prediction for the earthquake-induced free-field settlement of partially saturated soils.

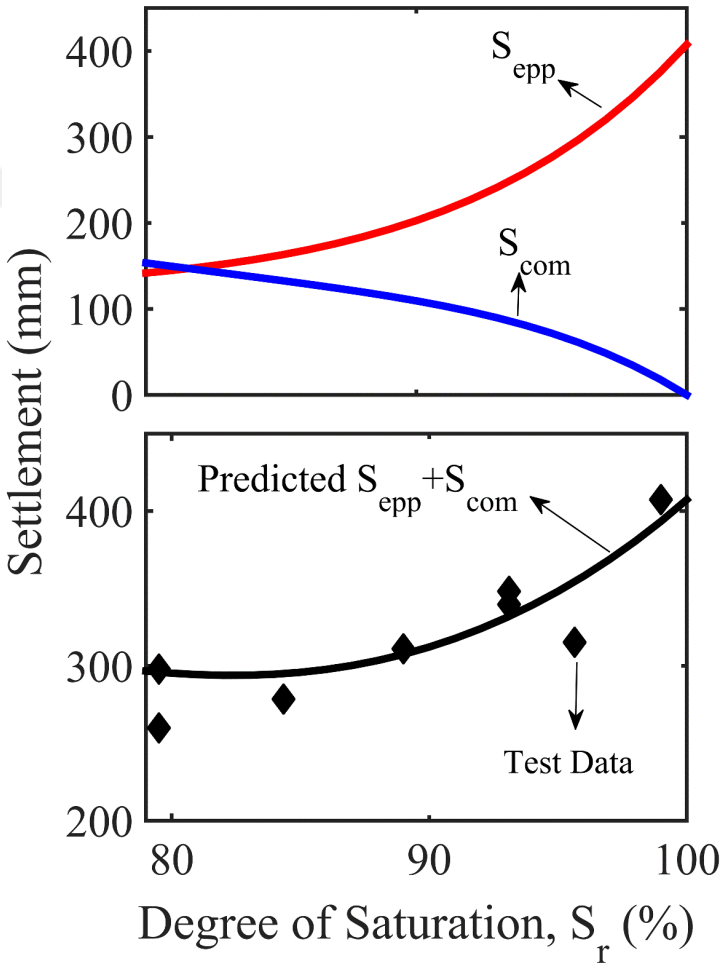

Figure 8.9– Comparison of the estimated total ground surface settlement with the measured centrifuge data.

8.4 Post-Liquefaction Reconsolidation of Soil

Section 6.3.1 reported an increased rate of settlement during the earthquake loading. Although the contribution of the post-seismic reconsolidation settlement to the total surface settlement is smaller in comparison with that of the co-seismic settlement, the former still deserves attention due to the related damage. The methodology in section 8.3 estimated the total settlement of the soil surface that an earthquake loading produced. In this section, the reconsolidation of soil layers following earthquake-induced liquefaction is examined separately to further the understanding on the post-liquefaction behaviour of partially saturated soils.

8.4.1 Reconsolidation Settlement

At the end of the earthquake, the liquefied soil has a very low effective stress state and stiffness. During reconsolidation, the contact forces between the soil grains are re-established as the excess pore pressures dissipate. The surface of the soil settles during this process where the loading of soil grains is monotonic.

The consolidation theory introduced by Terzaghi (1943) is widely used to study consolidation related problems. It assumes that (1) the soil is homogeneous, (2) the soil remains fully saturated at all times, (3) the soil particles and pore fluid are incompressible, (4) the compression and flow are one-dimensional (e.g. vertical direction), (5) strains are small, (6) Darcy's law is valid, (7) the coefficient of permeability, k, and one-dimensional stiffness of the soil, E_0, remain constant, and (8) there is a unique relationship, independent of time, between the void ratio and effective stress. Terzaghi's consolidation theory offers an opportunity to examine the reconsolidation of a liquefied soil layer. In particular, the assumption that the change in void ratio can be related to change in effective stress makes the analyses of reconsolidation much easier. The volumetric strains due to reconsolidation, $\varepsilon_{v-recon}$, can be estimated establishing a link between the changes in the void ratio, Δe, and the changes in effective stress, $\Delta\sigma'_v$, through one-dimensional oedometer stiffness, E_0:

$$\varepsilon_{v-recon} = \frac{\Delta e}{e_0+1} = \frac{\Delta\sigma'_v}{E_0} \tag{8.9}$$

where e_0 is the initial void ratio of the soil. The oedometer stiffness, E_0, can also be linked to the permeability of the soil, k, and coefficient of consolidation, c_v:

$$c_v = \frac{E_0 \cdot k}{\gamma_f} \tag{8.10}$$

where γ_f is the unit weight of the pore fluid. c_v is commonly used to examine the dissipation behaviour of soil as it incorporates both k and E_0.

It must be emphasised that some issues have been reported regarding the validity of some of Terzaghi's assumptions for reconsolidation of liquefied soil. Firstly, centrifuge test results often indicate that a constant and a single value of c_v cannot be used to accurately assess the reconsolidation of soil layers. For an accurate prediction, the value of c_v at the beginning of reconsolidation should be about three times smaller than that at the end (Brennan and Madabhushi 2011). Secondly, the permeability of soil increases as it liquefies, and one-dimensional stiffness of soil drops. Adamidis and Madabhushi (2016b) showed the variation of permeability and one-dimensional stiffness with effective stress and void ratio, and they pointed out the need for incorporating this variation to accurately replicate the reconsolidation settlement of saturated soil.

8.4.2 Permeability and One-Dimensional Stiffness

Partial drainage that occurs during an earthquake loading is often explained by a rapid change in the permeability of the soil at the very low effective stresses. Once the earthquake ceases, effective stresses start to increase, and the permeability drops back to its normal value. This causes a decrease in the rate of post-seismic settlement, compared to the co-seismic settlement rate. Haigh et al. (2012) provided experimental evidence of the change in the permeability of the liquefied soil with effective stress. They conducted fluidisation tests on Hostun sand where the permeability of the soils was tested by applying an upward hydraulic gradient. The permeability of the liquefied soil was shown to increase rapidly when the effective stress reached a near-zero effective stress state (typically below 0.1 kPa), as presented in figure 8.10.

Adamidis and Madabhushi (2016b) performed a series of three oedometer tests on the dry Hostun sand specimens with different initial void ratios to measure its one-dimensional stiffness. The variation of measured E_0 values with effective stresses was depicted (see the upper plot in figure 8.11). The relationships defining the dashed black line, as a function of σ_v' and e, were provided. They assumed that E_0 had a real, positive value at zero effective stress (non-zero one-dimensional stiffness). This assumption was to apply the consolidation equation throughout the reconsolidating layer, without dividing it into layers.

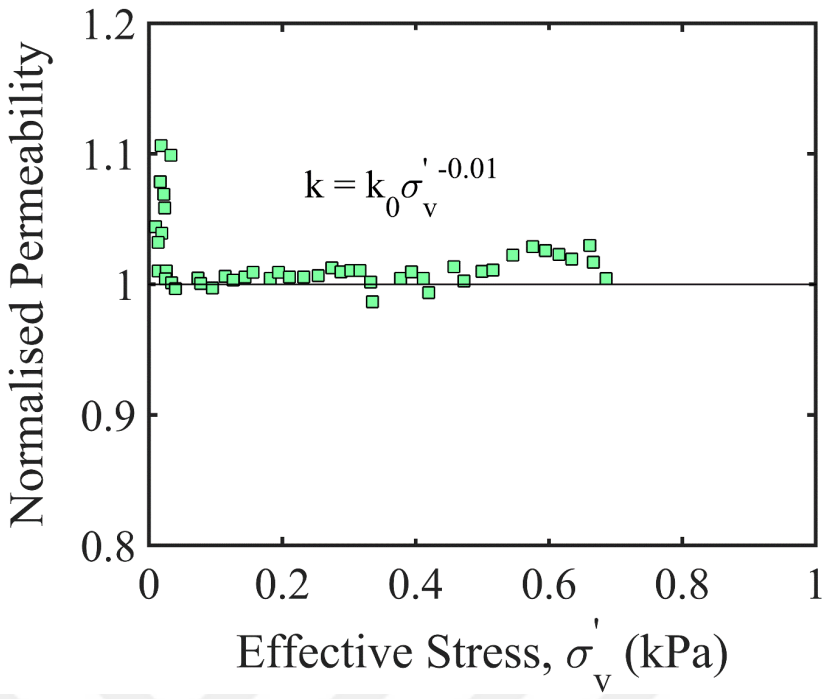

Figure 8.10– Variation of permeability with effective stress (after Haigh et al. 2012).

8.4.3 Centrifuge Test Results

The volumetric strains of soil deposit due to reconsolidation, $\varepsilon_{v-recon}$, were computed in each sub-layer using equation 8.9. In this equation, changes in effective stresses, $\Delta\sigma'_v$, during the dissipation of excess pore pressures were calculated by linking them to changes in excess pore pressure ratios ($\Delta\sigma'_v = r_{u-part} \cdot \sigma'_{v0}$). Here, r_{u-part} values were predicted using equation 8.7 and assuming full liquefaction of the saturated soil ($r_{u-sat} = 1$). The void ratio distribution corresponding to the beginning of the earthquake (e_0: 0.828) was considered for the calculation of E_0 values. This simplification was needed due to the difficulties in reliably estimating the actual distribution of void ratio with depth at the end of earthquake and beginning of the reconsolidation process. The computed volumetric strains were then summed to estimate the ground surface settlement associated with the reconsolidation of soil layer.

The predicted surface settlement was compared with the centrifuge test measurements, as depicted in the lower plot of figure 8.11. It is useful to note that initially original E_0 values (Adamidis and Madabhushi 2016b) were used in an attempt to assess whether they can reliably predict the centrifuge test measurements for the saturated soil ($S_r = \sim 99\%$). In this case, the predicted settlement was found to be relatively smaller than the centrifuge test measurements. The predicted lower bound for settlement was up to 1.3 times smaller than measured settlement.

Although the prediction was not too far off the observed settlement, smaller than original E_0 values (modified values) were selected in order to better match the experimental data. It can be seen that in all cases, good agreement with the experimental data was accomplished, using the E_0 values adjusted based on the centrifuge test measurements. The reconsolidation settlement reduced significantly with a decrease of S_r, and the decreasing trend was captured well by the predictions with an adequate accuracy.

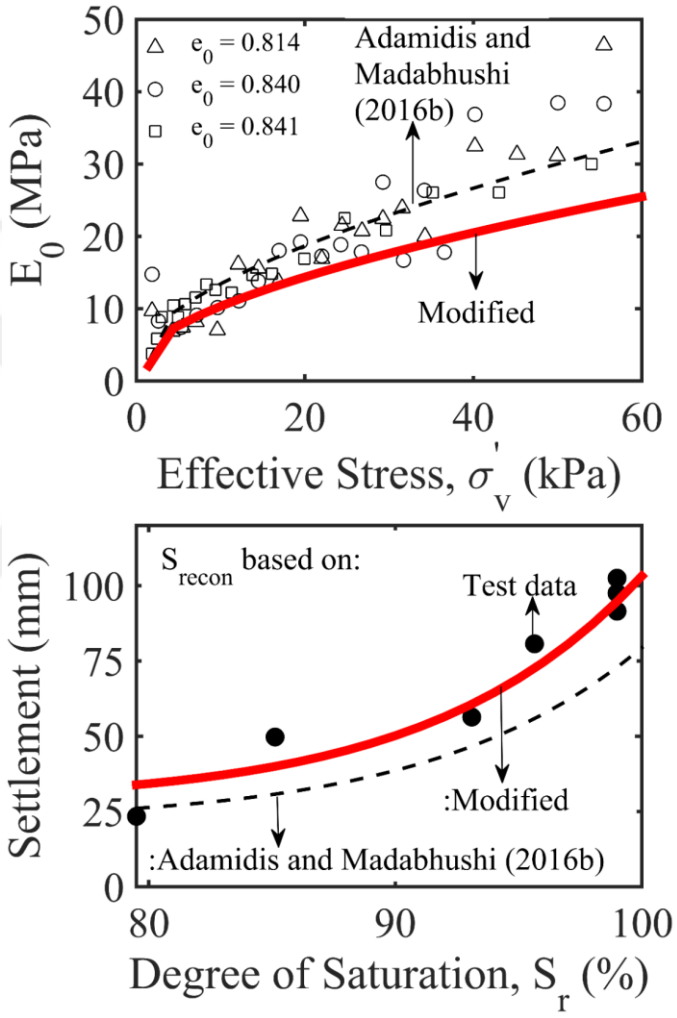

Figure 8.11– Comparison of the predicted reconsolidation settlement with the measured centrifuge data.

8.5 Summary

In this chapter, firstly the predictions of various semi-empirical methodologies, widely used in the state of practice for estimating the liquefaction-induced settlement of saturated soils in the free-field and beneath shallow foundations, were critically reviewed performing an extensive literature survey. In the following sections, a simplified effective stress-based methodology

was introduced to predict the earthquake-induced settlement of partially saturated soils in the free-field. The parameters required for the model were identified based on the experimental data and theoretical understanding. Subsequently, the performance and robustness of the proposed methodology was validated by comparing with the dynamic centrifuge test data.

The total settlement of a level deposit of partially saturated soil was estimated based on the superposition of the settlements due to (1) excess pore pressure generation/dissipation and (2) increased soil compressibility. The comparison of the estimates of the proposed methodology with the dynamic centrifuge measurements revealed that it successfully captured the nonlinear settlement trend followed by the experimental data. In a similar way, it was possible to reliably predict the reconsolidation settlement of partially saturated soil following the approach where the volumetric strains due to reconsolidation were linked to the changes in effective stress and one-dimensional stiffness.

Overall, the results show that the variation of degree of saturation is of most importance for the settlement of the free-field. As long as the ground surface settlement of a saturated soil layer is measured accurately, it will be possible to estimate the settlement of the same soil layer in a partially saturated condition reasonably well.

It should be emphasised that due to the complexities of the problem and lack of experimental verification, only the effect of certain parameters on the settlement behaviour was incorporated into the proposed methodology, which may reduce its ability to predict the settlement of more complicated cases in the field. Therefore, it will be of great value to examine the capacity of this sort of simplified method under a wider variety of circumstances. Further centrifuge testing with different test conditions can provide a larger database. The combination of such data with a large number of parametric analyses can lead to the calibration of the model, which may ultimately allow engineers to use it in their designs with a high level of confidence.

Chapter 9

Conclusions and Future Research

In earthquake prone areas, current engineering practice necessitates the effective remediation of the detrimental effects that earthquake-induced liquefaction has on the safety of shallow foundations and the serviceability of buildings. Although there are a number of remediation techniques which are readily available to ensure foundation safety prior to the commencement of construction, such methods are often costly and inconvenient to use for existing shallow foundations resting on deposits of liquefiable soil. There is ample evidence that the liquefaction resistance of soils will increase with reducing degree of saturation. In geotechnical engineering, air injection can be used in such a way to reduce degree of saturation and to ensure adequate foundation safety and satisfactory building performance. Nevertheless, this requires a proper understanding of the way it works. A comprehensive understanding of the interaction between the foundation and the amount of desaturation in the soil can pave the way for developing effective guidelines for the engineering design of this particular remediation measure.

This research endeavoured to highlight the important facets of air injection technique and its effects on the dynamic performance of liquefiable soil layers beneath shallow foundations. It also attempted to characterise the deformation mechanisms of earthquake-induced settlement in partially saturated soils. Subsequently, it tried to develop a simple, effective stress-based methodology for the prediction of seismically induced settlement in the free-field.

For this purpose, a wide variety of dynamic centrifuge tests at an increased gravitational field, a number of 1-g shaking table and one-dimensional vertical soil column tests were conducted. With the aid of the data collected, the impact of various key parameters on the settlement, excess pore pressure and acceleration response of foundations and soils was examined. This chapter presents the main conclusions derived from this research and discusses the implications of this research to practice. Finally, recommendations for further study are made.

9.1 Research Conclusions

9.1.1 Physical Modelling of Air Injection and Durability of Air

One of the objectives of this research was to examine the issues surrounding the physical modelling of air injection itself. Chapter 4 highlighted the importance of air injection pressure for the foundation safety. The influence of the distribution and magnitude of the desaturation on the seismic response of soils was discussed. In chapter 5, the durability of entrapped air was assessed to offer insights into the long-term reliability of air injection technique.

The zones where air injection effectively desaturated the soil were directly evaluated based on the changes in soil colour. The distribution of entrapped air and magnitude of desaturation were significantly affected by air injection pressure and preferential flow pathways. The extent of the air-entrapped zone and uniformity & magnitude of the desaturation in this region increased with increasing air injection pressure. The augmentation of air injection pressure, however, had associated detrimental effects: it produced an increased foundation settlement. The rate of air injection and maximum air injection pressure applied beneath an existing shallow foundation were found to be of most significance for its safety and efficient performance. The acceptable limits of air injection pressure that can be applied without causing significant foundation settlements were identified based on the collection of centrifuge test data. Although the data set was insufficient to suggest a rigorous design method, the guidelines as mentioned earlier in chapter 4 would still shed light on the practical application of air injection technique.

In view of engineering concerns regarding the long-term reliability of air injection technique, the durability of entrapped air in soil was extensively examined under different scenarios. Real field conditions were simplified capturing only important facets of the relevant situations and simulated in laboratory by using geotechnical centrifuge modelling and 1-g soil testing. It was concluded that although some of the air was lost over time, the majority of it remained entrapped within partially saturated soil under simulated field conditions. These results, in fact, revealed the reliability and practicality of the air injection technique in design practice and provided clues as to what the short and long-term behaviour of entrapped air in soil would be under changing field conditions. The test results can also be valuable to design engineers who may use another desaturation technique (e.g. drainage re-charge).

9.1.2 Performance of Air Injection as a Liquefaction Mitigation Measure

In chapter 6, the parameters that impact on the performance of air injection as a liquefaction remediation measure were examined using the dynamic centrifuge and 1-g shaking table tests with respect to settlement, excess pore pressure and acceleration behaviour.

General Trends

The dynamic response of saturated and partially saturated soils beneath shallow foundations and in the free-field was compared. Air injection was consistently found to be very successful in minimising the magnitude of excess pore pressures that were generated; in limiting soil softening and decrease of soil stiffness associated with liquefaction and in reducing foundation settlement. The test results reinforced the previous experimental findings in the literature and provided further insights into the less well-documented aspects. It was found that each of the parameters below dramatically affected the observed trends.

Degree of Saturation

Degree of saturation (S_r) was found to be of most importance for the dynamic response of partially saturated soils. The extent of generation and dissipation of excess pore pressures and associated foundation and surface settlements were closely linked to S_r. A decreasing trend in the build-up of excess pore pressures and related foundation settlements were observed with decreasing S_r.

The extent to which S_r was reduced affected the acceleration attenuation/amplification response of the soil and foundation. With decreasing S_r values, much higher accelerations were transmitted to the foundations through the unliquefied zone that existed beneath shallow foundations. In design practice, when the applied accelerations are deemed important to the extent that they will risk the global safety of foundations, and hence superstructures, taking precautionary measures against their detrimental effects will be necessary.

Confining Stress

The performance of air injection technique was examined at different confining stresses using geotechnical centrifuge and 1-g shaking table testing. The confining stresses were found to be of critical importance to the beneficial effects that air injection had on the foundation settlement and excess pore pressure generation.

Detailed analyses of the centrifuge test data revealed that a decrease of S_r using air injection was more effective in reducing the magnitude of excess pore pressures that built up in the deep soil layers than in the shallow soil layers. This was principally attributed to the increased confining (vertical) stresses and proximity of the air injector in this zone.

In the shallow soil layers, a similar mechanism of excess pore pressure generation took place in the saturated and partially saturated soils owing to low confining stresses and proximity of the drainage boundaries. Excess pore pressures were generated very quickly in the free-field, and liquefaction was reached in both cases. S_r of soils determined the depth of free-field liquefaction.

From the 1-g shaking table tests, it was found that a decrease of S_r using air injection or chemical method only produced a slight improvement. This finding was of particular importance for the researchers who investigate the air injection technique by employing 1-g shaking table testing apparatus, which is typically insufficient to produce high confining stresses. In general, the aforementioned test results signified the need for the incorporation of confining stresses in design practice, along with S_r.

Bearing Pressure

The impact of varying bearing pressure on the response of saturated and partially saturated soils beneath shallow foundations was investigated. It was found that the settlement of shallow foundation on the same soil layer and under the same earthquake motion reduced as bearing pressure increased. This was attributable to the level of foundation-induced stresses which potentially acted towards reducing the soil-softening.

It was observed that the beneficial effect of air injection on reducing the liquefaction-induced foundation settlements increased with increasing bearing pressure. The increased confining stresses that foundation imposed led to a larger resistance to excess pore pressure generation. On the other hand, larger accelerations were transmitted to the *heavy* foundation than its *light* counterpart owing to the larger foundation-imposed stresses and the formation of an area of increased stiffness beneath it.

Earthquake Motion

The impact of amplitude and duration of earthquake on the performance of air injection was explored subjecting the centrifuge models to successive earthquakes in increasing amplitude and number of cycles.

It was found that percentage reduction of the foundation settlement (gain in performance) increased with increasing amplitude of peak input acceleration.

The most interesting conclusion that could be drawn from this analysis was that air injection technique was very effective at reducing the liquefaction-induced deformations even during the moderate and strong amplitude of earthquakes that lasted for an unrealistically long period of time. This result was, in fact, very promising with respect to the long-term reliability of this particular remediation measure.

Seismic Settlement of Level Deposits of Saturated and Partially Saturated Soils

When the free-field response of saturated soils was examined, very high excess pore pressures built up during the earthquake loading, subsequently leading to significant soil-softening and a dramatic decrease of shear stiffness. The surface settlements primarily accumulated during the earthquake event, with comparatively smaller settlements developing during the post-seismic period of excess pore pressure dissipation. The increased rate of co-seismic surface settlement in the free-field was attributed to the partial drainage that occurred during the earthquake event. The upward flow from below was the cause of the high excess pore pressures that were maintained as the earthquake continued.

In the partially saturated soils, smaller excess pore pressures developed during the dynamic loading, minimising the soil-softening and loss of shear stiffness. This was ascribed to the presence of occluded air in the pore fluid that could potentially compress and reduce the build-up of excess pore pressures. The excess pore pressures started to drop while the earthquake continued, and pore fluid flow completed much earlier, in comparison with the saturated case. Most of the free-field settlements completed during the earthquake loading, limiting the extent of reconsolidation settlement. The free-field settlement of partially saturated soils was mainly attributable to the increased compressibility of the soil mass due to the presence of air bubbles.

9.1.3 Deformation Mechanisms

In chapter 7, the deformation mechanisms that developed under shallow foundations were examined through the utilisation of high-speed photography and particle image velocimetry (PIV) analysis. This allowed, for the first time, the visualisation and identification of the deformation mechanisms that developed in partially saturated soils during air injection process and earthquake loading. Chapter 7 also discussed the effects of key parameters.

Deformation Mechanisms during the Air Injection Process

The soil deformations that developed during the air injection process were studied using the data from a range of tests where air injection was performed in a different manner. It was found that for all cases, air injection resulted in some ground surface settlements (free-field) and shallow foundation settlements. The extent of such settlements, however, remained within the acceptable limits as long as the execution of air injection was performed in a controlled manner. The free-field settlements were attributable to positive volumetric strains caused by the decrease of effective stresses and increased compressibility of the soil mass. In the presence of foundations, air injection led to complete or partial bearing capacity deformations under the foundation-imposed static shear stresses, depending on the application of air injection process.

Deformation Mechanisms during the Earthquake Loading

When the response of saturated soils beneath shallow foundations was investigated, a significant extent of shallow foundation settlements was observed to take place. The soil in the free-field substantially liquefied, extending to a significant depth, and could not offer sufficient support. This allowed a bearing capacity failure mechanism to form. While the mechanisms of deviatoric and volumetric strain-induced deformation contributed to the settlement of shallow foundations, it was primarily driven by the former mechanism. This was evident from the strong tendency of the soil to move horizontally and formation of extended failure mechanisms within the saturated soil layers.

The foundations resting on partially saturated soils, on the other hand, suffered much smaller settlements. The deviatoric strain-induced deformations under the static and dynamic stresses were significantly minimised. The depth of liquefaction also markedly reduced, and a complete bearing capacity type of failure mechanism did not form under the shallow foundations.

Generally speaking, practising engineers have to strike a balance between the cost and efficiency of the proposed mitigation measure. Therefore, the estimation of the depth of soil that requires liquefaction treatment can be of significance. Furthermore, assessing to what extent and depth the mitigation measure can provide an improvement in the liquefiable ground can be equally important. This study showed that the visualisation of the soil deformations might ease such difficulties. It allowed for the identification of the deformation mechanisms, which are essential to define to what depth the remediation measure is required, and provided a better assessment of its adequacy for the engineering problem.

Degree of Saturation

A decrease of S_r did affect not only the build-up of and drainage of excess pore pressures but also influenced the deformation mechanisms. The reduction in S_r limited the depth of liquefaction and shortened the duration for which the liquefied soil at the shallow layer remained in a softened state. It subsequently prevented the formation of a bearing capacity failure mechanism within the soil layers. A decreasing trend in accumulated horizontal and vertical soil movements was observed with decreasing S_r. In general, the displacement mechanisms became much shallower and more localised as S_r reduced.

Confining Stress

Confining stress was an important parameter in assessing the deformation mechanisms that developed in the partially saturated soils.

It was shown by means of 1-g shaking table testing that a decrease of S_r was not sufficient to prevent the formation of a bearing capacity type of deformation, under the low confining stresses, at 1-g. Irrespective of the presence of air/gas bubbles in the soil, significant soil-softening took place, and large settlements were accumulated in both saturated and partially saturated soils.

On the other hand, the extent of soil deformation was found to decrease significantly when the partially saturated soils were examined, under increased confining stresses, in the centrifuge.

Bearing Pressure

The development of horizontal and vertical soil movements was directly linked to the level of foundation-imposed confining stresses and soil stiffness beneath shallow foundations.

In the case of saturated soils, an area of soil under and around the edges of the *heavy* and *light* foundations moved vertically downwards with the foundations. The inability of the liquefied soil of free-field to offer lateral confinement led to the lateral displacement of surrounding soil. The magnitude of horizontal and vertical displacements was comparatively much smaller when the *heavy* foundation was examined. This was attributable to the level of increasing stress field and decreasing soil-softening with an increase of foundation bearing pressure.

When the partially saturated soils were examined, increasing stress regime in the ground owing to increasing foundation bearing pressure was also found to decrease the magnitude of vertical and lateral soil displacements.

9.1.4 Methodology for Prediction of Settlement

As part of this research, an effective stress based methodology was described to predict the earthquake-induced settlement of partially saturated soils in the free-field. On the basis of theoretical considerations and experimental observations, the applicability of the selected relationships and input parameters was reassessed. The predictions of the proposed methodology were subsequently validated against the experimental set of data gathered from a series of dynamic centrifuge tests.

The model predictions were found to be capable of capturing a decreasing settlement trend with a reduction of S_r, as expected from partially saturated soils. Despite the complexities of the problem in question and experimental uncertainties, the informed predictions matched the experimental set of data to a level of accuracy that was fairly reasonable for engineering design.

The proposed methodology is of particular importance for design engineers who are currently reliant on the methods offered to predict the surface settlements of dry or saturated soil layers. A range of prediction methodologies used in the state of practice were revisited following an extensive review of the available literature. One of the problems inherent in using such methodologies for partially saturated soils is that they fail to account for the impact of S_r on the soil parameters and mechanisms of settlement. Nevertheless, the proposed method showed the possibility of acquiring reasonable predictions for the surface settlement of partially saturated soils, incorporating the effects of S_r.

9.2 Implications to Design Practice

9.2.1 Design of Air Injection

During this research, it was found that settlements of existing shallow foundations occur during the air injection process. Due to non-uniformity of the desaturation within the soils, asymmetric soil displacements beneath the foundations were also observable. Consequently, foundations suffered larger rotations in one direction than the other, causing concern with respect to the differential settlements.

The overall air -induced settlement of existing foundations may not be a major issue for their serviceability when liquefiable ground which they rest on is desaturated in a controlled manner.

Although the magnitude of differential settlements is small, they may still need a consideration in design practice. It can be advisable for design engineers to use different arrangement of air injection in such a way that the entire layer of foundation soil has uniform strength and desaturation. This can allow for averaging out the settlement across the footprint of foundations and minimising the possibility of differential settlements.

9.2.2 Reliability of Air Injection

The major engineering concern raised with regards to the air injection technique is the potential for air bubbles to lose their function over a period of time. Deciding how often the liquefiable ground beneath existing structures should be desaturated can be a difficult challenge for the design engineers who need to strike a balance between the safety and cost of the applied ground improvement method.

Through this research, it was shown that most of the air bubbles can remain entrapped in the desaturated soils for a long period of time. Even under the combined effects of different conditions, degree of saturation of the soils only increased marginally. The implication of this for design engineers is that they may not need to perform ground improvement work (air injection) very often, which allows them to save time and money.

9.2.3 Extent of Desaturated Zones

As shown through this research, a non-uniform desaturation of soils occurs even with the use of uniformly prepared beds of sand, which is essentially due to preferential flow of air. The implication of this to design practice is that when the air injection technique is used to mitigate a large area of heterogeneous deposits in the field, the desaturated zones may not extend sufficiently, and the desaturated zones may be narrower than those tested in this study. Consequently, this may result in a reduction in the efficacy of this technique. Therefore, more research is desirable to reduce the uncertainty regarding this aspect.

9.3 Research Limitations and Future Research

The primary aim of this research was to increase understanding on the air injection technique using physical modelling. The optimum outcome of future research on this subject would be

the development of a rational design tool that could benefit the practising engineers. The suggestions below for further study can be valuable to accomplish such a goal.

9.3.1 Experimental Modelling

Air Injection

In this study, the models were desaturated using an air injector pre-located on the centre-bottom of the model containers. Nevertheless, this would not be a realistic representation of the actual situation in the field (see figure 2.9). To better replicate the reality, a small diameter of pipes may be driven into the ground as the centrifuge is in-flight, and pressurised air can be injected.

Only one air injector extending along the plane strain direction was considered in this study. The extent and non-uniformity of the desaturated zones were found to be an issue. Different arrangement, positioning and number of air injectors may be worth further study. For instance, the aforementioned in-flight method might allow for altering the position of the air injector, and the entire volume of liquefiable soils can be desaturated. Besides, it would be possible to form layers of partially saturated soil in which the distribution of air, hence S_r, is reasonably uniform, and soil has a uniform strength.

This research solely focused on the uniform and loose sand stratification. Nevertheless, the soil deposits in the field have a heterogeneous and non-uniform nature, which can drastically affect the air flow behaviour. This could open up an avenue for further research on the alternative soil types and configurations.

The durability of air bubbles was examined in this research based on relatively simple boundary conditions and under particular field circumstances. Nevertheless, a wider range of realistic conditions (e.g. temperature change, horizontal flow, etc.) are yet to be examined for deriving more generalised conclusions. In addition, a combination of these conditions will occur in the field, and hence further research is required to determine the most critical case. Further study is also needed to address the question regarding the time scaling in centrifuge modelling for the problem under consideration.

Problem Parameters

A simple foundation model, without superstructure, was used while investigating the seismic response of partially saturated soils beneath shallow foundations. The foundation properties

(e.g. aspect ratio and sizes) and liquefiable soil properties (e.g. depth of liquefiable soil layer and relative density) remained unchanged between the tests. This allowed for the understanding of the complex soil behaviour and a direct comparison between the tests. Further research could focus on the effects of different foundation sizes, superstructure and changing the depth of liquefiable soil layer. It would be interesting to see to what extent such parameters affect the performance of air injection. For instance, shallow foundations used in this study had very low aspect ratios. However, the structures with high aspect ratios can potentially rock on top of the underlying partially saturated soil. This would be expected to have an important effect on the soil deformations associated with the soil-structure interaction.

The findings from this research showed that S_r was the most significant parameter for the partially saturated soil behaviour. However, the centrifuge tests involved only a small range of S_r values. A large database, ranging between 0 and 100%, could be invaluable to validate the predictions of the proposed methodology more accurately. Also, this could allow for a better understanding of the effects of S_r on the identified settlement mechanisms. Therefore, it would be necessary to extend the available database by performing further centrifuge experiments.

Deformation Mechanisms

The PIV analyses in chapter 7 highlighted that air injection noticeably affected the deformation of soils altering the pore fluid and soil compressibility. It could be of value to formulate the relationship between the compressibility of soil mass and a reduction in S_r. However, this would require a larger array of test data on the uniformly desaturated soil layers. Further element and centrifuge tests could perhaps be performed in the future to collect such data.

9.3.2 Numerical Modelling

Parametric studies through numerical modelling can provide a larger data repository that can allow for a better understanding of partially saturated soil behaviour and validation of the proposed prediction methodology. This would require the use of an advanced constitutive model that can capture the main facets of the problem. Currently, most numerical tools available for liquefaction problems (e.g. the Finite Difference Code FLAC) have certain shortcomings, even for the saturated soils. Nevertheless, once a comprehensive understanding of partially saturated soils is achieved with experimental studies, it would be possible to replicate the results of such tests using numerical modelling.

References

Adalier, K., and Elgamal, A. (2005). Liquefaction of over-consolidated sand: A centrifuge investigation, *Journal of Earthquake Engineering*, 9(1):127-150.

Adalier, K., Elgamal, A., Meneses, J., and Baez, J. I. (2003). Stone columns as a liquefaction countermeasure in non-plastic silty soils. *Soil Dynamics and Earthquake Engineering*, 23(7): 571-584.

Adamidis, O. (2017). *Earthquake-induced liquefaction of sand and response of structures with shallow foundations*. PhD thesis, University of Cambridge.

Adamidis, O., and Madabhushi, S. P. G. (2015). Insights into settlement mechanisms of shallow foundations on liquefiable layers. In *2015 SECED Conference: Earthquake Risk and Engineering towards a Resilient World*.

Adamidis, O., and Madabhushi, S. P. G. (2016a). Response of shallow foundations to successive earthquake-induced liquefaction events. In *1st international conference on natural hazards and infrastructure*, pages 1-9, Chania, Greece.

Adamidis, O., and Madabhushi, S. P. G. (2016b). Post-liquefaction reconsolidation of sand. *Proceedings of the Royal Society A: Mathematical, Physical and Engineering Science*, 472(2186): 20150745.

Balakrishnan, A., and Kutter, B. L. (1999). Settlement, sliding and liquefaction remediation of layered soil. *Journal of Geotechnical and Geoenvironmental Engineering*, 125(11):968-978.

Bertalot, D., and Brennan, A. (2015). Influence of initial stress distribution on liquefaction induced settlement of shallow foundations. *Géotechnique*, 65(5):418-428.

Bertalot, D., Brennan, A. J., and Villalobos, F. A. (2013). Influence of bearing pressure on liquefaction-induced settlement of shallow foundations. *Géotechnique*, 63(5): 391-399.

Bhattacharya, S., Hyodo, M., Goda, K., Tazoh, T., and Taylor, C. (2011). Liquefaction of soil in the Tokyo Bay area from the 2011 Tohoku (Japan) earthquake. *Soil Dynamics and Earthquake Engineering*, 31(11):1618-1628.

Bishop, A. W. (1959). The principle of effective stress. *Teknisk Ukeblad*, 106(39):859-863.

Bolton, M. D., and Wilson, J. M. R. (1990). Soil stiffness and damping. In *Structural dynamics*, pages 209-216. Balkema, Rotterdam.

Bray, J., Sancio, R., Durgunoglu, T., Onalp, A., Youd, T., Stewart, J., Seed, R., Cetin, O., Bol, E., Baturay, M., Christensen, C., and Karadayilar, T. (2004). Subsurface characterization at ground failure sites in Adapazari, Turkey. *Journal of Geotechnical and Geoenvironmental Engineering,* 130(7):673-685.

Brennan, A. J. and Madabhushi, S. P. G. (2005). Liquefaction and drainage in stratified soil. *Journal of Geotechnical and Geoenvironmental Engineering*, 131(7):876-885.

Brennan, A. J., and Madabhushi, S. P. G. (2011). Measurement of coefficient of consolidation during reconsolidation of liquefied sand. *Geotechnical Testing Journal*, 34(2):1-8.

Brennan, A. J., and Madabhushi. S. P. G. (2002). Effectiveness of vertical drains in mitigation of liquefaction. *Soil Dynamics and Earthquake Engineering,* 22(9-12):1059-1065.

Brennan, A. J., Madabhushi, S. P. G., and Houghton, N. E. (2006). Comparing laminar and equivalent shear beam (ESB) containers for dynamic centrifuge modelling. In *Wang, Y. H.,* editor*, Physical modelling in geotechnics: 6th ICPMG '06, volume 1-2 BT – of Balkema-proceedings and monographs in engineering, water and earth sciences,* pages 171-176. Taylor & Francis.

Brennan, A. J., Thusyanthan, N. I., and Madabhushi, S. P. G. (2005). Evaluation of shear modulus and damping. *Journal of Geotechnical and Geoenvironmental Engineering*, 131(12):1488-1497.

British Standards Institution. (2004). *Eurocode 8: Design of structures for earthquake resistance-part 1: General rules, seismic actions and rules for buildings*.

Casagrande, A. (1936). Characteristics of cohesionless soils affecting the stability of slopes and earth fills. *Journal of the Boston Society of Civil Engineers*, 23:13-32.

Cetin, K. O., Bilge, H. T., Wu, J., Kammerer, A. M., and Seed, R. B. (2009). Probabilistic models for cyclic straining of saturated clean sands. *Journal of Geotechnical and Geoenvironmental Engineering*, 135(3):371-386.

Cetin, K. O., Seed, R. B., Kiureghian, A. D., Tokimatsu, K., Harder, L. F., Kayen, R. E., and Moss, R. E. S. (2004). Standard penetration test-based probabilistic and deterministic assessment of seismic soil liquefaction potential. *Journal of Geotechnical and Geoenvironmental Engineering*, 130(12):1314-1340.

Chian, S., and Madabhushi, S. P. G. (2012). Effect of buried depth and diameter on uplift of underground structures in liquefied soils. *Soil Dynamics and Earthquake Engineering*, 41: 181-190.

Chian, S., Stringer, M. E., and Madabhushi, S. P. G. (2010). Use of automatic sand pourers for loose sand models. In Springman, S., Laue, J., and Seward, L., editors, *Physical Modelling in Geotechnics*, vol. 1, pages 117-121, Taylor & Francis, Zurich, Switzerland.

Cilingir, U., and Madabhushi, S. P. G. (2011). A model study on the effects of input motion on the seismic behaviour of tunnels. *Soil Dynamics and Earthquake Engineering*, 31:452-462.

Coelho, P. A. L. F. (2007). *In situ densification as a liquefaction resistance measure for bridge foundations*. PhD thesis, University of Cambridge.

Coelho, P. A. L. F., Haigh, S. K., Madabhushi, S. P. G., and O'Brien, A. S., (2007). Post-earthquake behaviour of footings when using densification as a liquefaction resistance measure. *Ground Improvement Journal-Special Issue on Ground Improvement Techniques*, 11(1):45-53.

Consentini, R. M., and Foti, S. (2014). Evaluation of porosity and degree of saturation from seismic and electrical data. *Géotechnique*, 64(4):278-286.

Cooke, H. G., and Mitchell. J. K. (1999). Guide to remedial measures for liquefaction mitigation at existing highway bridge sites. *Technical Report MCEER-99-0015*.

Cubrinovski, M., Bray, J. D., Taylor, M., Giorgini, S., Bradley, B., Wotherspoon, L., and Zupan, J. (2011). Soil liquefaction effects in the Central Business District during the February 2011 Christchurch Earthquake. *Seismological Research Letters*, 82(6):893-904.

Dashti, S., Bray, J. D., Pestana, J. M., Riemer, M., and Wilson, D. (2010). Mechanisms of seismically induced settlement of buildings with shallow foundations on liquefiable soil. *Journal of Geotechnical and Geoenvironmental Engineering*, 136(1):151-164.

DeJong, J. T., Mortensen, B. M., Martinez, B. C., and Nelson, D. C. (2010). Bio-mediated soil improvement. *Ecological Engineering*, 36(2):197-210.

Dobry, R., Ladd, R. S., Yokel, F. Y., Chung, R. M., and Powell, D. (1982). *Prediction of pore water pressure buildup and liquefaction of sands during earthquakes by the cyclic strain method*. Building science series, National Bureau of Standards, Washington, DC.

Elgamal, A.-W., Zeghal, M., and Parra, E. (1996). Liquefaction of reclaimed island in Kobe, Japan. *Journal of Geotechnical Engineering*, 122(1):39-49.

Ellis, E., Soga, K., Bransby, M., and Sato, M. (2000). Resonant column testing of sands with different viscosity pore fluids. *Journal of Geotechnical and Geoenvironmental Engineering*, 126(1):10-17.

Eseller-Bayat, E. (2009). *Seismic response and prevention of liquefaction failure of sands partially saturated through introduction of gas bubbles*. PhD thesis, University of Northeastern, Boston, MA.

Eseller-Bayat, E., Yegian, M., Alshawabkeh, A., and Gokyer, S. (2013). Liquefaction response of partially saturated sands. I: experimental results. *Journal of Geotechnical and Geoenvironmental Engineering*, 139(6):863-871.

Finn, W. D. L., Byrne, P. M., and Martin. G.R. (1976). Seismic response and liquefaction of sands. *Journal of the Geotechnical Engineering Division*, 102(8):841-856.

Flavigny, E., Desrues, J., and Palayer, B. (1990). Le sable d'Hostun. *Revue Francaise de Géotechnique*, 53:67-70.

Fredlund, D. G., and Rahardjo, H. (1993). *Soil mechanics for unsaturated soils*. Wiley, New York.

Gallagher, P. M., Mitchell, J. K. (2002). Influence of colloidal silica grout on liquefaction potential and cyclic undrained behavior of loose sand. *Soil Dynamics and Earthquake Engineering, 22(9):1017-1026.*

Gallagher, P. M., Pamuk, A., and Abdoun, T. (2007). Stabilization of liquefiable soils using colloidal silica grout. *Journal of Materials in Civil Engineering*, 19(1):33-40.

Ghosh, B., and Madabhushi, S. P. G. (2007). Centrifuge modelling of seismic soil structure interaction effects. *Journal of Nuclear Engineering Design*, 237(8):887-896.

Gokyer, S. (2009). *Inducing and imaging partial degree of saturation in laboratory sand specimens*. Master thesis, University of Northeastern, Boston, MA.

Green, P. A., and Ferguson, P. A. S. (1971). On liquefaction phenomena, by Professor A. Casagrande: Report of Lecture. *Géotechnique*, 21(3):197-202.

Haigh, S. K., Eadington, J., and Madabhushi, S. P. G. (2012). Permeability and stiffness of sands at very low effective stresses. *Géotechnique*, 62(1):69-75.

Hausler, E. A. (2002). *Influence of ground improvement on settlement and liquefaction: A study based on field case history evidence and dynamic geotechnical centrifuge tests*. PhD thesis, University of California, Berkeley.

He, J., Chue, J., and Ivanov, V. (2013). Mitigation of liquefaction of saturated sand using biogas. *Géotechnique*, 63(4):267-275.

Heron, C. M. (2013). *The dynamic soil structure interaction of shallow foundations on dry sand beds*. PhD thesis, University of Cambridge.

Houlsby, G. T. (1997). The work input to an unsaturated granular material. *Géotechnique*, 47(1):193-196.

Hsu, C.-C., and Vucetic, M. (2004). Volumetric threshold shear strain for cyclic settlement. *Journal of Geotechnical and Geoenvironmental Engineering*, 130(1):58-70.

Idriss, I., and Boulanger, R. (2006). Semi-empirical procedures for evaluating liquefaction potential during earthquakes. *Soil Dynamics and Earthquake Engineering*, 26(2-4):115-130.

Ishihara, K. (1985). Stability of natural deposits during earthquakes. *Proceedings of the 11th international conference on soil mechanics and foundation engineering*, San Francisco, August 1985. Vol. 1, (Balkema), pages 321-376.

Ishihara, K. (1993). Liquefaction and flow failure during earthquakes. *Géotechnique*, 43(3):351-451.

Ishihara, K., and Yoshimine, M. (1992). Evaluation of settlements in sand deposits following liquefaction during earthquakes. *Soils and Foundations*, 32(1):173-188.

Ishihara, K., Tatsuoka, F., and Yasuda, S. (1975). Undrained deformation and liquefaction of sand under cyclic stresses. *Soils and Foundations*, 15(1):29-44. *Journal of Geotechnical Engineering,* 116(2):165-185.

Ishihara, K., Tsuchiya, H., Huang, Y., and Kamada, K. (2001). Recent studies on liquefaction resistance of sand: Effect of saturation. In *the proceedings of the 4th international conference on recent advances in geotechnical earthquake engineering and soil dynamics*, San Diego, March, 2001, pages 1-7.

Ishihara, K., Tsukamoto, Y., and Kamada, K. (2004). Undrained behaviour of near-saturated sand in cyclic and monotonic loading. In *the international conference on cyclic behaviour of soils and liquefaction phenomena*, Bochum, March, 2004, pages 27-39.

Kammerer, A. M., Pestana, J. M., and Seed, R. B. (2002). *Undrained Response of Monterey 0/30 Sand under Multidirectional Cyclic Simple Shear Loading Conditions*. Technical report, UCB/GT/02-01, University of California, Berkeley.

Karol, R. H. (2003). *Chemical Grouting and Soil Stabilization*. Marcel Dekker, New York.

Knappett, J. (2006). *Piled foundations in liquefiable soils: accounting for axial loads*. PhD thesis, University of Cambridge.

Knappett, J. A., Haigh, S. K., and Madabhushi, S. P. G. (2006). Mechanisms of failure for shallow foundations under earthquake loading. *Soil Dynamics and Earthquake Engineering,* 26(2-4):91-102.

Kramer, S. L. (1996). *Geotechnical earthquake engineering*. Prentice Hall, Upper Saddle River, NJ 07458.

Kutter, B. I. (2013). Effects of capillary number, Bond number, and gas solubility on water saturation of sand specimens. *Canadian Geotechnical Journal*, 50 (2):133-44.

Lambe, P. C., and Whitman, R. V. (1982). Scaling for earthquake shaking tests on a centrifuge. *Proceedings of the international conference on soil dynamics and earthquake engineering*, Southampton, 1982. Vol. 1, (Taylor & Francis, New York), pages 91-106.

Lee K. L. and Albaisa A. (1974). Earthquake induced settlement in saturated sands. *Journal of Geotechnical Engineering Division*, 100(4):387-406.

Lee, F. H. (1985). *Centrifuge modelling of earthquake effects on sand embankments*. PhD thesis, University of Cambridge.

Lins, Y., Schanz, T., and Fredlund, D. G. (2009). Modified pressure plate apparatus and column testing device for measuring SWCC of sand. *Geotechnical testing Journal*, 32(5):450-464.

Liu, A. H., Stewart, J. P., Abrahamson, N. A., and Moriwaki, Y. (2001). Equivalent number of uniform stress cycles for soil liquefaction analysis. *Journal of Geotechnical and Geoenvironmental Engineering*, 127(12):1017-1026.

Liu, L., and Dobry, R. (1997). Seismic response of shallow foundation on liquefiable sand. *Journal of Geotechnical and Geoenvironmental Engineering*, 123(6):557-567.

Lu, N., Godt, J. W., and Wu, D. T. (2010). A closed form equation for effective stress in unsaturated soil. *Water Resources Research*, 46(5):1-14.

Luong, M., and Sidaner, J. (1981). Undrained behaviour of cohesionless soils under cyclic and transient loading. In *1st international conference on recent advances in geotechnical earthquake engineering and soil dynamics*, pages 215–220, University of Missouri-Rolla, St. Louis, USA.

Luthin, J. N., and Miller, R. D. (1953). Pressure distribution in soil columns draining into the atmosphere. Proceedings of Soil Science Society of America, 17:329-333.

Madabhushi, S. P. G. (1994). Effect of Pore Fluid in Dynamic Centrifuge Modelling. In *Proceedings of Centrifuge `94*, pages 127-132. Balkema, Rotterdam.

Madabhushi, S. P. G. (2014). *Centrifuge Modelling for Civil Engineers*. Taylor & Francis, London.

Madabhushi, S. P. G., Houghton, N. E., and Haigh, S. K. (2006). A new automatic sand pourer for model preparation at University of Cambridge. In *proceedings of the 6th international conference on physical modelling in geotechnics*, volume 1-2, pages 217-222. Taylor & Francis.

Madabhushi, S. P. G., Schofield, A. N., and Lesley, S. (1998). A new Stored Angular Momentum (SAM) based earthquake actuator, pages 111-116. Balkema.

Marasini, N. P., and Okamura, M. (2015). Air injection to mitigate liquefaction under light structures. *International Journal of Physical Modelling in Geotechnics*, 15(3):129-140.

Marulanda, C., Culligan, P. J. and Germaine, J. T. (2000). Centrifuge modelling of air sparging-a study of air flow through saturated porous media. *Journal of Hazardous Materials*, 72(2-3):179-215.

Mitchell, J. K., and Santamarina, J. C. (2005). Biological considerations in geotechnical engineering. *Journal of Geotechnical and Geoenvironmental Engineering*, 131(10):1222–1233.

Mitchell, J. K., Baxter, C. D. P., and Munson, T. C. (1995). Performance of improved ground during earthquakes. *Soil Improvement for Earthquake Hazard Mitigation, Geotechnical Special Publication,* 49:1-36.

Mitrani, H. (2006). *Liquefaction remediation techniques for existing buildings*. PhD thesis, University of Cambridge.

Mitrani, H., and Madabhushi, S. P. G. (2008). Centrifuge modelling of inclined micro-piles for liquefaction remediation of existing buildings. *Geomechanics and Geoengineering,* 3(4):245-256.

Montoya, B. M., DeJong, J. T., and Boulanger, R. W. (2013). Response of liquefiable sand improved by microbial-induced calcite precipitation. *Géotechnique,* 63(4):302-312.

Muhunthan, B., and Schofield, A. N. (2000). Liquefaction and dam failures. *Slope Stability 2000, ASCE Special Publication*, pages 266-280.

Muraleetharan, K. K., Mish, K. D., and Arulanandan, K. (1994). A fully-coupled nonlinear dynamic analysis procedure and its verification using centrifuge test results. *International Journal for Numerical and Analytical Methods in Geomechanics*, 18(5):305-324.

Naesgaard, E., Bryne, P. M., and Wijewickreme, D. (2007). Is P-wave velocity an indicator of saturation in sand with viscous pore fluid? *International Journal of Geomechanics*, 7(76):437-443.

Ogata, H., and Okamura, M. (2006). Experimental study on air behavior in saturated soil under air injection. In *proceedings of the symposium on natural disaster prevention*. Japan Society of Civil Engineers, Tokushima, Japan, pages 89-90.

Okamura, M., and Inoue, T. (2012). Preparation of fully saturated models for liquefaction study. *International Journal of Physical Modelling in Geotechnics*, 12(1):39-46.

Okamura, M., and Noguchi, K. (2009). Liquefaction resistance of unsaturated non-plastic silt. *Soils and Foundations*, 49(2):221-229.

Okamura, M., and Soga, Y. (2006). Effect on liquefaction resistance of volumetric strain of pore fluid. *Soils and Foundations*, 46(5):703–708.

Okamura, M., and Teraoka, T. (2005). Shaking table tests on desaturated soil as liquefaction countermeasure. *Geotechnical Special Publication*, 145:282-293.

Okamura, M., and Tomida, Y. (2015). Full scale test on cost effective liquefaction countermeasure for highway embankment. In *Proceedings of the 6th international geotechnical symposium on disaster mitigation in special geoenvironmental conditions*, IIT Madras, Chennai, India, Vol. 1, (Indian Geotechnical Society, Chennai Chapter), pages 208-212.

Okamura, M., Ishihara, M., and Oshita, T. (2003). Liquefaction Resistance of Sand Deposit Improved with Sand Compaction Piles. *Soils and Foundations* 43(5):175-187.

Okamura, M., Ishihara, M., and Tamura, K. (2006). Degree of saturation and liquefaction resistances of sand improved with SCP. *Journal of Geotechnical and Geoenvironmental Engineering*, 132(2):258-264.

Okamura, M., Takebayashi, M., Nishida, K., Fujii, N., Jinguji, M., Imasato, T., Yasuhara, H., and Nakagawa, E. (2011). In-situ desaturation test by air injection and its evaluation through field monitoring and multiphase flow simulation. *Journal of Geotechnical and Geoenvironmental Engineering*, 137(7):643-652.

Poulos, S. J. (1981). The Steady State of Deformation. *Journal of the Geotechnical Engineering Division*, 107(5):553-562.

Reddy, K. R., and Adams, J. A. (2001). Effects of soil heterogeneity on airflow patterns and hydrocarbon removal during in situ air sparging. *Journal of Geotechnical and Geoenvironmental Engineering*, 127(3):234-247.

Robertson, P., List, B., and Hofman, B. (1994). CANLEX (Canadian Liquefaction Experiment): A One year Update. In *5th US-Japan workshop on earthquake resistant design of lifeline facilities and countermeasures against soil liquefaction*.

Robinson, D. A., Jones, S. B., Wraith, J. M., Or, D., and Friedman, S. P. (2003). A review of advances in dielectric and electrical conductivity measurement in soils using time domain reflectometry. *Vadose Zone Journal*, 2:444-475.

Rollins, K. M., and Seed, H. B. (1990). Influence of buildings on potential liquefaction damage. *Journal of Geotechnical Engineering,* 116(2):165-185.

Sancio, R. B., Bray, J. D., Stewart, J. P., Youd, T. L., Durgunoglu, H. T., Onalp, A., Seed, R. B., Christensen, C., Baturay, M. B., and Karadayilar, T. (2002). Correlation between ground failure and soil conditions in Adapazari, Turkey. *Soil Dynamics and Earthquake Engineering*, 22(9-12):1093-1102.

Schofield, A. (1980). Cambridge geotechnical centrifuge operations. *Géotechnique*, 30(3):227-268.

Schofield, A. N. (1981). Dynamic and earthquake geotechnical centrifuge modelling. In *1st international conference on recent advances in geotechnical earthquake engineering and soil dynamics*, pages 1081-1100, University of Missouri-Rolla, St. Louis, USA.

Schofield, A. N., and Wroth, C. P. (1968). *Critical state soil mechanics*. McGraw-Hill, London.

Seed, H. B. (1979). Soil liquefaction and cyclic mobility evaluation for level ground during earthquakes. *Journal of the Geotechnical Engineering Division*, 105(2):201-255.

Seed, H. B., and Idriss, I. M. (1971). Simplified procedure for evaluating soil liquefaction potential. *Journal of the Soil Mechanics and Foundations Division*, 97(9):1249-1273.

Seed, H. B., and Lee, K. L. (1966). Liquefaction of saturated sands during cyclic loading. *Journal of the Soil Mechanics and Foundations Division*, 92(6):105-134.

Seed, H. B., Mori, K., and Chan, C. K. (1977). Influence of seismic history on liquefaction of sand. *Journal of the Geotechnical Engineering Division*, 103(4):255-270.

Seed, R. B., and Harder, L. F. (1990). SPT-based analysis of cyclic pore pressure generation and undrained residual strength. In Duncan, J. M., editor*, Proceedings of the H. B., Seed Memorial Symposium*, Vol. 2, pages 351-376, BiTech Publishers, Richmond.

Seed, R. B., Cetin, K. O., Ress, M. O. S., Kammerer, A. M., Wu, J., Pestana, J. M., Riemer, M. F., et al. (2003). Recent advances in soil liquefaction engineering: A unified and consistent framework. *Proceedings of the 26th Annual ASCE Los Angeles Geotechnical Spring Seminar*, Long Beach, California, USA, pages 301-371.

Semer, R., Adams, J. A., and Reddy, K. R. (1998). An experimental investigation of air flow patterns in saturated soils during air sparging. *Geotechnical and Geological Engineering*, 59(1):59-75.

Sherif, M. A., Tsuchiya, C., and Ishibashi, I. (1977). Saturation effect on initial soil liquefaction. *Journal of the Geotechnical Engineering Division*, 103(8):914-917.

Soga, K. (1998). Soil liquefaction effects observed in the Kobe earthquake of 1995. In *Proceedings of Institution of Civil Engineers, Geotechnical Engineering*, 131(1):34-51.

Steedman, R. S. and Madhabushi, S. P. G. (1991). Wave propagation in sand medium. In *the 4th International Conference on Seismic Zonation*. EERI.

Stewart, D. P., Chen, Y.-R., and Kutter, B. L. (1998). Experience with the use of methylcellulose as a viscous pore fluid in centrifuge models. *Geotechnical Testing Journal*, 21(4):365-369.

Stringer, M. E., and Madabhushi, S. P. G. (2009). Novel computer-controlled saturation of dynamic centrifuge models using high viscosity fluids. *Geotechnical Testing Journal*, 32(6):559-564.

Stringer, M., Heron, C. M., and Madabhushi, S. P. G. (2010). Experience using MEMS-based accelerometers in dynamic testing. In *the 7th international conference on physical modelling in geotechnics*, pages 389-394.

Takahashi, H., Kitazume, M., Ishibasi, S., and Yamawaki, S. (2006). Evaluating the saturation of model ground by P-wave velocity and modelling of models for a liquefaction study. *International Journal of Physical Modelling in Geotechnics*, 1:13-15.

Terzaghi, K. (1943). *Theoretical soil Mechanics*. John Wiley & Sons Inc., New York, NY.

Tokimatsu, K. and Seed, H. B. (1987). Evaluation of settlements in sands due to earthquake shaking. *Journal of Geotechnical Engineering*, 113(8):861-878.

Tokimatsu, K., and Yoshimi, Y. (1983). Empirical correlation of soil liquefaction based on SPT N-value and fines content. *Soils and Foundations*, 23(4):56-74.

Tsukamoto, Y., Kawabe, S., Matsumoto, J., and Hagiwara, S. (2014). Cyclic resistance of two unsaturated silty sands against soil liquefaction. *Soils and Foundations,* 54(6):1094–1103.

Vaid, Y. P., and Chern, J. C. (1983). Effect of static shear on resistance to liquefaction. *Soils and Foundations*, 23(1):47-60.

Van Genuchten, M. T. (1980). A closed-form equation for predicting the hydraulic conductivity of unsaturated soils. *Soil Science Society of America Journal*, 44(5):892-898.

Venter, K. (1987). *Modelling the response of sand to cyclic loads*. PhD thesis, University of Cambridge.

White, D. J. (2002). *The measurement of particle size distribution using the Single Particle Optical Sizing (SPOS) method*. University of Cambridge Department of Engineering, Technical Report, University of Cambridge, CUED/D-SOILS/TR321.

White, D., Take, W., and Bolton, M. (2003). Soil deformation measurement using particle image velocimetry (PIV) and photogrammetry. *Géotechnique*, 53(7):619-631.

Wu, J., and Seed, R. B. (2004). Estimating of liquefaction-induced ground settlement (case studies). In *the proceedings of the 5th international conference on case histories in geotechnical engineering*, New York, April, 2004, No. 3.09, pages 1-8.

Yasuhara, H., Kochi, M., and Okamura, M. (2008). Experiments and predictions of soil desaturation by air injection technique and the implications mediated by multiphase flow simulation. *Soils and Foundations*, 48(6):791-804.

Yegian, M. K., Eseller-Bayat, E., Alshawabkeh, A., and Ali, S. (2007). Induced partial saturation (IPS) for liquefaction mitigation: Experimental investigation. *Journal of Geotechnical and Geoenvironmental Engineering*, 133 (4):372-380.

Yoshimi, N., Rolando, P. O., Fumiaki, T., Naitaka, K., Masayuki, H., and Yukio, N. (2011). Measurement of degree of saturation on model ground by digital image processing. *Soils and Foundations* 51(1):167-177.

Yoshimi, Y., and Tokimatsu, K. (1977). Settlement of buildings on saturated sand during earthquakes. *Soils and Foundations*, 17(1):23-38

Yoshimi, Y., Yanaka, K., and Tokimatsu, K. (1989). Liquefaction resistance of a partially saturated sand. *Soils and Foundations*, 29(3):157-162.

Youd, T. L., Hansen, C. M., and Bartlett, S. F. (2002). Revised multilinear regression equations for prediction of lateral spread displacement. *Journal of Geotechnical and Geoenvironmental Engineering*, 128(12):1007-1017.

Zeybek, A., Madabhushi, S. P. G. (2017a). Centrifuge testing to evaluate the liquefaction response of air-injected partially saturated soils beneath shallow foundations. *Bulletin of Earthquake Engineering*, 15(1):339-356.

Zeybek, A., and Madabhushi, S. P. G. (2017b). Influence of air injection on the liquefaction-induced deformation mechanisms beneath shallow foundations. *Soil Dynamics and Earthquake Engineering*, 97:266-276.

Zeybek, A., Madabhushi, S. P. G. (2017c). Physical modelling of air injection to remediate liquefaction. *International Journal of Physical Modelling in Geotechnics*, http://dx.doi.org/10.1680/jphmg.16.00049.

Zeybek, A., and Madabhushi, S. P. G. (2017d). Durability of partial saturation to counteract liquefaction. *Proceedings of the Institution of Civil Engineers - Ground Improvement,* 170(2):102-111.

Appendix-A Centrifuge Test Programme and Model Layouts

This appendix describes the centrifuge model layouts with instrumentation positions given in model scale. The centrifuge testing programme summarised in table 3.5 (section 3.3.6) is also detailed. The convention for each phase of centrifuge test is [*Centrifuge Test (CT) ID*, *Air Injection* (*A*) or *Earthquake (EQ) Number*].

Table A.1– Testing programme for CT1.

Centrifuge Test: CT1		
Aim: ***to assess the seismic response of a heavy shallow foundation resting on a saturated soil deposit (benchmark test)***		
Model box	: *Window box*	
Model layout	: *(see figure A.1)*	
Model foundation	: *MF1 (see table 3.3)*	
Initial relative density	: *~40.8%*	
g-level (*N*)	: *70*	
Test sequence:		
Swing-up 1	(SWGUP1)	: 1-g to 70-g
Earthquake 1	(CT1EQ1)	: 50 Hz, 1.194 V, 0.4 seconds (~12.6 g peak input acceleration)
Earthquake 2	(CT1EQ2)	: 50 Hz, 0.752 V, 0.4 seconds (~14.7 g peak input acceleration)
Earthquake 3	(CT1EQ3)	: 50 Hz, 0.504 V, 0.4 seconds (~16.1 g peak input acceleration)
Air Injection 1	(CT1A1)	: Degree of saturation (reduced from ~99.0% to ~88.3%)
Earthquake 4	(CT1EQ4)	: 50 Hz, 0.507 V, 0.4 seconds (~16.1 g peak input acceleration)
Swing-down 1	(SWGDOWN1)	: 70-g to 1-g

Table A.2– Testing programme for CT2.

Centrifuge Test: CT2		
Aim: ***to assess the seismic response of a heavy shallow foundation resting on a partially saturated soil deposit mitigated by air injection (improved soil deposit)***		
Model box	: *Window box*	
Model layout	: *(see figure A.1)*	
Model foundation	: *MF1 (see table 3.3)*	
Initial relative density	: *~40.0%*	
g-level (*N*)	: *70*	
Test sequence:		
Swing-up 1	(SWGUP1)	: 1-g to 70-g
Air Injection 1	(CT2A1)	: Degree of saturation (reduced from ~99.0% to ~89.0%)
Earthquake 1	(CT2EQ1)	: 50 Hz, 1.2 V, 0.4 seconds (~12.6 g peak input acceleration)
Air Injection 2	(CT2A2)	: -
Earthquake 2	(CT2EQ2)	: 50 Hz, 0.755 V, 0.4 seconds (~14.7 g peak input acceleration)
Air Injection 3	(CT2A3)	: -
Earthquake 3	(CT2EQ3)	: 50 Hz, 0.501 V, 0.4 seconds (~16.1 g peak input acceleration)
Air Injection 4	(CT2A4)	: -
Earthquake 4	(CT2EQ4)	: 50 Hz, 0.504 V, 0.4 seconds (~16.1 g peak input acceleration)
Swing-down 1	(SWGDOWN1)	: 70-g to 1-g

Table A.3– Testing programme for CT3.

Centrifuge Test: CT3		
Aim: ***to assess the seismic response of a heavy shallow foundation resting on a partially saturated soil deposit mitigated by air injection (improved soil deposit)***		
Model box	: *Window box*	
Model layout	: *(see figure A.1)*	
Model foundation	: *MF1 (see table 3.3)*	
Initial relative density	: *~39.9%*	
g-level (*N*)	: *70*	
Test sequence:		
Swing-up 1	(SWGUP1)	: 1-g to 70-g
Air Injection 1	(CT3A1)	: Degree of saturation (reduced from ~99.0% to ~86.0%)
Earthquake 1	(CT3EQ1)	: 50 Hz, 1.25 V, 0.4 seconds (~12.6 g peak input acceleration)
Air Injection 2	(CT3A2)	: -
Earthquake 2	(CT3EQ2)	: 50 Hz, 0.752 V, 0.4 seconds (~14.7 g peak input acceleration)
Air Injection 3	(CT3A3)	: -
Earthquake 3	(CT3EQ3)	: 50 Hz, 0.499 V, 0.4 seconds (~16.1 g peak input acceleration)
Air Injection 4	(CT3A4)	: -
Earthquake 4	(CT3EQ4)	: 50 Hz, 0.501 V, 0.4 seconds (~16.1 g peak input acceleration)
Swing-down 1	(SWGDOWN1)	: 70-g to 1-g

Table A.4– Testing programme for CT4.

Centrifuge Test: CT4		
Aim: ***to assess the seismic response of a light shallow foundation resting on a saturated soil deposit (benchmark test)***		
Model box	: *Window box*	
Model layout	: *(see figure A.2)*	
Model foundation	: *MF2 (see table 3.3)*	
Initial relative density	: *~40.2%*	
g-level (*N*)	: *70*	
Test sequence:		
Swing-up 1	(SWGUP1)	: 1-g to 70-g
Earthquake 1	(CT4EQ1)	: 50 Hz, 1.202 V, 0.4 seconds (~12.6 g peak input acceleration)
Earthquake 2	(CT4EQ2)	: 50 Hz, 0.748 V, 0.4 seconds (~14.7 g peak input acceleration)
Earthquake 3	(CT4EQ3)	: 50 Hz, 0.505 V, 0.4 seconds (~16.1 g peak input acceleration)
Air Injection 1	(CT4A1)	: Degree of saturation (reduced from ~99.0% to ~87.2%)
Earthquake 4	(CT4EQ4)	: 50 Hz, 0.506 V, 0.4 seconds (~16.1 g peak input acceleration)
Swing-down 1	(SWGDOWN1)	: 70-g to 1-g

Table A.5– Testing programme for CT5.

Centrifuge Test: CT5

Aim: ***to assess the seismic response of a light shallow foundation resting on a partially saturated soil deposit mitigated by air injection (improved soil deposit)***

Model box	: *Window box*
Model layout	: *(see figure A.2)*
Model foundation	: *MF2 (see table 3.3)*
Initial relative density	: *~39.9%*
g-level (*N*)	: *70*

Test sequence:

Swing-up 1	(SWGUP1)	: 1-g to 70-g
Air Injection 1	(CT5A1)	: Degree of saturation (reduced from ~99.0% to ~93.1%)
Earthquake 1	(CT5EQ1)	: 50 Hz, 1.198 V, *0.4 seconds** (~12.6 g peak input acceleration)
Air Injection 2	(CT5A2)	: -
Earthquake 2	(CT5EQ2)	: 50 Hz, 0.749 V, *0.4 seconds** (~14.7 g peak input acceleration)
Air Injection 3	(CT5A3)	: -
Earthquake 3	(CT5EQ3)	: 50 Hz, 0.502 V, 0.4 seconds (~16.1 g peak input acceleration)
Air Injection 4	(CT5A4)	: -
Earthquake 4	(CT5EQ4)	: 50 Hz, 0.500 V, 0.4 seconds (~16.1 g peak input acceleration)
Swing-down 1	(SWGDOWN1)	: 70-g to 1-g

**Note:* The duration of the first and second earthquake was comparatively longer than usual (see section 3.5.3 for further details).

Table A.6– Testing programme for CT6.

Centrifuge Test: CT6

Aim: ***to assess the seismic response of a heavy shallow foundation resting on a partially saturated soil deposit mitigated by air injection (improved soil deposit) and to investigate the durability of air bubbles under the simulated field conditions***

Model box	: *Window box*
Model layout	: *(see figure A.2)*
Model foundation	: *MF2 (see table 3.3)*
Initial relative density	: *~40.1%*
g-level (*N*)	: *70*

Test sequence:

Swing-up 1	(SWGUP1)	: 1-g to 70-g
Air Injection 1	(CT6A1)	: Degree of saturation (reduced from ~99.0% to ~79.5%)
Earthquake 1	(CT6EQ1)	: 50 Hz, 1.214 V, *0.4 seconds** (~12.6 g peak input acceleration)
Air Injection 2	(CT6A2)	: -
Earthquake 2	(CT6EQ2)	: 50 Hz, 0.749 V, *0.4 seconds** (~14.7 g peak input acceleration)
Air Injection 3	(CT6A3)	: -
Earthquake 3	(CT6EQ3)	: 50 Hz, 0.500 V, 0.4 seconds (~16.1 g peak input acceleration)
Air Injection 4	(CT6A4)	: -
25 Minutes Flight (Hydrostatic)		: -
Increasing g-level		: 70-g to 90-g in 10-g steps
Earthquake 4	(CT6EQ4)	: 50 Hz, 0.501 V, 0.4 seconds (~16.1 g peak input acceleration)
Swing-down 1	(SWGDOWN1)	: 90-g to 1-g

**Note:* The duration of the first and second earthquake was comparatively longer than usual (see section 3.5.3 for further details).

Table A.7– Testing programme for CT7.

Centrifuge Test: CT7

Aim: ***to assess the seismic response of a light shallow foundation resting on a partially saturated soil deposit mitigated by air injection under low confining (vertical) stress level***

Model box	: *Window box*
Model layout	: *(see figure A.2)*
Model foundation	: *MF3 (see table 3.3)*
Initial relative density	: *~40.2%*
g-level (*N*)	: *40*

Test sequence:

Swing-up 1	(SWGUP1)	: 1-g to 40-g
Air Injection 1	(CT7A1)	: Degree of saturation (reduced from ~99.0% to ~84.34%)
Earthquake 1	(CT7EQ1)	: 50 Hz, 1.202 V, *0.7 seconds** (~7.2 g peak input acceleration)
Air Injection 2	(CT7A2)	: -
Earthquake 2	(CT7EQ2)	: 50 Hz, 0.749 V, 0.7 seconds (~8.4 g peak input acceleration)
Air Injection 3	(CT7A3)	: -
Earthquake 3	(CT7EQ3)	: 50 Hz, 0.497 V, 0.7 seconds (~9.2 g peak input acceleration)
Air Injection 4	(CT7A4)	: -
Earthquake 4	(CT7EQ4)	: 50 Hz, 0.503 V, 0.7 seconds (~9.2 g peak input acceleration)
Swing-down 1	(SWGDOWN1)	: 40-g to 1-g

**Note:* The trace of the first earthquake was not symmetrical (see section 3.5.3 for further details).

Table A.8– Testing programme for CT8.

Centrifuge Test: CT8

Aim: ***to assess the seismic response of a saturated and partially saturated soil deposit in the free-field and to investigate the durability of air bubbles under the simulated field conditions***

Model box	: *Window box*
Model layout	: *(see figure A.3)*
Initial relative density	: *~40.2%*
g-level (*N*)	: *70*

Test sequence:

Model foundation		: *No foundation (Free-field Test)*
Swing-up 1	(SWGUP1)	: 1-g to 70-g
Earthquake 1	(CT8EQ1)	: 50 Hz, 1.202 V, 0.4 seconds (~12.6 g peak input acceleration)
Air Injection 1	(CT8A1)	: Degree of saturation (reduced from ~99.0% to ~86.58%)
Earthquake 2	(CT8EQ2)	: 50 Hz, 0.748 V, 0.4 seconds (~14.7 g peak input acceleration)
Air Injection 2	(CT8A2)	: -
Earthquake 3	(CT8EQ3)	: 50 Hz, 0.505 V, 0.4 seconds (~16.1 g peak input acceleration)
Air Injection 3	(CT8A3)	: -
Increasing g-level		: 70-g to 90-g in 5-g steps
Swing-down 1	(SWGDOWN1)	: 90-g to 1-g

Table A.9– Testing programme for CT9.

Centrifuge Test: CT9

Aim: ***to assess the seismic response of a saturated and partially saturated soil deposit in the free-field and to explore the durability of air bubbles***

Model box	: *Laminar box*
Model layout	: *(see figure A.4)*
Initial relative density	: *~40.1%*
g-level (*N*)	: *70*

Test sequence:

Model foundation		: *No foundation (Free-field Test)*
Swing-up 1	(SWGUP1)	: 1-g to 70-g
Air Injection 1	(CT9A1)	: Degree of saturation (reduced from ~99.0% to ~85.12%)
30 Minutes Flight (Hydrostatic)		: -
Earthquake 1	(CT9EQ1)	: 50 Hz, 1.200 V, 0.4 seconds (~12.6 g peak input acceleration)
Increasing g-level		: 70-g to 90-g in 5-g steps
30 Minutes Flight (Hydrostatic)		: -
Earthquake 2	(CT9EQ2)	: 50 Hz, 0.751 V, 0.4 seconds (~14.7 g peak input acceleration)
Swing-down 1	(SWGDOWN1)	: 90-g to 1-g

Table A.10– Testing programme for CT10.

Centrifuge Test: CT10

Aim: ***to assess the seismic response of a saturated and partially saturated soil deposit in the free-field***

Model box	: *Laminar box*
Model layout	: *(see figure A.4)*
Initial relative density	: *~39.4%*
g-level (*N*)	: *70*

Test sequence:

Model foundation		: *No foundation (Free-field Test)*
Swing-up 1	(SWGUP1)	: 1-g to 70-g
Air Injection 1	(CT10A1)	: Degree of saturation (reduced from ~99.0% to ~95.65%)
30 Minutes Flight	(Hydrostatic)	: -
Earthquake 1	(CT10EQ1)	: 50 Hz, 1.203 V, 0.4 seconds (~12.6 g peak input acceleration)
Swing-down 1	(SWGDOWN1)	: 70-g to 1-g

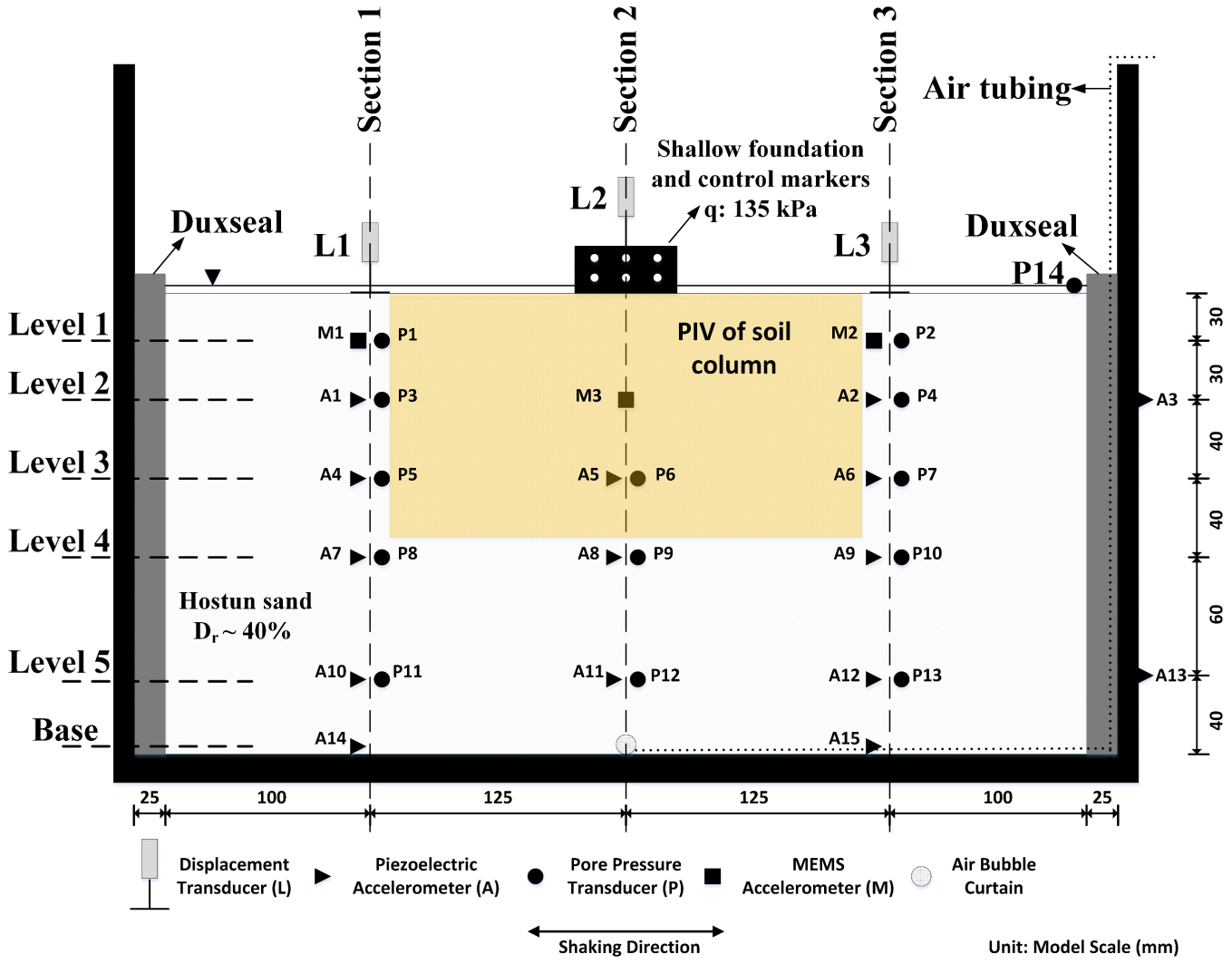

Figure A.1– Model layout for CT1, CT2 and CT3, dimensions in model scale.

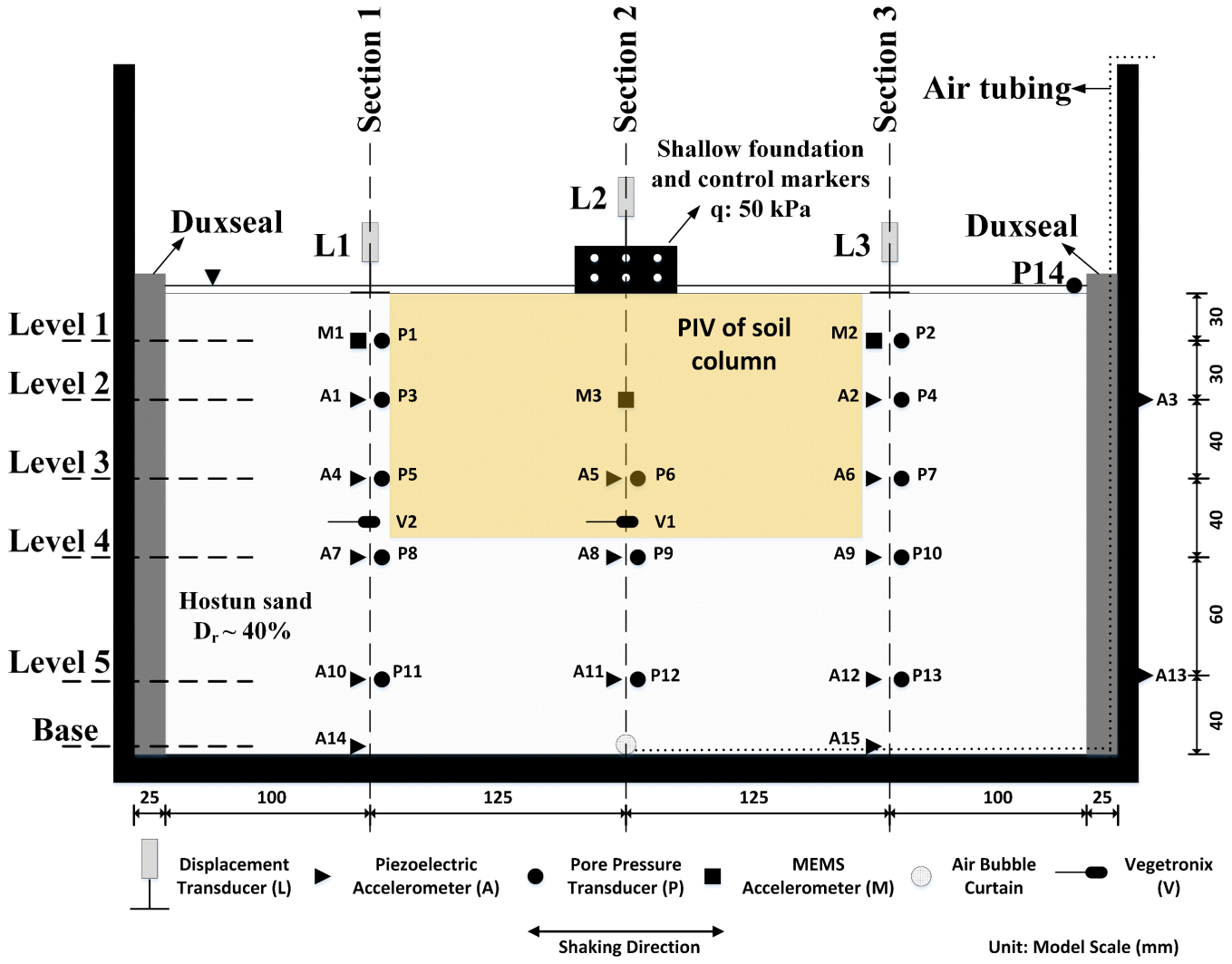

Figure A.2– Model layout for CT4, CT5, CT6 and CT7, dimensions in model scale.

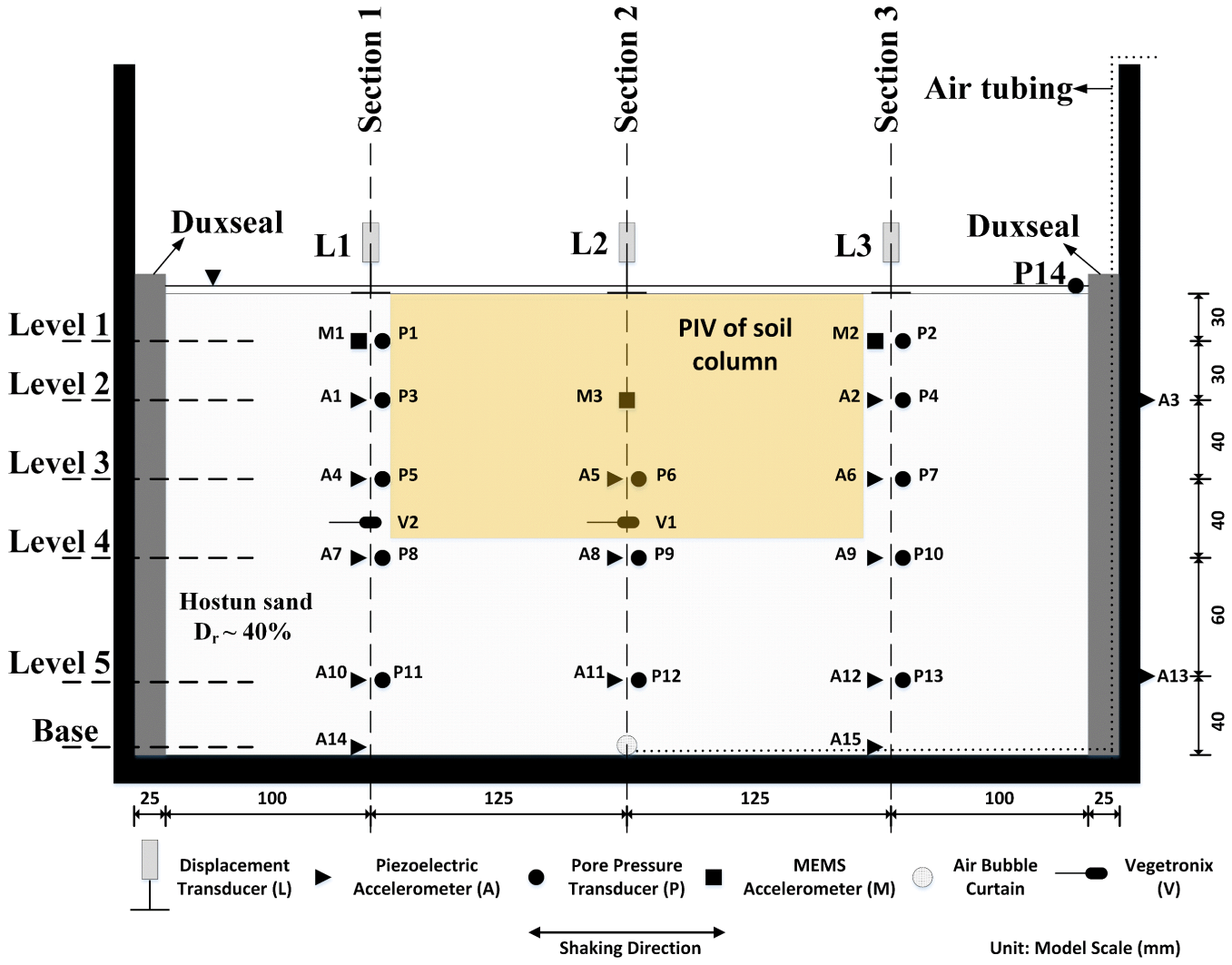

Figure A.3– Model layout for CT8, dimensions in model scale.

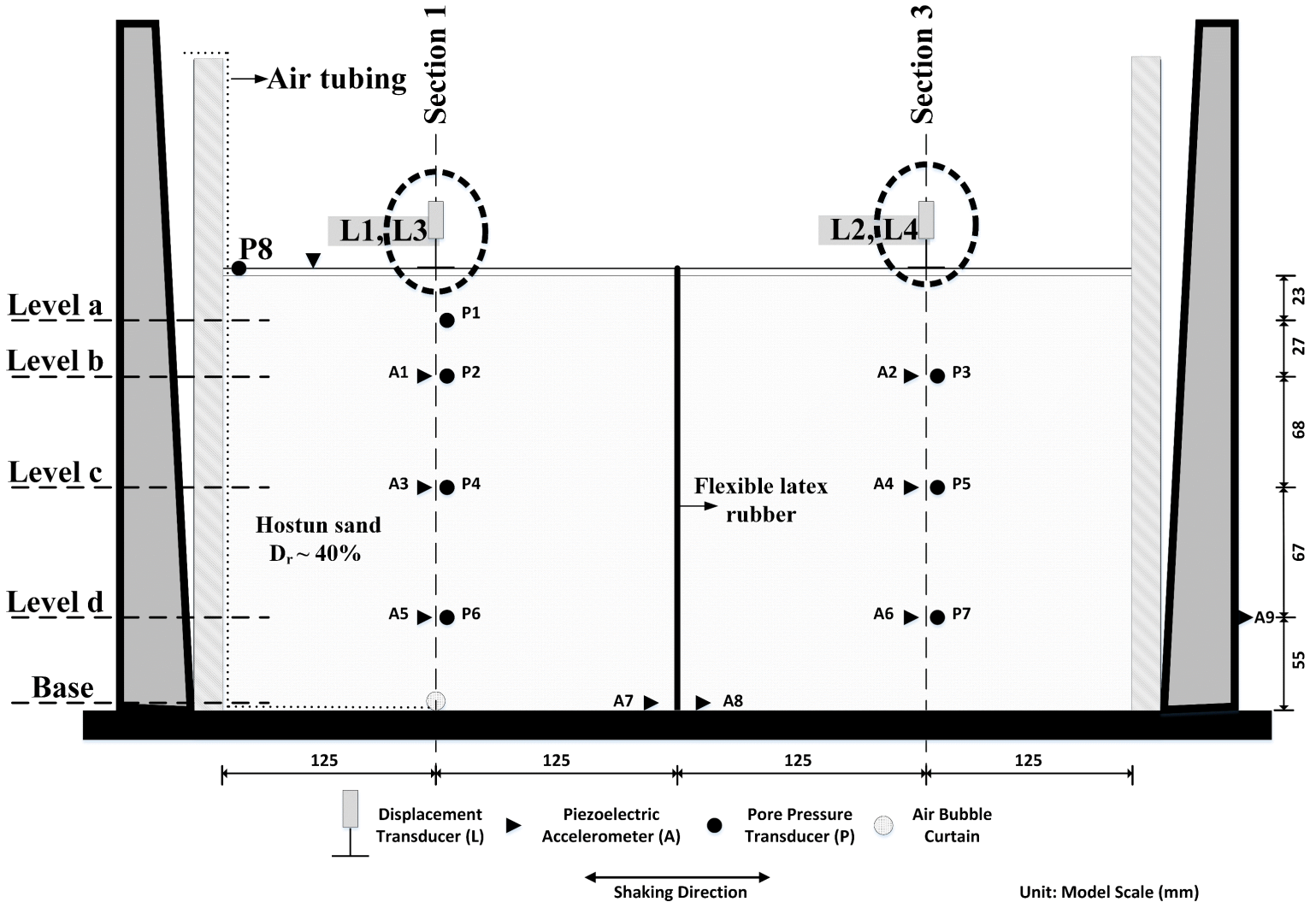

Figure A.4– Model layout for CT9 and CT10, dimensions in model scale.